NORWEGIAN UNIVERSITY OF SCIENCE AND TECHNOLOGY
DEPARTMENT OF CIVIL AND ENVIRONMENTAL ENGINEERING

Appendix A - REPORT I

Finite Element Modelling principles on the interaction between railway tracks, culverts and backfills in PLAXIS 2D

- ***Includes examples of track modelling, moving train loads, dynamic assessments and modelling of soil-culvert interactions based of norwegian backfill and compaction procedures***

By Dan Sergei Sukuvara

Aknowledgement

Writing this report I've gotten several contributions which helped me tremendously during the process of creating the models. I want to show my appriciation to

- **Kenneth Sundli** from NTNU for gaining me access to three powerfull work stations. This project would never been feasible if I hadn't gotten access to such power computers and large amount of disk space

- The professors from the geotechnical group at NTNU, **Steinar Nordal**, **Gustav Grimstad** and **Gudmund Eiksund** for interesting discussions and learning experiences regarding modelling in PLAXIS

- **Albert Lau** from NTNU for always supporting me with guidance and questions on topics regarding railways and for creating the Fast Fourier Transformation (FFT) code in Matlab

- **Geir Svanø** and **Alf-Helge Løhren** for sharing their experiences and comments during the project

- **Peder Hembre** from ViaCon Norway for his support and providing me with alot of background information and referance projects of flexible steel-soil culverts

- **Jan Vaslestad** from Statens Vegvesen for sharing his valuable experiences with flexible steel-soil composite bridges, providing me with litterature and always answering questions

- **Ole-John Fossum** from Farbu & Gausen As for sharing his practical knowledge from field and answering questions regarding installation and backfilling of railway culverts

- **Åsmund Tøsse** and **Aziz kameran** from Bane NOR for sharing their knowledge on norwegian railway culverts and the transition slab

- **Andreas Andersson** from KTH for providing me with litterature but also sharing his expertise

- **Amer Wadi** from ViaCon Sweden for sharing his knowledge on flexible steel-soil composite bridges and experiences with modelling and backfilling in PLAXIS 2D

Summary

This report is written as a supplementary report for the master thesis «Stiffness variations on railway tracks over culvert underpassing», and involves all the principles and background information for the finite element models created to study railway transition zones.

This report is divided into three main parts, that is railway tracks, moving train loads with backfilling and construction of railway culverts.

The second chapter purposes a methodology for constructing a railway track in PLAXIS 2D. This track was then used for calibration of ballast and railpad stiffness, which also included a comparison to the classic theory for beam on elastic foundation, namely Zimmermanns theory. It is generally found that this railway track behaves with good correlation to theory, statically speaking.

The third chapter introduces a method for modelling horisontally moving point loads in PLAXIS. This method is used to model a moving train based of any desired speed and axle spacing. The chapter also involves dynamic assessments of the model were several frequency domains were found. This analysis made it possible to damp away unrealistic frequencies without misusing rayleigh damping factors.

Chapter 4-6 involves construction and backfilling of railway culverts. It is generally found that catching the field behaviour when constructing flexible steel-soil composite culverts in a model is crucial in order to get the structure to behave as it would in field. It was therefore created a methodology with a Hardening Soil model for catching the internal forces that develops on a flexible culvert during backfilling and compaction.

The methodology involves creating layers, compacting with static line loads and unloading. From two field test were the structural response of flexible culverts has been monitored, it was possible to validate this methodology by simulating all the fundamental backfilling stages. In general, good agreement is found with this methodology. The simulation examples also shows how big of an influence the use of heavier compaction equipment has on these structures, were heavier equipment (or magnitudes of the line loads) in general leads to better structural resistance against surface loads in terms of bending and displacements of the culverts crown.

Another aspect considered of flexible steel culverts, is how its interact with the backfill over time. In Hardening Soil models, after the first loading cycle of the soil has occoured and assuming that this load doesn’t change, it behaves almost completely elastic afterwards when it is being unloaded. It was a desire to validate the models behaviour after several train passages as this would be similar to «a long-term behaviour»of the interaction, i.e when the model starts to behave elastic. After comparison to two long-term fieldmeasurements from Norway, good agreement in general was found, and it could be concluded that the methodology presented in these chapters shows high good accuracy as long as certain field conditions are known.

Since the backfill procedures of rigid and flexible culverts are very alike, the same methodology defined for flexible culvert was also applied for concrete culverts in the final models.

Table of contents

Notations

a	Sleeper spacing (Chapter. 2)	[m]
a	Soil attraction	[kPa]
A_s	Sleeper contact area with ballast	[m^2]
C	Ballast coefficient	[N/m^3]
c	Cohesion	[kPa]
c_{inter}	Interface cohesion in structure-soil interaction in PLAXIS	[kPa]
c_{ref}	Effective cohesion at failre	[kPa]
C_u	Soil coefficient of uniformity	[-]
d_{10},d_{50},d_{60}	Soil gradings	[-]
E	Elastic modulus	[MPa]
e_0	Initial void ratio	[-]
E_{50}^{ref}	Secant stiffness from a standard triaxial test	[MPa]
EA	Axial stiffness	[kN]
EI	Bending stiffness	[kNm^2]
E_{oed}^{ref}	Tangent stiffness from a oedometer apparatus	[MPa]
$E_{pad,10mm}$	Elastic modulus of railpad	[kN/mm^2]
$E_{soil,k}$	Characteristic secant modulus of soil after compaction	[MPa]
E_{ur}^{ref}	Unloading-reloading stiffness	[MPa]
f	Frequency	[Hz]
h_c	Height of soil cover	[m]
K	Earth pressure in a soil-culvert interaction	[-]
k	Fundation spring stiffness (Chapter. 2)	[kN/m]
L	Characteristic lenght (Chapter. 2)	[m]
M	Bending moment	[kNm]
m	Modulus ratio of soil	[-]
m	Power modulus for load distribution in Hardening soil	[-]
n	Stiffness ratio number between culvert and soil (λ in SDM)	[-]
η(x/L)	Deflection distribution along rail	[-]
μ(x/L)	Moment distribution along rail	[-]
N_A	Archingfactor (S_{ar} in SDM)	[-]
p	Uniform pressure above a pipe	[kPa]
P_{ref}	Atmospheric pressure with referance at 100 kPa	[kPa]
q	Equvalent live load over a burried pipe	[kPa]
r_0	Radius	[m]
R_{inter}	Interface roughness in structure-soil interaction in PLAXIS	[-]
S_v	Friction number	[-]
T	Circumferential thrust around a flexible pipe	[kN]
Ts	Fundamental frequency in soil	[Hz]
v	Possions ratio	[-]
v	Wave speed (Ch. 3.5)	[m/s]
v_p	Compression wave velocity	[m/s]
v_s	Shear wave velocity	[m/s]
v_{ur}	Unloading-reloading possions ratio	[-]
x	Ordinat from applied point load	[m]
y	Rail deflection (ch.2)	[mm]
α	Rayleigh damping factor for the influence of mass (ch3)	[-]
γ	Unit weight of soil	[kN/m^3]
δ	Settlement	[mm]
λ	Wave lenght (Ch. 3.5)	[m]
τ	Shear strenght at soil failure	[kPa]
ψ	Dilatancy angle at failure	[°]
ω	Angular velocity	[1/rad]

β	Rayleigh damping factor for the influence of stiffness (chapter. 3)	[-]
β	Stress exponent (chapter. 4.2.2)	[-]
ρ	Soil density	[g/cm^3]
σ_h	Horisontal stress	[kPa]
σ_v	Vertical stress	[kPa]
φ'	Effetive friction angle at failure	[°]
φ_k	Characteristic friction angle according to SDM	[°]

1 Introduction

The purpose of this report is to provide a detailed background basis for all the decisions and principles that were used when modelling transition zones for the final report. The methods presented in this report contains several simulation examples and comparisons to field measurements.

1.1.1 Setup of the report

This report is written in total 7 chapters. A typical chapter that involves modelling starts with general principles of creating the model, then compares it to either theory or field measurements. A summary of this reports structure is presented in figure 1.1

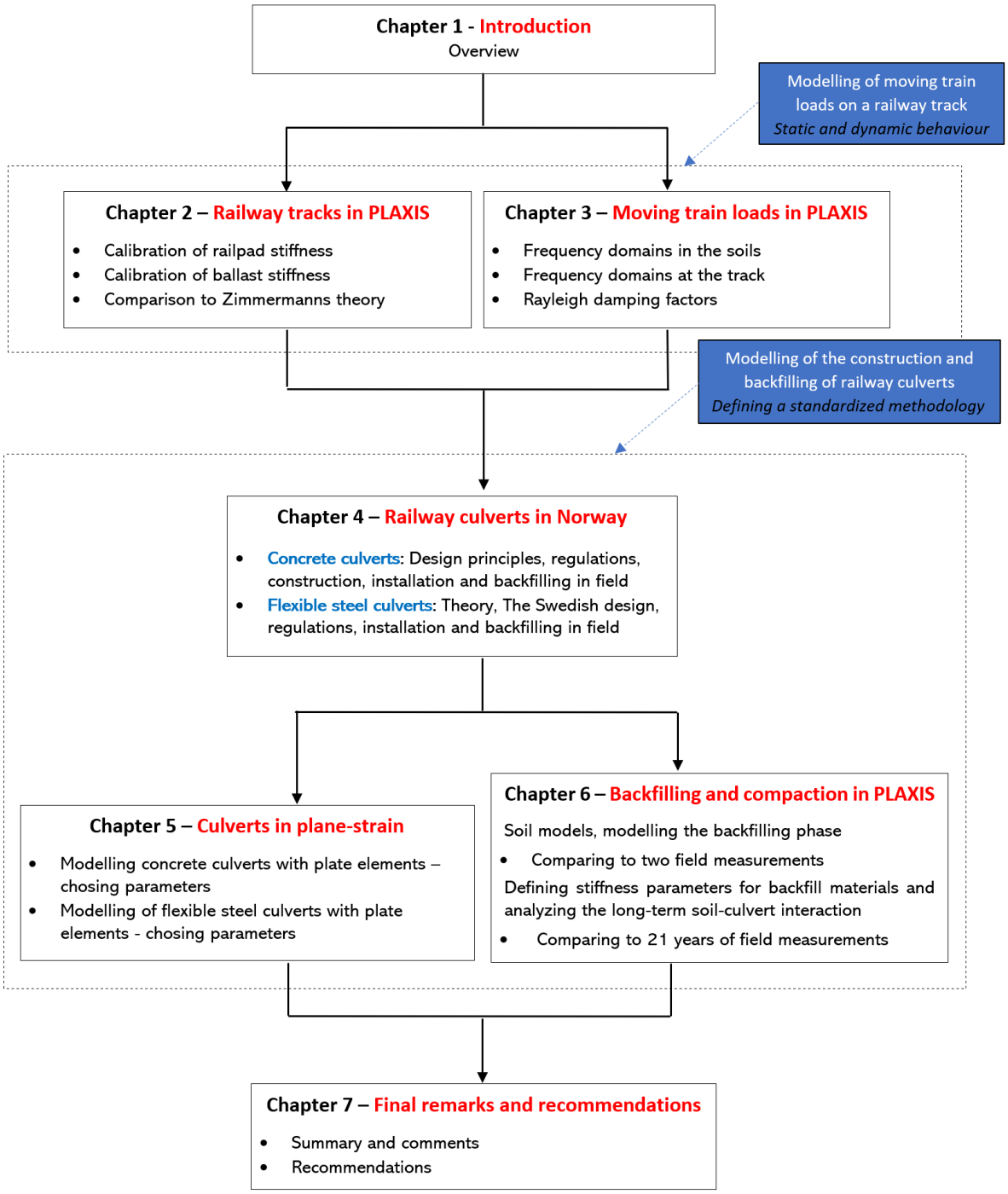

Figur 1.1 – Overview: Structure of this report

As seen in figure 1.1, chapter 2 involves modelling of a railway track in PLAXIS. The focuse of this part of the model has been to best obtain a realistic static behaviour of a real track, as it primarily is the quasi-static aspect of the transition zone that has been of interest in this project. Background descriptions for decisions made are first presented then followed by comparison to classic theory for beam on elastic foundation. Two calibration examples are also given in this chapter, one for calibrating the railpads compressive stiffness and one for calibrating the ballasts elastic stiffness.

Chapter 3 involves the aspect of moving train loads. It was found that using the multiplier functions in PLAXIS dynamic mode makes it possible to create an artificial load that moves horisontally. Instead of thinking in terms of trains, the chapter outlines a methodology for spacing point loads on the basis of the axle spacing of a real train with the option of given them any desired speed. .

When using the methodology for moving train loads and running dynamic analyses, it has frequently been seen that severe vibrations occours in the displacements. As a part of chapter 3, results from Fast Fourier Transformation (FFT) analysis are presented which exposed two frequency domains in the model which shouldn't be there. Those frequency domains were located from the loads entering the model and one was located from the railpads spacing on each sleeper.

Another point that is discussed in this chapter is a problem that has been observed with the Hardening Soil model in PLAXIS and dynamic loads.

Chapter 4-6 involves background information and principles of constructing railway culverts in PLAXIS. The first chapter (ch.4) starts with presenting some general background information on rigid concrete cul-verts and flexible steel-soil composite bridges. The purpose of this chapter was to provide information on railway culverts that especially applies for norwegian conditions. This chapter was used as the basis for several of the assumptions later made in the final models of the transition zones.

Chapter 5 shows principles of transforming culverts into plane-strain, involving two examples of how to chose stiffness parameters of concrete and steel elements when modelling them as elastic plates in PLAXIS.

Chapter 6 outlines a comphrehensive methodology for catching the effect of compaction during backfilling. The methodology was created using a Hardening Soil model, and the compaction equipments sentrifugal forces was modelled as static line loads. Comparisons of this methodology was made to two independent field measurements were good agreement was found.

When comparing to external field measurements, calculation procedures from the Swedish Design Method (SDM) were used and compared to other approaches for estimating stiffness parameters of the backfill.

Later in this chapter, the effect of changing backfilling materials, compaction loads and increasing the unloading stiffness of the backfill was compared to the results from long-term fieldmeasurements at two large spann flexible culverts from Norway.

2 Railway tracks in PLAXIS

This chapter describes the principles and methodology for modelling a railway track structure in PLAXIS 2D. The methodology includes background principles for modelling the interaction between rail, sleeper and ballast with plate elements. The basis behind the assumptions made in this chapter are deriven from the current norwegian design requirements for new railway lines, were technical design basis for the norwegian InterCity project, a report published by Bane NOR, are followed [1].

2.1 Track components

According to Bane NORs technical design basis for new InterCity lines, the standard rail and sleeper that must be used is the 60E1 rail and concrete JBV 60 sleeper [1]. For the JBV 60 sleeper, the current standard fastening system is the Pandrol Fastclip FE 1404 system followed by Pandrol 10 mm rubber pads with clusters knobs [2], see figure 2.1.

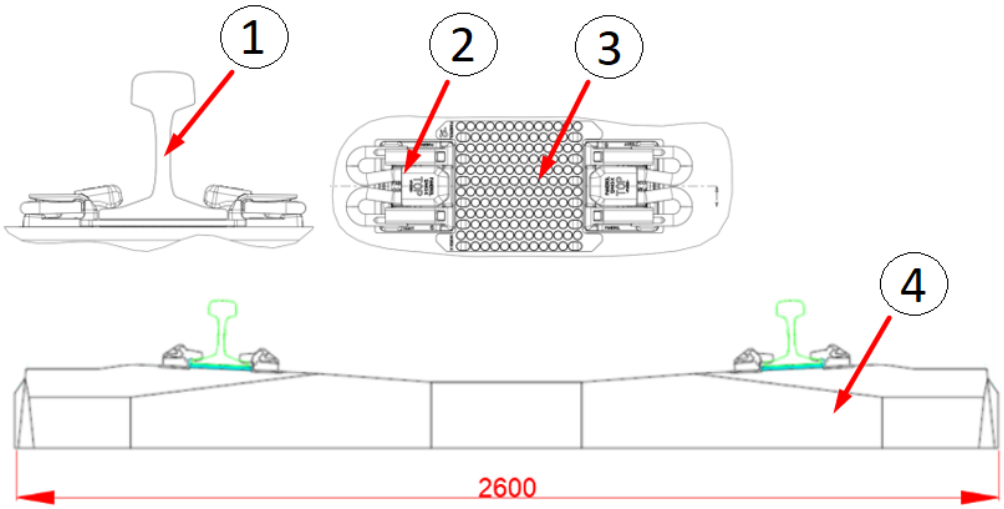

Figure 2.1 – The current standardized railway track in Norway based on the InterCity design basis, showing the ① 60E1 rail, ② Pandrol Fastclip FE 1404 system, ③ Pandrol 10 mm rail pad and ④ the JBV 60 sleeper (Modified after Teknisk regelverk 2019)

2.2 Modelling of the interaction between rail, sleeper and ballast

The interaction between track components is modelled in PLAXIS 2D with plate elements. The intended purpose of the track model is to distribute any load from the train wheels as realisticly as possible down to the ballast layer.

Figure 2.2 shows a section of the model which shows the system at one sleeper. The rail ① is considered a continuous plate element in the model, as if it was a case of a continuously welded rail (CWR) on a real track, and has been elevated 10 mm from the sleepers through two vertical plate elements, as if there was a small rail pad ③ between the sleeper ④ and rail ①.

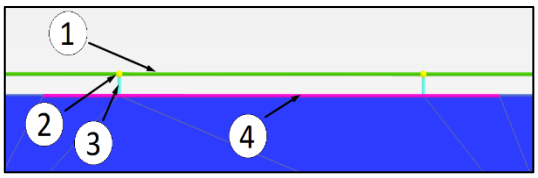

Figure 2.2 – Illustration of the track structure in PLAXIS 2D, showing the interaction of the track components in the system at one sleeper. Element ① shows the rail, element ② the hinged connection between rail and pad, element ③ the sleeper pad and ④ the sleeper on top of the ballast

The sleepers plate element is placed directly on top of the ballast without interfaces, as this might give nummerical problems or prevent the track from being lifted from ground on the sides when being subjected to a point load.

The connection between the rail and the pad is defined as freely rotating hinges ②, ensuring that the connection to the rail is not affected by any stiffness properties from the sleeper or pad element. The connection between the rail pad ③ and sleeper ④, is assumed completely fixed as the pads main intension in respect to the sleeper is to elevate the the rail, and in respect to the rail to reduce the point concentration from the wheel loads.

This system allows the model to simulate a real scenario as if the rail was founded on discrete supports, but without affecting the bending behaviour of the rail unfavourable when it is being subjected to external loads. If given proper axial stiffness, the pad will enable this system to reduce the point concentration of each wheel load at the rail by compressing, which causes the rail to distribute the load better to the nearby sleepers as the stiffness under the load is decreased by pads compressing ability.

2.2.1 Plate elements and plane-strain in PLAXIS 2D

PLAXIS 2D offers two options for modelling structures in two dimensional planes, plane-strain and axisymmetry. This model is based on the principles of plane-strain, where the model represents a uniform cross-section of the geometry in 2D with an effective width of 1.0 meter in- and out of the plane, defined as the z-axis by PLAXIS [3].

The principle of effective width applies for both structural and soil elements, which is a predefined sectional plane in the models z-direction. The displacements and strains for this plane in its z-direction always remains zero, meaning that the model can only displace and strain in its x or y-direction as illustared in figure 2.3A).

Structures in PLAXIS 2D may be constructed as plate elements, which is line elements connected by nodes, where each node has three degrees of freedom. PLAXIS offers two varieties of plate elements, the 3-noded or 5-noded variety. The 5-noded variety is automatically activated by PLAXIS when using a 15-node triangle elements for the soil cluster, which is standard setting.

The 5-node variety has four pairs of Gaussian stress points which is located at a distance governed by the equivalent plate thickness parameter (d_{eq}). Whats important to highlight is that this equivalent plate thickness is defined by the relationship between the axial- and bending stiffness of the plate element (EA and EI).

A change in the ratio EI/EA, changes the distance of the stress points in the plate element, which changes the distribution of the bending moments in the plate element [3].

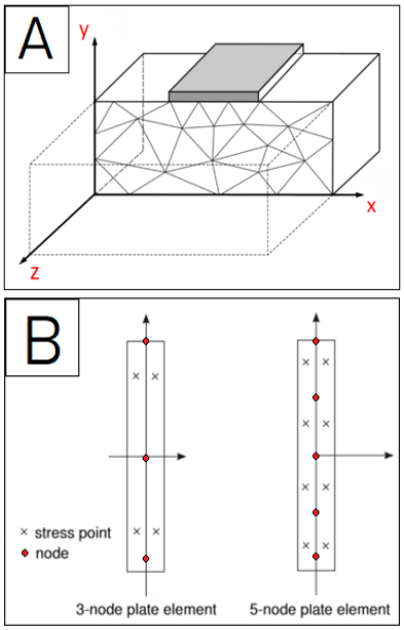

Figure 2.3 – Illustration of plate elements where figure A) shows the principles of plane-strain and figure B) shows the principles of plate elements (Modified after PLAXIS reference manual, 2019)

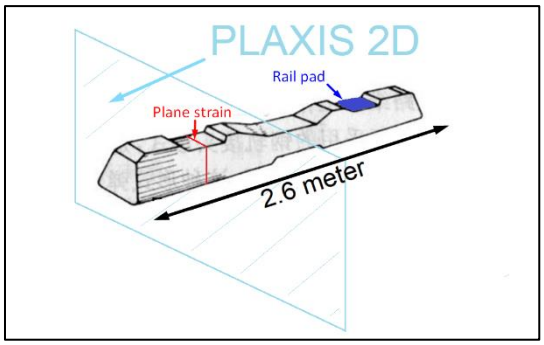

Figure 2.4 –Principles for transforming the track components into a sectional plane after the principles of plane-strain

Transforming the track components into plane-strain can be done under the assumption that the sleeper is governing the effective width. A prerequisite for doing this is that the load is equally distributed bellow the sleeper at any given plane in the models z-direction.

This means that instead of considering the axle loads, rails and rubber pads as pairs on top of the sleeper, they're transformed into planes with an effective width of 1.0 meter, as if every element intersected by these planes had equal properties along the entire sleeper. Such approach may be achieved by dividing the sum of any desired track component by the sleepers width.

2.2.2 Modelling of rails and sleepers as plate elements

By following the principles of plane-strain described (section 2.2.1), the rail together with the sleeper is to be modelled as plate elements. The properties of each element is based of the properties of a 60E1 rail and JBV 60 concrete sleeper.

The sleeper plate element is modelled under the assumption that it is very stiff, both in its axial and bending direction while its weight and width is transformed into plane-strain. This is because the main intent of the sleeper element in the model is only to distribute the loads from the rail to the soil without considering the behaviour of the sleeper it self when the track is subjected to external loads.

Not considering the behaviour or stresses at the sleeper itself, allows for neglecting how the ratio between the axial and bending stiffness (EI/EA) might affect the equvivalent thickness of the plate. The weight on the other hand plays an important role in the rail bending behaviour, as neglecting the weight will contribute to unrealistic upward deflections of the rail when it is being subjected a downward force.

Figure 2.5 is derived from design drawings from Bane NOR, and shows that the width of the sleeper varies. For the principles in section 2.2.1 to be valid, an average width of 0.25 meter is used as the lenght of every sleeper plate element in the model.

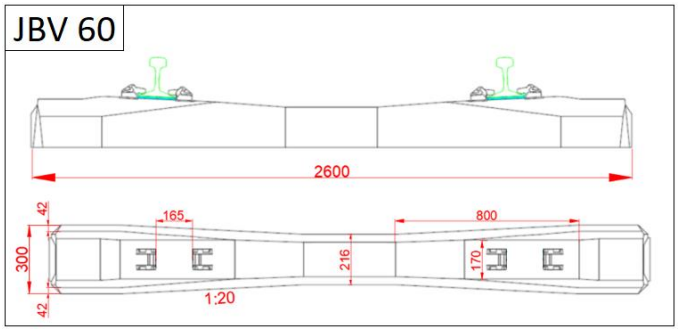

Figure 2.5 – The JBV 60 sleeper (Modified after Teknisk regelverk, 2019)

As each sleeper weighs 285 kg, one could either transform it into plane-strain by transforming the weight into force and divide it by the lenght of the sleeper (2.6 m) and the width (0.3 meter) which yields 4.3 kN/m/m, or just multiply the height of the sleeper with the unit weight of concrete, which yields 4.08 kN/m/m. Both approaches gives the weight pr. effective meter plane pr. effective meter plate.

The rails weight, bending- and axial stiffness is transformed into plane-strain by following the same principles as described in section 2.2.1, where the sleeper width is the basis for the rails properties pr. effective meter plane. This means that the rails bending stiffness (EI), axial stiffness (EA) and weight (w) is to be multiplied by two, then divided by 2.6 meter. From the norwegian railway normal, *teknisk regelverk* the properties of a 60E1 rail is presented in table 2.1.

Table 2.1 – Properties of a 60E1 rail (Modified after Teknisk regelverk, 2019)

60E1 Rail properties		
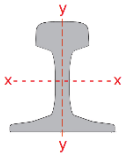	Weight	w = 60,21 kg/m
	Cross-section area	A = 76,7 cm^2
	Moment of inertia, strong axis	I_{x-x} = 3038,3 cm^4
	Moment of inertia, weak axis	I_{y-y} = 512,3 cm^4

The transformed parameters for both the 60E1 rail and JBV 60 sleeper is presented in table 2.2.

Table 2.2 – Properties of a 60E1 rail and JBV 60 sleeper transformed to plane-strain in PLAXIS 2D

	60E1 Rail	**60E1 Rail, Plane-strain**	**JBV 60 sleeper**	**JBV 60 sleeper, Plane-strain**
Bending stiffness, EI	6380 kNm^2	4908 kNm^2/m	-	$1.0*10^6$ kNm^2/m
Axial stiffness, EA	$1.61*10^6$ kN	$1.239*10^6$ kN/m	-	$1.0*10^6$ kN/m
Weight, w	60.21 kg/m	0.45 kN/m/m	285 kg	4.3 kN/m/m
Possions ratio, v	-	0.3	-	0

2.2.3 Modelling of the rail pad as plate elements

Rail pads in general reduces both the point concentration and impact loads on the track when a train is passing a sleeper by absorbing much of the energy transfered from the rail. According to the norwegian electronic railway textbook series, jernbanekompetanse.no, the properties of a pad has shown to have a tremendous effect on the long-term tear and maintenance of track components, especially at higher speeds [4]. This demonstrates the importance of including the pads behaviour in a track model.

The geometric properties of the «Pandrol 10 mm» railpad are presented in figure 2.6, which shows it has an bearing area of approximately 150x150 mm, web thickness 7.4 mm and knob thickness of 10.1 mm. This information led to the assumption that the maximum distance between the two vertical plate elements representing the pad in the model should not be larger than 150 mm.

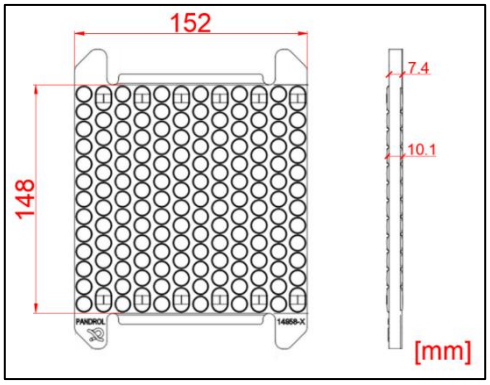

Figure 2.6 – The geometric properties of a Pandrol 10 mm rail pad with kluster knobs (Modified after Teknisk regelverk, 2019)

According to jernbanekompetanse.no, ensuring as realistic track behaviour in respect to the rail pad can be achieved by defining a static compressive stiffness required for the pad when it is being subjected to vertical loads. This stiffness has in field been determined by comparing the pads compressive behaviour when compressed by the systems own weight (rails weight with fastening force) and secondly when compressed under a static, average axle load, see figure 2.7.

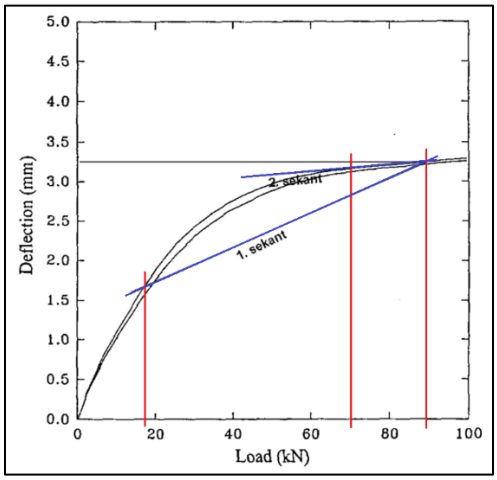

Figure 2.7 – Illustration: Loading vs deformation plot showing how the pad deflect as a function of compressive force (Jernbanekompetanse.no, 2019)

Comparing the two loading schemes, 18 kN is thought of as the average compressive force from the fasteners in combination with the rails weight, while 90 kN is the average wheel load on the basis of mixed traffic (with an average axleload of 180 kN) [4].

Figure 2.7 shows a graph of the Pandrol 10 mm pads compressive response under these loading cicrumstances, where two secants are drawn between 18 kN to 90 kN, and 18 kN to 70 kN. These secants, according to jernbane-kompetanse.no, are calculated as:

$$E_{pad,10mm} = \frac{(Upper\ load - lower\ load)}{(Upper\ deformation - lower\ deformation)} \quad \text{(Eq. 2.1)}$$

The first secants slope coefficient of 40-55 kN/mm should according to jernbanekompetanse.no represent the static stiffness of the rail pad when it is being subjected by an average axle load of 180 kN [4].

Jernbanekompetanse.no from this test therefore suggests using a static stiffness of ca. 45 kN/mm. A static stiffness of 45 kN/mm means that it requires 45 kN of force to compress to pad 1 mm. By expressing this behaviour as a linear spring, Eq. 2.2 bellow permits the transformation of this compressive stiffness to axial stiffness for the vertical plate elements in PLAXIS.

$$F = k*\delta \quad \text{(Eq. 2.2)}$$

where

F being the applied force
k being the spring stiffness
δ being the displacement

By following the same principles as described in section 2.2.1 when transforming the pads spring stiffness into plane-strain, the stiffness is to be multiplied by 2 then divided by the sleepers width of 2.6 meters. Since we have two vertical plate elements representing the pad, this stiffness is again to be divided by two, which yields an axial stiffness of 17.3 kN/m when convertet into plane-strain.

As the calculation example in section 5.3 suggests however, a pad stiffness of 17.3 kN/m makes the track structure to soft as it deflect to much. The cause of this exaggerated deflection is mainly due to the pad compressing with an unrealistical magnitude. As figure 2.7 shows, the deflection-curve of the pad starts to flatten when the graph passes 3.0 mm compression. Elastic plate elements in PLAXIS 2D doesn't catch the non-linear behaviour of the pad, as seen in figure 2.7.

2.3 Comparing the track behaviour in PLAXIS to classic railway theory – Beam on elastic foundation

This section evaluates the track behaviour in PLAXIS 2D from the purposed methodology from section 2.2, and one way of validating the modell is to compare the static behaviour under the circumstance that the track is founded on a elastic foundation. The behaviour of the model under these circumstance can then be compared to theoretical solution purposed by Herman Zimmermann from 1880, known as Zimmermanns theory. Despite the theory being simple, it is still considered in modern railway technology to be sufficient for quick and easy static calculations [4-6].

The theory assumes that a continuously welded rail (CWR) can be expressed as a continuously Euler-Bernulli beam founded on a winkler springbed (elastic foundation), see in figure 2.8.

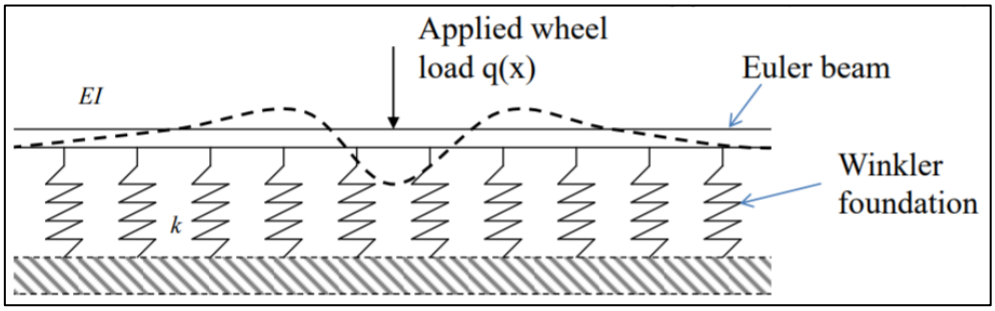

Figure 2.8 – Principle sketch: The main principles of Zimmermanns theory, a continuously welded rail (CWR) can be expressed as an Euler-bernullis beam founded on a winkler springbed

The theory assumes that the rails bending stiffness (EI) and the winkler spring stiffness (k) is constant, which in equilibrium gives the following fourth order differential equation

$$EI\frac{d^4y}{dx^4} + k*y(x) = q(x) \qquad \text{(Eq. 2.3)}$$

where

EI being the beams bending stiffness
y(x) being the downward deflection of the beam
k being the fundations spring stiffness
q(x) being the evenly distributed load

The solution for this differential equation can be solved as

$$y = e^{-x/L}(A*\sin(x/L) + B*\cos(x/L)) + e^{x/L}(C*\sin(x/L) + D*\cos(x/L)) + y_p \qquad \text{(Eq. 2.4)}$$

where

y_p being the particular solution corresponding to q(x)/EI

For a case of a single point load applied at a contact point x = 0, the evenly distributed load (q) will also be equal to zero, which leads to the particalur solution (y_p) also to be equal to zero. The solution for the differential equation (Eq. 2.3) in the case of a point load, can thereby be rewritten as

$$y = e^{-x/L}(A*\sin(x/L) + B*\cos(x/L)) + e^{x/L}(C*\sin(x/L) + D*\cos(x/L)) \quad \text{(Eq. 2.5)}$$

Where the lenght (L) is the characteristic lenght accounting for the relationship between the beams bending stiffness and the fundations spring stiffness. This characteristic lenght governs the tracks ability to distribute any concentrated loads at the track, and is expressed as

$$L = \sqrt[4]{\frac{4*EI}{k}} \quad \text{(Eq. 2.6)}$$

Zimmermann also purposed another way of defining the fundations spring stiffness (k) by including the contact area under a sleeper, spacing and ballast coefficient, but still maintaining the properties of the linear elastic springbed, expressed as

$$k = \frac{C*As}{a} \quad \text{(Eq. 2.7)}$$

where

C being the ballast coefficient
A_s being the bottom contact area of the sleeper
a being the sleeper spacing

By setting the boundary conditions at $y(\infty) = 0$ and $y(0) = 0$ with the effect of the point load (Q) at an infinite distance being equal to zero, the final expression for the deflection distribution is given as

$$y = \frac{Q}{2*kL} e^{-x/L}(\sin(x/L) + \cos(x/L)) = \frac{Q}{2*kL} * \eta(x/L) \quad \text{(Eq. 2.8)}$$

Deriven twice, equation 2.7 is transfered into to the following expression for moment distribution

$$M = \frac{QL}{4} e^{-x/L}(-\sin(x/L) + \cos(x/L)) = \frac{QL}{4} * \mu(x/L) \quad \text{(Eq. 2.9)}$$

where

x being the distance from the applied point load
L being the characteristic lenght, as expressed in Eq. 4
η(x/L) being the deflection (y) at any given point (x), from the applied point load Q
μ(x/L) being the bending moment (M) at any given point (x), from the applied point load Q

Assuming that both the spring- and rails bending stiffness is constant, the distribution from the ordinat where the point load is being applied will show the same characteristics in its characteristic distribution regardless of the magnitudes for both the spring stiffness (k) or rail bending stiffness (EI). The characteristic lenght however, are influenced by these parameters which further influences the section of the track which is affected by the point load (i.e the distribution along the rail).

In respect to evaluating the tracks behaviour, the characteristic distributions can be compared to the behaviour of the track in PLAXIS. Deriven from equation 2.5 and 2.9, a typical characteristic distribution from Zimmermanns theory is presented in figure 9, showing both moments and deflection under a static point load.

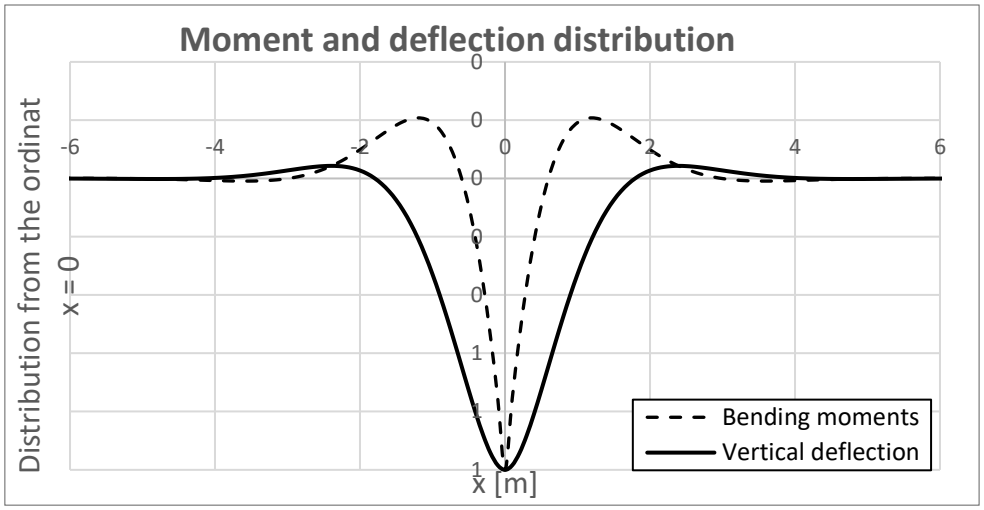

Figure 2.9 – Illustration: The characteristic distribution of the rails deflection and bending moment when a point load is being applied deriven from Zimmermanns theory

Figure 2.9 shows that the characteristic moment- and deflection distributions after Zimmermanns theory, and suggests a maximum upward ratio for the bending moments in the order of 20%, while 5% for the deflections seen from the applied point load (i.e at x=0 in the figure).

In the following example, the track principles from section 5.2 for PLAXIS are compared to Zimmermanns theory. The ballast is modelled with a linear-elastic soil model with an elastic modulus set to 275 MPa, unit weight 20 kN/m^3 and possions ratio 0.3.

The rail is assumed to be of the type 60E1, the sleepers JBV 60 and the rail pad of the type Pandrol 10 mm with cluster knobs. The properties transformed into plane strain are represented in table 2.3.

Table 2.3 – Properties of the 60E1 rail, JBV 60 sleeper and Pandrol 10 mm rail pad transformed into plane strain

	60E1 Rail,	**JBV 60 sleeper**	**Pandrol 10mm rail pad**
Bending stiffness, EI	4908 kNm^2/m	1.0*10^6 kNm^2/m	1.0*10^6 kNm^2/m
Axial stiffness, EA	1.239*10^6 kN/m	1.0*10^6 kN/m	17.3 kN/m
Weight, w	0.45435 kN/m/m	4.3 kN/m/m	0
Possions ratio, v	0.3	0	0.3

Figure 2.10 shows that the soil body in this example has a total lenght of 20 meters, is 7 meters thick and the track itself is 19.2 meters long. This ensures that the influenced lenght from the point load doesn't extend beyond the tracks lenght while the bottom boundaries ensures that the bedrock doesnt affect the rails deflection. The point load is set to 84.9 kN, based of a 22.5 tonn axle load.

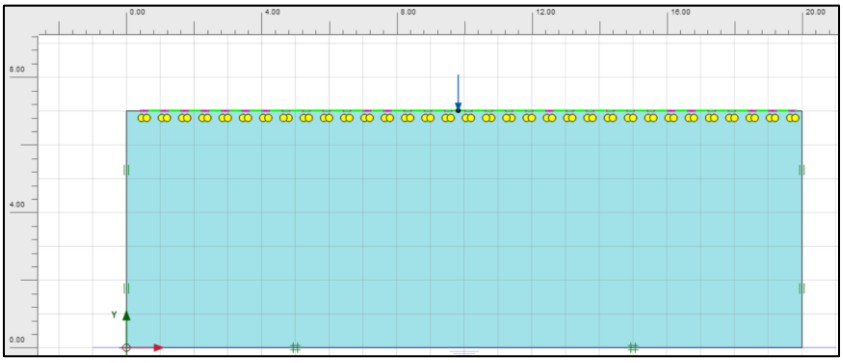

Figure 2.10 - Illustration: Geometry and boundaries for the static loading example

Figure 2.11 presents the results from this static example where it shows a reasonable track behaviour in comparison to Zimmermanns theoretical, see figure 2.11.

The hinged connection between the pad and rail ensures that the rails bending behaviour is not affected by any of the track components, illustrated by the smoothness of the moment distribution in figure 2.11B).

The moment distribution spreads approximately 5 meters to each side from the applied point load, indicating a reasonable influenced lenght compared to theory. The maxi-mum upward deflection is 20.5 % of the the downward deflection, which is reasonable when comparing to the theoretical solution.

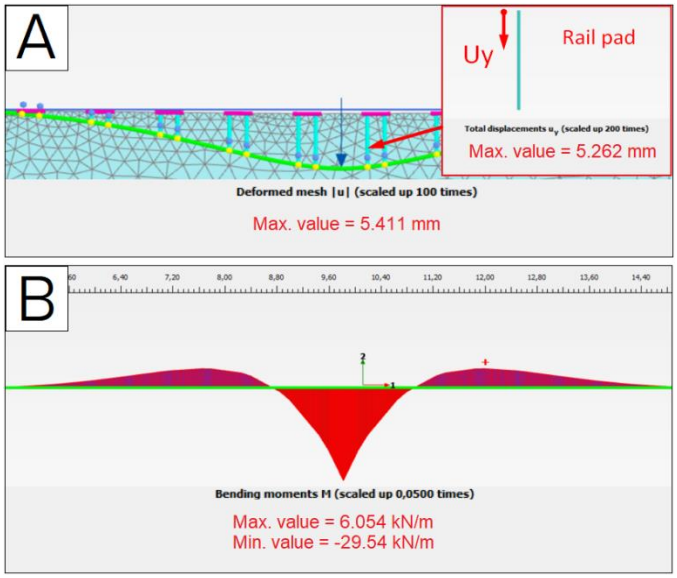

Figure 2.11 – Results from the example: Figure A) shows the deformed mesh including the rail pad, figure B) shows the moment distribution

Despite the characteristic distributions showing similarities to the theoretical distributions, having in mind that the subsoil in this example is relatively stiff, the deflection suggests that the track structure in this model is to soft. From experience, a typical track deflection should be in the order of 1.0 - 2.0 mm when assuming the properties from section 2.1 and a static axle load. In PLAXIS this track shows more than 5 mm deflection which is not acceptable for any track in Norway.

Figure 2.11A) shows that the rail pad compresses together with the track, suggesting that the exaggerated deflections in fact is caused by compression of the rail pad. Recapping the load-deflection curve for the Pandrol 10 mm pad in figure 2.7, it shows that the curve starts to flatten when the pad is compressed more than 3.0 mm (or when the applied force increases from 80 kN and further).

This demonstrates that the transformation of the compressive stiffness to axial stiffness in plane strain, leads to an unrealistically soft behaviour of track when converting the pad stiffness to elastic plates in PLAXIS. The following section as a result, provides two calibration examples in order to tune the properties of both the ballast and railpad stiffness to behave as realistic as possible compared to a real track.

2.3.1 The railpads effect on point load concentration and defining a railpad stiffness

As section 5.3 has shown, when transforming the railpad stiffness pruposed by jernbanekompetanse.no directly to plane-strain and using elastic plate elements for the railpad in PLAXIS, it behaves to soft in the system. The following calculation example illustrates both the pads influence on the point load concen-tration effect on the track, and a more accurate axial stiffness for the pad in respect to the model. The calibration is based of experience numbers for deflections purposed by Bane NOR.

In order to inspect how the pads axial stiffness in PLAXIS affects the track in terms of point load conecntration, figure 2.12 shows the results of using two different pad properties, where A) is when the railpads axial stiffness is set to 10000 kN/m, and B) when it is set to EA = 100 kN/m.

The same PLAXIS model as for section 3.3 are used, and the properties used are summarized in table 2.4.

Table 2.4 – Input parameters for simulation of inspecting the pads effect on point load concentration

Input parameters – PLAXIS 2D	
Ballast elastic modulus, E	275 MPa
Rail bending stiffness, EI	4908 kNm^2/m
Static pointload	89.4 kN/m
Pad_1, EA	$1.0*10^5$ kN/m
Pad_2, EA	100 kN/m
Sleeper stiffness, EI = EA	$1.0*10^6$

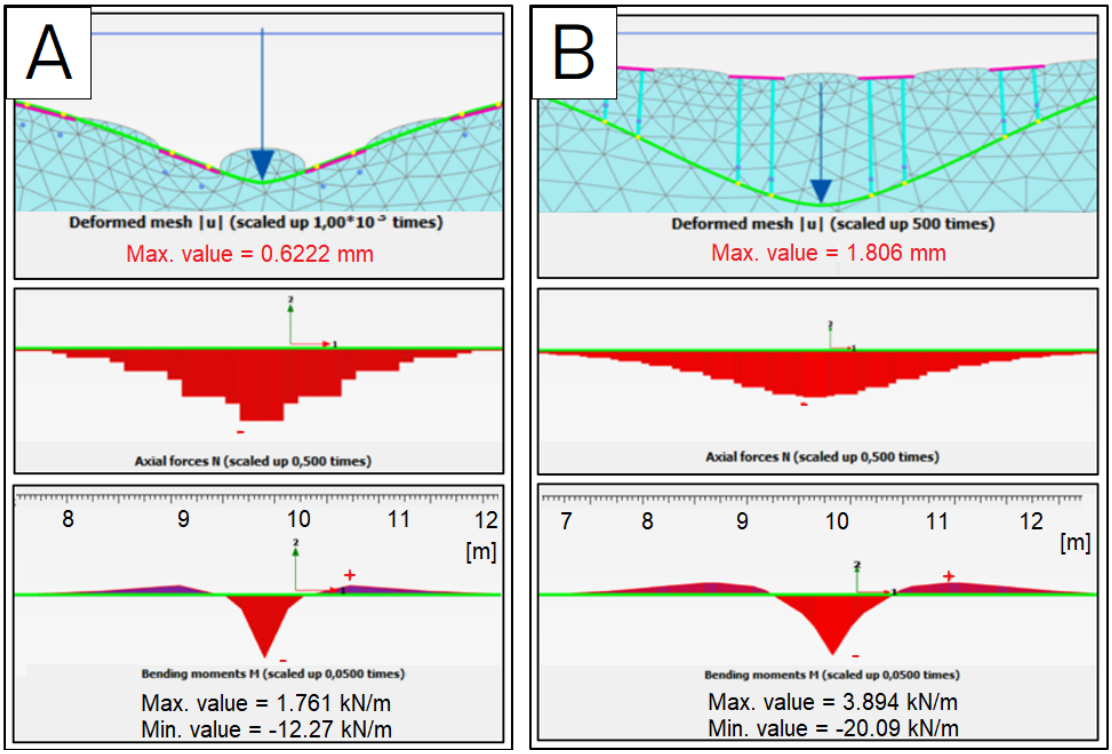

Figure 2.12 – Results of the deformations, axial forces and bending moment from PLAXIS 2D when usen A) an axial stiffness of the pad element of 10000 kN/m, and B) using a axial stiffness of the pad element of 100 kN/m

Figure 2.12 clearly demonstrates the effect of including a pad with compressive properties. Excluding the compressive behaviour of the pad shows that most of the displacement of the track comes from soil settlement (fig. 2.11A), while including a pad decreases the point concentration trem-endously by making the pad compress (fig. 2.11B). Thinking in terms of characteristic lenghts (Eq. 2.6), including a railpads compressive properties for PLAXIS increases the characteristic lenght of the system, and causes both the moment and deflections distributes better along the rail.

For calibrating purposes, in order to define a more accurate railpad stiffness in respect to the elastic behaviour of the plate element in PLAXIS, a practical approach is used. By assuming a 22.5 tonn referance axle, experience quantities from Bane NOR suggests that on a normal track with 60E1 rails, if the referance axle was placed directly above one concrete sleeper over 0,75 meter ballast (the minimum requirement) and it was founded on a rigid bedrock, the track is expepcted to not deflect more than 1.0 mm.

By creating another calibration modell were the boundaries are fixed and placing the track structure from section 2.2 on top with a 750 mm thick ballast bed, one could base this calibration of the railpad by assuming that the track must not displace more than 1.0 mm under a 84.9 kN/m point load (corresponding to a 22.5 tonn axle). A model were created for this particular case where the point load was place above a sleeper, see figure 2.13.

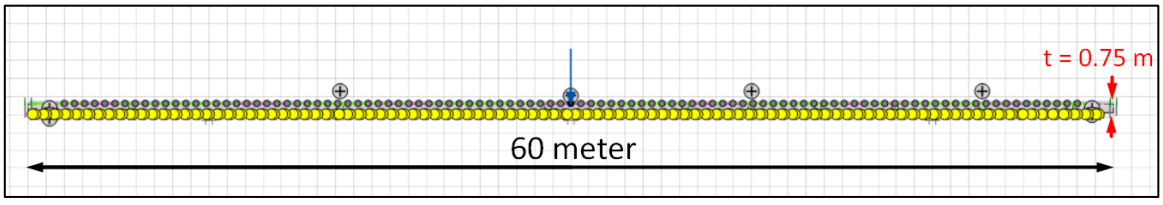

Figure 2.13 – Calibration model created for defining a realistic railpad stiffness

For this calibration example it was desired to use a lower ballast stiffness than 275 MPa, because to high of a stiffness would influence the result in the sense that the pad stiffness could be overestimated. According to Nålsund, plate loading tests has shown that compacted layers of crushed rock could yield a deformation modulus ranging in between 180-260 MPa [31]. According to Coenraad Esveld, the elastic modulus of ballast could aswell range between 100-150 MPa [5].

Variables such as track quality and number of load cycles that has been exposed to the ballast, makes it difficult to point out an exact quantity for the ballasts elastic modulus. From various calibration attempts in PLAXIS, it was found that minor variations of the ballast stiffness (for example changing ranges between 10-50 MPa) influences the orders of the deflection to a neglectible degree compared to changing the pad elements axial stiffness. An elastic modulus of 180 MPa was selected for the ballast.

All input parameters used for this calibration example are given in table 2.8, and after some trails, a pad stiffness of 225 kN/m seem to corresponds well to a track deflection of 1.0 mm.

Table 2.8 – Input parameteres for calibrating the pad stiffness

Input parameters – PLAXIS 2D	
Ballast elastic modulus, E	180 MPa
Rail bending stiffness, EI	4908 kNm^2/m
Rail weight, w	0.4543 kN/m/m
Pad axial stiffness, EA	225 kN/m
Sleeper stiffness, EI = EA	1.0*10^6
Sleeper weight, w	4.08 kN/m/m
Wheel load, Q	84.9 kN/m

Whats important to highlight here is that a railpad stiffness of 225 kN/m is defined under the prerequisite that an axle load of 22.5 tonn is used. Since the railpad in PLAXIS doesn't catch the nonlinear behaviour shown in the diagrams from section 2.2.3, any deviation from the referance axle should be checked.

Before a pad stiffness of 225 kN/m can be considered a valid choice, an additional check is performed for a 18 tonn referance axle which is typical for norwegian passenger trains [1]. Transfered into plane-strain by the principles from section 2.3, a 18 tonn axle corresponds to an point load of 67.91 kN/m in PLAXIS. Under the circumstances presented in figure 2.14, this yields a track deflection in the order of 0.8 mm. For comparison, a 22.5 axle load (corresponding to a point load of 84.9 kN/m in plane-strain) yields a track deflection in the order of 0.99 mm, see figure 2.14A) and 2.14B).

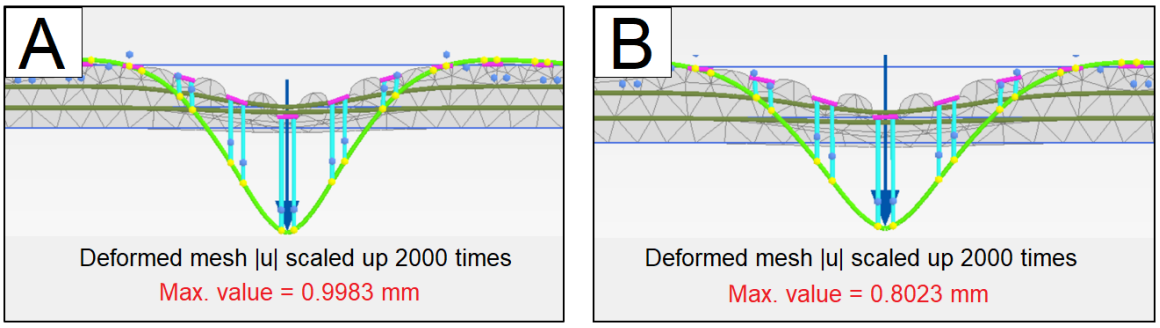

Figure 2.14 – Rail deflection under A) a 22.5 tonn referance axle (89.4 kN/m) and B) a 18 tonn referance axle (67.9 kN/m)

It is hereby concluded that a railpad stiffness of 225 kN/m is a reasonable quantity to use as the stiffness of the pad elements in PLAXIS 2D, up to 22.5 tonn axle loads. Any increase in axle load should be checked further due to the plate elements linear behaviour in the programme.

2.3.2 Calibrating the ballast stiffness with experience quantities from Deutche Bahn

One way of calibrating the ballast stiffness in PLAXIS could be to isolate its effect on track deflection under the influence of a static load, then compare it to Zimmermanns theory. For such approach, the circumstances in the model should be as close to the circumstances in Zimmermanns formulation as possible, i.e using the same bending stiffness of a 60E1 rail and sleeper area for the JBV60 sleeper, but also neglecting their weight as this is not considered in the theory.

According Coenraad Esveld [5], based on track classifications ranging from poor to good, certain limiting values for second load cycles during plate load tests (E_{v2}) should correspond to a certain ballast coefficient (C) based on experiences from Deutche Bahn, see table 2.4.

Table 2.4 – Purposed ballast coefficients based of track quality (From Esveld. C, 2016)

Classification	E_{v2} [N/mm^2]	C [N/mm^3]
Poor	10	0.03
	20	0.04
Moderate	50	0.07
Good	80	0.09
	100	0.11

The track quality in this calibration example is assumed to be moderate, yielding a ballast coefficient in the order of $70*10^6$ N/m^3. For calibration purposes, the magnitude of the deflections given from this ballast coefficient should match the calculated ones from Zimmermanns theory best possible.

By assuming a 22.5 tonn referance axle load, it corresponds to a static point load of 110 kN at one single rail. In respect to the plane-strain in PLAXIS, an average sleeper width of 0.25 m is used, leading to a sleeper contact area of 0.65 m^2. This sleeper area is to be divided by two in respect to one single rail in Zimmermanns theory[5]. Assuming a sleeper spacing of 0.6 meter per sleeper, the linear spring stiffness (k) for the winkler bed can be calculated according to equation 2.7, see section 2.3.

From knowing the bending stiffness of a E601 rail, all variables for calculating the characteristic lenght (L_c) of the system are given, and input parameters for the calculation and results after Zimmermanns theoretical formulation are given in table 2.5 and 2.6.

Table 2.5 – Input parameters for calculating moments and deflection according to Zimmermanns theory

Input parameters – Zimmermanns theory	
Ballast coefficient, C	$70*10^6$ N/m^3
Sleeper contact area, A_s	0.325 m^2
Sleeper spacing, a	0.6 m
Rail bending stiffness, EI	6384 kNm^2
Wheel load, Q	110 kN

Table 2.6 – Results showing spring stiffness, characteristic lenght, deflection and bending moment according to zimmermanns theory

Results	
Winkler spring stiffness, k	3790 kN/m^2
Characteristic lenght, L_c	0.905774 m
Vertical deflection, y_0	1.61 mm
Bending moment, M_0	25 kN/m

From using equation 2.8 and 2.9 from section 2.3, the deflection and moment distribution along the rail are calculated in a spreadsheet, and further presented in figure 2.15.

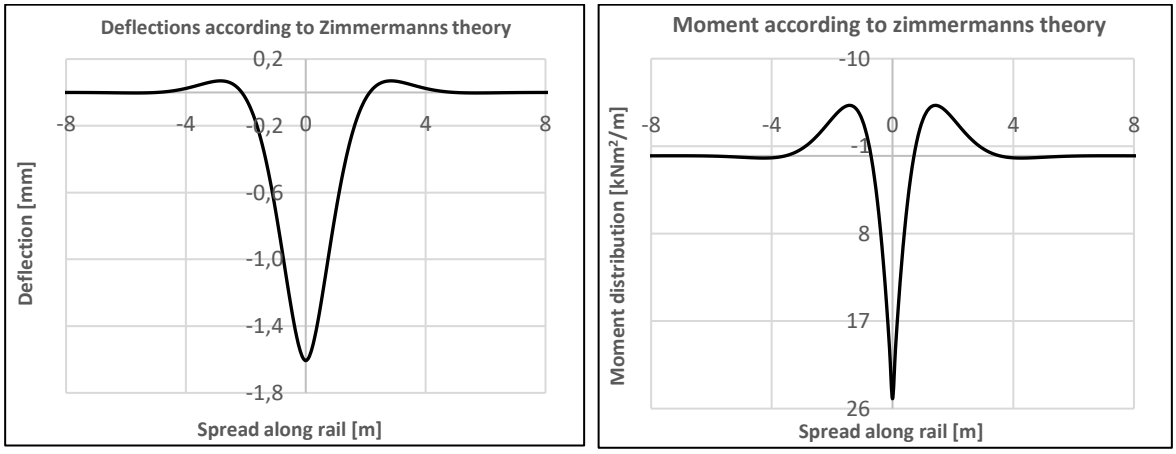

Figure 2.15 – Deflection and moment distribution along the left and right side of the applied point load at the oordinat x = 0

In order to calibrate the ballast in PLAXIS after these quantities, the calibration model should be created under circumstances that is as close to the circumstances of the theory as possible. The soil body is therefore made of a completely homogeonous ballast layer modelled with a linear-elastic soil model. The weight of the rail and sleeper has been neglected as this is not included in the theory. The depth of the model is kept to ensure that the bedrock does not influence the deflections, and the track made long enough to ensure that the load spread doesn't reach the end boundaries of the model, see figure 2.16.

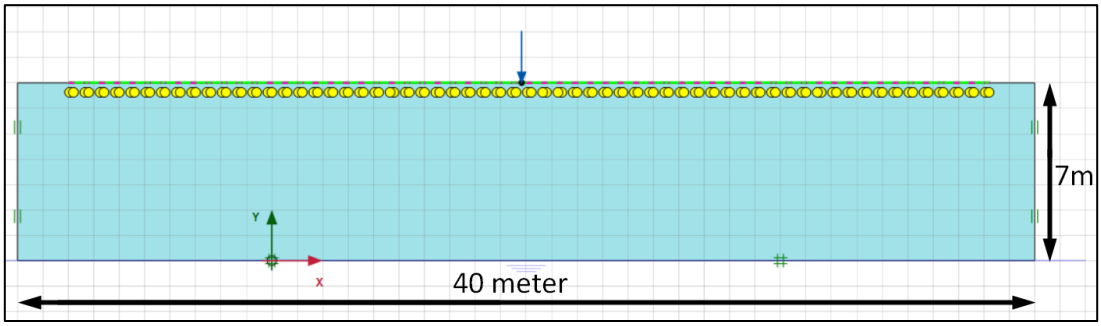

Figure 2.16 – Calibration model in PLAXIS 2D for calibrating the ballast stiffness, consisting of a 7 meter thick completely homogenious soil layer representing the ballast.

According to Coenraad Esveld [5], the formulation of the spring stiffness in Zimmermanns theory (Eq. 2.7) can be expressed in various ways

$$L = \sqrt[4]{\frac{4*EI}{k}} = \sqrt[4]{\frac{4*EI*a}{k_d}} = \sqrt[4]{\frac{4*EI*a}{C_{rs}*A_{rs}}} = \sqrt[4]{\frac{4*EI*a}{C_{bs}*A_{bs}}} = \sqrt[4]{\frac{4*EI*a}{C_{sb}*A_{sb}}} \qquad \text{(Eq. 2.10)}$$

where

k being the coefficient of continous support
k_d being a spring constant of discrete supports
a being the spacing between center of the discrete support
C_{rs} being the foundation modulus at contact area between rail and sleeper
C_{bs} being the foundation modulus at contact area between baseplate and sleeper
C_{sb} being the foundation modulus at contact area between sleeper and ballast bed
A_{rs} being the contact area between rail and sleeper for half sleeper
A_{bs} being the area between baseplate and sleeper for half sleeper
A_{sb} being the contact area between sleeper and ballast bed for half sleeper

It has been under discussion in this project if these formulations of the foundation modulus accounts for the railpads stiffness. When looking at the last formulation it is seen that the foundation modulus (C_{sb}) is defined between the sleeper the ballast bed, while the third formulation (C_{rs}) is defined as the foundation modulus between the rail and sleeper. For these to be equal, the contact area must be different.

As a result from these definitions, two calibration attempts were performed in correlation to Zimmermanns theory, one with including a railpad stiffness of 225 kN/m and one with excluding it.

The 22.5 axle load as with all other track components transfered into plane-strain. After some attempts, an elastic modulus of 138 MPa for the ballast stiffness when using a railpad, and 86 MPa for ballast stiffnes when not including it seems to yield the same deflections as purposed by Zimmermanns theory. The final input parameters for this analysis is presented in table 2.7.

Table 2.7 – Input parameters for the calibration example

Input parameters – PLAXIS 2D	
Ballast stiffness$_1$, E	138 MPa
Ballast stiffness$_2$, E	86 MPa
Rail bending stiffness, EI	4908 kNm^2/m
Static pointload	89.4 kN/m
Railpad$_1$, EA	225 kN/m
Railpad$_2$, EA	10000 kN/m
Sleeper stiffness, EI = EA	1.0*10^6

Moving the ordinat of the pointload in PLAXIS to the same ordinat as in Zimmermanns theory (x=0), a comparison for both deflection and bending moment distribution along the rail is presented in figure 2.17.

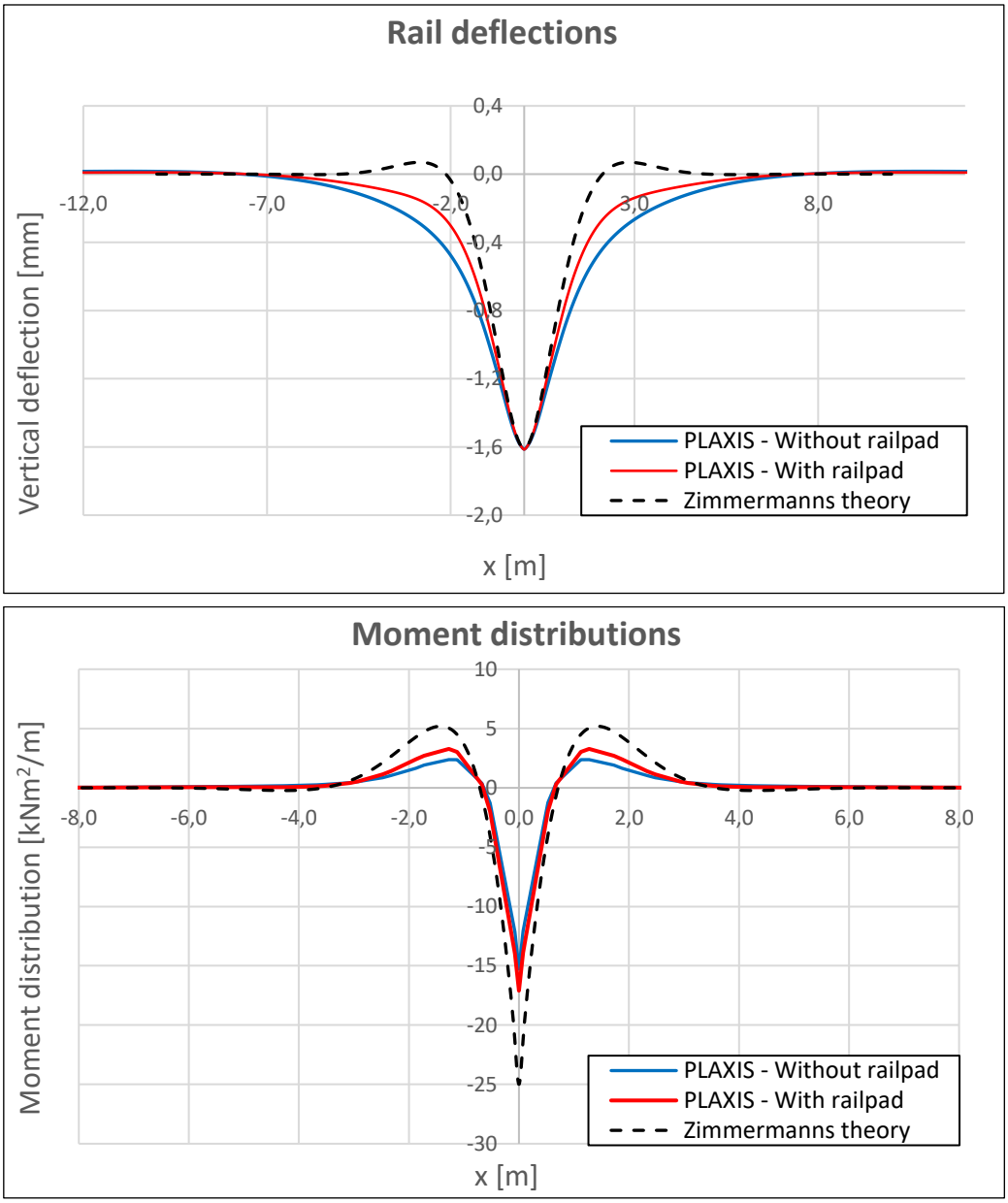

*Figure 2.17 – Comparison between the track behaviour from Zimmermanns theory and PLAXIS for deflections and bending moment distributions when a ballast coefficient of 70*10E6 is used*

As these results suggests, there is some deviation compared to Zimmermanns theory in the distribution of deflections and magnitudes at the maximum bending moments for both cases. Neither case also seem to catch the uplifting part of the rail at the deflections, which can be seen in Zimmermanns solution.

Some uplifting tendencies can be seen from PLAXIS further out (at approximately 8 meters along the rail). The reason for this is unclear, but the effect of including the railpad stiffness in the system makes the track behave closer to the behaviour from theory at the concave downward deflection part. The nonuplifting behaviour in PLAXIS is thought of as more realistic than the behaviour purposed by Zimmermanns theory.

This assumption is based of how the sleepers are supported when comparing PLAXIS and theory. The sleepers in PLAXIS supports the rail discretely, while the theory assumes that the entire rail is supported by a continous elastic spring bed. From equation 2.7 it can be seen that the spring stiffness is also expressed by the sleeper spacing, which may lead to the confusion that the theory accounts for discrete suppert. It is important to be aware of the presumptions of this theory in fact is based on continous and not discrete support despite the foundation modulus being expressed by sleeper spacing.

These differences in support causes a difference in reaction forces when the beam loaded with a concentrated point load, where the case with discrete supports shows more the realistic behaviour of a real track than this theory.

When it comes to the results for moment distributions it can be seen that both results from PLAXIS deviates from theory. When comparing the upper concave parts from PLAXIS it can be seen that the simulation with railpad deviates less than the simulation without railpad. Recapping a point made in chapter 2.3 of the characteristic uplift ratio of the moment distribution in Zimmermanns theory, it was said to be 20%. The PLAXIS simulations however, shows 19.2% uplifting in the case of including the railpad and 15.6% uplifting when excluding it.

These findings suggests that when including the railpad in the model it behaves closer to Zimmermanns theory compared to excluding it.

The second point to be made is that the elastic modulus used in these simulations where 138 MPa was used (for the case with railpad) and 86 MPa (without a railpad). By knowing that these quantities is based of experience numbers from a «moderate track» which has been exposed for two million load cycles, it is hard to believe that the ballast stiffness can be less than 90 MPa.

From this it is concluded that the calibration attempt with including the railpad is more representative than the latter case, and an elastic modulus of 140 MPa is chosen as ballast stiffness.

3 Moving train loads in PLAXIS

This chapter describes a methodology for modelling moving trains as point loads in PLAXIS, and provides a full example followed up by showing how the same principle can be used for modelling two norwegian trains. The chapter also highlights several dynamic aspects of the model one should be aware of, such as frequency domains and limitations tied to the Hardening Soil model in dynamic mode.

3.1 An example for modelling a moving train in PLAXIS 2D

PLAXIS 2D does not offer the same luxury as PLAXIS 3D where it is possible to assign any defined path for a continuous moving point load. Nevertheless, this effect is possible to catch in PLAXIS 2D by placing several point loads continously along the section of interest, using the dynamic option for the given phase by defining how each point load acts at any given time through the multiplier option. The multiplier option allows the user to specify how much force each point load acts with at any given time, and with several point loads, this enables the user to simulate a horisontally moving load between the them by keeping the sum of the multipliers equal to 1.0 at all times, expressed by the multiplier function.

If one is to model a moving train for example, this option can be used to determine at what given time each of the trains axles is passing any given point. Since trains have fixed distances between their axles, the time delay can be manually calculated as long as the velocity of the train is known. If the velocity of the train is constant, then the delay between each axle will also be constant. Depending on the number of point loads, train lenght and number of axles, the total time intervall of the segment will be defined as from the first axle hits the first point load, to the last axle leaves the last point load.

An example of this is shown in figure 3.1, where a section of 50 point loads resulting in a total lenght L_1 between the first and last point load (P_1 and P_{50}). The train in the figure has eight axles with a total distance L_2 between the first (A_1) and the last (A_8) axle. The total time intervall will then be the sum of the trains lenght and the total lenght of study ($L_1 + L_2$), divided by the velocity of the train. The time intervall between each axle hitting each point load will then be determined by the distance between them divided by the trains speed. This means that each point load will be loaded then unloaded in total eight times during the analysis as if the train was passing them.

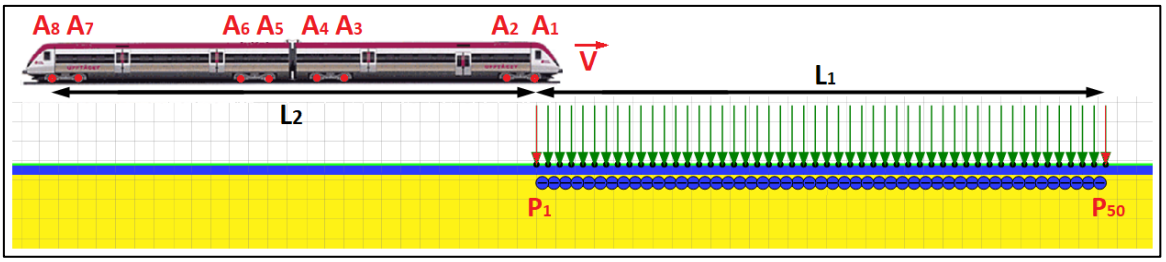

Figure 3.1 – Principles and necessary background information for modelling a moving train in PLAXIS 2D

The multiplier option in PLAXIS allows the user to define how many percent of the selected point load is working at any given time. This is favourable since it opens for fading of the load (i.e gradual loading), which will mimic as if the load moving horisontally between the point loads with a predefined speed, as long as the sum of the multiplayer (i.e the load) at all times is equal to 1.0 between two point loads. Following such procedure for every point load through the section of interest will then simmulate a continous horisontally moving load through the section of point loads.

Continuing the example above while aiming for a linear transition between each point load, a train speed of 50 m/s (180 km/t) and a distance of 0.6 meter between each point load is selected. This yields a total lenght of 29.4 meter between the first and last point load. For the train veichles, an axle spacing of 2.7 meter for each bogie is selected while having a distance of 16.4 meter between each bogie. This yields a total train lenght of 48.7 meter, resulting in a total traveling distance of 78.1 meter for the sequence, see figure 3.2.

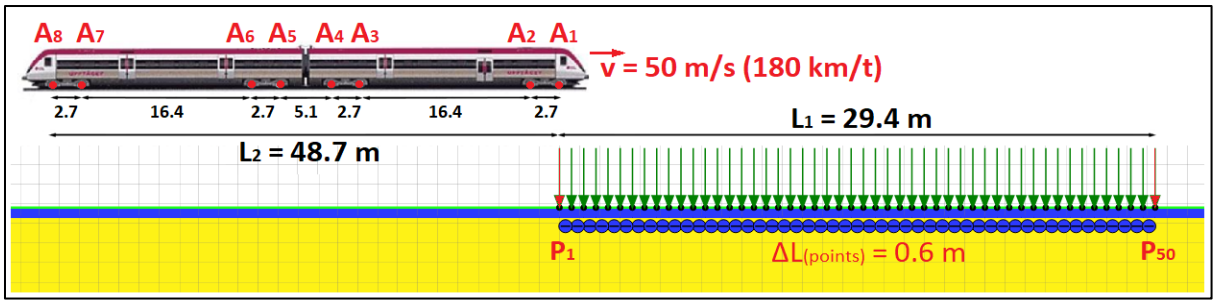

Figure 3.2 – The section which is to be studied consisting of 50 point loads with a distance of 0.6 meter between each load, resulting in a traveling distance of 29.4 meter. The train is based on a X52-commuter train configuration

The multiplier signal in PLAXIS must first be set from «harmonic» to «table», which gives the opportunity to define the dynamic multiplier factors manually. Calculating the multipliers for each point load can be done efficiently in for example a spread sheet, where the main effords will lie in calculating the multipliers for the first and second point load. Following the example above, the next task will be calculate the time segments during the train passage, which is shown in table 3.1 for this particular case.

Table 3.1 shows that it will take this train in total 1.562 seconds to pass the model with a time segment of 0.012 seconds between each point load. It will take each axle to hit the same point load 0.054, 0.328 and 0.102 seconds respectively. On the basis of the decimal places of the total time segment (1.562 seconds) and the time segment between each point load (0.012 seconds), a time step of 0.001 seconds for the fade «in» and «out» for each point load in the multiplier is preselected.

Table 3.1 – Time functions and time segments

Time functions	Time [seconds]
t(0.6 m)	0.012 s
t(78.1 m)	1.562 s
t(2.7 m)	0.054 s
t(16.4 m)	0.328 s
t(5.1 m)	0.102 s

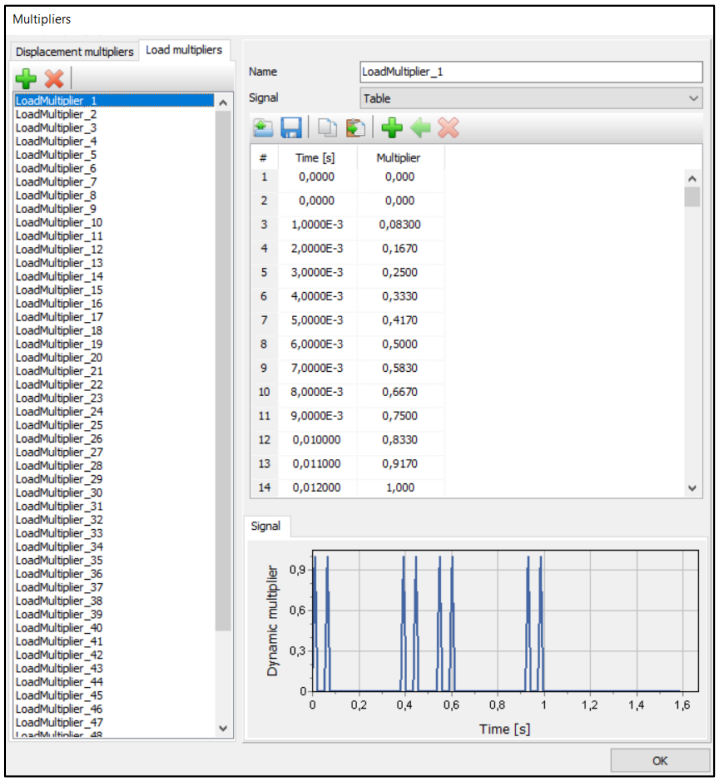

Figure 3.3 –The multiplier option output in PLAXIS 2D, showing the first twelve steps for tbe first axle in the first point load

The next step is to assig a multiplier for each point load, defining when each axle hits any given point. This can be done by repeating *_loadmultiplier* in the command window, the selecting one multiplier for each point load. A loads multiplier factor will determine to what magnitude the load is working at any given time, where a factor of 1.0 means that the point load is acting with full force. This function also opens for the possibility of assigning different magnitudes for the different axles, simulating different axle loads.

As shown in figure 3.3 for this example, each multiplier are deriven in such a way that the loads is introduced gradually in 12 steps with 0.001 second time increment between each step. The multiplier will then decrease gradually again with the same phase untill it has reached zero, simulating that the axle has passed that point load. The dynamic multiplier in the graph shows at what time each axles from the train in figure 3.2 is passing the first point load of the section.

Whats important to highlight here is that the magnitude of each axle should at all times be equal to 1.0. This is achieved by keeping the phase of the multiplier segment between the two pointloads in such a way that the sum of the multiplier at all times is equal to 1.0.

An example of this is illustrated in table 3.2, showing the segments of multiplier 1 and 2 (i.e first and second point load) for the trains front bogie. The table shows that when the first axle hits the first point load with a magnitude of 1.0 (at 0.012 seconds), the second axle is working with zero magnitude. When the magnitude of this multiplier starts to decrease, the magnitude of the second multiplier (point load 2) starts to increase with the exact same phase, keeping the sum of the load equal to 1.0 at all times. Axle number two follows the same principle with an added time delay of 0.054 seconds on the basis of the trains velocity and the wheel distance.

Table 3.2 – The dynamic multiplier factor shown for axle 1 and 2 for the trains front bogie, following the properties illustrated in figure 3.2. In order to simulate an moving load, the sum of the multiplier must be equal to 1.0

Point load 1 – Multiplier 1			
AXLE 1		AXLE 2	
Multiplier	Time [s]	Multiplier	Time [s]
0.000	0.000	-	-
(0/12)	0.000	(0/12)	0.054
(1/12)	0.001	(1/12)	0.055
(2/12)	0.002	(2/12)	0.056
(3/12)	0.003	(3/12)	0.057
(4/12)	0.004	(4/12)	0.058
(5/12)	0.005	(5/12)	0.059
(6/12)	0.006	(6/12)	0.060
(7/12)	0.007	(7/12)	0.061
(8/12)	0.008	(8/12)	0.062
(9/12)	0.009	(9/12)	0.063
(10/12)	0.010	(10/12)	0.064
(11/12)	0.011	(11/12)	0.065
(12/12)	0.012	(12/12)	0.066
(11/12)	0.013	(11/12)	0.067
(10/12)	0.014	(10/12)	0.068
(9/12)	0.015	(9/12)	0.069
(8/12)	0.016	(8/12)	0.070
(7/12)	0.017	(7/12)	0.071
(6/12)	0.018	(6/12)	0.072
(5/12)	0.019	(5/12)	0.073
(4/12)	0.020	(4/12)	0.074
(3/12)	0.021	(3/12)	0.075
(2/12)	0.022	(2/12)	0.076
(1/12)	0.023	(1/12)	0.077
(0/12)	0.024	(0/12)	0.078

Point load 2 – Multiplier 2			
AXLE 1		AXLE 2	
Multiplier	Time [s]	Multiplier	Time [s]
0.000	0.000	-	-
(0/12)	0.012	(0/12)	0.066
(1/12)	0.013	(1/12)	0.067
(2/12)	0.014	(2/12)	0.068
(3/12)	0.015	(3/12)	0.069
(4/12)	0.016	(4/12)	0.070
(5/12)	0.017	(5/12)	0.071
(6/12)	0.018	(6/12)	0.072
(7/12)	0.019	(7/12)	0.073
(8/12)	0.020	(8/12)	0.074
(9/12)	0.021	(9/12)	0.075
(10/12)	0.022	(10/12)	0.076
(11/12)	0.023	(11/12)	0.077
(12/12)	0.024	(12/12)	0.078
(11/12)	0.025	(11/12)	0.079
(10/12)	0.026	(10/12)	0.080
(9/12)	0.027	(9/12)	0.081
(8/12)	0.028	(8/12)	0.082
(7/12)	0.029	(7/12)	0.083
(6/12)	0.030	(6/12)	0.084
(5/12)	0.031	(5/12)	0.085
(4/12)	0.032	(4/12)	0.086
(3/12)	0.033	(3/12)	0.087
(2/12)	0.034	(2/12)	0.088
(1/12)	0.035	(1/12)	0.089
(0/12)	0.036	(0/12)	0.090

Each multiplier for the 50 point loads must be defined manually using the same procedure for all eight axles. Another thing to bear in mind is to keep the total duration of each multiplier the same, only changing the loads location. In this example the total train passage would've taken 1.562 seconds. Considering the first axle (A_1) «fading in» when entering the first point load, and the last axle (A_8) «fading out» when leaving the last point load, the total dynamic time for this segment will be 1.586 seconds.

To complete this example, the input parameters used in the phase properties of PLAXIS is shown in figure 3.4.

Setting the dynamic time interval to minimum 1.586 seconds is required to cover the behaviour of each point load during this train passage. If set to exactly 1.586 seconds, while setting the number of max steps manually to 1586, then each step will reflect the trains location with 0.001 second increments in real time, which can be usedful for determing the trains location at any given time.

In this case were the train speed was set to 50 m/s, each step would then reflect as if the train was moving 5 centimer at the time incrementally between each step. This is favourable in terms of further analyses since if saving each step this way for a simulation, it will be possible to create dynamic animations of the train passages which during this project was valuable for assessing different aspects of the model.

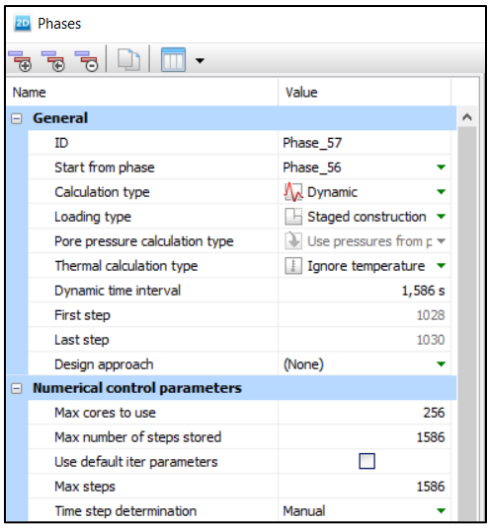

Figure 3.4 – Phase option with calculation type set to «dynamic». A minimum dynamic time intervall of 1,586 seconds is required to cover this train passage over all the 50 point loads

3.2 Modelling after specifications of two commonly used trains in Norway

This chapter presents the properties of two typical norwegian trains which is to be modelled by the principles from section 3.1 and further used for the final report. The trains are the norwegian airport express train type BM 71, currently used as a passenger train at the line «Gardemoenbanen» while the second train is a freight train consisting of a CE119 front locomotive combined with two SNGS wagons, see figure 3.5.

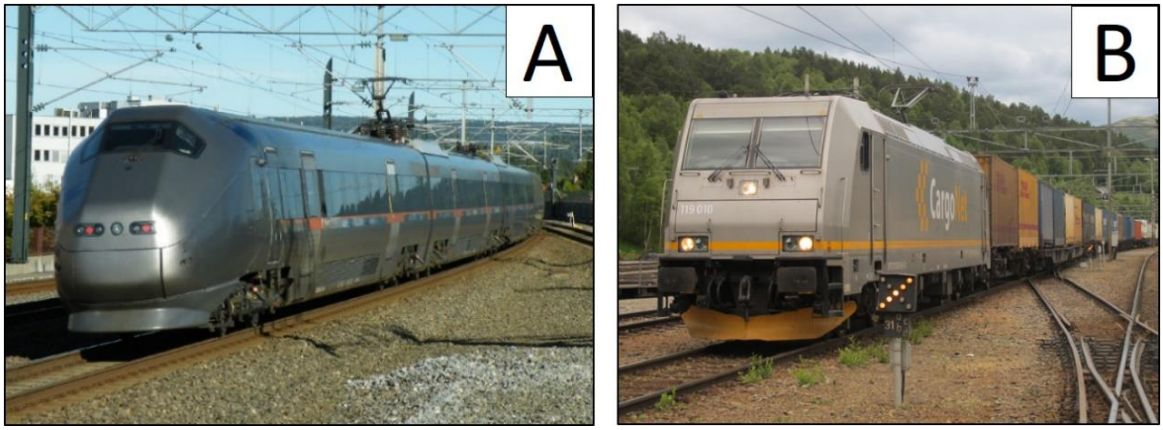

Figure 3.5 – Illustration of two common trains in Norway: A) The norwegian airport express train BM71 and B) A freight train from Cargonet consisting of an electric CE119 front veichle (Photo: Stig Baumeyer and Andreas B. Westheimer)

The trains are chosen particularly to disperse train variables such as axle configurations, velocity and axle loads. The properties of each train configuration is selected according to the current norwegian regulations for axle loads, train classes and speed limits.

The section used for the model for both trains are a standardized section defined with a total of 101 point loads, placed with a distance of 0.56 meter between them. This makes a total travelling lenght of 56 meter. To avoid any influence end boundaries might have on the track, an offseth of 0.2 meter for the track was set, see figure 3.6.

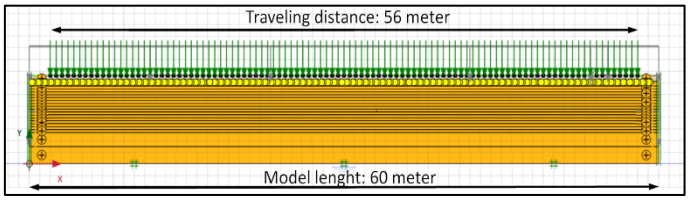

Figure 3.6 – The generalized track section, showing the traveling distance of 56 meter which is used for all simulations

3.2.1 The norwegian airport express train, type BM71

The BM 71 airport express train was designed by Terje Meier in 1999, and looks very similar to the NSB type 73 passenger train, both of which are delivered by Bombardier transportation, Germany.

The BM type 71 train is designed to reach velocities up to 210 km/h, and according to old design drawings from NSB, were designed with a 16.5 tonn axle load at the front bogies and 15.5 tonn axle loads at the inner bogies [7]. With respect to the specification for the new Intercity project, an axle load of 18 tonn is assumed for all axles as this is specified as a design criteria by Bane NOR [1].

The train speed for this «train» is set to 56 m/s (201.6 km/h), which means it will take one axle a total 1.0 second to pass all the 101 point loads. Considering the trains lenght of 74.52 meter (from first to last axle), its axle configurations and speed results in a delay from the first to the last axle of 1.33 seconds. The fading time between each point load is set to 0.01 seconds and is performed in 10 steps, making up for a total traveling time of 2.351 second for the entire train passage, see figure 3.7.

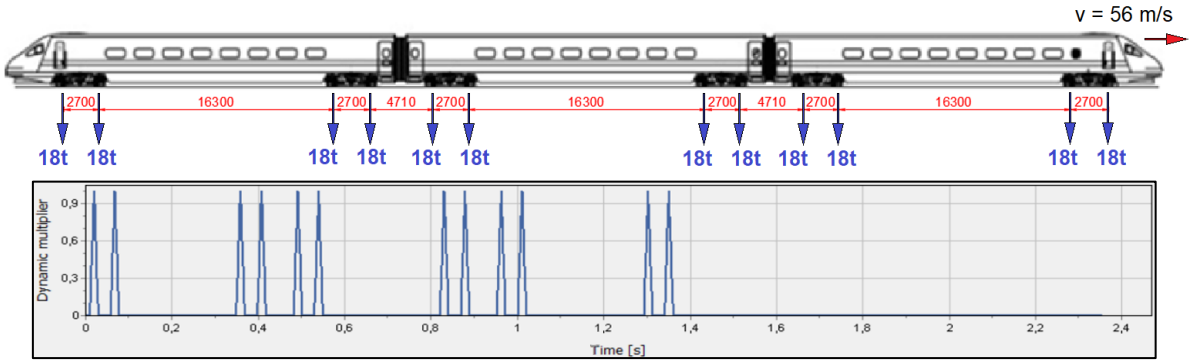

Figure 3.7 – Train specifications based of a BM type 71 train, showing its speed, axle configurations, and time increments based of the multiplier for the first point load in PLAXIS (After www.wikipedia.org)

3.2.2 A freight train consisting of CE119 front veichle and two SGNS-wagons

The front locomotive is based of the Bombardier Traxx type CE119, a commonly used locomotive by the company Cargonet in Norway. The wagons were selected to furfill requirements from NS-EN 15528:2015 for load limits, and EN 1991-2:2003 describing load limits on bridges for spacing between each wagon. The specifications of a SNGS wagon in combination with the CE119 locomotive seem to satisfy an allowable axle load up to 22.5 tonn and a traveling velocity up to 100 km/h.

The train configuration for PLAXIS was therefore defined as a CE119 locomotive in the front followed by two SNGS wagons with axle loads of 22.5 tonn. The train speed is set to 28 m/s (100.8 km/h), which means one axle will use 2.0 seconds to pass all 101 point loads. The fading time is set to 0.02 seconds performed in 10 steps, resulting in the sequence taking a total of 3.948 seconds. The multipliers is set to 0.93 of an 22.5 tonn axle for the front locomotive to disprese them from the wagon, see figure 3.8.

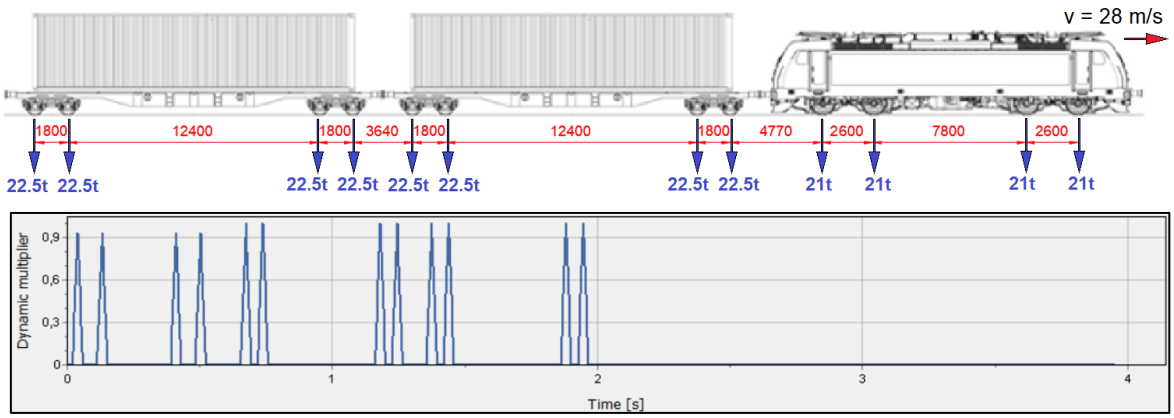

Figure 3.8 – Train specifications for the CE 119 locomotive followed by two SNGS wagons, showing its speed, axle configurations, and time increments for the first point load in PLAXIS (After www.greencargo.com and www.wikipedia.com)

3.3 Static and dynamic boundary conditions

As a minimum for both the static and dynamic boundary conditions the horisontal boundary is set to «fixed-fixed» by line displacement, enclosing the bottom boundary completely in both x and y direction. This would simulate as if there was a rigid bedrock beneath the soil body.

At the vertical end boundaries the line displacements are set to «fixed-free», preventing the soil from escaping the model horisontally while enabling it to displace vertically at the boundaries, see figure 3.8.

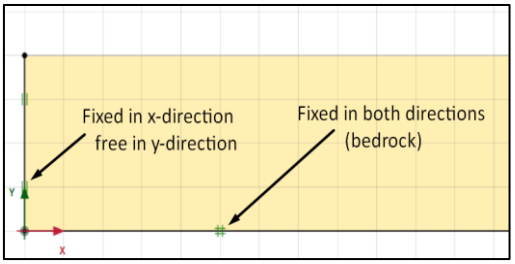

Figure 3.8 – Illustration: General boundaries used in all simulations, placing a rigid bedrock beneath the soil body by keeping it «fixed-fixed»

When considering the shear waves which propagates from a dynamic load, it should be considered how the boundaries reflect these. If the boundaries in the option «model conditions» under «model explorer» are set to none, the waves which propagates from the source are trapped inside the model, which might influence the results. The PLAXIS manual states that this should as a minium be considered at the vertical boundaries in order to catch a far-field behaviour for any dynamic load [8].

Under the circumstances presented in figure 3.8, the shear waves propagated from a railway superstructure should be reflected at the bedrock while being able to move continously at the vertical end boundaries. To catch the far field behaviour the PLAXIS manual suggests to either use the «viscous» or «free field» option at the X_{min} and X_{max} boundaries. When the source of the vibrations comes from a structural elements however, the viscous option are not recommended in the manual [8].

The dynamic boundaries for this model are set to «none» at the lower horisontal boundaries while «free-field» at the vertical end boundaries. Such specification will enable the shear waves propagated from the train loads to be relfected by the bedrock and being minimally reflected at the vertical end boundaries. Whats important to mention here is that in order for the "free field" option to work properly, interface elements must be created at both the vertical model boundaries inside the model [8], see figure 3.9.

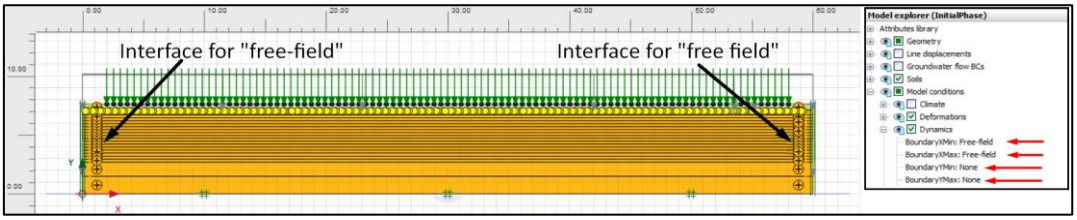

Figure 3.9 – Illustration: Interfaces placed at the end boundaries inside the model and set to «free-field» in dynamic mode

3.4 Example: Using Rayleigh damping factors

The focuse of this project has been to keep the quasi-static behaviour of the moving loads on the track as realistic as possible. As the following section will show, if the dynamic aspect of the model is completely ignored results for displacements reveals a dominant frequency domain which excites the displacmeents of the entire model. The aim of this section is to identify some of the frequencies associated with this noise.

Getting rid of the vibrations seen at the displacements could be as simple to just include a high damping factor, which when being high enough eventually will damp away all accelerations. Considering the quasi-static part of the system exclusively, such approach can be sufficient. However, rayleigh damping factors can easily be misused when the root cause of the problem are not identified and might even affect the displacements if their high enough.

The following section shows that investigating the problem under a «full train passage» tends to mask the problem under these simulations. Fast Fourier Transformations (FFT) has later revealed that some of the noise seen are tied to how the track structure is built, but the main source of it is tied to how the loads is entering the model, independent of speed.

3.4.1 Undamped train passages and principles of damping in PLAXIS 2D

In the following section results for displacements of two undamped train passages are presented, together with some background principles for Rayleigh damping factors in PLAXIS 2D. The soil models in this simulation are completely Linear-Elastic for both ballast and backfill as experience from simulations has suggested that the problems root cause is not tied to soil models. The steel culvert and backfill is in this case constructed simultaneously in one single phase. Four nodes are to be inspected, where two of them placed on the rail, one is placed in the soil and one at the culvert, see figure 3.10.

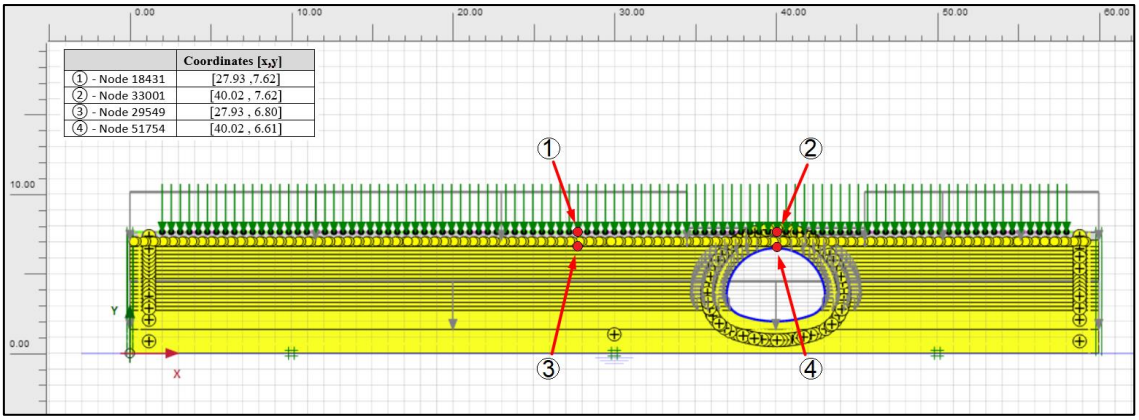

Figure 3.10 – The extendend model from section 3.4.1 using linear-elastic soil models. In this model, a full train configuration from section 3.2 are used

The railway track is built on the basis of a 60E1 rail, JBV 60 sleeper and pandrol 10 mm railpad, see chapter 2.2. The properties of the steel-soil composite bridge are based on the Enköping test-culvert which was presented by Lars Pettersons in 2007 [9], later used for validating the backfill procedure in chapter 6.3.1, see figure 3.11.

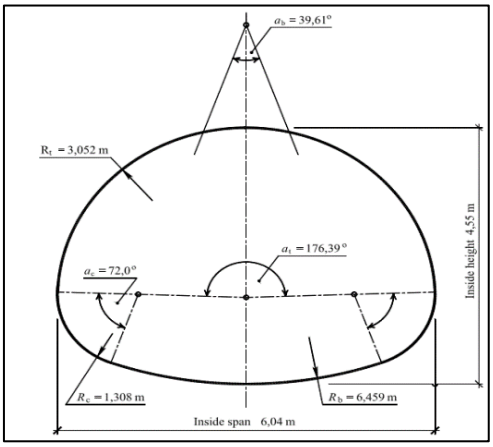

Figure 3.11 – Enköping test culvert used for various full-scale field tests (From Lars Petterson, 2007)

Enköping was of the type closed pipe arch and had a span lenght of 6.04 meter. The steel plates was built with a 200 x 55 mm corrugation and its thickness was set to 3.0 mm.

The culvert are constructed in PLAXIS after the principles demonstrated in chapter 5.2. The soil cover above the culvert is set to 1.0 meter, were 0.5 meter of ballast is placed on top of 0.5 meter of backfill. The ballast stiffness was set to 200 MPa in this calculation since it was performed before the calibration of section 2.3.2. Input parameters for are presented in table 3.3 and table 3.4.

Table 3.3 – Inputparameters for soil material

	Unit weight, γ [kN/m^3]	Possions ratio, v [-]	Elastic modulus, E [MPa]
Ballast	20	0.3	165
Backfill	20	0.3	200

Table 3.4 – Structural inputparameters for culvert and track

	EA [kN/m]	EI [kNm^2/m]	w [kN/m/m]
60E1	1.239*10^6	4908	0.4543
Railpad	225	1.0*10^6	-
Sleeper	1.0*10^6	1.0*10^6	4.08
Culvert	7.434*10^5	284.13	0.2355

Results from a undamped train simulation with the configuration of a freight train are presented in figure 3.12. The figure shows the vertical displacements of the rail in the free track ①, the rail above the culvert ②, the soil ③ and the steel plate at the crown of the culvert ④. In this simulation, the train loads were set to a velocity of 28 m/s, see section 3.2.2.

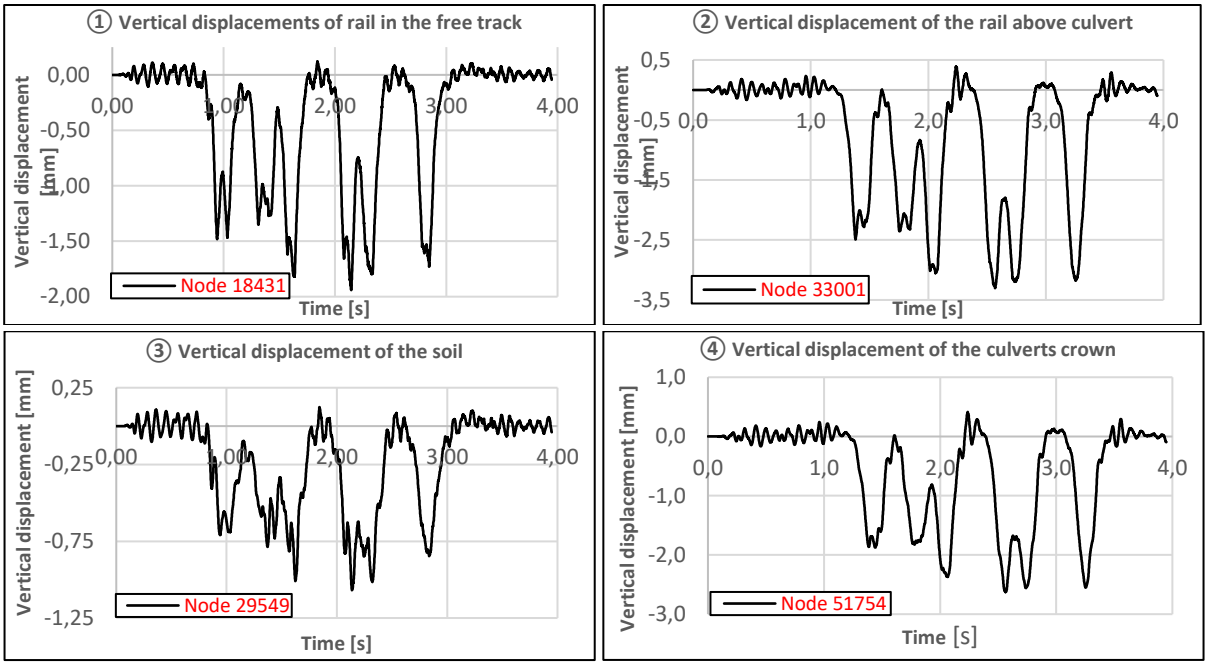

Figure 3.12 – Vertical displacements of rail, soil and culvert in an undamped case of a train passage corresponding to the configuration of the freight train in section 3.2.2. Nodes are placed according to figure 3.10

From figure 3.12 it is shown that the frequency of the vibration seen at the displacement of the rail, approximately has the same frequency as in the soil and steel plate on culvert. The frequency of this vibration seem to be in between 10-15 Hz, where its influence on the peak displacements of rail in the free track ① and in the soil ③ seem to be more severe than its influence on the rail above the culvert ② and at the steel plate of the culvert ④. The severity of the vibraiton also has the tendency of being larger when the first axle is closing in on the node compared to when the entire load set has passed.

Another train simulation is performed in an identical model, this time by replacing the configurations of the freight train with the passenger train from section 3.2.1, and remaining the same axle loads, see figure 3.13.

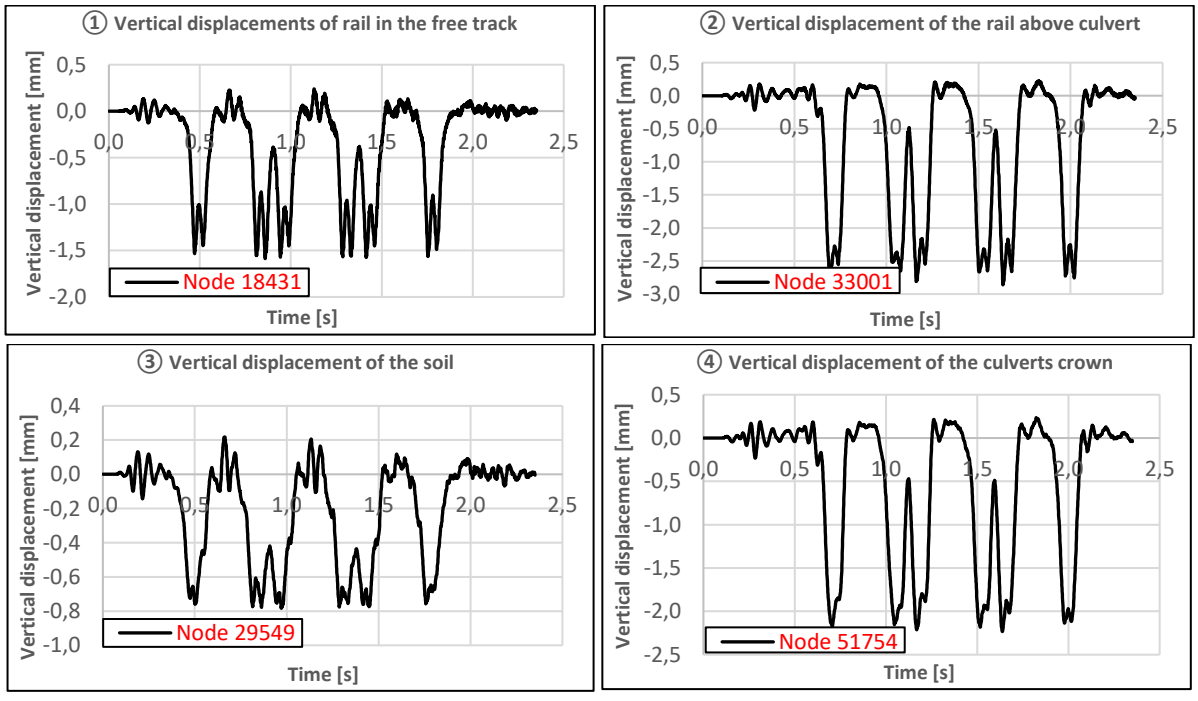

Figure 3.13 - Vertical displacements of rail, soil and culvert in an undamped case of a train passage, corresponding to the configuration of the passenger train in section 3.2.1. Nodes are placed according to figure 3.10

From figure 3.13 it is shown that the same tendency as for the freight train occours for the passenger train, were the vibrations is seen in all sections of the model with a nearly constant frequency. The frequency in this case seem to be slightly higher than it was for the freight train, in an order of 15-20 Hz. The vibration shows the same tendency as for the previous case where the amplitudes are largest as the train is nearing the measurement point, and decreases when the train loads has passed over.

The challenge with selecting accurate damping factors in PLAXIS 2D when the cause of the noise is dispersed, is that they are based on single degree of freedom equivalence for each material. This makes it impossible to only damp a certain frequency range sufficient without affecting other frequencies.

The PLAXIS manual [8] provides a simplified chart for roughly explaining the effect of damping certain frequency ranges, see figure 3.14.

From figure 3.14 it can be seen that the influence of β is tied to damping the higher frequencies while α is more associated to the lower frequencies. The α parameter determines the influence mass has on damping the system, while β, the influence stiffness has on damping. The general, simplified formulation of the damping matrix C, are given as

(Eq. 3.1) $$[C] = \alpha[M] + \beta[K]$$

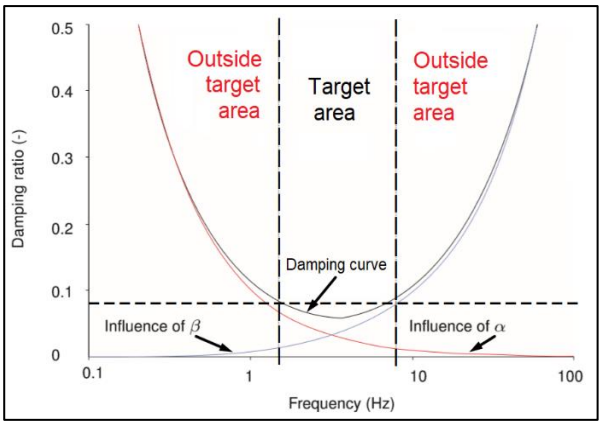

Figure 3.14 – Influence damping a target section has on rest of the frequency ranges (Modified after PLAXIS manual, 2019)

PLAXIS 2D purposes Rayleigh damping factors (α and β) automatically on the basis of damping ratios ξ_1 and ξ_2 and the target frequencies f_1 and f_2. A common practice is to define the damping ratio in target 1 the same as in target 2 [10]. When a certain target damping is desired for a certain frequency range, this range is labeled as the target area.

In the target area it can be seen from the damping curve in figure 3.14 that the effect of damping will be slighltly less than the inserted damping ratios ξ_1 and ξ_2, and higher outside this range. Figure 3.14 also shows that the further away the frequency is from the damped frequency of the target area, the more it will be damped. This means that if the target area covers a low frequency range, all higher frequencies will be significantly damped, increasing as the frequencies is further away from the target area.

As an closing example, another simulation is performed in the same model as used in this section, damping the frequency range of 135-190 Hz with 5% in the ballast and 2.5% in the subsoil. The configurations of the freight train in section 3.2.2 is still used. Displacements results are presented in fig. 3.15.

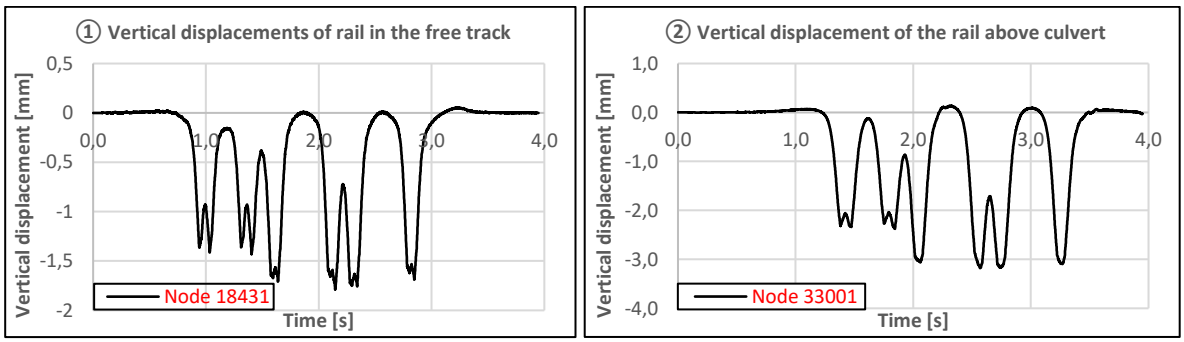

Figure 3.15 - Vertical displacements of rail, soil and culvert in an damped case in the frequency range of 135-190 Hz

As figure 3.15 shows, all vibrations seen for the undamped cases has nearly disappeared. An important point to highlight here is that this doesn't mean that the problem is tied to the frequency range of 135-190 Hz, it could aswell be tied to higher or lower frequencies as these were damped more in this case.

3.4.2 Damping the end boundaries of the model

This section is written after the findings of section 3.5, where it was found that the frequencies of the amplitudes seen at the displacements likely is caused by the impact of the sudden entry of the train loads at the entry and exit of the model, leading to several waves propagating in the soil at 11-14 Hz. One way of removing this «pulse» without ruining the dynamic behaviour of the model, is to only use damping under the first few point loads at the end boundaries (i.e only a small section).

By dividing the soil at the end boundaries into three individual zones which are damped, the unrealistic vibrations seem to be significantly reduced while it provides a gradual transition to the nondamped soil medium. The ballast and backfill of all three zones are damped within the frequency range of 5-50 Hz, which commonly are recognized with lower frequencies [6,11,12]. The first zone is damped with 400%, the second with 200% and the third with 100% where the middle section remains completely undamped, see figure 3.16.

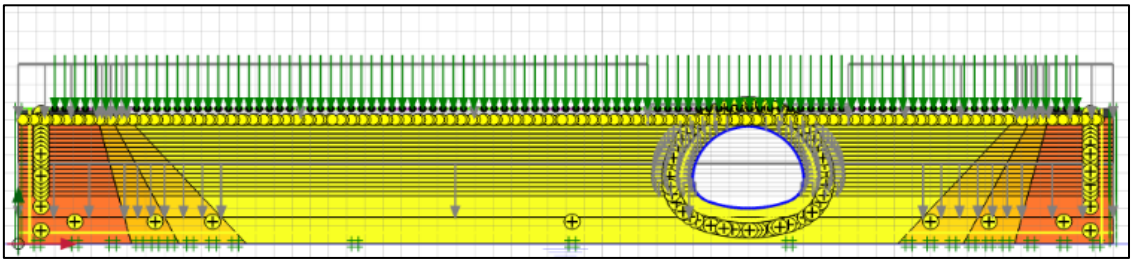

Figure 3.16 – Principles for damping the entry and exit of the model. Using the highest damping under the first point loads at the end boundaries of the model, gradually decreasing to no damping

At the first attempt of removing the amlitudes in the displacements, only a section of the model was improved. From this it was concluded that the train loads when exiting the model led to similar vibrations as previously seen.

In figure 3.17 an example is provided for illustrating this where vertical displacement at two nodes are presented, that is one in the free track at the coordinates [20.13, 7.62] and one at the culverts crown, at [40, 6.61]. As these results show, only damping the entry reveals that the rapid removal of the train loads also causes similar tendencies as previously seen at 11-14 Hz, see figure 3.17.

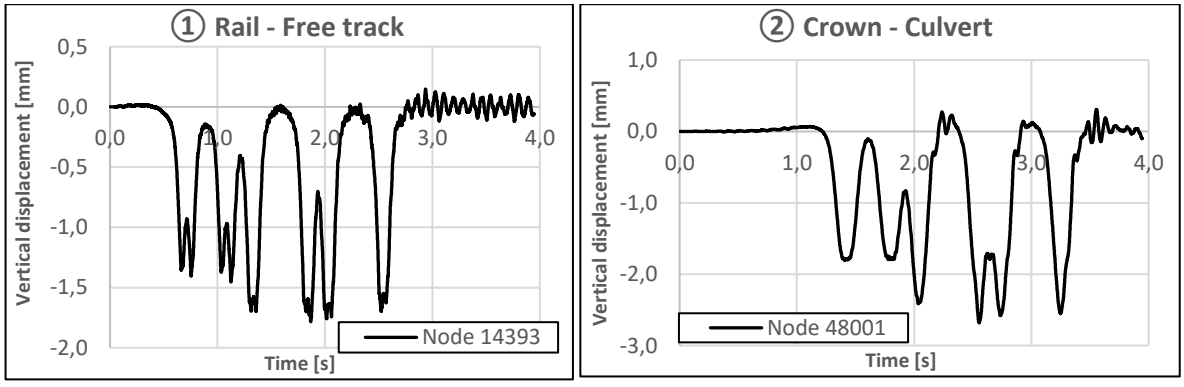

Figure 3.17 – Example: Only damping the entry of the train loads, showing the noise still occouring at the exit

If the principles of damping is used on both sides of the model, then the amplitudes seen at the exit is also removed which underlines that the problem is related to the loads entering and leaving the model.

In figure 3.18 four plots are presented, two at the rail ① and②, one in the soil ③ and one on the top point of the culvert ④. This simulation is performed with using the same model as used in section 3.4.1, but now only introducing damping at the end boundaries also. In this, case both sides of the model are damped while keeping the middle section of the model undamped. The three transition zones for damping decreases from high to no damping in total three steps, as before where 5-50 Hz are damped with 400%, 200% and 100 % respectively.

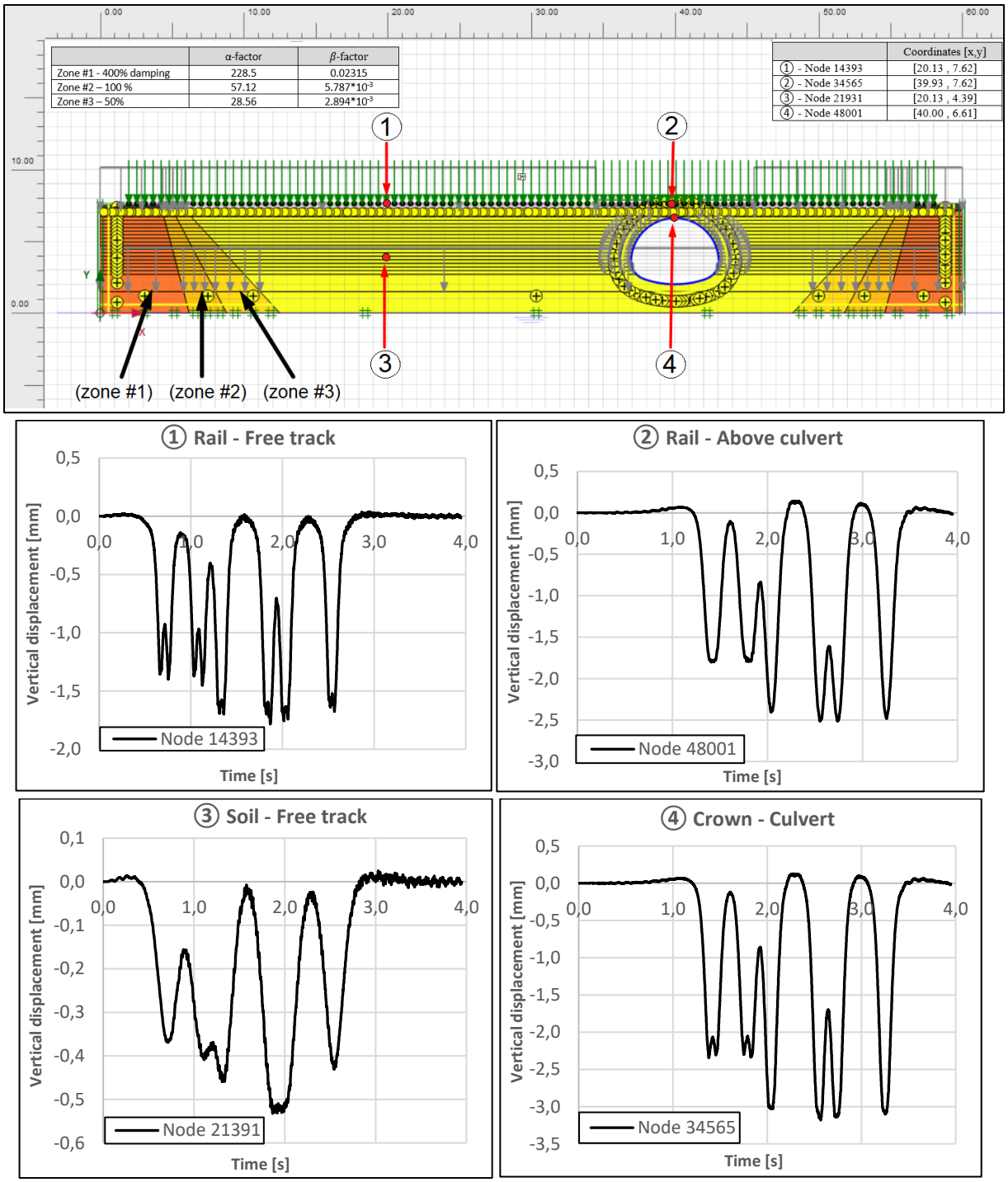

Figure 3.18 - Vertical displacement of rail and soil at various sections of the model during moving train loads at 28 m/s.

As these results shows, the spikes seen in the completely undamped case is reduced to something that looks more realistic, suggesting that the source of the amplitudes previously seen at the displacements has been located. Indeed, some amplitudes can still be seen at 11-14 Hz, suggesting that it to some degree still occours in the model but the main «pulse» is gone.

The source of the smaller amplitudes are not clear, but might be related to the fading time between the point load themselves. Even if the track is loaded and the sum of the multipliers remains 1.0, how the point loads are modelled (rapid loading-unloading) might cause the same phenomenom as seen for the first point loads, but in a much smaller degree. In terms of evaluating the quasi-static aspect of the system this solution as demonstrated in this section is considered to be sufficient.

3.5 Identifying the problem via FFT, point load test and geodynamics

One way to investigate the sources of the excitement seen at the displacements could be to run a simulation with only one single point load moving through the model, and Fast Fourier Transform (FFT) the displacements from time domain to amplifications in frequency domain. This approach might reveal dominant frequency domains in the given signal which later can be identified to what frequency they are associated with.

Changing the load configuration to only one single point load removes any influence the axle spacing might have on the noise. Forthis simulation, the culvert was also removed for the same purpose. The previous Linear-Elastic soil model used as backfill material is now also replaced with a Hardening Soil model, where each single layer are compacted with a static load, an approach used to investigate the influence of the methodology used in the final models, see chapter 6.

The point load is modelled by multipliers and has a predefined running distance of 56 meter. The load represents an axle load of 22.5 tonn, corresponding to a 84.9 kN/m point load in PLAXIS. The model is built by layers, is in total 6.76 meter high and is 60 meters long, see figure 3.19.

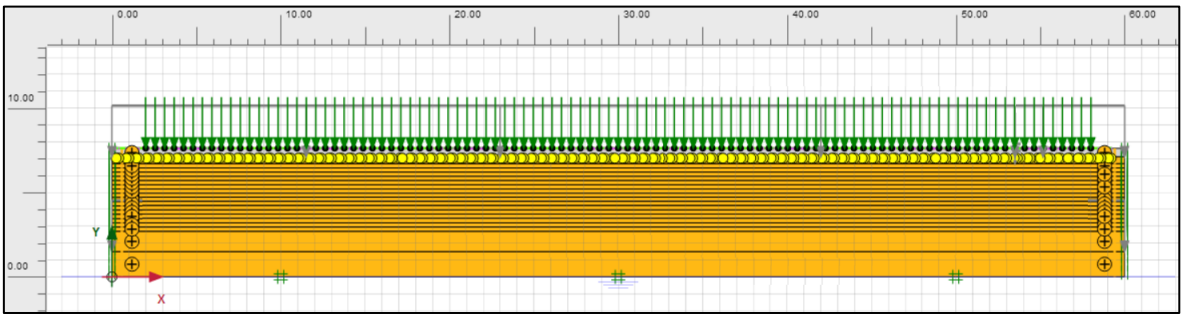

Figure 3.19 – Model used for this simulation with a single moving point load and using a Hardening soil model for the backfill

The process of creating each layer are performed in total three individual phases, which first is to create a new layer, load it («compaction»), then unload it. Each layer is laid out alternately in 0.3 meter thick layers, and are compacted with a static line load of 25 kN/m representing a small vibroplate. The static load is then removed and the process is repeated for all layers. The ballast thickness is set to 0.5 meter. Additional information on this backfilling methodology and Hardening Soil, can be found in chapter 6.

Input parameters for the backfill material are based of the example in chapter 6.3, the unloading stiffness in this calculation was set to ten times the referance stiffness in order to simulate a long term stiffness. At this point of the project, the unloading stiffness had not been predefined, see chapter 7.2.1. Dilatancy (ψ) and friction angle (φ) is set to 5° and 36° as if this was a course material, see table 3.5.

Table 3.5 – Input parameters for Hardening Soil model used as backfill material

	E_{50}^{ref} [MPa]	E_{oed}^{ref} [MPa]	E_{ur}^{ref} [MPa]	φ	Ψ	c [KPa]	v_{ur}	Unit weight γ [kN/m^3]
Backfill	27.5	27.5	275	36°	5°	1.0	0.2	17.8

The ballast are modelled as a Linear-Elastic soil model and the railway track is built on the basis of a 60E1 rail, JBV 60 sleeper and pandrol 10 mm railpad, see chapter 2.2. The properties used for these material are presented in table 3.6 and 3.7 respectively.

Table 3.6 – Inputparameters for the ballast

	Unit weight, γ [kN/m^3]	Possions ratio, v [-]	Elastic modulus, E [MPa]
Ballast	20	0.3	165

Table 3.7 – Structural input parameters for culvert and track

	EA [kN/m]	EI [kNm^2/m]	w [kN/m/m]
60E1	$1.239*10^6$	4908	0.4543
Railpad	225	$1.0*10^6$	-
Sleeper	$1.0*10^6$	$1.0*10^6$	1.08

3.5.1 Investigating frequency domains from the track superstructure

Fast Fourier Transformations (FFT) of the results from PLAXIS are performed with the use of a prewritten Matlab script used for the displacement data with time domain from PLAXIS directly to frequency domains with amplitudes. The script was written by Albert Lau at NTNU.

Two FFT results are presented per simulation where two point load tests is carried out, traveling at 28 m/s and 56 m/s in order to correspond to the train configurations of chapter 3.2. From each simulation, measurements of the passage above and between two sleepers are presented at the rail. Indeed, it would've been more advantagous to FFT track displacements of the moving load itself rather than a single point at the track, where the quality of the signal varies with time. This limitation is set by PLAXIS which to begin with doesn't offer the option of creating horisontally moving object.

Two ways of investigating the frequency domains seen from the FFT results is to compare them with frequencies of the track and the tracks pinned-pinned frequencies. From knowing the loads speed, it is possible to calculate the frequency over a sinusodial rail irregularity from the classic expression

$$f = \frac{v}{\lambda} \qquad \text{(Eq. 3.2)}$$

where

f being the frequency
v being the wave speed
λ being the wave lenght

The expression from eq. 3.2 is accepted for investigating excitation frequencies for railways [6]. It shows that longer wave lenghts or lower veichle speeds leads to lower frequencies. This expression can roughly be used for comparison to the results seen at frequency domains, see figure 3.20.

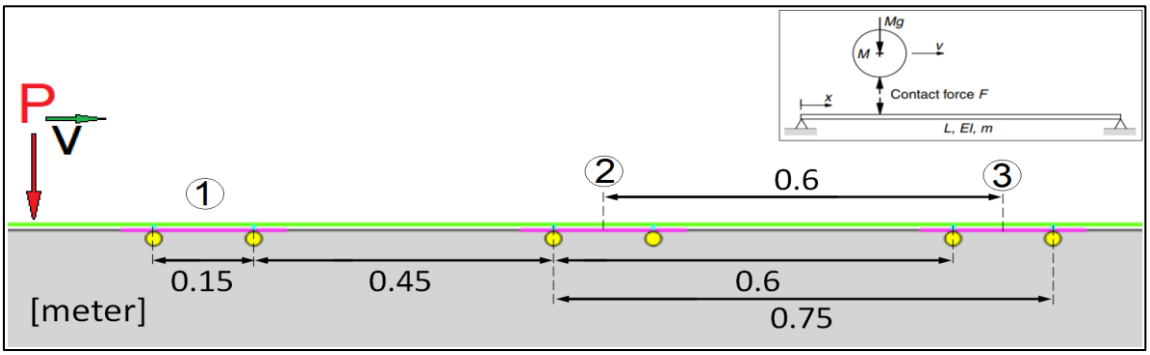

Figure 3.20 – Basis for investigating exciting frequencies occouring at the track with the moving point load test, showing a traveling point load with the various pinned-pinned frequenciesoccouring when the train passes from sleeper to sleeper

Creating the railpad by two plate elements was a good solution for maintaining the static behaviour of the system, but creates frequency domains which does not exist in a real track. For sleeper ① it can be seen that the distance between left pad (LP) and right pad (RP) is 0.15 meter. Having two plate elements for the pad also creates other irregularities such as the distance between the RP at sleeper ① to LP at sleeper ② of 0.45 meter, and LP at sleeper ② to RP at sleeper ③ of 0.75 meter. The distance between LP at sleeper ② to LP at sleeper ③ has the same spacing as the spacing as the sleepers at 0.6 meter.

Based of the track model presented in Figure 3.20, the various frequencies that might occour for a single point load traveling at 28 m/s and 56 m/s are presented in table 3.8.

Table 3.8 – Frequencies at the track for a point load at 28 m/s and 56 m/s

Source	28 m/s Frequencies	56 m/s Frequencies
$Pad_{1.1}$ - $Pad_{1.2}$ (0.15 m)	186.7 Hz	373.33 Hz
$Pad_{1.1}$ – $Pad_{2.1}$ (0.6 m)	46.7 Hz	93.33 Hz
Sleeper spacing (0.6 m)	46.7 Hz	93.33 Hz
$Pad_{1.2}$ - $Pad_{2.1}$ (0.45 m)	62.2 Hz	124.44 Hz
$Pad_{1.1}$ – $Pad_{2.2}$ (0.75 m)	37.33 Hz	74.66 Hz

To check the potential of resonance, one can estimate the pinned-pinned frequen-cies of a track system through beam theory. According to Tore Dahlberg [6], the angular frequency (ω) is the same as the fundamental frequency of a simply supported beam with the lenght L, which means the fundamental frequencies of a track system can be expressed as

$$f_{\text{fundamental}} = \frac{\omega}{2\pi} = \frac{1}{2\pi}\pi^2\sqrt{\frac{EI}{mL^4}} \qquad \text{(Eq. 3.3)}$$

where

f being the fundamental frequency
ω being the angular velocity
EI being the beams bending stiffness
m being the beams pr. unit lenght in meters
L being the lenght of the beam

From using the rail properties previously transfered into Plane-strain, the estimated pinned-pinned frequencies of the track model in based of the simple Euler bernulli beam formualtion is presented in table 3.9.

If the frequencies from the model is close to the pinned-pinned frequencies, it can be stated that there might have occoured resonance in the track. It is important to bear in mind that the pinned-pinned frequencies provided by equation 3.2 is only a rough estimate

Table 3.9 – Estimated pinned-pinned frequencies of the track when the speed is 28 m/s of the moving load

Source	Frequencies
$Pad_{1.1}$ - $Pad_{1.2}$ (0.15 m)	22730 Hz
$Pad_{1.1}$ – $Pad_{2.1}$ (0.6 m)	1420 Hz
Sleeper spacing (0.6 m)	1420 Hz
$Pad_{1.2}$ - $Pad_{2.1}$ (0.45 m)	2525 Hz
$Pad_{1.1}$ – $Pad_{2.2}$ (0.75 m)	1420 Hz

Regarding uncertainties tied to the pinned-pinned frequencies, the rule of thumb is that Euler-Bernullis beam theory becomes less accurate the shorter the wave lenght of the signal compared to the height of the beam becomes. From experience, it is found that the resonanse frequencies usually are lower in reality compared to theoretical ones [6]. However, from comparing the frequencies of the track in table 13 to the pinned-pinned frequencies in table 3.9, the major difference between them suggests that resonanse of the track most likely has nothing to do with the vibrations seen in section 3.4.1.

The point load test in PLAXIS is performed in two simulations, one traveling at 28 m/s and one at 56 m/s, which are then converted to Matlab the displacement in time domain transfered to frequency domain. The displacements of the two points at the rail is presented, one above a sleeper and one in between them, at the x and y coordinates [29.73, 6.76] and [30, 6.76], see figure 3.21. The amplitudes are scaled logaritmic in order to locate the frequency domains better, where the purposed locations of the frequencies at the track are labeled as ①, ② and ③, see figure 3.21A) and figure 3.21B).

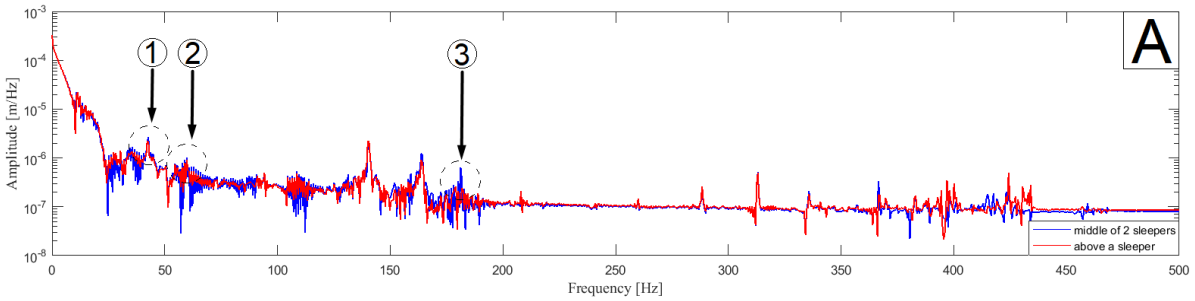

Figure 3.21 – Fast Fourier Transformed (FFT) results for a completely undamped case in frequency domain, showing A) results when the point load is traveling at 28 m/s. Located frequencies of the track are denoted as ①, ② and ③ (Matlab script written by Albert Lau)

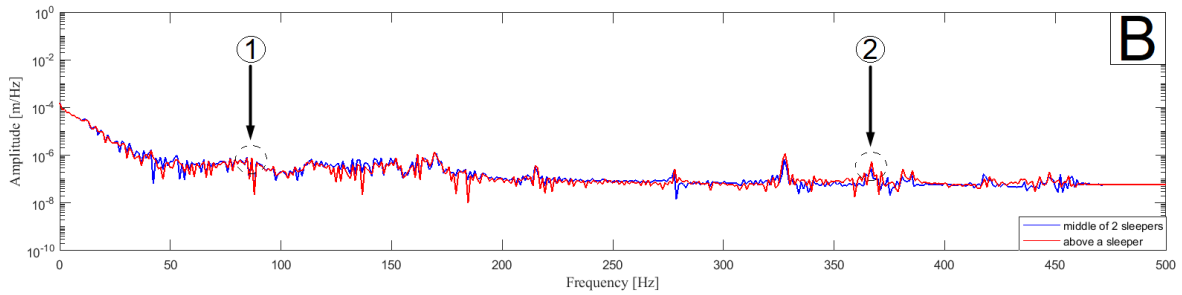

Figure 3.21 – Fast Fourier Transformed (FFT) results for a completely undamped case in frequency domain, showing B) results from a point load traveling at 56 m/s. Located frequencies of the track are denoted as ① and ② (Matlab script written by Albert Lau)

The FFT results from both simulations shows several amplitudes along the signals frequency domain, which reflects the potential contribution of a particular frequency to the noise often seen. Some of these spikes can be associated with the track frequencies while some cannot. In this section only frequencies associated with the track (> 30 Hz) are discussed.

By comparing the FFT results of the point load traveling at 28 m/s (figure 3.21A) to the amplitudes of the frequencies at the track, the sleeper passing frequency ①, the $Pad_{1.2}$ - $Pad_{2.1}$ passing frequency ② and $Pad_{1.1}$ - $Pad_{1.2}$ passing frequency ③ is seen in the frequency domain. As a consequence of how the track is constructed in chapter 2 were the pad elements was built by vertical plate elements, the FFT results suggest that this leads to some unrealistic noise at the track as these loads are moving.

Comparing the FFT results of the second simulation (56 m/s, figure 3.21B) to the amplitudes of the frequencies at the track, the passing frequencies of the track seems less visible. Only the sleeper passing frequency ① and the $Pad_{1.1}$ - $Pad_{1.2}$ passing frequency ② was located, where the sleeper passing frequency only is intimated. Judging from the magnitudes of the spikes, the FFT results clearly demonstrates that the pad element frequencies influences the frequency domains.

Recapping the problem with severe vibrations that was seen in section 3.4, they typically had a frequency of 10-20 Hz. It can be argued for that this frequency might be excited from frequencies of the track. But having in mind that the amplitudes are logaritmic and by styding the order of the displacements tgese frequencies lower than 20 Hz, the amplitudes of the lower frequencies are between 100-1000 times higher than the frequencies seen at the track, underlining that the source of the severe vibrations seen in the entire model most likely does not have their origin from the track.

3.5.2 Investigating frequencies dissipating in the soil

From comparing the displacements of the single load simulation to the FFT results in frequency domain, it is evident that the lower frequencies dominates the signal. When investigating the influence speed has on the excitement seen at the rail, upose to a full train simulations seen in section 3.4 the single point load test suggests that the frequencies more or less is the same, independent of traveling speed.

From investigating the fundament frequencies of the ballast and subsoil it has been possible to locate the lower frequencies (10-20 Hz) often seen at the displacements in all sections of the model. The aim of this section is to give a better basis for understanding how the load configuration creates both shear and compression waves which propagates through the soil, with a suprizingly similar frequency seen at the displacements.

In figure 3.22 results from an undamped point load traveling at 28 m/s is presented. The prerequisites of the model is the same as previously illustrated in section 3.5, where the backfill is modelled with a hardening soil model and the culvert is removed. Vertical displacement from four nodes in the model are presented, that is three at the rail and one in the soil, see figure 3.22.

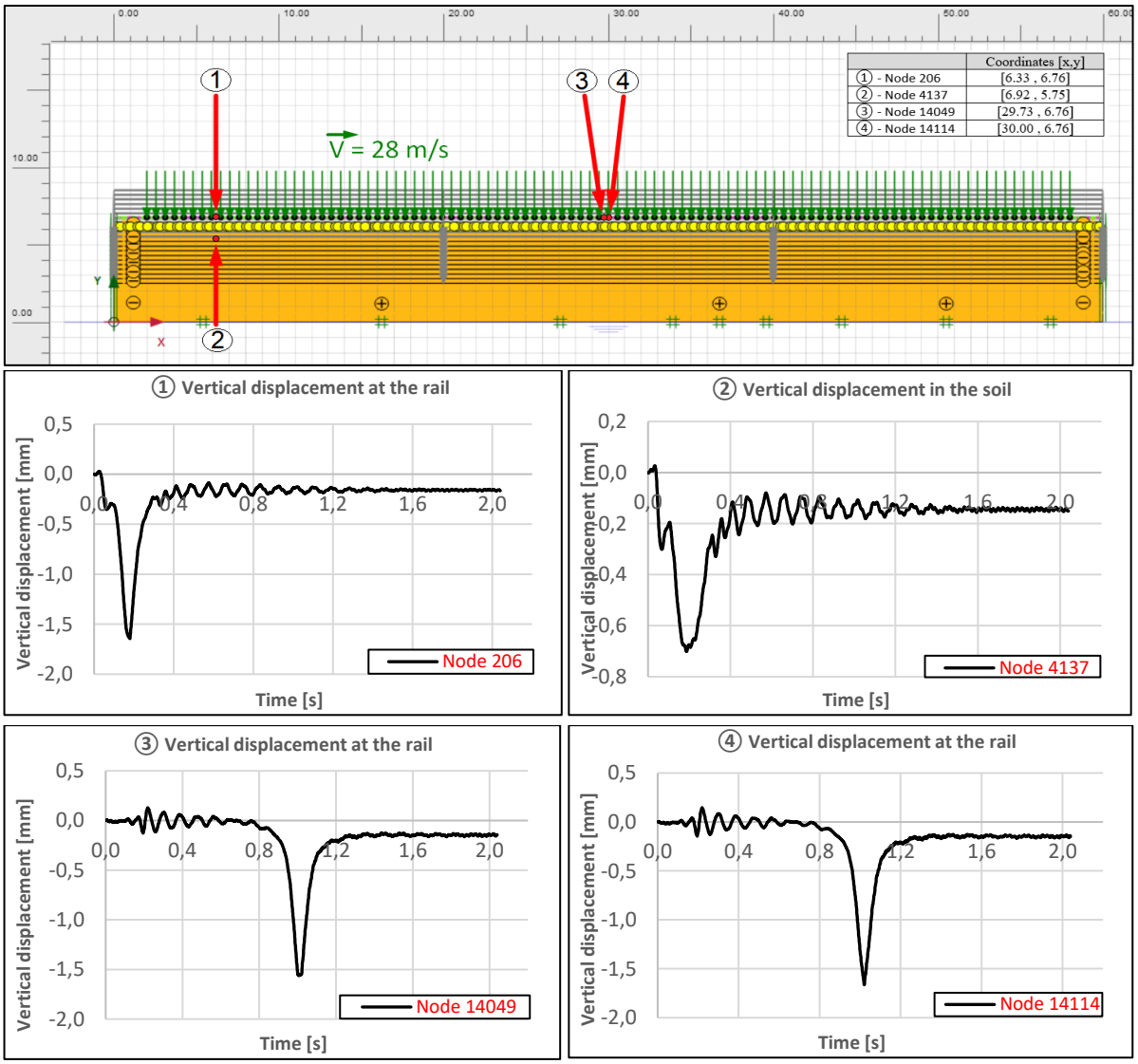

Figure 3.22 – Vertical displacement of the rail and soil at various sections in the model during a moving point load at 28 m/s

From the plots it can be seen that the point load hits the beginning of the model (plot ① and ②), causing severe vibrations with a frequency of 12-15 Hz. At the rail in the middle of the model (plot ③ and ④), it can be seen that the wave created at the beginning hits the measuring point long before the point load has reached the same point, suggesting that the wave travels much faster than the point load. It is also evident that this wave is gradually dissipating, as if it was caused by a impact force.

Recapping the Fast Fourier Transformed results at the middle of the model, the waves seen at 12-14 Hz can clearly be seen in the beginning of the frequency domain, both between and above the sleepers. The peak is in the order of 10-100 times larger than the peaks previously seen at the track, see figure 3.23.

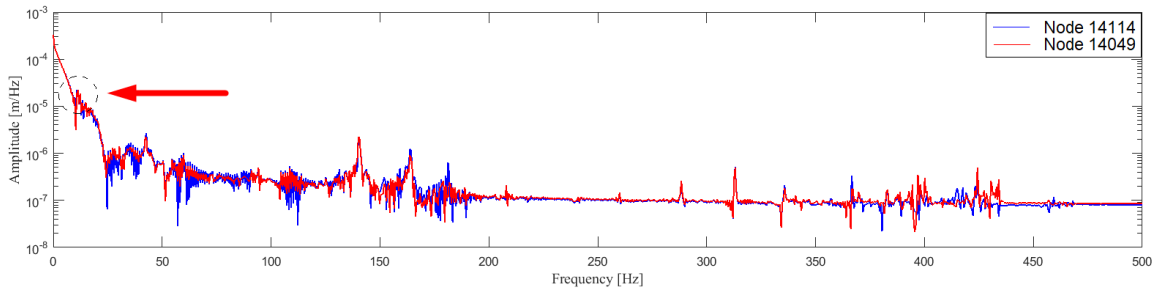

Figure 3.23 – FFT results for node 14114 and 14049, clearly showing the impact created at the beggining of the model

To study the influence of speed, the same simulation is performed once again but with a point load traveling at 56 m/s corresponding to the speed of the BM71 passenger train in section 3.2.1. Vertical displacement at four nodes is presented, that is two at the rail and two in the soil, see figure 3.24.

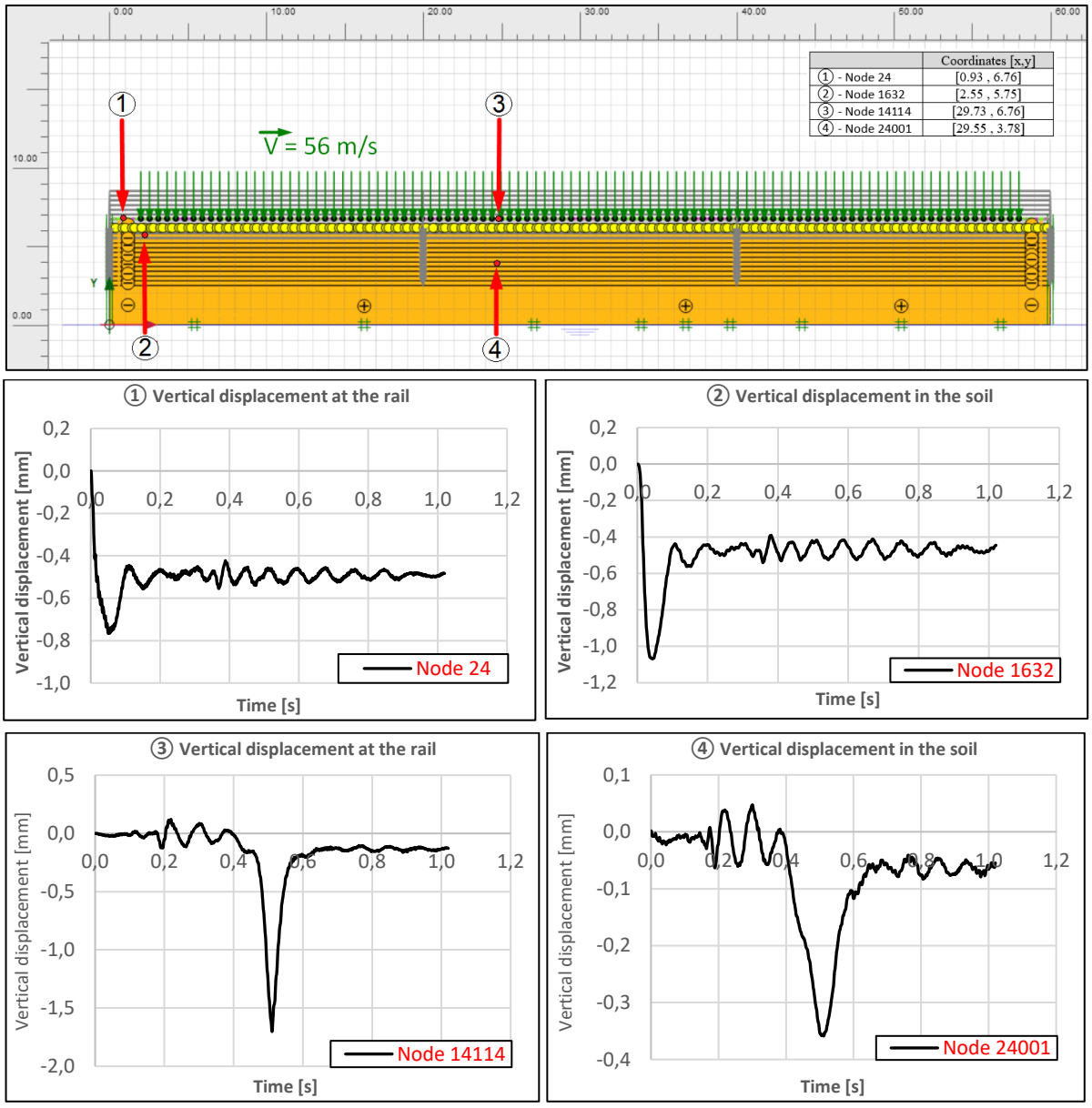

Figure 3.24 - Vertical displacement of rail and soil at various sections of the model during a moving point load of 56 m/s

Similar to the simulation with the point load traveling at 28 m/s, it is evident that when the load enters the model (plot ① and ②), it causes some kind of a pulse with propagates through the model. This pulse is clearly seen in the middle of the model both at the rail and in the soil (plot ③ and ④), suggesting the same tendency as previously. It is also seen that the amplitude has disipated more at the rail ③ compared to the soil ④, suggesting that this frequency primarily propagates through the soil and has little to do with the frequency domains at the track.

Another interesting observation is that the frequency of the wave created by this pulse is suprizingly similar to the pulse in the case of the load traveling at 28 m/s. Upose to their differences when the full train configuration was used, the frequency now is around 12-15 Hz for both cases. When the point load hits any node in the model the plots also suggest that the pulse that was created at the beginning is followed by a smaller wave, with approximately the same frequency, see ③ in figure 3.24.

Considering the train configurations from section 3.2, the BM71 passenger train has a total lenght of 74.52 meter while the freight train 53.41 meter. This information shows that through the entire simulation, the pulse is never able to die completely out until a new one is created by a new axle entering the model. The tendency of creating several pulses will therefore occour for both trains, see figure 3.25.

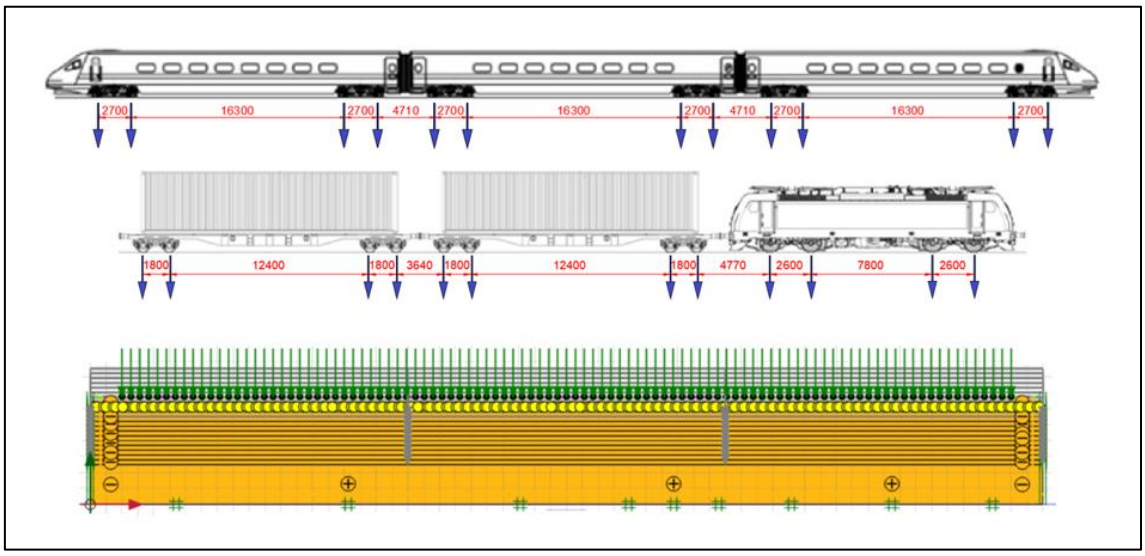

Figure 3.25 – Train configurations from section 3.2 scaled according to the model for illustrating their differences in lenght

In order to better understand the how this «pulse» created at the entry of the model propagates through the soil, fundamental frequencies of the soil are investigated. According to Nordal and Kramer [11,12], the general expression for a resonance frequency in a soil medium is

$$\lambda = \frac{2H}{n-(\frac{1}{2})} \text{ for n = 1,2,3..} \qquad \text{(Eq. 3.4)}$$

where

λ being the wave lenght
H being the height of the soil medium
n being the eigenmode of the given fluctuation

As the expression shows, the first wave in the soil medium will be the larges one, gradually decreasing for each oscillation. The eigen modes of the three first modes in a soil layer formulated after the illustration in figure 3.26.

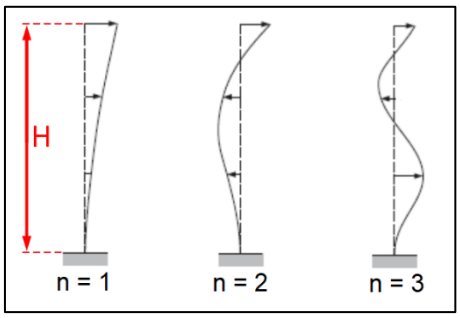

Figure 3.26 – Eigen modes of the first three modes of a soil layer (Modified after Nordal. S, 2017)

According to Steven Kramer, in the case of a uniform, damped soil on a rigid bedrock, this causes the highest amplification to occour at the lowest natural frequency (the first mode), refered to as the fundamental frequency [11]. The fundamental frequency for a shear wave can hereby be expressed as

$$T_s = \frac{\lambda}{vs} = \frac{4H}{vs} \qquad \text{(Eq. 3.5)}$$

where

T_s being the period of vibration corresponding to the fundamental frequency
H being the height of the soil medium, see figure 3.36
v_s being the velocity of the wave propagating in the soil

Rewriting equation 11, we obtain the general expression for a fundamental frequency of a soil medium

$$f = \frac{vs}{4H} \qquad \text{(Eq. 3.6)}$$

There are two types of waves which can be identified in a soil medium, that is the compression wave (primary wave) and the several shear waves which follows. There are several ways of adressing these waves, but the compression wave is herafter labeled as «P-wave» and shear wave as «S-wave». The compression wave will travel the fastest while the shear wave often contains more energy [12].

The compression wave may be describes as a sound wave which characteristics depend on the volumetric and shear properties of the soil model [11,12]. The P-wave can be expressed as

$$v_p = \sqrt{\frac{M}{\rho}} \quad \text{(Eq. 3.7)}$$

with

$$M = \frac{E(1-v)}{(1+v)(1-2v)} = K + \frac{4}{3}G \quad \text{(Eq. 3.8)}$$

and

$$G = \frac{E}{2(1+v)} \quad \text{(Eq. 3.9)}$$

where

v_p being the compression wave velocity
M being the confined modulus
ρ being the soil mediums density
K being the bulk modulus
G being the shear modulus
E being the elastic modulus

From theory of elasticity, the bulk modulus (K) is a quantity that controls the change in volume (i.e the relation between volumetric strain and mean stress) while the shear modulus (G) controls the stiffness related to change in shape [13].

Shear waves can be defined by assuming that the soil medium provides a linear elastic medium for low amplitude waves. This assumption is normally accepted since the lower amplitudes travels faster than the higher amplitudes of such signals [11,12]. From this, the potential of a shear wave velocity can be expressed as a function of shear modulus and specific density as

$$V_s = \sqrt{\frac{G}{\rho}} \quad \text{(Eq. 3.10)}$$

where

v_s being the shear wave velocity
G being the shear modulus
ρ being the soil mediums specific density

From these relationships a check is performed on the natural frequencies of the soil in the model. Recapping the geometric properties of the model, it consists of 0.5 meter ballast founded on 6.26 meter of backfill. In order to use the expressions derived above, average parameters for stiffness and possions ratio must be defined.

For Hardening Soil models, it is the unloading stiffness parameters (E_{ur}) and (v_{ur}) which mostly reflects the backfill materials elastic behaviour in terms of loading. Recapping the material parameters from section 3.5, we obtain

- $E_{average} = E_{ballast} + E_{backfill} = \frac{0.5}{6.76} * 165 + \frac{6.26}{6.76} * 275 = 266.7$ MPa
- $v_{average} = v_{ballast} + v_{backfill} = \frac{0.5}{6.76} * 0.3 + \frac{6.26}{6.76} * 0.2 = 0.207$
- $\rho_{average} = \rho_{ballast} + \rho_{backfill} = \frac{0.5}{6.76} * 20 + \frac{6.26}{6.76} * 17.8 = 1796$ kg/m^3

From equation 3.8 for the confined modulus (M), the p-wave velocity through the soil medium in the model can be calculated as

- $v_p = \sqrt{\frac{M}{\rho}} = \sqrt{(\frac{E}{\rho} * \frac{(1-v)}{(1-v)(1-2v)})} = \sqrt{(\frac{266.7*10^6}{1796} * 1.12)} = 408$ m/s

From equation 3.9 for the shear modulus (G), the s-wave velocity through the soil medium can be calculated as

- $v_s = \sqrt{\frac{G}{\rho}} = \sqrt{(\frac{E}{\rho*2(1+v)})} = \sqrt{(\frac{266.7*10^6}{1796*2(1+0.207)}} = 248$ m/s

According to Nordal. S [12], typical values for s-waves in sands has from international tests been reported between 250-400 m/s, arguing for that the calculated values are within reasonable limits.

By knowing the velcoities of the waves in the soil deposit and the total soil depth, from equation 3.5 the fundamental frequencies of the compression and shear waves are calculated as

- $f_{compression} = \frac{vp}{4H} = \frac{408\ m/s}{4*6.76} = 15$ Hz
- $f_{shear} = \frac{vs}{4H} = \frac{248\ m/s}{4*6.76} = 9.17$ Hz

From this rough estimate it is found that the fundamental frequencies of the soil deposit are within the same range of the frequencies seen at the displacement in the model. This potential in the soil suggests that the rapid loading at the beginning of the model creates a pulse which propagates through the soil, leading to severe vibrations seen at the entire model. This effect is created by an mechanism which is not realistic, and should be removed.

3.6 Dynamic problems with the Hardening Soil model

Findings related to a combined problem between moving loads (dynamics) and the Hardening Soil model are discussed in this section. It has been found that whenever using a undamped Hardening Soil model during simulations with moving train loads, there occours persisten plastifications at any parts in the model independent of the number of simulations. In other words, the model never seem to plastify and reach its full elastic state, evidently leading to unrealistic deformations.

This problem is seen at the displacement in any part of these models as either the rail or the soil is able (i.e behave elastic) to move back to their original position after the load has passed. It is also found that this problem gradually worseness as several point loads is passing a node or the depth to bedrock (or concrete culvert) is decreased. An example of how this problem propagates for a ① single moving point load and ② a full train passage is shown in figure 3.27, where displacements for the rail in a regular embankment is presented. The soil models for the backfills in both cases were Hardening Soil.

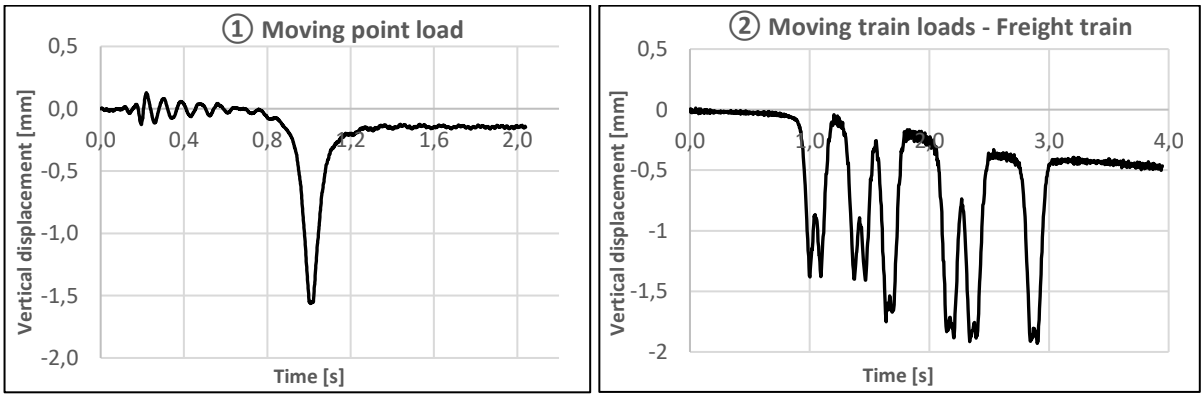

Figur 3.27 – Demonstration of the persisten plastification occouring in the Hardening Soil model

As the plots in figure 3.27 shows, the displacement at the rail never goes back to zero for either case. Whats interesting here is that the simulation with several moving loads tends to create a «stair» for each moving load passing that node, gradually increasing the displacement peak while never being able to go back to zero. The more loads involved, the more deviation is seen at the displacements.

In the following simulation example, results from three simulations are discussed to show that this issue is more related to the Hardening Soil model in the materials than the behaviour of the model itself. It was found that whenever damping a Hardening Soil model or using a Linear-Elastic soil, this problem was either significantly reduced or completely removed.

Two models were created, the first one being built with a Hardening Soil model in the backfill, alternately placing out each layer and comapcting them according to chapter 6.1.2, see figure 3.28.

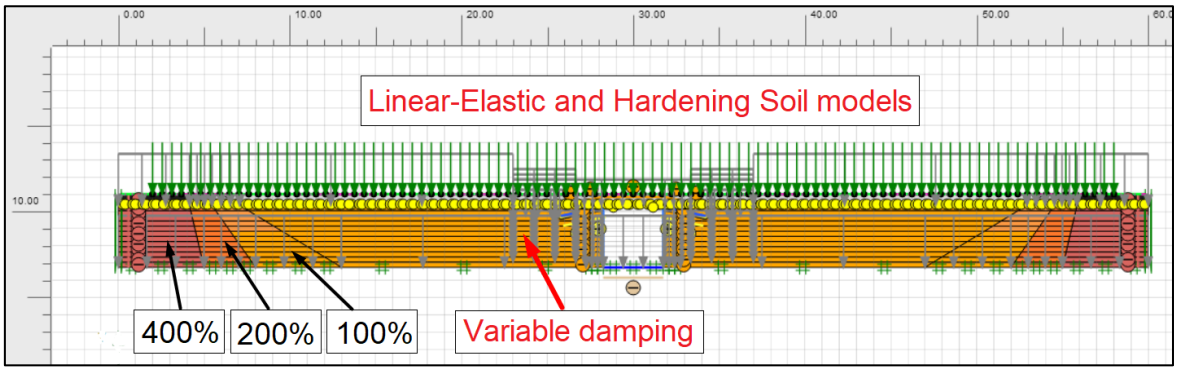

Figure 3.28 – Model conditions for the simulations using a Hardening soil model as backfill material

In this model, the end boundaries were damped as described in section 3.4.2 by using 400% damping in the frequency ranges 5-50 Hz, gradually decreasing the damping towards zero. The regular backfill has been defined as «Variable damping», and is runned with zero damping in the first simulation and 100% damping in the second one at 5-50 Hz.

It was decided to remove the foundation in these simulations in order to isolate the problem and remove other variables that influences the Hardening soil model.

The backfill in these simulations consist of crush-ed rock and a thin corrective layer of sand beneath the slab. Each layer is built alternately, first compacted (loaded) and then unloaded, see chapter 6.2.2.

The soil cover of the culvert is built with a combination of a 0.65 meter thick ballast bed and 0.1 meter thick crushed rock layer. The ballast is modelled with a Linear Elastic soil model, see figure 3.29.

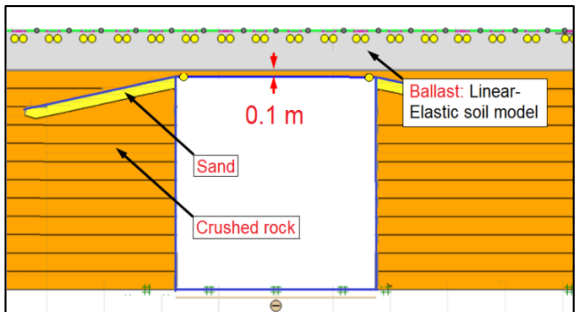

Figure 3.29 – Soil conditions. Only Hardening soil models are in the contact surrounding the culvert, see chapter 6.2.2 for more

Based of the materials defined in chapter 6.4, the same crushed rock and sand defined there is used for these simulations. It should be mentioned that in the final simulations in the main report, it was decided to use a lower unloading stiffness compared to what was used here. Material properties for the hardening soil materials are shown in table 3.10.

Tabell 3.10 – Hardening soil parameters used for the backfill and sand

	E_{50}^{ref} [MPa]	E_{oed}^{ref} [MPa]	E_{ur}^{ref} [MPa]	φ	Ψ	c [KPa]	Unit weight γ [kN/m^3]
Backfill	45	45	360	40°	15°	0.1	20
Sand	30	30	150	36	5°	1°	20

In order to match the deformations from the Hardening Soil simulations, the Linear-Elastic case was calibrated and a elastic stiffness of 170 MPa, which seems to lead to similar deformations when using a Linear-Elastic backfill. A ballast stiffness of 140 MPa was also selected based of the cali-bration from chapter 2.3.2. The elastic materials used for this simulation are presented in figure 3.11

Table 3.11 – Material parameters for ballast and when the backfill is modelled with a Linear-Elastic soil model

	Unit weight, γ [kN/m³]	**Possions ratio, v [-]**	**Elastic modulus, E [MPa]**
Ballast	20	0.3	140
Backfill	20	0.3	170

Lastly, the track were modelled according to chapther 2.2 and material parameters based of the calibrations made for the track (ch. 2.3), see table 3.12

Table 3.12 – Material parameters for the track structure

	EA [kN/m]	**EI [kNm²/m]**	**w [kN/m/m]**
60E1	$1.239*10^6$	4908	0.4543
Railpad	225	$1.0*10^6$	-
Sleeper	$1.0*10^6$	$1.0*10^6$	1.08

The model conditions of the Linear-Elastic simulations where slightly differentiated in order to also investigate the effect of damping the entry and exit of the loads, see figure 3.30

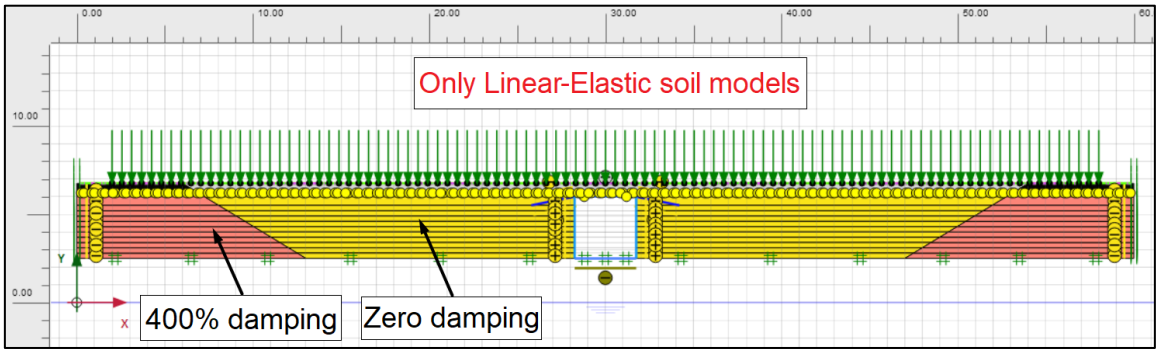

Figure 3.30 – Model conditions for the simulations using only Linear-Elastic soil models

Geometrically speaking, the backfill of this model is identical to the backfill of the model using Hardening soil (figure 3.28). The main difference here is that the culvert, backfill and track were built simultaneously in one single phase in this case (compared to the hardening soil simulations where each layer is compacted). Instead of gradually decreasing the damping in this simulation, the damping goes from being damped with 400% at 5-50 Hz to zero damping simultaneously.

In total three simulations where performed, one undamped Linear-Elastic simulation and two Hardening Soil simulations. In the Hardening Soil simulations all the material properties remained identical except for the damping at the regular backfill material, where it in the first case remained at zero damping and in the second case being damped with 100% at 5-50 Hz.

The vertical displacements of four locations were investigated, that is 1) at the free track, 2) above the transition slab, 3) above the culvert and 4) at the concrete of the culverts top element. As the results from these locations shows, the tendency of this problem in the undamped Hardening Soil simulations can be seen at the free track, but is gradually worsening as the train loads are closing in on the stiff culvert. This is thought related to the «rigid foundation» provided by the culvert being moved closer to the surface and nummerical problems in PLAXIS.

Results for vertical deformations at these four locations are presented in figure 3.31, showing deformations from all three simulations.

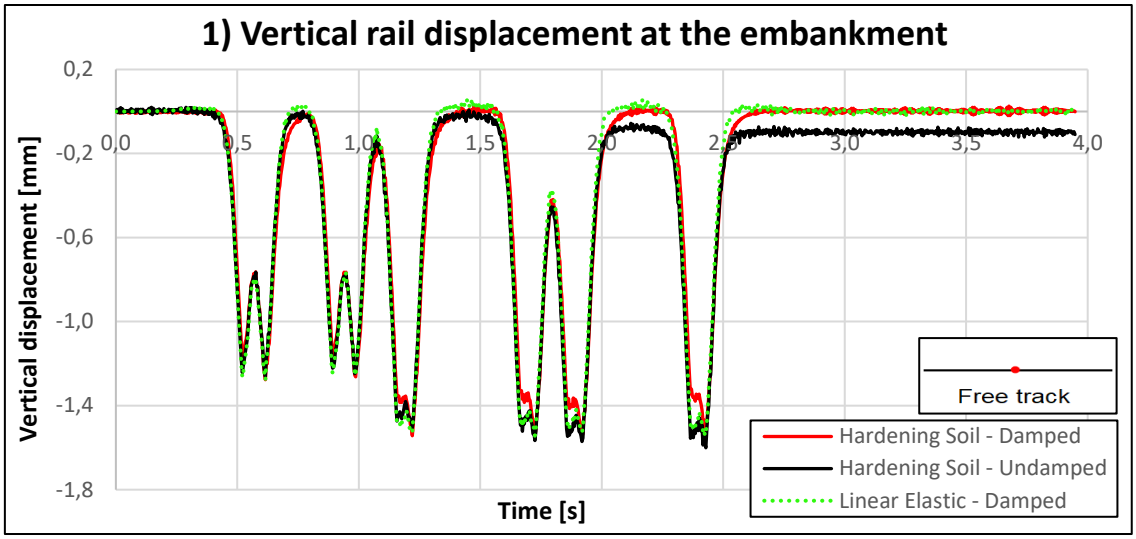

Figur 3.31 – 1) Vertical displacement of the rail when the train loads is passing a node at the free track

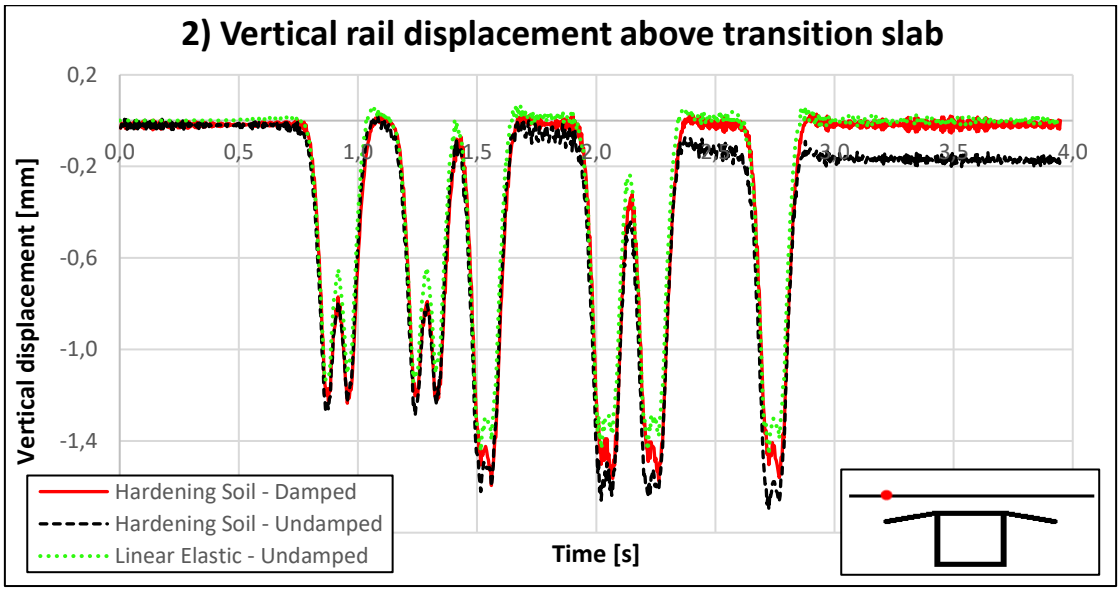

Figure 3.31 – 2) Vertical displacement of the rail when the train loads is passing a node over the slab

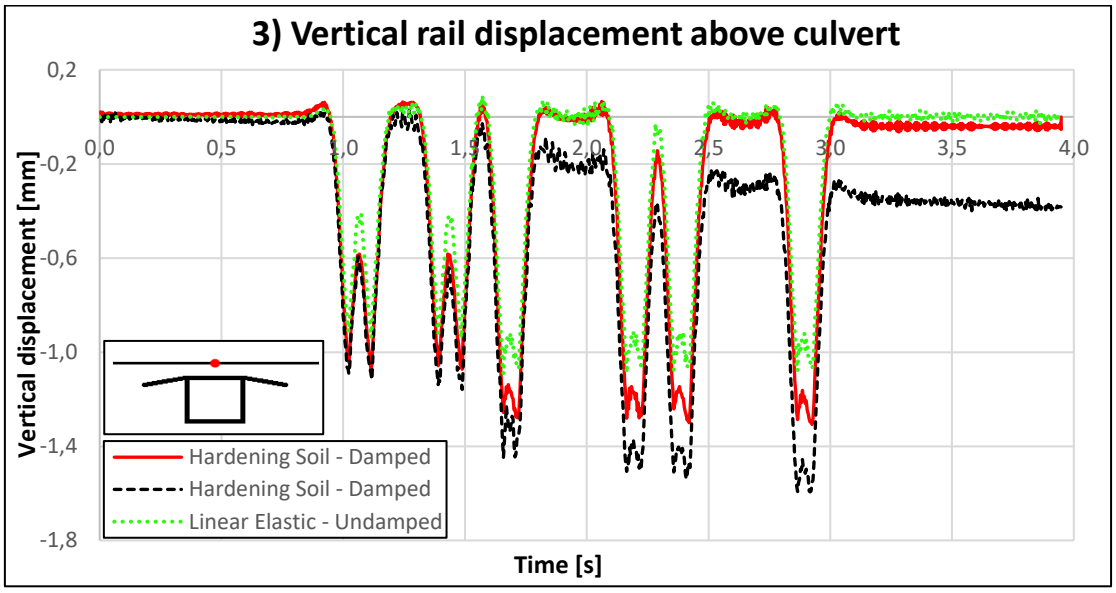

Figure 3.31 – 3) Vertical displacement of the rail when the train loads is passing a node over the culvert

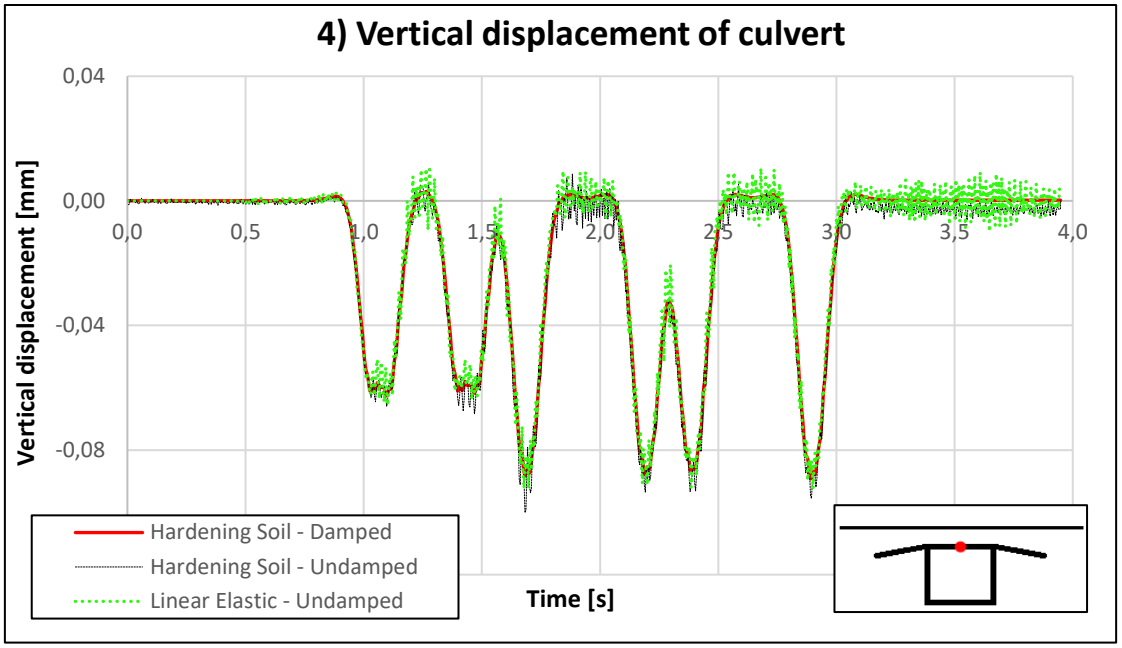

Figure 3.31 – 4) Vertical displacement of the concrete when the train loads is passing a node over the culvert

As the first three plots shows, only the case with an undamped Hardening Soil model creates the so-called «stair». This «stair» gradually becomes steeper as the train loads are closing in on the culvert, suggesting that the problem is also related to stresses.

This problem is not fully understood from that it is removed by introducing damping. But it is thought to be related to tension forces. A way of removing this problem without ruining the model with to much damping is to unhook the «tension cut-of» option in material explorer and run 3-5 train simulations. The problem then tends to converegate towards zero.

At the latest stages of the project it was found that this problem likely were related to the Hardening Soil model not being able to take tension forces. A hypotheses is that the elastic ballast layer on top of the fill with Hardening soil extends when the train loads is passing and, forces the Hardening Soil material to extend which PLAXIS does not allow it to do. The exact mechanisms involved in this problem is considered complex and was not studied in detail, but another way of solving this while also keeping the model undamped, is to unmark the «Tension cut-off» option in the materials mode and run 4-6 train simulations. It seems like this solution enables the model to convergate the problem away after enough simulations.

Doing this forces the material to only take compression which seems to solve this problem without ruining the dynamic behaviour of the model. This approach are not discussed in Appendix A because it was discovered at the latest stages of this project, but is considered a better way of solving this problem compared to using damping.

4 Railway culverts in Norway

This chapter outlines background information on the current practice for building and installing two types of culverts in norwegian railway fills. Design principles, structural and geotechnical considerations and installation procedures will be highlighted for both flexible steel-soil composite and stiff concrete culverts. The main purpose of this chapter is highlight the principles of constructing and designing these structures, which were used as a basis for several of the choices made in the models.

4.1 Construction and design of rigid, square concrete culverts

Concrete as a building material has long ties in Norway which over the years has led to relatively high usage of concrete in structures. From the norwegian railway database *Banedata*, it states that more than 90% of the norwegian railway culverts is built with concrete.

From the fact that concrete culverts is rigid (i.e not exploiting the strenght of the adjecent soil) and is required to be built with transition slabs- a concrete plate which extends out from the top of the culvert into the backfill, it is thought of as a reliable solution in Norway. The slab covers the closest meters from the bridge end, an area which particulary is proun to settlements and historically has caused alot of problems in railway transition zones.

The following section highlights the fundamental structural and geotechnical principles, the current practice for constructing and installing, and examples of installation and backfilling and field.

4.1.1 Transition slab and backfilling

The norwegian railway normal *teknisk regelverk* states that all bearing structures under railways with free span lengths more than 2.0 meter, is defined as railway bridges [2]. The fact that a concrete culvert is rigid and will deform minimally when being subjected to loads makes it unable to exploit the strenght of its surrounding soil, leading to higher internal forces. The structure is therefore way more massive than the flexible variety, but making it completely undependent on the backfill (i.e self-bearing).

Teknisk regelverk specifies that all culverts must as a minimum be designed with corbells and transition slabs which must be connected together through a simple reinforced connection to ensure that the slab can't displace over time. The intention of this system for a railway track is to provide a gradual stiffness transition for the track structure over the embankment to the culvert while also accounting for potential differential settlements which experience suggests may occour between the bridge deck and backfill.

The transition slab is as a result to be installed on the corbell in such a way that the slabs inner section is at the same elevation as the bridge deck, having a 1:5 slope into the backfill. This is both to provide a gradual stiffness transition to the bridge for the track structure and prevent differential settlement the closest meters from the bridge to occour, as shown in figure 4.1.

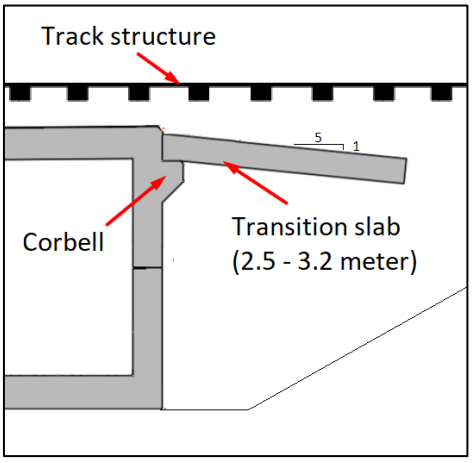

Figure 4.1 – Main principles of the transition slab interacting with the track structure and bridge

Depending on the span lenght of the culvert, the concrete slabmust minimum be 2.5-3.2 meter long and 0.3 meter thick.

For backfilling to the bridge, teknisk regelverk has not specified any distinctive requirements for execution and compaction, and refers further to the same standards used by the norwegian public road administration, *Handbook R761 - Processcode 2* and *NS-3458: Compaction, require-ments and execution.*

The main principles for backfilling against a culvert are summarized in figure 4.2, showing that the backfilling zone is defined by a section extending minimum 1.0 meter out from the bridge, geometrically defined by either a minimum distance H out from the bridge ends or having a maximum sloping angle of 1:2. The backfill zone is further separated into two parts, the inner- and outer zone.

To prevent any risk of damaging the bridge due to vibrations from compaction, the inner zone should be compacted with more caution than the outer, allowing for only using T1-backfill material of crushed rock with maximum stone size being 125 mm and compaction equipment not weighing more than 300 kg [14].

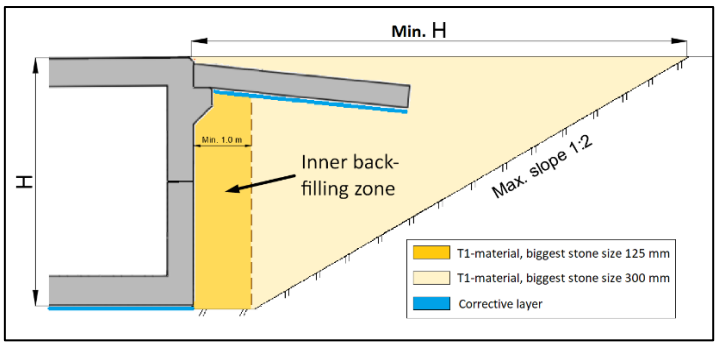

Figure 4.2 – Illustration of the inner- and outer backfilling zone which is differentiated by their distance from the bridge end.

In the outer zone, the norwegian standards allows the use of crushed rock with maximum stone size up to 300 mm and compaction equipment weighing up to 1500 kg. The backfill material here is also to be laid out in layers, being maximum 0.3 meter thick at the inner zone and 0.5 meter thick for the outher zone. Each layer must be compacted with minimum 6 over passing each [14].

According to compaction standard *NS-3458: Compaction - Requirements and execution*, following such procedure for 20/120 mm crushed rock material will normally result in 90-95% degree of compaction (standard proctor) for the inner meter, and about 95-100% degree of compaction for the outer zone.

4.1.2 Function of the transition slab in the transition zone

The transition slab is advantagous for distributing earth pressure as it moves the effect of any live load from the railway track away from the bridge to the end of the slab. This reduces the earth pressure that acts at the bridge end significantly, which decreases the potential of differential settlements. Assuming that the slab rotates freely at the corbell, the effect of any payload will be distributed at the plates support A and B approximately equal. This results in support A taking up about 50 % of the acting load while the other 50% will be distributed into the backfill at support B, as shown in figure 4.3.

There are two common designs used in Norway for the reinforced connection between slab and bridge, shown as option I and II in figure 4.3. Regardless of their differences in design, their intended function is to prevent the slab of displacing of the corbell over time but enabling it to rotate freely. The reinforcement compared to the slabs weight will be so slender that any moment capacity provided by any of the solutions may be neglected and hence, their main function can be assumed to be identical.

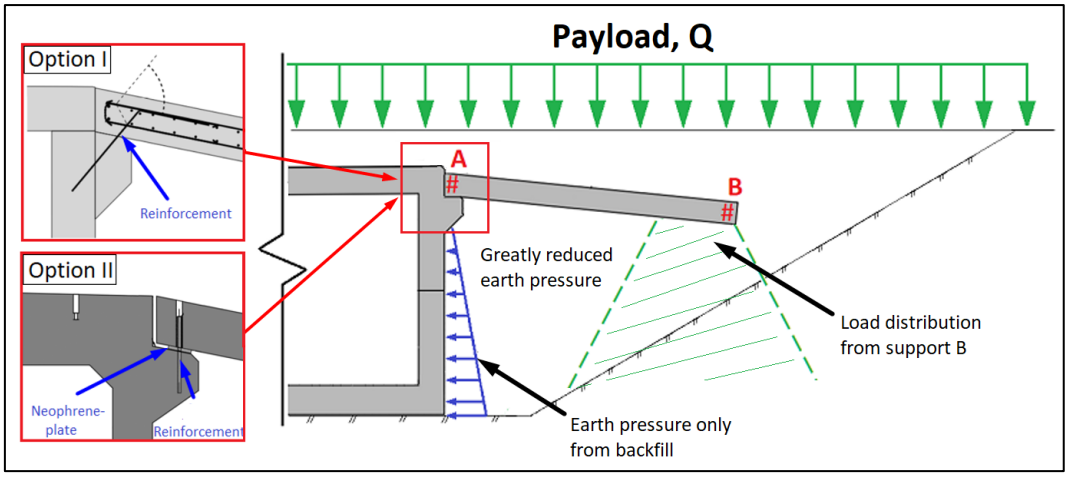

Figure 4.3 – Earth pressure distribution of the transition slab when being subjected to an external payload, showing two options commonly used in Norway for the reinforced connection between slab and corbell

4.1.3 Construction and structural properties

Concrete culverts can in general be built by two different principles, cast-in-place directly at the construction site or pre-cast at a factory. Cast-in-place means that the entire culvert is constructed manually with formwork, reinforcement and concrete at the site while pre-casting means that the culvert is built at a factory normally in elements, then later transported to the site for installtion.

The cast-in-place principle is more flexible in terms of adaptations during construction but with the cost of having longer construction time. Figure 4.4 illustrates both metods.

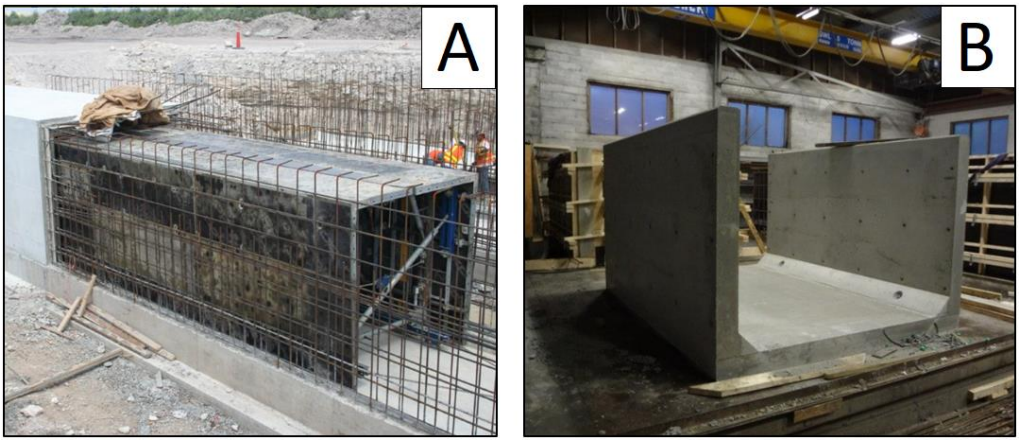

Figure 4.4 – Principles of contructing a culvert with method A) cast-in-place at construction site, and B) pre-cast at a factory in elements (Source: www.doka.com and www.aakrasement.no)

The cast-in-place method gives the opportunity to make the square cross-section of the culvert completely integrated (i.e jointless). For comparison, the standard norwegian element culvert will typically be made of U-elements which is stacked upon eachother longitudinally, creating several joint systems along the culvert. For connecting these elements longitudinally there are different methods depending on the manufacturer which are not discussed further here.

The upper U-element is built directly upon the lower element and has no reinforcement in their connection, making the connection unable to take up any bending moments. This means that the upper and lower elements are only held together by the systems own weight as illustrated by the example in figure 4.5, showing the element culvert that was installed at the Gjøvik railway line in 2018.

When designing railways for speeds above 200 km/h, *Eurocode 1: Actions on structures - Part 2: Traffic loads on bridges* requires that the designer performs dynamic analyses for proving that any risks of resonance or additional vibrations from the bridge is within the tolerable limit.

According the the bridge department from Bane NOR, doing such analyses is much more demanding for the jointed variety compared to the integrated one. It is therefore a common preferance in Norway to construct new railway lines with the use of the integrated variety, especially at higher speeds.

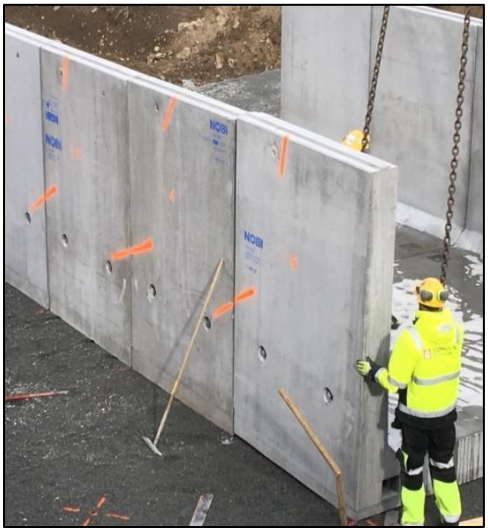

Figure 4.5 – Installation of a element culvert at Gjøviksbanen in 2018, showing the connection between the lower and upper U-element (Source: Støholen Entreprenør AS)

Bane NOR has as a consequence limited jointed culverts to a maximum speed of 200 km/h. This doesn't mean that element culverts with joints is not suited for higher speeds than 200 km/h, but must be designed with caution and other considerations than the integrated case, and is therefore avoided.

4.1.4 Installation

The method of installation at the site will depend on local conditions such as accessibility to the site, if it is to be built in an existing or new railway or the traveling speed at the line. If the concrete culvert variety is to be built in a new railway for example, construction of the culvert might occour directly at its intended location which is advantageous for the cast-in-place method, while installing it in a existing railway line might be more advantageous for the element variety due to its short installation time.

In the case of an existing railway, the culvert will often have to be installed in a very short period of time, typically during traffic stops in between 24-72 hours. Although one of the biggest advantages of the pre-cast element variety is its construction time, installation following both construction principles has been performed in Norway during short traffic breaks.

The procedure of preparing a culvert for installation in a existing railway fill involves removing the track structure, excavating the section of installation and preparing the fundation of the culvert with proper frost protection. A pre-cast element culvert will often be lifted into place element by element with a mobile crane. If the culvert is cast-in-place on the other hand, it will be to heavy to be installed by this method and other installation equipment such as a transportation transformer, a trailer designed for moving heavy structures is often used to move it into place.

Figure 4.6 shows an example of two culvert installations in Norway for illustrating both installation methods, where figure A) shows how the fully integrated, cast-in-place culvert from Hans Edges vei in Lørenskog was installed in 2018 at the Oslo line with a transportation transformer, while figure B) shows how the the pre-cast element culvert at the railway line «Bergensbanen» was installed in 2007 with the use of a mobilecrane.

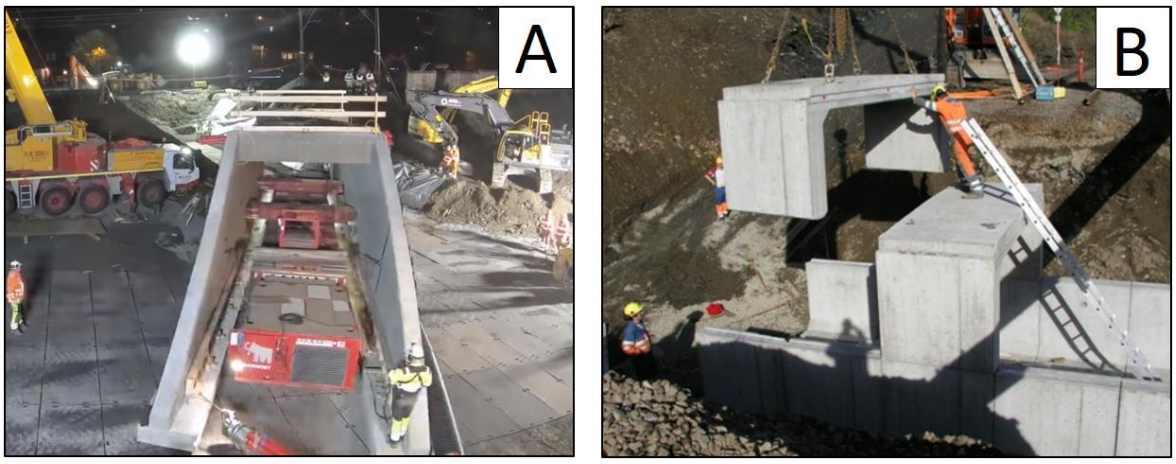

Figure 4.6 – Principles of installation during traffic stops, showing A) the installation of the cast-in-place, fully integrated culvert at Hans Edges Vei in 2018 with a transportation transformer trailer, and B) installation of the element culvert at Bergensbanen in 2007 with a mobile crane (Source: www.PEAB.no and www.Banenor.no)

4.1.5 Backfilling and compaction in field

The culverts fundation is usually created on the basis of requirements set to the frost protective layer which often consists of crushed rock. This layer is compacted with heavy equipment, for example a heavy vibration roller. If the culvert has a closed cross section (i.e not built on a continous plate), a finer corrective layer is placed directly on top of the frost protective layer before the installation takes place, see figure 4.7A).

After the culvert has been installed the backfilling and compaction work will normally start immediately. For backfilling, the normal practice for contractors is to follow the procedures from processcode 2 [14], compacting the closest meter to the culvert with a vibroplate weighing maximum 300 kg and using heavier equipment such as a light vibration roller further out.

Even though the norwegian codes allows to use crushed rock with stone sizes, up to of 300 mm in the outer backfill zone, contractors suggests that using anything above 120 mm in stone size is less practical because of the complications with separating the inner- and outer layers and compacting the larger stones with a relatively small vibroplate. It is therefore more common to use crushed rock ranging in between 20/120 mm for the entire backfill during short traffic stops.

The material is laid out alternately in 0.3 thick layers and compacted with 6 overpassings. Figure 4.7B) and 4.7C) illustrates a close up of 20/120 mm crushed rock material and how a typical compaction sequence of the backfill is performed for a rigid concrete culvert.

Figure 4.7 – Illustration: Backfilling and compaction during different steps of building of the Kilnes element culvert, showing A) the finer corrective layer underneath the culvert, B) a closeup of the 20/120 mm crushed rock material and C) how the compaction work is performed in the different zones (FOTO: Farbu & Gausen AS)

4.1.6 Installation of the transition slab

When the backfilling has reached the corbel level of the culvert, preparation for installing the transition slab will typically take place. This involves laying out the corrective layers and mounting the reinforced connection between the slab and culvert, as seen in figure 4.8A) and 4.8B).

Experience from contractors suggests that it is more practical to keep the thickness of the corrective as low as possible because of the relative steep slope the slab is to be installed with. The slope also makes it hard to compact the corrective layer which may displace during compaction, and a common practice for solving this has been to use the slabs own weight to compress this layer, see figure 4.8C). The end result after installation of the slab will normally look as illustrated in figure 4.8D).

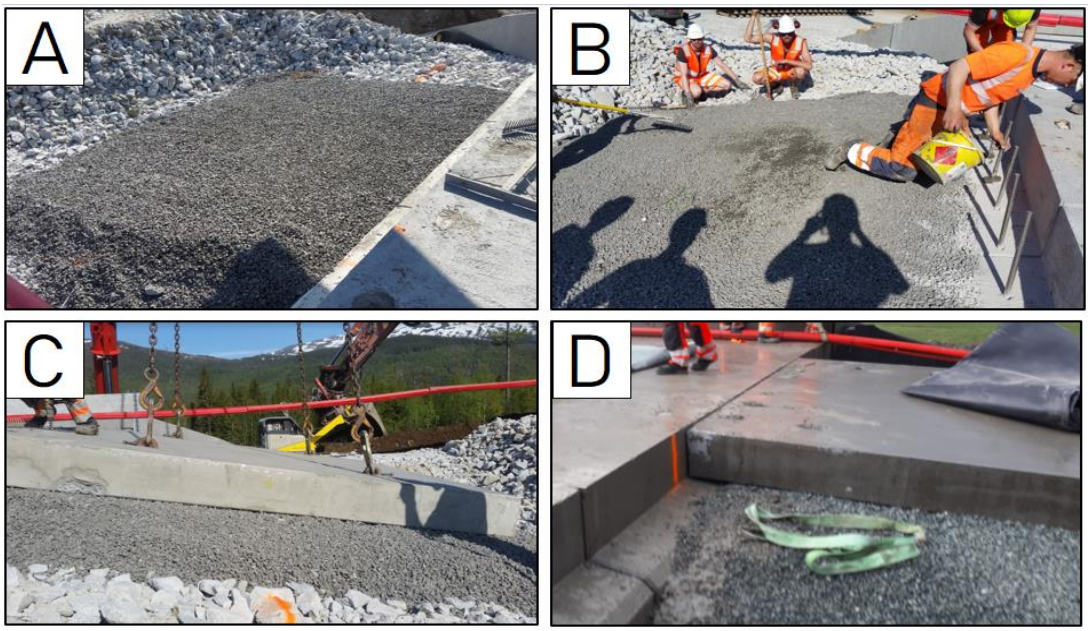

Figure 4.8 – Illustration of the steps wise installation of a transition slab for Svenningsdal culvert in 2016, showing A) the corrective layer under the slab, B) mounting of the reinforced connection to the slab, C) compaction of the corrective layer and D) the finished installation of the slab (FOTO: Farbu & Gausen AS)

4.2 Construction and design of flexible steel-soil composite culverts

According to the norwegian railway database *Banedata*, it states that less than 10% of all the norwegian railway culverts is built of the type flexible Steel-Soil Composite Bridges (SSCB).

There are currently no defined norwegian design method or procedure for designing steel-soil composite bridges, and teknisk regelverk has only required that the soil cover from top of the ballast down to the culverts crown should be minimum 1.1 meter seen from the surface of the ballast. The norwegian railway normal further refers to the specifications and recommendations provided by the Norwegian Public Roads Sdministrations Hand Book (HB), N400 and V220s chapter 12. HB N400 has specified that there is currently no required counter measurement for the transition from embankment to bridge due to the structures circular geometry [15], and recommendations for design based on experience are provided in HB V220 [16].

The following section highlights some of the background theory for how flexible corrugated steel pipes maintains so high bearing capacity by exploiting the strenght of its surrounding soil. The sections also includes recommendations for design from HB V220, and design principles from the Swedish Design Method (SDM). The SDM-method for design is after its last edition considered completely code independent and is often used for design in Scandinavia.

4.2.1 Positive arching, earth pressure distribution and ring compression theory

This section explains how the soil interactions for a flexible steel pipe or arches leads to a advantageous redistribution of the acting earth pressures on the structure. Some of the background theory is the basis behind the principles for design in handbook V220 and SDM, and will involve both a combination of arching and earth pressure theory. Arching theory was develeoped by Jan Vaslestad in 1990, and is now a part of the swedish design in the SDM-manual [19].

In general, SSCB has much lower stiffness in bending but higher in ring compression than the stiffness of the surrounding soil. This leads to two advantages, a favourable redistribution of the vertical to horisontal earthpressure and positive arching. When considering the effect of arching, the overburding vertical earth pressure distribution can be expressed as

$$\sigma_v = N_A * \gamma * h_c \qquad \text{(Eq. 4.1)}$$

where

N_A being the archingfactor for redistribution of the overburding earth pressure
γ being the soils unit weight
h_c being the cover height above the culvert

On square, stiff culverts recommended N_A factors from HB V220 range between 1.2-1.35, while for flexible steel pipes less than 1.0. The magnitude of the N_A factor in the flexible case are governed by the pipes ability to deflect and how the soil rearranges when the structure is exposed to live loads [16]. These assumptions are based on several field measurements which has shown that the vertical earth pressure on top on a stiff pipe, in fact will have a greater magnitude than the soil prisms own weight above the structure, but for flexible cases this condition is reversed as illustrated in figure 4.9A) and 4.9B).

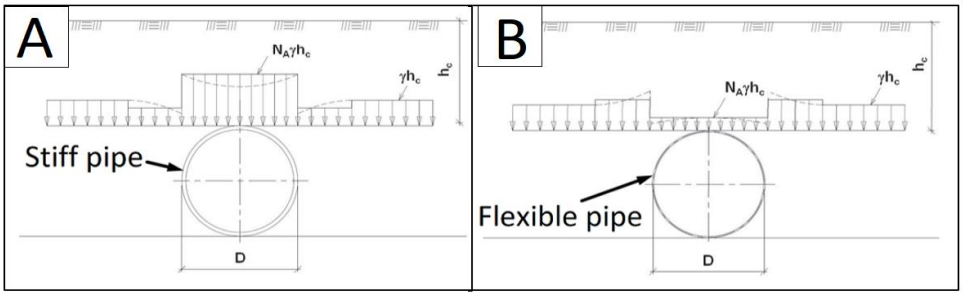

Figure 4.9 – The vertical earth pressures on top of a pipes top arch in the case of A) a stiff pipe and B) A flexible pipe (Modified after HB V220, Statens Vegvesen 2018)

The characteristics of how a flexible pipe bends and interacts with its surrounding soil can be asseset by a stiffness ratio [17,18], expressed as

$$n = \frac{EI}{MD^3} \quad \text{(Eq. 4.2)}$$

where

M being the confined modulus (i.e oedometer modulus) of the soil
D being pipes span lenght
E being the youngs modulus of the pipe
I being the moment of intertia of the pipe

From equation 4.2, table 4.1 shows how the characteristics of the pipe-soil interaction can be ranged into three categories, where ranges of the n-factor bellow 0.1 is characterized as flexible while a n-factor above 1.0 characterized as rigid. As the following section will show, the characteristics defined from the n-factor will either contribute or aggrevate the soil covers effect on a pipe in terms of arching.

Table 4.1 – Characteristics of a pipes stiffness on the basis of the n-factor

Range	Characteristics
n < 0.1	Flexible
n = 0.1 – 1.0	Intermediate
n > 1.0	Rigid

Vaslestad when developing the arching factor stated that on the basis of several field tests, if a pipes soil interaction had a stiff characteristic (n > 1.0), shear stresses in the soil would cause the load on the pipe to be greater than the weight of the soil prism above. The uposite would be the case for a flexible pipe (n < 0.1) as this would cause the shear stresses to reduce the effect of the weight above the culvert. This effect of either contributing or aggravating the vertical overburden pressure was labeled as positive or negative arching [17].

The arching effect comes into play from the fact that the soil above the culvert wants to settle differently in respect to the soil at the free embankment. The difference in settlement rate between these two soil bodies leads to a plane of vertical shear stresses at the edges of the pipe, see figure 4.10.

If the settlement rate in the soil body above the culvert is lower than the settlement rate of the soil body in the free embankment, negative arching occours as the vertical shear stresses from the embankment zone tries to «pull down» the soil prism above the culvert, contributing to its weight. Without any compressive material above a stiff culvert, negative arching will therefore increases the earth pressure acting on the culvert as illustrated in figure 4.10.

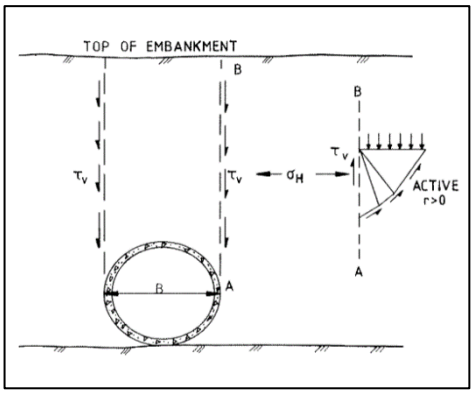

Figure 4.10 – Illustration: Shear stresses at the edges of a stiff pipet caused by difference in settlement ratio (Modified after Jan Vaslestad, 1990)

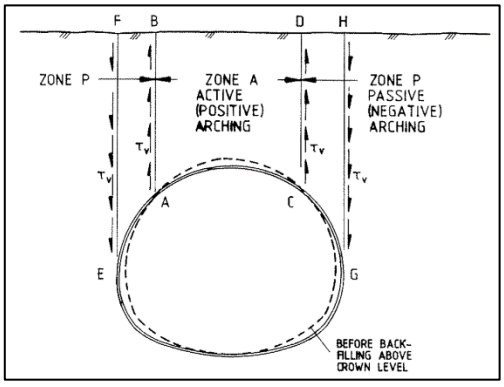

Figure 4.11 – Shear stresses at different planes over a flexible pipe caused by a combination of vertical deflections and difference in settlement ratio (From Jan Vaslestad, 1990)

The uposite will be the case for a flexible pipe, as the settlement rate will be higher above the culvert compared to the free embankment, causing upward shear stresses. These shear stresses will reduce the effect of the soil prisms weight on the pipe.

It is important to highlight that this effect only occours at a specific zone of the top arch, where negative arching still can occour at the edges of the culvert because of the outher section of the pipe being pushed upwards when the middle section is being pushed down, causing the settlement rate to be higher at this part of the pipe. The plane which separates the positive- and negative arching shear planes is governed by how the pipes changes shape when being compressed [17], as illustrated in figure 4.11.

The resulting shear stresses from this phenomenom will as a rule of thumb always cause a reduction of the resulting soil prisms weight above the culvert as long as the culverts has a flexible interaction with the adjecent soil (i.e n < 0.1). Increasing the soil cover will therefore contribute to this effect considerably, making larger soil covers very advantageous for flexible culverts compared to rigid ones.

The arching factor can according to Vaslestad, be formulated after Janbu's friction number [17,33], as

$$N_A = \frac{1-e^{-A}}{A} \quad \text{(Eq. 4.3)}$$

with

$$A = 2*S_v*\frac{hc}{D} \quad \text{(Eq. 4.4)}$$

and

$$S_v = |r|*\tan\rho*K_A = \frac{r*tan\rho}{\left(\sqrt{1+\tan^2\rho}-tan\rho\sqrt{1+r}\right)^2} \quad \text{(Eq. 4.5)}$$

where

N_A being the arching factor
S_v being the friction number developed by Janbu. N in 1979
D the culverts span lenght
h_c being the height of cover
tanρ being the mobilized friction
r being the roughness ratio
K_A being the active earth pressure coefficient

According to Vaslestad [17], the n-factor could also be used to express how a pipes flexible behaviour affects the redistribution of earth pressures, as

$$K = \frac{0.18+n*K_A}{0.18+n} \quad \text{(Eq. 4.6)}$$

The K-coeffecient from equation 4.6 will vary after how the stiffness of the pipe affects the interaction with the soil (assuming n < 0.1), where flexible pipes often leads to K ≈ 1.0 and rigid ones (with n > 1.0) often leads to a K which is in between K_A and K_0 (rest pressure) [17], see figure 4.12.

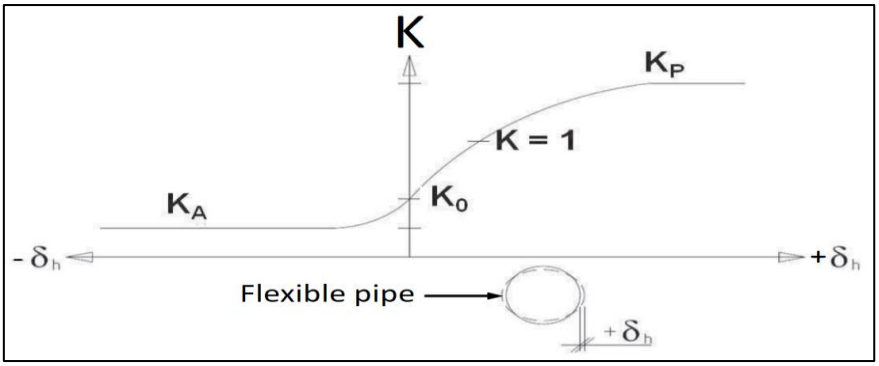

Figure 4.12 – Principal diagram on how the horisontal earth pressure coefficient for a flexible circular pipe changes by how the pipe is deflecting (Modified after Statens Vegvesen 2018)

According to HB V220, from the classic expression for transforming the vertical to horisontal earth pressure, the horisontal earth pressure against a flexible pipe can be expressed as

$$\sigma_h = \sigma_v*K \quad \text{(Eq. 4.7)}$$

where

σ_h being the horisontal earth pressure
σ_v being the vertical earth pressure
K being the earth pressure coeffecient on the side of the pipe

When n < 0.1, equation 4.7 suggest under the assumption of K ≈ 1.0 that the vertical earth pressure is equal to the horisontal. Some field measurements has reported that the horisontal earth pressure can even be higher than the vertical, reaching almost full passive state. A common practice is to assume that the horisontal earth pressure is equal to the vertical in cases of flexible pipes [16-18].

In the study of sectional forces around a closed pipe, it has been found that most loads applied on a burried culvert, except during backfilling, is taken in ring compression. The original ring compression theory was developed by White. H.L an Layer J.P in 1960, and is background theory in the original SCI-method developed by Duncan which stated that even if steel pipes are flexible in bending, they are more than 25 times stiffer than the backfill in ring compression [18]. Modifications of the original SCI-method is still being used in the swedish design [19].

Ring compression theory is only valid for closed flexible pipes and soil covers higher than 1/8 of the pipes diameter [17]. The theory states that once a flexible pipe has been installed, the thrust on the wall is nearly constant around the entire circumferentia. profile which reflects the overburden pressure. From the theory, the overburden pressure is simplified to a uniform pressure (p), which roughly reflects the overburden pressure plus any live loads, as

$$p = \gamma H + q \qquad \text{(Eq. 4.8)}$$

where

H being the depth of cover
γ being the unit weight of the soil
q being the equivalent live load

According to ring compression theory, the circumferential thrust can be calculated as

$$T = p\frac{D}{2} \qquad \text{(Eq. 4.9)}$$

Assuming that the circumferential thrust remains constant, the soil pressure p at any point along the profile can be written as

$$p = \frac{T}{R} \qquad \text{(Eq. 4.10)}$$

where

T being the circumferential thrust
D being the diameter of the pipe
R being the radius of curvature at the point under consideration

Equation 4.10 shows that the soil pressure is proportional to the radius of the pipes curvature, where a lower radius yields a higher soil pressure and reversed in a latter case.

The soil pressure distribution around the pipe can thereby be illustrated for different profile shapes on the basis of the change in their sectional radius. Figure 4.13 shows how the soil pressures around three pipe-profiles will vary depending on their radius at any given section.

It is shown that for case A the soil pressure remains constant, while for case B and C the relative low radiuses in their corners leads to earth pressure concentrations. This concentration is especially severe in the corners of case C, the pipe-arch.

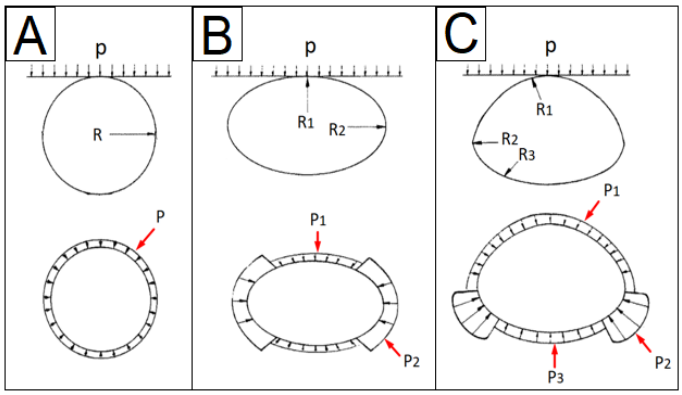

Figure 4.13 - Illustration: The soil pressure as a function of radius for A) a circluar pipe with constant radius, B) an elliptic pipe and C) a pipe arch with varied radiuses (Modified after Jan Vaslestad, 1990)

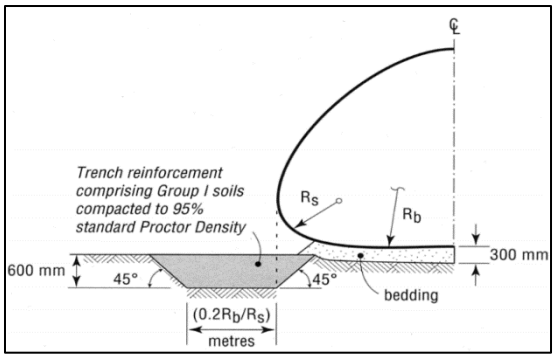

Figure 4.14 – Illustration: Recommendations for constructing a reinforced side trench (Modified after HB V220, 2018)

From a practical standpoint, HB V220 recommends to always ensure that the side trenches of a pipe arch has sufficient capacity as this in worst case can lead to total collapse of the culvert. This phenomena can be explained by the classic ring compression theory which showed that lower radiuses in the corners of the culvert leads to stress concentrations.

Where the ground condition is especially poor, HB V220 highly recommends to always construct a reinforced trench to provide sufficient soil support with the principles shown in figure 4.14.

From these formulations it can therefore be stated that when a flexible pipe deflects, it will exploit the strenght of the surrounding soil by bending in such a degree that it leads to a significant decrease in the bending moments that acts on the pipe itself which is rather taken in ring compression. The uposite is the case for a stiff pipe because it will deform minimally and distribute the overburden pressure poorly, increasing the acting bending moments that acts on the structure considerably.

4.2.2 The Swedish Design Method (SDM), principles for design

This section highlights key points from The Swedish Design Method (SDM) in respect to the previous section and the problem formulation in this project. The SDM was originally developed by Lars Pettersson in 2000 under the initiative from the Swedish road administration, which at the time saw an demand for a more defined method particulary for traffic loads, larger spans and smaller cover heights.

The calculation methods presented in SDM is based on two main theories with some modifications, that is the principles from Duncans Soil Culvert Interaction method (SCI-method) for calculating forces and moments around the culvert [18], and the theory for buckling calculations described in the Klöppel and Glock method from Germany.

Modifications that has been introduced in SDM for the SCI-method involves:

- Reduction of normal forces around the pipe at larger cover heights, following the principles of arching developed by Jan Vaslestad
- Reduciton of load-bearing capacity, taking into account second order theory
- Methods for calculating soil modulus, based on Lars Andrèasson laboratiry findings in 1973

The Swedish Design Method has during development and later been verified by comparing calculations to several full-scale from [19]. The method also provides ultimate capacity calculations using either the national or European codes, making the standard considered code independent.

Similar to the n-factor used by Duncan and Vaslestad [17,18], the relationships between stiffness of the soil and conduit is also formulated in the swedish design by a flexibility number (λ_f). The flexibility number in SDM is defined similar to eq. 4.2, but dividing the soil modulus and span lenght (Mr^3) by the bending stiffness of the pipe instead of the uposite. The quantity is formulated similar to the n-factor, but with a range between $100 \leq \lambda_f \leq 50000$ for flexible pipes [19].

The modified version of Duncans SCI-method in SDM, includes the arching factor which allows a reduction in sectional forces. The modification also involves a method for estimating the tangent modulus of the backfill compared to the one developed by Duncan in 1979. The SDM-manual provides two methods for calculating the soil tangent modulus, that is Duncans «Method A» and the modified «Method B» from Lars Andreassons laboratory findings.

Method A was developed on the basis of characteristic curves provided from FEM-simulations [18], which stated the secant stiffness of any backfill material can be expressed as

$$E_{soil,k} = 1{,}3*1{,}17^{(RP-95)}*[1.25*\ln(h_c + H/2)+5.6] \quad \text{(Eq. 4.11)}$$

where

$E_{soil,k}$ being the characteristic secant modulus for the backfill material
RP being the degree of compaction corresponding to a standard proctor
H_c being the height of cover
H being the distance from the culverts neutral axis to its crown

According to Duncan, the secant modulus represents the soil stiffness at first time loading, i.e after compaction. This quantity is representative as an average stiffness of the entire backfill [18]. Duncan also stated that the secant modulus should be considered a «first time loading stiffness», and yields very conservative values if comparing it to a stiffness as a result from repeated loading.

It is well known that the simplified formulation from Duncan leads to very conservative values for soil stiffness, but is still considered valid in SDM for estimatiing a tangent modulus for design. This is due to the low amount of input parameters requred to calculate the stiffness.

When developing the SDM, a second and more complex method was developed from modifying Janbu's formulation of soil stiffness [9, 19] from stress dependent soil modulus to soil gradation and initial void ratios.

It was found from laboratory tests in Sweden that the particle size distribution and the relative degree of compaction is the dominating factors for soil stiffness [9]. From these findings the soil modulus number, stress exponent and angle of friction was expressed by soil graduation, initial void ratio but also including the arching factor [9], as

$$E_{soil,k} = 0.42*m*100*k_v*\left(\frac{(1-\sin(\varphi k)*\rho*Sar*(hc+\frac{H}{2})}{100}\right)^{1-\beta} \quad \text{(Eq. 4.12)}$$

where

$E_{soil,k}$ being the characteristic tangent modulus
m being the modulus ratio
k_v being a notation in the tangent modulus
φ_k being the characteristic angle of friction
S_{ar} being the arching factor
β being the stress exponent

with

$$m = 282*C_u^{-0.77}*e_0^{-2,83} \quad \text{(Eq. 4.13)}$$

$$e_0 = \frac{\rho s}{\rho} - 1 \quad \text{(Eq. 4.14)}$$

$$\beta = 0.29*\log\left(\frac{d50}{0.01}\right) - 0.065*\log(C_u) \quad \text{(Eq. 4.15)}$$

$$k_v = \frac{1-v-2v^2}{1-v} = \frac{\sin(\varphi k)*(3-2\sin(\varphi k))}{2-\sin(\varphi k)} \quad \text{(Eq. 4.16)}$$

$$\varphi_k = 26° + 10*\frac{(RP-75)}{25} + 0.4*C_u + 1.6*\log(d_{50}) \quad \text{(Eq. 4.17)}$$

where

C_u being the uniformity coefficient
e_0 being the initial void ratio
ρ_s being a referance number for density, at 26 kN/m^3 according to SDM
ρ being the occouring density of the backfill
d_{50} being the partice size distribution at 50% passing percentage

In general, method B returns higher values for the soil secant modulus compared to method A but with the cost of requiring more information on the backfill material. Similar to Duncans formulation in method A, method B represents the average soil tangent stiffness at first time loading in the backfill, labeled as «engineered soil» in figure 4.15.

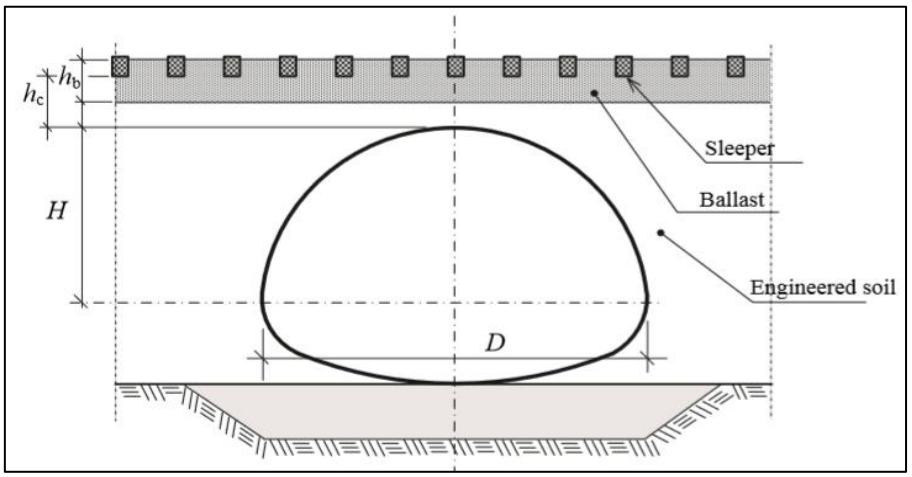

Figure 4.15 – Definitions used when calculating soil secant modulus for the engineered soil in SDM

When considering the manual in respect to train speed, it is important to highlight that the design from SDM does not apply for railways with line speeds exceeding 200 km/h. This is a limitation rather set by the european codes than the manual itself as it required that all bridges under railway lines with operating speeds above 200 km/h, is to be proven analytically not to pose any risk of resonance or additional vibrations.

No methods currently exist for performing such dynamic analyses for flexible steel-soil composite bridges and is under research in Sweden. As a full scale test from 2012 suggested, the structures interacting nature with its surrounding soil makes structural dynamic analyses based on beam theory less applicable and controlling acceleration levels for these structures is more likely to be related to soil dynamics [20].

4.2.3 Structural properties of Steel-soil composite bridges

Steel-Soil Composite Bridges (SSCB) are in principle built with a low bending stiffness (EI) compared to the axial stiffness (EA). This enables the structure to behave flexible while maintaining a high circumferential capacity, exploiting the strenght of its surrounding soil by bending.

The properties of the steels corrugation is defined by the distance between each wave in the corrugation (L), depth (h) and thickness of the steel (t) as shown in figure 4.16.

There are several corrugations used in todays marked, but most bridges with diameters higher than 2.0 meter, are either built with the 152 x 51 mm corrugation, the 200 x 55 mm (Multiplate) or 381 x 140 mm (SuperCor) corrugation. In 2011, an even deeper corrugation was developed with geometric properties 500 x 237 mm, named UltraCor. Figure 4.16 shows a comparison between three different corrugations.

The bending stiffness of a flexible steel pipe is governed by its corrugation, where a deeper corrugation yields a higher bending stiffness. SuperCor for example, has 9 times higher bending stiffness than the relative shallow 152x51 mm corrugation [21], assuming the same steel thickness.

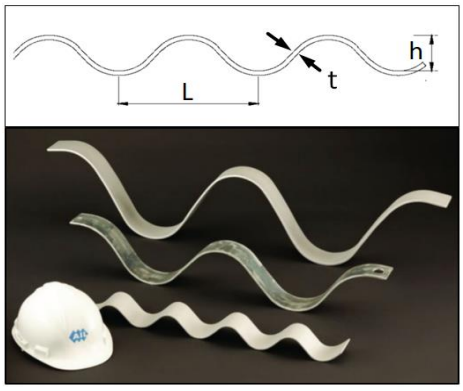

Figure 4.16 - Comparison between UltraCor, SuperCor and the 152x51 mm corrugation profile (Modified after Williams et al., 2012)

However, increasing the thickness (t) of the steel will for any corrugation increase the structural capacity of the steel. When a certain span width is desired, limitations of the given corrugation is rather set by the manufacturers which only delivers a certain thickness range for a given corrugation. This has led to the common practice of moving towards bigger corrugations as the span width of a flexible steel-soil composite bridge increases.

On norwegian railways, span lenghts for flexible SSCB rarely exceeds 8 meter. This has led to often using the MP 200 x 55 mm corrugation which according to norwegian suppliers such as Viacon can be delivered with steel thickness up to 8.0 mm [22].

The SDM-manual offers in total 8 different shapes of steel-soil composite bridges, consisting of both fully closed pipes, open arches and a box variety. For a certain shape type to be defined there is a certain relationship between the different radiuses along its profile that must be forfilled for the design steps in SDM to be valid. But this doesn't mean that the design from the manual is not valid for culverts that deviates from the purposed profiles, but must be analyzed with special considerations in order to apply [19]. The 8 profile types covered in the manual is shown in figure 4.17.

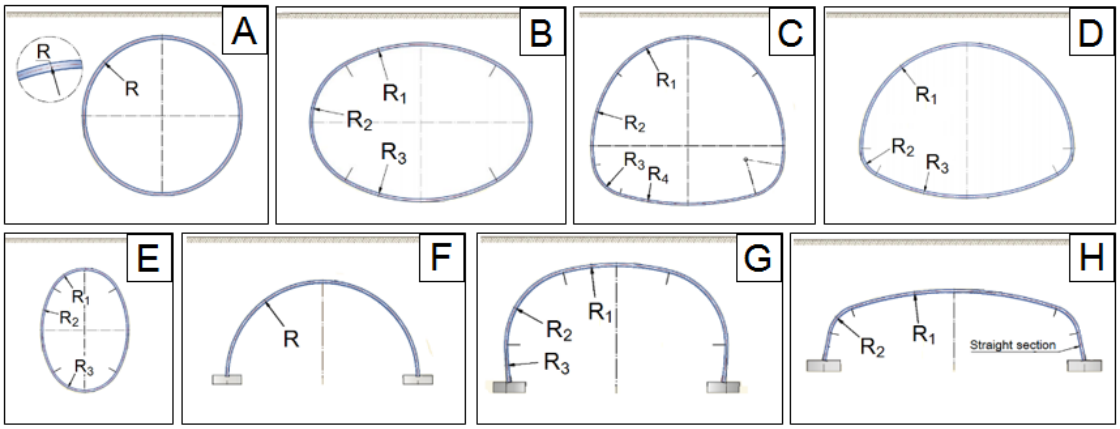

Figure 4.17 – Illustration of the 8 different profile types covered by the SDM manual, showing A) a circular pipe, B) a horisontal ellipse, C) and D) a pipe arch, E) a vertical ellipse, F) an arch with a signle radius, G) an arch with two or three radiuses and H) a box culvert (From Petterson. L and Sundquist. H, 2014)

The box-type is different from the other varieties as it is more square like. It is designed for cases where especially low cover heights in combination with larger spans are desired, putting more demand the structures steel. For severe cases and using this variety, the corners or crown area of a box culvert can be stiffened by adding reinforced ribs which has proven to increase the structures capacity considerable [19].

In Poland where steel-soil composite bridges are often used, quasi-static field tests with using a single locomotive showed that for the box culvert Prabuty, measured vertical deflections at the crown in the order of 3.5 mm. The bridge was built with SuperCor, had a span lenght of 8.8 meter and a total cover height of 0.95 meter [23].

The other categeories (A-G in figure 4.17) has a more circular characteristic than the box variety. For these shapes, it is normally not very expedient to distinguish between the open or closed varieties because of their similarities in how they interact at the top shelf with the soil. Field tests has shown that it is actually the top shelf of a flexible steel arch that plays the most important role in this interaction as two field mea-surements in Poland concluded [24,25].

4.2.4 Installation

When the diameter or lenght of a SSCB reaches a certain limit and it is not possible to ship the entire culvert as a whole, a common practice is for the steel plates to be shipped to the construction site in bundles, which is bolted together plate by plate into sections. These sections are then mounted together, completing the entire pipe as shown in figure 4.18.

Figure 4.18 – The merging process of an SSCB, showing A) the steel plates delivered in bundles, B) bolting of the steel plates together in sections and C) sections being mounted together (Modified after Viacon, 2015)

Depending on if the bridge is to be built in a new or existing railway, the pipe can either be constructed at its intended position or nearby for later installation. In existing railways the culvert will typically be prepared in advance as the culvert will often have to be installed during a 24-72 hour traffic break.

One of the biggest advantages with steel-soil composite bridges under installation is its relatively low weight, which decreases the need for heavy equipment but also reduces its installation time. Figure 4.19 shows how the Solheim underpassing was installed in 2009, during a 48 hour traffic break at Ofotbanen railway using only two small wheel loaders when moving it into place.

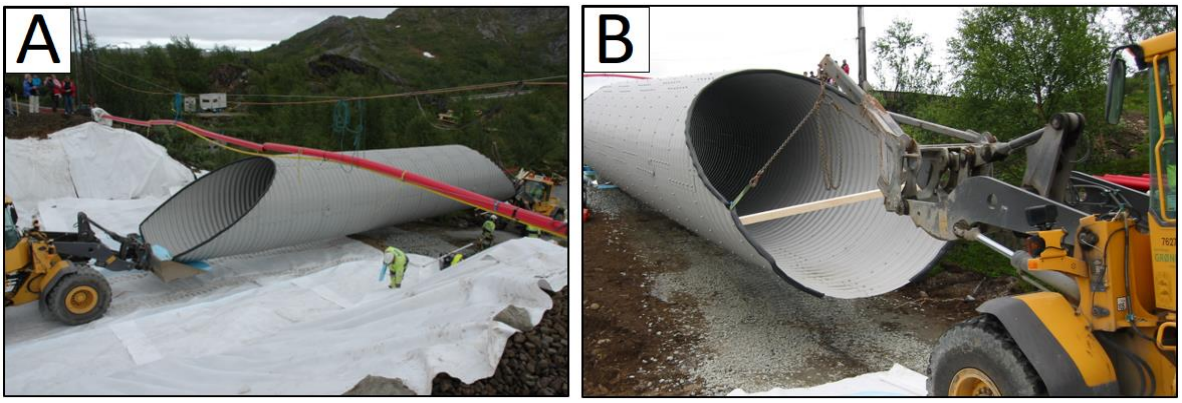

Figure 4.19 – Installation of Solheim culvert in 2009 with wheel loaders at Ofotbanen railway line. The culvert had a circular cross section and a diameter of 3.0 meter (Source: Viacon Norway)

When the size of the culvert becomes large another, will another alternative be to lift the culvert into place with a mobile crane. This was for example the case for the norwegian culvert «Sel Fv. 438» which was built as a road underpassing in 2002. The culvert was lifted into place in one single operation, see figure 4.20.

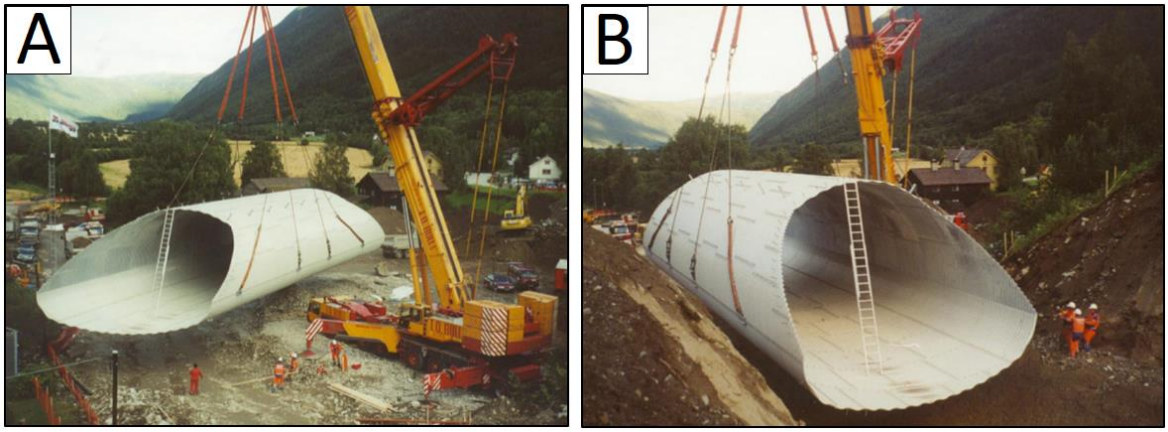

Figure 4.20 - Installation of Sel Fv. 438 pipe arch culvert in 2002 with a mobile crane under the Dovrebanen railway line. The culvert had a span lenght of 9.6 meter (Source: Jan Vaslestad)

4.2.5 Backfilling and compaction

It is important to distinguish the backfill against a flexible pipe and the backfill against rigid one. The backfill surrounding a flexible pipe must be considered as a part of the structure from the fact that a flexible pipe gains most of its capacity from the surrounding soil [19]. Years of experience has shown that it is the quality of the backfill that mostly will govern the long term behaviour of an SSCB, which has led the Swedish design manual to specify that for the manual to apply, certain procedures and tolerance limits must be followed and forfilled when backfilling in a certain zone around the culvert.

Figure 4.21 arederiven on the basis of the specifications in the SDM and recommendatios from HB V220, which summarizes the fundamentals for backfilling around a flexible pipe. As with the rigid self-bearing culvert, the fundation underneath a flexible pipe should be prepared on the basis of the frost protection. This zone is defined after the pipes biggest diameter (D), and is to be built by layers of well compacted crushed rock which must reach a minimum frost depth (Z_f) and 98% Standard proctor.

Before the culvert can be installed, a additional layer must be placed out as a bedding for the culvert. This layer should consist of a finer, uncompacted material which is adapted to the culverts bottom geometry, enabling the culvert to settle into the bedding over time.

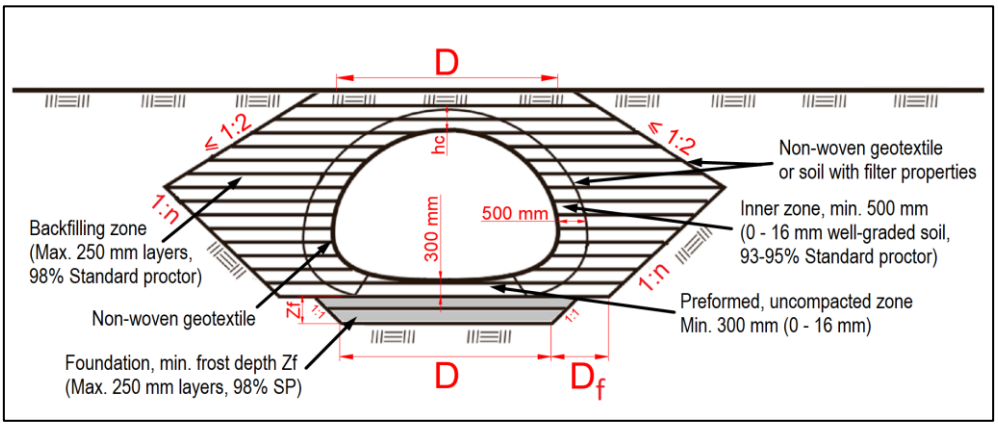

Figure 4.21 – Principle sketch: The main principles for backfilling at a flexible steel-soil composite bridge (Modified after Petterson. L and Sundquist. H, 2014 and Statens Vegvesen, 2018)

The backfill on the sides of the pipe is divided into two parts, an inner- and outer zone. Geometrically speaking, the outer zone is defined by an inclination 1:n, which extends out a distance (D_f) from the end of the frost protective layer. The extension (D_f) is according to the SDM-manual defined as min{D/2 ; 3.0m}, were the slope 1:n represents the soil volume defined only after the strenght character-istics of the material used in the backfill.

The inner zone must consist of finer material (0 – 16 mm), extending minimum. 500 mm out from the culvert around its circumferential profile, ensuring that the soil-culvert interaction maintains over time without damaging the culvert by larger stones of the backfill.

Figure 4.22 – Illustration: Soil blowing on the sides of Haugenstua pipe culvert in 2008 (Source: Gjermnudshaug Gruppen)

A especially challenging section to access and compact has been the bottom part on the sides of the culvert. For smaller profiles with diameters less than 4.0 meter, it has for a long time been considered sufficient to adapt a preformed, uncompacte layer at this section [16].

For larger profiles, HB V220 suggests to perform additional measurements for adapting the bedding of the culvert to its curvature, such as premading a template on the basis of the pipes geometry. This approach is now considered discontinued, and more modern practices is to either compact the sides by hand-stamping or to blow soil into the sides with a pressure hose, as shown in figure 4.22.

The SDM-manual has distinguished a loads effect on a culvert on the basis of what material is being used for the backfill and soil cover. This can better be understood from for example Vaslestads formulation of arching where a higher angle of friction causes a higher friction number Sv, and hence a lower arching factor. This means that if using a crushed rock material with a higher angle of friction comapred to a gravel for example, it will be advantogous for the arching effect (i.e lower arching factor) and hence, the sectional forces of the pipe will be reduced.

For backfilling, it is a common practice in Norway to use 20/120 mm crushed rock for the outer zone, while either use sand, gravel or finer crushed rock ranging in between 0/16 mm for the inner zone. Figure 4.23 shows two examples were sand and fine crushed rock material were used for the inner section.

Figure 4.23 – Backfilling at A) Solheim culvert in 2009 and B) Ydsedal culvert in 2018. For case A) sand were used as the inner layer while for case B) a finer crushed rock were used. In both cases crushed rock ranging in between 20/120 mm were used for the outer zones (Source: Viacon Norway and Farbu & Gausen AS)

As with cases of a rigid culvers, the regulations for compaction are distinguished on the basis of an inner- and outer backfill zone. The norwegian guidelines in HB V220 states that each layer must be laid out alternately on both sides of the culvert being maximum 250 mm thick, where the difference between the fill height on each side of the pipe should not exceed one layer thickness.

Recommendations from HB V220 states that the allowed compaction equipment should be distinguished on the basis of what material is being used in the backfill.

Table 4.2 shows that if crushed rock is being used in the inner zone, the compaction equipment is limited to weighing maximum 200 kg to prevent any damages on the pipe when compacting.

Table 4.2 - Compaction limitations based on the backfill material used in the inner and outer zone (After Statens Vegvesen 2018)

	Compaction (Inner zone)	**Compaction (Outer zone)**
Crushed rock as backfill material	Vibroplate, 100 – 200 kg	Drum roller, 10 – 15 tonn
Sand/gravel as backfill material	Vibroplate, 200 – 500 kg	Drum roller, 10 – 15 tonn

During backfilling, the pipe will start to deform because of the high earth pressures caused by the compaction. This will lead to the top point (the crown) of the pipe to start displacing upward. Backfilling on the sides of the culvert is considered the most crucial part since the vertical earth pressure from the overfilling will push the crown at the top arch to displace back into its intended position again. Both HB V220 and the SDM-manual has specified that the crown area of the culvert must not displace more than 2% of the pipes total diameter during backfilling.

As figure 4.24 shows, the inner and outer backfill zone must be separated in such a way that it maintains a filter criteria. From the fact that the material of the inner zone is considered permable, it is not considered necessary to use any additional geotextiles between these layers. This is because of the complications with compacting the transition between an inner- and outer zone.

The part where the risk of mixing between the inner and outer zone is highest, is the top arch of the culvert which also is the section that is most affected by live loads [19]. Figure 4.24 illustrates a common practice of separating the inner and outer zone on the top arch of the pipe with a non-woven geotextile for reducing any risks of largers stones reaching the culvert. The 20/120 mm crushed rock material is thereafter placed directly on top of the geotextile.

Figure 4.24 – Illustration: Using a non-woven geotextile as a separation medium for the upper top arch of a pipe, reducing the risk of materials from the inner and outer zone to mix (Source: Farbu & Gausen AS)

The SDM-manual specifices that the same material used for the outer sections, must also be used as soil cover. The absolute minimum soil cover required, is 0.5 meter. In order to retain this cover height for a culvert under a railway fill, an additional 0.5 meter (total 1.0 meter) is required to ensure that the required soil cover (i.e 0.5 meter) is retained during maintenance. Teknisk regelverk has specified that the minimum distance from the top of a sleeper down to the crown on a flexible steel pipe must be minimum 1.1 meter [2], which is similar to SDMs 1.0 meter requirement [19].

If the swedish design is done accordingly and the backfilling properly executed, the interaction between a flexible culvert and soil can provide a large load-bearing capacity even if the soil cover is at its minimum [19]. The influence of traffic loads on the pipe however, will largely dependen on the soil cover since lower soil covers causes larger influence from live loads to be greater on the pipe.

5 Culverts in plane-strain

This chapter outlines the main modelling principles for building flexible and rigid culverts in PLAXIS 2D. Based of the descriptions of chapter 4, both structures are assumed to be fully integared where the flexible culvert will have the geometry of a closed pipe and the rigid variety a closed square. Both structures are modelled after the principles of plane-strain, where an example for defining structural input parameters are given.

5.1 Modelling of square concrete culverts with transition slabs

Based of the principles of plane-strain, the concrete culvert is modelled with elastic plate elements as a fully integrated square cross section. The slab is installed at the top point of the culvert as a plate element, and given the geometric properties required in Bane NORs regulations [2].

By assuming a fully integrated cross section, it is possible to neglect any extensive considerations that might have followed the jointed element variety, see section 4.1.3. It is assumed that the joints between elements for the sake of the transition zon are not factors that has a mentionworthy influence.

For the model to be as accurate as possible, it is a prerequisite that the track superstructure is centered on the transition slab. By only transforming the section of the culvert which has a slab into plane-strain, it can be stated that since the track is centered above the slab the load distribution will also be symmetrical, see figure 5.1A)

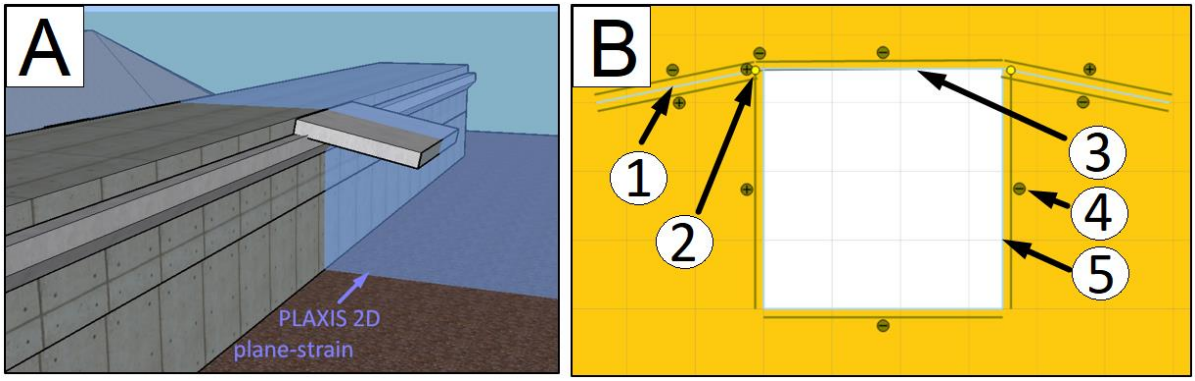

Figure 5.1 -Modelling principles for a square concrete culvert, showing A) A 3D sketch of the plane in PLAXIS, and B) when the plane is transfered into PLAXIS showing ① the transition slab, ② the freely rotating hinge between culvert and slab ③ the roof/bottom elements, ④ the interfaces outside the culvert and ⑤ wall elements

From only considering the section which covers the slab (fig. 5.1), constructing the culvert in PLAXIS is a simple task, see figure 5.1 B). The culvert is completely square and the transition slab ① is installed at the top, connected to the culvert by a freely rotating hinge ②. An important factor to bear in mind here is that the difference in concrete thickness for the different elements will affect the properties of the plate elements in PLAXIS. The wall thickness ⑤ for example, might be different from the roof/fundation thickness ③, evidently leading to different properties.

5.1.1 Example: Transfering a 3.5 x 3.5 meter concrete railway culvert into plane-strain

The following section is based on the shortest slab lenght required for norwegian railway bridges of 2.5 meter, which accor-ding to teknisk regelverk is allowed for culverts that are less than 3.5 meter high. It is assumed that the short slab in combination with the lowest height of cover will yield the most extreme case for a concrete culvert. Teknisk regelverk has also specified that the slab must be minimum 0.3 meters thick and minimum 3.2 meter wide [2].

Norwegian manufacturers of concrete element such as Nobi and Overhalla Betongbygg suggests that a typical 3.5x3.5 meter U-element railway culvert are delivered with walls that are about 0.3 meter thick and roof/cellar elements about 0.45 meter thick, see figure 5.2A) and 5.2B).

After some simulations in PLAXIS, it can be said from experience that using a long term elastic modulus for concrete, i.e reducing it due to creep and shrinkage as suggested in Eurocode 2 – Design of concrete structure – Part 1-1, the concrete when transformed into PLAXIS 2D behaves to soft in respect to the track. This is found from to the fact that the deflections at the culverts deck is directly affecting the displacement of the railway track during train a passage, where calculations has shown that following such procedure leads to higher deflections of the rail above the culvert than in the free track, which is unrealistic.

As a result it is thought that when a train is passing a rigid concrete culvert in PLAXIS 2D, one should not expect much happening with the culvert itself. The chosen elastic modulus is therefore viewed more at as a serviceability limit state (SLS) parameter than a ultimate limit state (ULS).

From assuming a balanced reinforced concrete in stadium I (i.e the concrete is completely uncracked and takes both compression and tension), the elastic modulus of the concrete can be used directly to represent the elastic modulus of the reinforced concrete of the culvert. On the basis of suggestions from EC2 for a C40 concrete, a elastic modulus (E_{cm}) in the order of 35 GPa is selected. The unit weight of the concrete is set to $\gamma_c = 24$ kN/m^3.

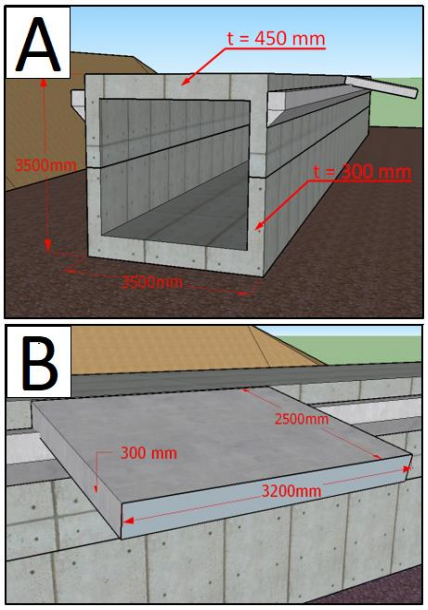

Figure 5.2 – Necessary dimensions for the 3.5 x 3.5 meter culvert when transformed into plane-strain

When calculating the moment of inertia (I) and area (A) for the top/bottom plate elements of the culvert, a lenght being 3.5 meter and height 0.45 meter is used. Accounting for the top and bottom plate elements, the wall elements are defined as 0.3 meter long with a height of 2.6 meter. When determing the moment of inertia of the plates (i.e top/bottom element and slab), an effective widt of 1.0 meter is assumed. Calculations are shown in table 5.1.

Table 5.1 – Calculations when transforming the properties of the concrete into plane-strain

Calculation – Inputparameters in PLAXIS 2D	
Area, top/bottom elements	A = (3.5*0.45) = 1.575 m^2
Area, wall elements	A = (2.6*0.3) = 0.78 m^2
Area, transition slab	A = (2.5*0.3) = 0.75 m^2
Moment of inertia, top/bottom elements	I = (1.0*0.45^3)/12 = 7.59375 * 10^{-3} m^4
Moment of inertia, wall elements	I = (0.3*2.6^3)/12 = 0.4394 m^4
Moment of inertia, transition slab	I = (1.0*0.3^3)/12 = 2.25 * 10^{-3} m^4
Weight, top/bottom elements	w = γ_c*0.45 = 10.8 kN/m^2
Weight, wall elements	w = γ_c*0.3 = 7.2 kN/m^2
Weight, transition slab	w = γ_c*0.3 = 7.2 kN/m^2

Considering the elastic modulus purposed by EC2, table 5.2 showing input parameters are obtained.

Table 5.2 – Input parameters for top/bottom element, wall elements and transition slab in PLAXIS

	EA [kN/m]	**EI [kNm^2/m]**	**w [kN/m/m]**
Top/bottom elements	55.125 * 10^6	2.6578 * 10^5	10.8
Wall elements	27.3 * 10^6	15.379 * 10^6	7.2
Transition slab	26.25 * 10^6	7.875 * 10^4	7.2

5.2 Modelling of flexible steel-soil composite bridges

By assuming that the steel plates behaves as if the pipe was fully integrated (i.e neglecting the fact that the plates are bolted together), the steel-soil composite bridge can be modelled as plate-elements by following the principles of plane-strain, se figure 5.3. The plate elements ② are tied together as «fixed» continously along the pipes geometry, enabling for transmission of bending moments and axial forces around the structures entire cross section. To provide a proper steel soil interaction, interfaces ① are placed respectively to the plate elements, se figure 5.3B).

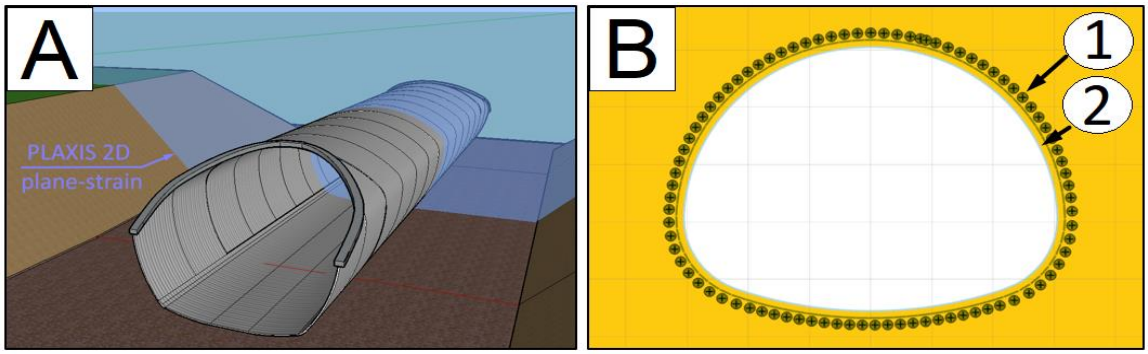

Figure 5.3 - Modelling principles for a steel-soil composite bridge, showing A) A 3D sketch of the plane in PLAXIS, and B) transfering it into PLAXIS were ① shows the interfaces and ② fixed plate elements

PLAXIS 2D offers the option of creating tunnels in structures mode. When the geometry of the pipe starts to deviate from a circle however, using this option may become challenging and it may be more convenient to draw its geometry in AutoCAD, then later import it into PLAXIS as shown in figure 5.4.

When drawing in AutoCAD, is it important to ensure that the polylines are closed. Using the point style option enables for creating any amount of connecting dots along the pipe geometry which makes it considerably easier to draw the plate elements and interfaces in PLAXIS, see figure 5.4.

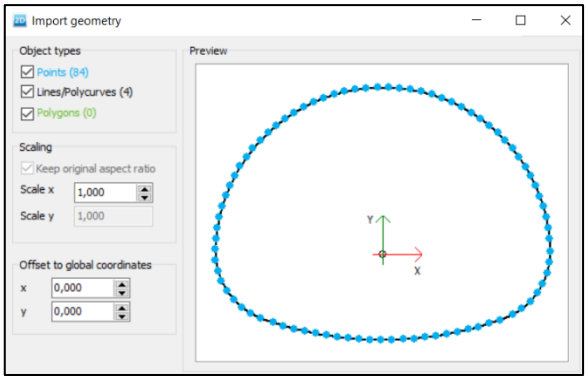

Figure 5.4 – Importing a pipe geometry from AutoCAD to PLAXIS 2D, including connecting dots

5.2.1 Example: Transfering corrugated steel plates into plane-strain

The Swedish Design Manual (SDM) offers cross-sectional data for the different corrugations as a function of thickness [19]. This means that the calculated axial- and bending stiffnesses from the provided charts already is transfered into plane-strain.

According to Eurocode 3 – Design of steel structures – Part 1, unit weight of steel qualities S235, S275, S355, S420, S450, S460 is 78.5 kN/m^3. By assuming E = 210 GPa as Young's modulus, the properties for corrugation type MP 200x55 mm can be obtained and is presented in table 5.3.

Table 5.3 - MP 200x55 profile showing properties of area (A), moment of inertia (I), axial stiffness (EA) and bending stiffness (EI) as a function of plate thickness (t). (Modified after Petterson. L and Sundquist. H, 2014)

t [mm]	A [mm^2/mm]	I [mm^4/mm]	EA [kN/m]	EI [kNm^2/m]	W [kN/m/m]
2.00	2.36	898	4.956 * 10^5	188.58	0.1570
3.00	3.54	1353	7.434 * 10^5	284.13	0.2355
4.00	4.73	1811	9.933 * 10^5	380.31	0.3140
5.00	5.92	2273	12.43 * 10^5	477.33	0.3925
6.00	7.10	2739	14.91 * 10^5	575.19	0.4710
7.00	8.29	3208	14.73 * 10^5	673.68	0.5495

6 Backfilling and compaction in PLAXIS

What governs most of the long term behaviour of flexible steel-soil composite culverts is the execution of backfill and service loads. As a result from this has it been a priority to catch the normal forces, bending moments and internal thrust forces that develops during backfilling as it is these aspects that governs these structures long-term behaviour. Field measurements and longterm monitoring has shown that the sectional forces surrounding a burried pipe changes insignificant longterm compared to the change the structure undergoes during construction [21,26].

This chapter will go more in depth on how these forces can be catched in PLAXIS 2D by simulating the fundamental steps of backfilling and compaction through phases. By using a hardening soil model for all backfill materials, transfering the compactions centrifugal forces into line loads and using proper soil parameters has made it possible to create a general procedure in PLAXIS which is representative to field behaviour when backfilling.

The following chapters first outlines the main principles behind the Hardening Soil model, followed by examples for back-filling against flexible steel pipes. These examples are compared to real field measurements where the pipes structural behaviour during backfilling was monitored. The downside with rigid culverts is that little to no documentation exists for how it behaves and is affected by construction which made it a challenge to define a standard procedure for stiff culverts. When the calibration results were carried out for steel-soil composite bridges however, it was thought that the same procedure could be applied for rigid culverts aswell as the norwegian procedure for both type of culvert is somewhat similar.

6.1 Soil models

This section highlights the background principles for the two soil models used in this project, which is the Linear-Elastic and Hardening Soil model.

From a practical point of view, the ballasts interacting behaviour may be considered complex but by assuming that the ballast helds high quality and has reached full stability (i.e all initial settlements has surpassed), it can be thought of as a continous elastic springbed providing a certain amount of damping to the track and with these assumptions in mind, a Linear-Elastic soil model is considered reasonable.

The main advantage that follows a Hardening soil model compared to simpler models such as Mohr Coloumb or the Linear-Elastic soil model for backfilling comes from its ability to behave much stiffer when unloading-reloading compared to virgin loading. This ability is very valuable when soil deformations are of interest. For such purpose, the Mohr Coloumb soil model behaves to elastic to simulate a realistic backfill procedure in the same steps as in field.

6.1.1 The Linear-Elastic soil model

The Linear-Elastic soil model is the simplest soil model offered by PLAXIS and only involves two elastic stiffness parameters, that is the effective Young's modulus (E') and possions ratio (v').

This model is soely based on theory of elasticity, namely hooks law meaning that when the soil is loaded it will strain linearly, and when it is being unloaded it will also unstrain linearly back to its original shape, see figure 6.1.

What should be kept in mind for this model in terms of the using it as backfill material, is that its inbuilt formulation of stiffness is not stress-dependent, meaning that it doesn't account for stiffness increase with depth if this is not specified manually. Options in PLAXIS only offers to define a linear increase in stiffness pr. meter depth for this soil model.

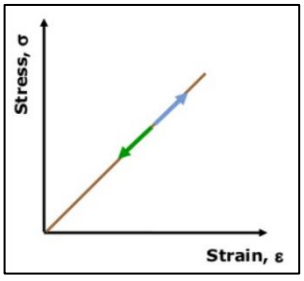

Figure 6.1 – Illustration, the simple Linear-Elastic soil model

6.1.2 The Hardening Soil model and relations between stiffness parameters

The Hardening Soil model is an advanced soil model were the behaviour of both stiff and soft soils can be simulated. Following the complexity of Hardening Soil, the number of input parameters is also higher. This section will outline the general background for Hardening Soil, followed by a description of the most related input parameters for this project. Parameters which PLAXIS defines by default is considered less important and will not be discussed.

In contrast to simpler models such as Mohr Coloumb where the yield surface is set by the Coloumb criterion, the yield surface in Hardening Soil can expand due to plastic straining. This expansion leads to isotropic hardening of the soil which is connected to the two following plastic yield surfaces, the «cone» and «the cap», illustrated in a stress space in figure 6.2A).

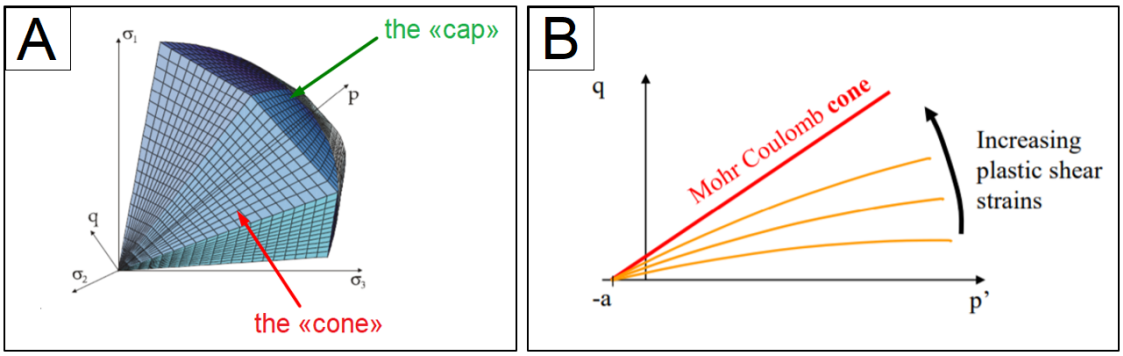

Figure 6.2 – Illustration of A) the «cone» and the «cap» in a principle stress space for the two yield surfaces that governs hardening and B) how permanent plastic strains bellow the MC failure line occours (From Nordal. S 2018)

The general Mohr-Coloumb failure criterion can be expressed as

$$\tau = \sigma * \tan(\varphi) + c \qquad \text{(Eq. 6.1)}$$

where

τ being the shear strenght at failure
σ being the normal stress
φ being the materials friction angle
c being the materials cohesion

The «cone» is expressed by the Coloumb criterion as in eq. 6.1, but the mobilizied friction tan(ρ) replaces the failure friction tan(φ). The cone will gradually expand when loading the material towards failure, and gives plastic strains that is constrolled by the increase in mobilized friction, causing shear hardening. The elastic strains will increase gradually as the loading reaches failure (see figure 6.3B) and the cone when being unloaded will stay at its outer position. The expanded region within the cone now becomes elastic. The elasto-plastic stiffness for the «cone» is governed by a secant stiffness E_{50}^{ref} [8,13].

The «cap» in Hardening Soil is a spherical surface that controls the preconsolidation stress. If the loading p' ($(\sigma_1' + \sigma_2' + \sigma_3')/3$) reaches the cap, it has reached the preconsolidation level. If p' is increased further, there will be plastic volumetric strains as a consequence. Theoretically speaking, we will never go outside the cap since it is pushed out by the stress state [13]. In the normal consolidated region, the stiffness is given by the oedometer parameter E_{oed}^{ref} [8,13].

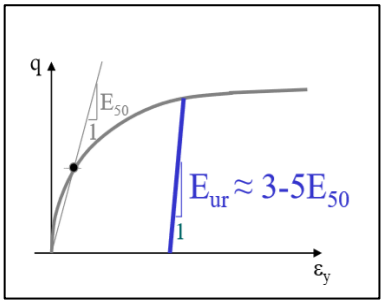

Figure 6.3 – Loading stiffness compared to unloading stiffness expressed in a stress-strain plot (From Nordal. S 2018)

In Hardening Soil it is the elastic parameters that handles the unloading stiffness. As with convential parameters for stiffness (E') and possions ratio (v), they are now describing the unloading stiffness (denoted as E_{ur}^{ref} and v_{ur}). E_{ur}^{ref} is often in the range of 3-5 times E_{50}^{ref}, and v_{ur} in the range of 0.1-0.2 [8,13], see figure 6.3 where E_{50} is refered to as E_{50}^{ref}.

From figure 6.3 it can be stated that the soil in a Hardening Soil model will never become stiffer than its unloading stiffness. Assuming that a load is being applied with the same magnitude in cycles, most of the plastification will occour after first time loading.

Another important input parameter is the dilatancy parameter (ψ), often refered to as «the climbing angle». The property of this parameter can easilest be explained by illustrating a densely packed sand with spheres in a simple two dimensional model, see figure 6.4.

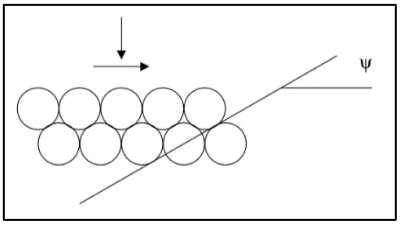

Figure 6.4 – A simple two-dimensional model of sand where the grains are considered as spheres (From Nordal. S 2018)

When applying shear strains, the spears in figure 6.4 must climb above each other which demands an increase in volume. Thinking like this in a three dimensional case, the spheres moves easiler and more free if the dilatancy angle is lower. In Hardening Soil, the dilatancy angle is only related to the cone where it will affect the volumetric plastic strains bellow the Coloumb line as long as it is nonzero [13].

Default parameters which is defined manually for a Hardening Soil model are presented in table 6.1.

Table 6.1 – Necessary input parameters for determining stiffness and strenght parameters in a hardening soil model

Parameter	**Description**
Stiffness	
E_{50}^{ref}	Secant stiffness in standard drained triaxial test
E_{oed}^{ref}	Tangent stiffness for primary oedometer loading
E_{ur}^{ref}	Unloading/reloading stiffness
Power (m)	Power of stress-level dependency of stiffness
v_{ur}	Possions ratio for loading/unloading
Strenght	
c'_{ref}	Effective cohesion at failure
φ'	Effective angle of friction at failure
ψ	Dilatancy angle at failure

Assuming linear elasticity and a typical possions ratio of 1/3, the relationship between the oedometer stiffness (E_{oed}^{ref}) and youngs modulus (E) can be expressed via the possions ratio as

$$E_{oed} = \frac{E(1-v)}{(1-2v)(1+v)} = \frac{3}{2}E \qquad \text{(Eq. 6.2)}$$

According to Nordal [13], from the study of nummerical values from trixial testing (denoted as the secant stiffness E_{50}^{ref}) and oedometer testing (denoted as the tangent stiffness E_{oed}^{ref}), it has been shown that both quantaties are almost identical, leading up to the formulation

$$E_{50}^{ref} \approx E_{oed}^{ref} \qquad \text{(Eq. 6.3)}$$

A advantage of Hardneing Soil compared to Mohr Coloumb is its built in formulations that make the stiffness stress dependent. According to Nordal [13], all stiffness moduli included in Hardening Soil can be described with expressions similar to

$$E_{50} = E_{50}^{ref}\left(\frac{\sigma 3' + a}{Pref + a}\right)^{m} \qquad \text{(Eq. 6.4)}$$

where

E_{50}^{ref} being the input parameter for stiffness
σ_3' being the horisontal effective stress, calculated in the program
a being the attraction
p_{ref} being the atmospheric pressure at 100 kPa
m being the power modulus

The formulation in eq. 6.4 will determine how the stiffness in Hardening Soil increases with depth, were the power modulus (m) describes the characteristics of this distribution. The power modulus is usually ranging between 0.5-1.0. For clays it it typically set to 1.0, while for sand 0.5 [13]. This means that the stiffness increase for a sand (assuming m = 0.5) will propagate in the soil as a square root function.

6.2 Backfilling in PLAXIS 2D

This section demonstrates the principles for constructing and backfilling against rigid and flexible culverts in PLAXIS 2D. The procedures purposed in this section are based on a combination of norwegian experiences from contractors, descriptions in handbooks the SDM manual [16,19,27], also see chapter 4.1.5 and 4.2.5.

6.2.1 Constructing and backfilling against a flexible steel-soil composite bridge

A purposed general procedure for modelling the soil-structure interaction for culverts are outlined in this section. When thinking of backfilling in field, there will always be variables which cannot be acounted for but from simulating the construction steps in field the end goal of this methodology has been to create a procedure which can distinguish the fundamental differences that affects the end result of a culvert. Such variables are for example what material that is used in the culverts inner and outer zones, differences in layering and differences in compaction equipment.

A summary of the various steps involved in this methodology are presented in figure 6.5, showing A) preparation of a fundation, B) construction of the culvert, C) backfilling and D) the culvert at construction finish with the various materials involved in this methodology.

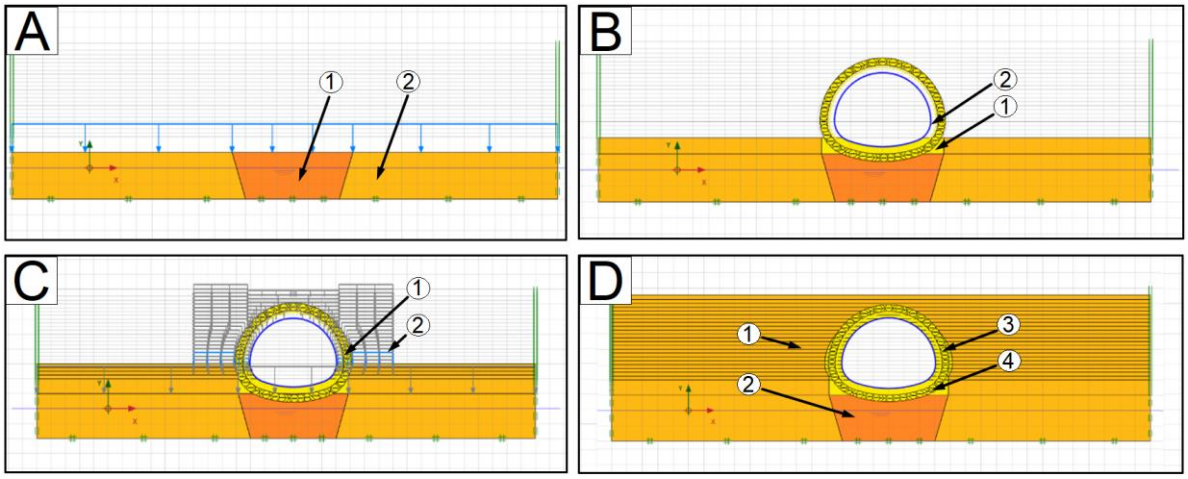

Figure 6.5 – Summary: The methodology of the construction steps for a steel soil composite bridge, showing A) preparation of the fundation, B) construction of the culvert, C) backfilling and D) all materials covered in the methodology

In order to limit other soil variables which influence the transition zone to only the interactions of the backfill and bridge, the subsoil (i.e bellow culvert) is assumed to be preconsolidated to such a degree that any settlement bellow the culvert can be neglected. The stiffness of the foundation should as a result be high. It may be debatable if a regular embankment has the same stiffness as a backfill due to use of higher quality materials, but from assuming that the embankment has been consolidated over many years, then sany difference between them can be considered to be so small that they may be neglected.

In figure 6.5A) the generalized foundation is presented, showing that it is divided into the zones of ① the foundation bellow culvert and ② the «subsoil» at the regular embankment. This solution plays the biggest role for the final track structure compared to the backfilling process, but is included here since it was included in the final models.. In order to avoid any influence the rigid bedrock may have on the track stiffness, the foundation height is as a minimum set to 3.0 meter, but should be increased if the culverts span is long enough. This layer is then compacted with a static line load of 50 kN/m, as if a vibro drum-roller were used. The foundations is constructed in total three steps, first constructing the layer, loading, then unloading.

The reason for separating the foundation into two sections is that previous train simulations has shown that PLAXIS suggests unrealistic displacements of the track over the culvert. This is tied to the Hardening Soils inbuilt formulation of stiffness and stress dependency. Since Hardening Soil threats the stiffness as a stress dependent quantity any stress conditions lower than 100 kPa (the referance pressure) will actually behave softer than what the stiffness of the material really is. This leads to a effective stress situations in the soil under the culvert that causes the foundation to behave much softer than it should, always leading to a lower stiffness of the track level over a culvert.

If the quality of the subsoil is poor, then a typical norwegian practice has been to excavate to the minimum frost susceptible depth and replace the masses with highly permeable crushed rock and then compact it with heavy equipment [27], also see section 4.1.5. By assuming that this procedure has been followed, it is reasonable to suggest that the foundation bellow the culvert always should be stiffer than it would be at the free embankment or regular backfill. This can be solved in PLAXIS by defining the unloading stiffness (E_{ur}^{ref}) to double bellow the culvert compared to the regular subsoil, but can also be solved by decreasing the power modulus (m) from 0.5, see the formulation of eq. 6.4 in chapter 6.1.2.

Following the preparation of the foundation, figure 6.5B) shows that the next layer and culvert is built simultaneously in one single phase, where the culvert ① is placed directly on a uncompacted bedding ②. It is important to adjust the bedding according to the geometry of the culvert so that the culverts entire bottom remains in contact with the soil. Although the bedding bellow the culvert is uncompacted, the same material is defined for the culverts entire inner zone. In the outher zones, a different and stiffer material may be used, see section 4.2.4 and 4.2.5.

In figure 6.5C) a summary of the compaction procedure used for this methodology are illustrated. Each layer is to be built alternately in total three phases where the layer is first actived, then loaded (i.e compacted), then unloaded which finishes a layer. This procedure is used for all layers methodically, where each layer can maximum be 0.3 meter thick, never exceeding the height difference of one single layer on the other side of the culvert [19].

The compaction loads are divided into two types of loads, hereby refered to as ① «light compaction» based of a 300-500 kg vibroplate and ②, «heavy compaction» based of a medium vibro drum-roller. Transfering sentrifugal forces into static line loads in plane strain definitelly brings uncertainty. The rule of thumb is that for lighter compaction equipment the influence of weight compared to the vibration force will be low while for heavier equipment, the influence of weight will be higher.

According to manufacturers of compaction equipment such as dynapac, a 300 kg vibroplate yields 39 kN/m of centrifugal force while a 5.0 tonn drum-roller, 89 kN/m of force. After some calibration attempts for compaction, a static line load of 25 kN/m seems to correspond well to a 300 kg vibro plate. This quantity has also been used by other authors when modelling similar problems [27-28]. To avoid overshooting the effect of heavier compaction forces and taking into consideration all the variables tied to the contractor, a static line load of 50 kN/m is set for the heavier compaction equipment.

When all layers are constructed with the principles of figure 6.5C), the end result for a finished steel-soil composite bridge should look as shown in figure 6.5D). The figure shows that the foundation bellow culvert ② is given the same material properties as the backfill material used in the outher zone ① except for a double unloading stiffness. This is based of that a 20/120 mm crushed rock material is used in both these sections except for the fundation that isbeing compacted with heavier equipment compared to the sides of the culvert, see chapter 4.1.5 and 4.2.5.

The inner section ③ and ④ are built with a finer material than what is used for the outer zones where the only difference between them is that a bedding of the culvert remains uncompacted. The SDM-manual requires a minimum distance for the inner zone from the culvert to be 0.5 meter around its entire circumferential cross section, but a distance of 1.0 meter is used. It should be highlighted that dividing different materials of the inner and outer zones are not a requirement. In Sweden there has been several cases where the same sand has been used in both the inner and outer sections of a backfill. Dividing these sections are done to account for norwegian conditions where this is a normal practice.

6.2.2 Constructing and backfilling against a rigid concrete culvert with transition slab

What benefit it will have to perform the same construction phases for a rigid case compared to a flexible one is debatable. It can be argued for that if enough train simulations are performed and the displacements are set to zero between each simulation then this will take care of most of the plastifications around the culvert.

From running some simulations it has been found that the plastification from compacting leads to a different elastic end behaviour compared to only plastifying the backfill from running train simulations. To ensure that the backfill under the slab does not behave to soft, compacting all layers for the rigid cases are also considered a prerequisite. A summary of all steps are given in figure 6.6.

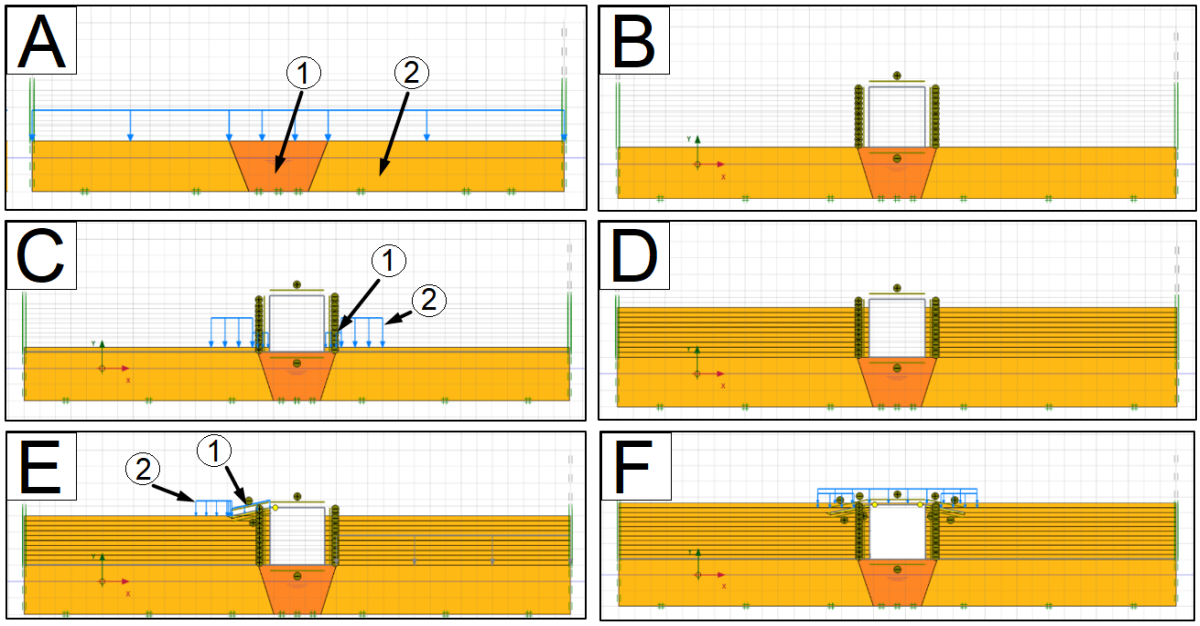

Figure 6.6 - Summary: The methodology showing all construction steps for a rigid culvert built with a transition slab, showing A) preparation of the fundation, B) construction of the culvert, C) backfilling and D) when reaching the level of the transition slab, E) constructing the layers bellow the slab and F) compacting the material above the culvert

As with flexible culverts, figure 6.6A) shows that the construction of the culvert starts with first preparing a foundation. Bellow the culvert the unloading stiffness compared to the free subsoil ② is doubled. When the fundation has been prepared the culvert can then be built simultaneously in one single phase as seen in figure 6.6B).

The compaction procedure is summarized in figure 6.6C) where it is seen that it is executed in similar manner as for the flexible case. The inner section ① is compacted with «light equipment» the closest meter from the culvert, and with «heavy equipment» ② further out.

It is important to be aware of that only one backfill material is used for the regular backfill here. This is based of several experiences from contractors which has stated that only using 20/120 mm crushed rock is more convenient than separating the inner and outer zones during short traffic breaks, see chapter 4.1.5.

When the level of backfill has reached the slab section, two elevated layers with the regular backfill materials is palced close to the culvert where a third corrective layer ② is placed on top of of the elevated 20/120 mm layer ①, see figure 6.7. The elevated corrective layer are compacted with a force equal to the weight of the slab and the horisontal layer of normal backfill with «light equipment», see 6.6E) but also see section 4.1.6.

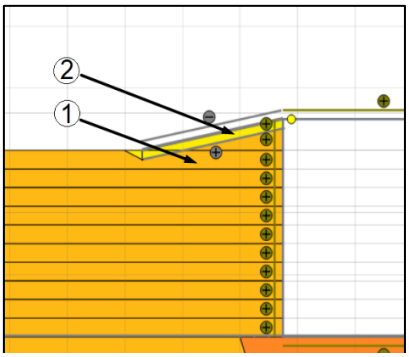

Figure 6.7 – Layering bellow the slab, showing the geometry of the corrective layer ②

After the layers bellow the slab has been compacted, and prepared the slab is ready to be constructed. The slab is built in one individual phase followed by the same compaction procedures seen in figure 6.6C). The difference is only that «light equipment» i sused here, corresponding to 25 kN/m. This procedure is followed until the formation plane bellow the ballast layer has been reached.

6.3 Comparing to two individual field measurements of backfilling

Studies on rigid culverts during backfilling is rarely a incidence as the main prerequisite for these structures is that uppose to flexible culverts, its bearing capacity should be maintained independent of backfill. From this standpoint the thought has been if one can prove that the methodology from section 6.2 leads to an accurate response of the soil-structure interactions of flexible SSCB, then the same methodology can be applied for rigid culverts.

This section compares finite element simulations in PLAXIS to two selected field measurements carried out for monitoring the culverts structural behaviour during backfilling phases. The examples refered to here is the full-scale test on a flexible pipe arch from Sweden [9], and the most recent full-scale test on a horizontal ellipse from Canada [29,30]. Estimation of soil secant modulus of the backfill according to SDM will also be discussed, also see chapter 4.2.2.

6.3.1 The Enköping pipe arch, a test culvert from Sweden 1987

This section involves the findings from the Enköping test culvert from Sweden, which was a part of a series of tests in the period 1987-1990. The culvert was located close to the city Enköping, appro-ximately 100 km west of Stockholm.

The findings from this full-scale test were used for calibrations and comparisons in development of the Swedish Design Method (SDM) for flexible steel-soil composite bridges, where the findings of this culvert was later reported by Lars Petterson in 2007 [9].

For this culvert, it was decided to keep the culverts wall stiffness as low as possible to particulary get a better understanding of the structural response during backfilling. Enköping was built with MP 200x55 corrugation and a steel thickness of 2.95 mm, having a maximum inside span of 6.04 meter and height 4.55 meter, see figure 6.8.

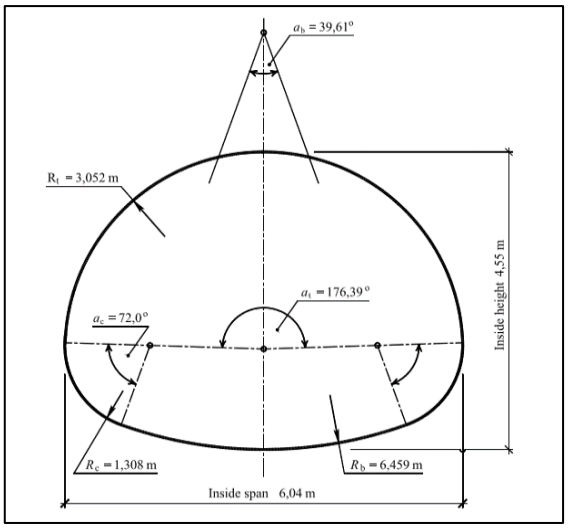

Figure 6.8 – Geometrical properties of the pipe arch «Enköping» from Sweden (From Petterson. L, 2007)

A gravel pit was first excavated and prepared for the culvert to be installed in followed by creating a foundation which was preshaped after the bottom of the culvert, see figure 6.9A). The culvert was then placed upon this layer, followed by the backfilling procedures as shown in figure 6.9B and 6.9C).

Figure 6.9 – Installation of the Enköping test culvert from Sweden in 1987, showing A) preparation of the fundation, B) installation of the culvert in the excavation pit and C) backfilling (Modified after Petterson. L, 2007)

Geometrical properties of the culvert in relation to the gravel pit are given in figure 6.10, showing that the compacted fundation was laid with a thickness of 0.6 meter followed by a uncompacted bedding of 0.75 meter for the culvert.

Several soil samples of the backfill were collected at the site and rutinely measurements with a nuclear densometer (Troxler) for evaluating the degree of compaction were carried out. A plate loading test was also performed a little out in backfill at the crown level, denoted as [PLT] in figure 6.10.

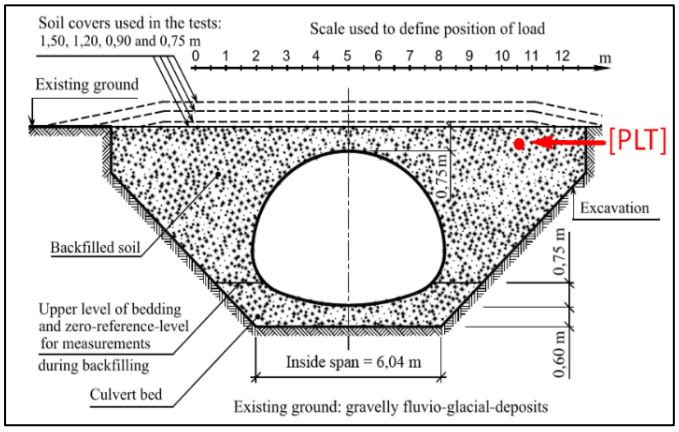

Figure 6.10 – Geometrical properties of the culvert in the excavated pit, showing the plate loading test denoted as [PLT] (From Petterson. L, 2007)

Each backfill layer was compacted alternately with a vibroplate weighing about 450 kg, where each layer was 0.3 meter thick and was compacted with four passages approximately two meters from the culvert and out. The backfilling level was kept to the same height at both sides of the culvert to keep the deformations symmetrical. Strain- and deflection gauges was also installed on the culvert before the backfilling began for measuring the culverts structural response.

Three soil samples were collected, that is one at the culverts foundation bed and one on each sides of the culverts backfill. Graduation curves showed that the number of fines were relatively low (less than 5% < 0.06mm), leading to the sand being classified as a free draining, uniformly graded- or poorly graded sand according to the unified soil classification system. From the graduation curves, d_{10}, d_{50} and d_{60}- values were determined for defining the coefficient of uniformity (Cu), see table 6.2.

Table 6.2 – Results from sample graduations taken at the site (From Petterson. L, 2007)

Sample no.	d_{50}	$Cu = d_{60}/d_{10}$
1	0.93	1.20/0.31 = 3.9
2	0.97	1.20/0.41 = 2.9
3	0.83	1.00/0.31 = 3.2

From laboratory studies it was found that the maximum dry density was in the order of 1.98 g/cm^3 with 9.5 % in water content. Results from the nuclear densometer suggested that a modified proctor of 92% common at each layer.

Three plate loading tests were also performed, but only one carried out in the backfill, where a secant modulus of 56 MPa for the first load cycle followed by 107 MPa at the second load cycle was measured in the pressure interwalls of 150 and 350 KPa [9].

In figure 6.11 the gradual development of displacements and internal bending moments are presented. As the figure shows, when the backfill procedure begins, the crown level of the culvert is gradually pushed upwards when each layer is placed out and compacted. The plot also reveals the effect of compaction in some of the layers where the crown displaces despite the layers being at the same level.

This figure shows that the maximum vertical deflection of the crown was in the order of 65 mm, corresponding to a deformation of 1.1 % of the culverts span which is within limits according to SDM (< 2%). It can also be seen that when the backfill has reached the top point of the culvert, the crown is then pushed down again to approximately 58 mm. At the culverts quarter point the same tendencies can be seen but to a smaller degree. Similar development of bending moments are given in figure 6.11B).

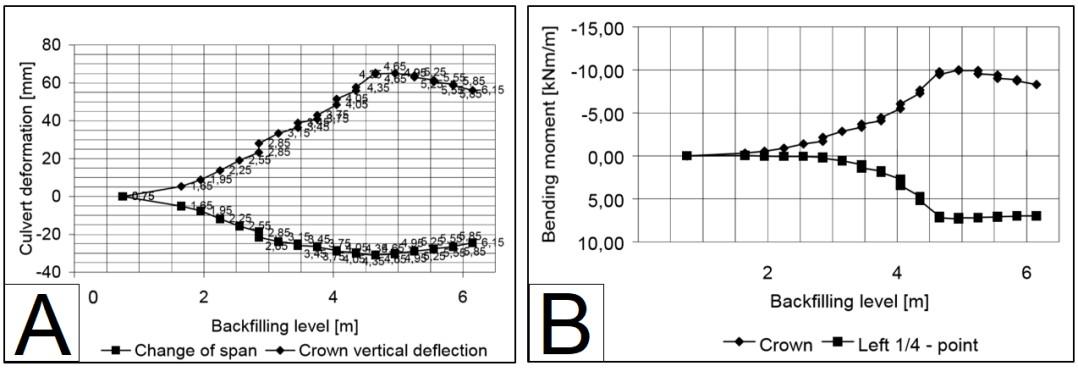

Figure 6.11 – Measurements during backfilling of Enköping, showng A) Vertical deformation at crown level and change in span at the culverts quarter point, and B) change in moment at crown level (From Petterson. L, 2007)

A summary from the deflections, moments and axial forces (wall thrust) at the various backfilling stages (0-1.5 meter) are given in table 6.3.

Table 6.3 – Summarized results from backfilling, showing deflections, moments and normal forces (From Petterson. L, 2007)

δ^{crown} at h_c = 0.0 m [mm]	M^{crown} at h_c = 0.0 [kNm/m]	M^{crown} at h_c = 1.5 [kNm/m]	N^{max} at h_c = 0.0 m [kN/m]	N^{max} at h_c = 0.75 m [kN/m]	N^{max} at h_c = 1.5 m [kN/m]
65	-10.0	-8.3	-120	-128	-173

Before any simulations in PLAXIS are carried out, stiffness parameters based of applications of the equations found in SDM are used, see chapter 4.2.2 or the SDM-manual [19]. An estimation of the soil modulus based of the plate loading test in the backfill will also be performed.

The SDM suggests that a modified proctor relates to the standard proctor with a difference of 5% [19], i.e the Standard Proctor (SP) in this backfill should be in the order of 97 %. From the test and geometry of the culvert, it is found that the distance from crown level to its neutral axis (H) is 3.052 meter while the height of cover (h_c) is 1.5 meter. On the basis of Duncans formulation from chapter 4 (Eq. 4.11) we obtain a secant modulus of the soil in the order of

- $E_{soil,k} = 1.3*1.17^{(97-95)}*[1.25\ \ln(1{,}5 + \frac{3.052}{2}) + 5.6] = \underline{12.42\ MPa}$

From the modified method for calculating secant stiffness (Method B), it is required to know the co-efficient of uniformity (C_u) and coefficients for particle size distributions (d_{10}, d_{50}, d_{60}) in addition to the the quantities used for method A. The background of this method is somewhat limited, but according to Petterson [33] based of a reformulation of Janbus expression for stress dependent soil modulus by a statistical approach. The application of this method is therefore soely using these expressions.

Average values from table 6.2 are used, corresponding to 0.91 for d_{50} and 3.33 for C_u. From the formulations in SDM (chapter 4.2.1 and 4.2.2), the following are obtained

Characteristic angle of friction

- $\varphi_k = 26° + 10*\frac{(97-75)}{25} + 0.4*0.91 + 1.6*\log(3.33) = 36.06°$

Arcing factor

- $S_v = \frac{0.8*\tan(\varphi k)}{\left(\sqrt{1+\tan^2(\varphi k)}+0.45*\tan(\varphi k)\right)^2} = \frac{0.8*0.728}{\left(\sqrt{1+0.728^2}+0.45*0.728\right)^2} = 0.2379$
- $A = 2*S_v*\frac{hc,red}{D} = 2*0.2292*\frac{(1.5-0.015*6.1)}{6.1} = 0.1098$ (Refered to as «κ» in SDM)
- $N_A = \frac{1-e^{-\kappa 1}}{\kappa 1} = \frac{1-e^{-0.1058}}{0.1058} = 0.9488$ (Archingfactor, refered to as «S_{ar}» in SDM)

In SDM it is stated that the arching factor must be calculted with a designed angle of friction. This has not been included here and only made a difference in the order of 0.001. How the change in shape influences height of cover is according to SDM accounted for by introducing a reduced height of cover ($h_{c,red}$).

Density and initial void ratio

- $\rho = (\frac{RP}{100\%})* \rho_{s,max} = (\frac{97\%}{100\%})* 1.98 = 1.9206$ g/cm3 $\Leftrightarrow \rho = 18.84$ kN/m^3
- $e_0 = \frac{\rho s}{\rho} - 1 = \frac{26}{18.4} - 1 = 0.38$ (ρ_s is set to 26 kN/m^3 after recommendations in SDM)

Stress exponent, modulus ratio and notation K_v

- $\beta = 0.29*\log(\frac{d50}{0.01}) - 0.065*\log(C_u) = 0.29*\log(\frac{0.91}{0.01}) - 0.065*\log(3.33) = 0.5341$
- $m = 282*C_{u,average}^{-0.77}*e_0^{-2,83} = 282*(3{,}33^{-0.77})*(0.91^{-2,83}) = 1725{,}7$
- $k_v = \frac{\sin(\varphi k)*(3-2\sin(\varphi k))}{2-\sin(\varphi k)} = \frac{\sin(36)*(3-2\sin(36))}{2-\sin(36)} = 0.7603$

From these relations we obtain the secant stiffness of the soil modulus from method B

- $E_{soil,k} = 0.42*m*100*k_v*(\frac{(1-\sin(\varphi k)*\rho*Sar*(hc+\frac{H}{2})}{100})^{1-\beta}$
- $E_{soil,k} = 0.42*(1725{,}7)*100*(0.7603)*(\frac{(1-\sin(36)*18{,}84*0.9488*(1{,}5+\frac{3{,}052}{2})}{100})^{1-0.5341} = \underline{27.36\ MPa}$

In order to evaluate what might be consider a reasonable stiffness for PLAXIS, results from plate the load test is also used for estimating the tangent modulus of the soil after first time loading in field (i.e compaction).

In order to evaluate the results corresponding to 56 MPa (E_{v1}) and 107 MPa (E_{v2}) in figure 6.12, an expression for soil modulus is deriven through the simple formulation

$$F = k*\delta \qquad \text{(Eq. 6.5)}$$

where

F being the applied force
k being the elastic spring stiffness
δ being settlement or displacement

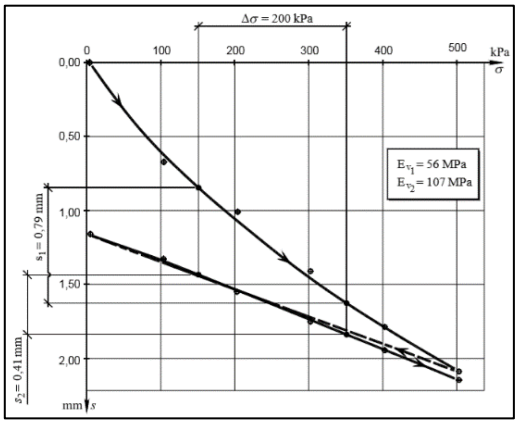

Figure 6.12 – Results from plate loading test showing E_{v1} and E_{v2} based of Boussinesqs soultion

The spring stiffness is defined via Lysmers analogue model for a circular footing in an elastic half space [32], which is equivalent to Boussinesq formulation [12], and expressed as

$$k = \frac{4G*r_0}{1-v} \qquad \text{(Eq. 6.6)}$$

Inserting (Eq. 3.9) from chapter 3 for shear modulus (G) in equation 6.6, we obtain

$$k = \frac{4\frac{E}{2(1+v)}*r0}{1-v} = \frac{2*E*r0}{(1-v)(1+v)} = \frac{E*D}{(1-v)(1+v)} \qquad \text{(Eq. 6.7)}$$

where

G being the shear modulus
E being the elastic modulus
r_0 being the radius of the footing
D being the diameter of the footing
v being the possion ratio of the soil body

Typical values of possion ratio ranges between 0.3-0.5 for soils. According to Nordal [13] based of theory of elasticity it can be assumed a possions ratio in the order of 1/3 for sands. However, when determining the possions ratio of a layered and compacted structure, the handbook on laboratory «HB R211: Feltundersøkelser» suggests that it should be higher.

According to HB R211, the possions ratio for a plate load test at a pavement structure should be as high as 0.5. Using v = 0.5 inserted into Eq. 6.7, we obtain

$$k = \frac{E*D}{(1-\frac{1}{2})(1+\frac{1}{2})} = \frac{4}{3} E*D \qquad \text{(Eq. 6.8)}$$

Inserted into eq. 6.5 and isolating the elastic modulus (E), we obtain

$$E = \frac{3}{4} * \frac{F}{\delta * D} \qquad \text{(Eq. 6.9)}$$

Transforming the force (F) into stress (σ) by

$$\sigma = \frac{F}{A} \qquad \text{(Eq. 6.10)}$$

Inserted into Eq. 6.9 and knowing that the circular plate had a diameter of 300 mm [9], we obtain

$$E = \frac{3\pi}{16} * \frac{\sigma}{\delta} * D \qquad \text{(Eq. 6.11)}$$

where

E being the soil modulus
σ being the applied stress on the plate
D being the plates diameter
δ being the settlement bellow the plate

From figure 6.12 it was seen that for first time loading of the change in stress was within the order of 200 MPa and the registered settlement was about 0.79 mm. When these are inserted into equation 6.11, we obtain

- $E = \frac{3\pi}{16} * \frac{\Delta\sigma}{\Delta\delta} * D = \frac{3\pi}{16} * \frac{200}{0.79} * 300 = \underline{44.73 \text{ MPa}}$

This soil modulus is slightly lower than E_{v1} which was calculated based of Boussinesqs expression for stress in an elastic half space and using the same possions ratio (0.5). All three soil modulus numbers from SDM and the plate loading test are summarized in table 6.4, which represents the soil modulus of the backfill after first time loading (i.e after compaction of all the layers up to crown level of the culvert).

Table 6.4 – Soil modulus numbers after first time loading from SDM and plate load test

SDM - Method A	SDM - Method B	Field - Plate load test
12.42 MPa	27.36 MPa	44.73 MPa

When chosing stiffness parameters for PLAXIS, it is important to be aware of that those stiffness parameters represents the stiffness of the material in its neutral condition, i.e without considering any interactions with any structures or influence of compaction beforehand. According to Nordal [13] triaxial tests has revealed that most sands shows a refererence stiffness in the range of 15-50 MPa, corresponding to E_{50}^{ref}, see chapter 6.1.2.

The ranges purposed by Nordal reflects a «virgin sand» in its natural condition. Cases of a really dense sand might for example show a higher value while a very loose sand lower values. Thinking that the stiffnes for the Enöping backfill already accounts for compaction, it might be argued for not using them for PLAXIS. Having in mind what could be expected to be a typical stiffness, the plate loading test showed something that seems more reasonable than the values obtained from SDM. The plate loading test also suggests that the SDM procedure yields conservative results as even in the comprehensive method B, a stiffness 39% less than the ones obtained from the plate load test was returned.

From this it can be stated that the stiffness used for PLAXIS in a hardening soil model, should probably range between 27.36 – 44.73 MPa. A secant stiffness of 30 MPa is chosen for this sand with the same angle of friction calculated from SDM. The calculated density is also used here, where a «climbing angle» (dilatancy angle) of 5° is defined. The oedometer stiffness are set to the same as the refereance stiffness, and the unloading stiffness to three times the referance stiffness.

Following the logic from section 6.1.2, the parameters used for this simulation are presented in table 6.5

Table 6.5 – Input parameters for the PLAXIS simulation showing stiffnes, density, friction- and dilatancy angle

E_{50}^{ref} [MPa]	E_{oed}^{ref} [MPa]	E_{ur}^{ref} [MPa]	γ [kN/m^3]	φ [°]	ψ [°]
30	30	90	18.9	36	5

It is important to get the proper correlation between cohesion, interface and stiffness when determining the stress which acts on a flexible pipe in PLAXIS. As various simulations untill now has shown, the quantity that really plays an important role is the cohesion and interface (R_{inter}). A weakness with PLAXIS is that the interface is either completely rigid (i.e $R_{inter} = 1.0$) and there is full contact with soil and structure or it has to be defined manually for determining a weaker contact (i.e $R_{inter} < 1.0$).

The interface roughness chosen in PLAXIS mostly affects to what degree the angle of friction is working in the structure-soil interaction, but also other quantities such as interface stiffness [8]. The interface role in a Hardening Soil model in relation to a soil-structure interaction can be explained via the Mohr Coloumb criteria where a reduction in cohesion leads to a reduction in the angle of friction.

As the PLAXIS manual states [8], the relationship between interface and cohesion has a direct correlation, expressed as

$$c_{inter} = R_{Inter} * c \qquad \text{(Eq. 6.12)}$$

where

c_{inter} being the acting cohesion at the soil-structure interaction
c being the input cohesion for PLAXIS
R_{inter} being the interface roughness

As Eq. 6.12 shows, if the R_{inter} is low then the cohesion is significantly reduced which has a direct effect on the angle of friction, see Eq. 6.1 in section 6.1.2.

According to the PLAXIS manual, a typical soil-structure interaction should have an R_{inter} in the order of 2/3 [8]. One could argue that it might be lower when backfilling and compacting due to vibrations, but this recommendation is the basis for the finished structure, and hereby used.

The PLAXIS programme also suggests as a standard input to use a minimum cohesion in the order of 0.1 KPa, but may be argued for to be higher for a compacted sand. The effect of compaction will thoughtfully create some cohesion. With respect of remaining 0.7 as an interface value, a cohesion of 1 kPa is set for the sand.

The model created for this validation test is in total 35 meters long and 6.75 meters high, see figure 6.13. All steps from section 6.2.1 are followed here, where a 2 meter fundation is created having twice the unloading stiffness ($6xE_{50}^{ref}$) compared to the free embankment. For backfilling this does not affect the results as significant as it does for train passages, but were used with respect to the final model.

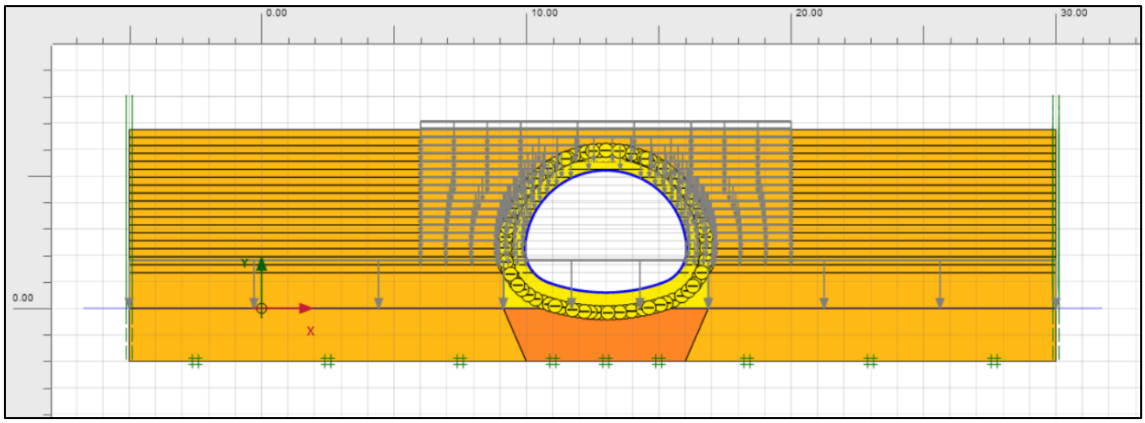

Figure 6.13 – Geometric properties of the PLAXIS model used for simulating the backfill at Enköping, Sweden

The backfill is divided into two parts, that is the inner and outer zone. With respect to the case of Enöping, the same sand is used for both zones. After the foundation was created the culvert with the bedding are laid where it in is total 1.35 meter high reaching 0.75 meter up from the bottom of the culvert, see figure 6.10. After the culvert is constructed the displacements are set to zero as reported by Petterson. L [9]. The backfill in total consist of 18 layers corresponding a height of cover of 1.5 meter after the last layer.

A static line load of 25 kN/m were used, representing a 450 kg vibroplate. According to Petterson. L [9], the backfill were compacted approximately 2 meters out and around the entire culvert while for PLAXIS this zone was extendend to 4 meters. One could argue that the sides of the pit would provide some support compared to a completely new embankment as it is created in PLAXIS, but simulations has shown that this influence (2 compared to 4 meter wide compaction) is insignificant as long as the load remains the same. The loads are placed with an offseth of 0.1 m away from the culvert to avoid nummerical problems.

The reported profile for Enköping was MP 200x55x2.95. Assuming a plate thickness of 3 mm the structural properties from SDM can be used directly and is presented in table 6.6.

Table 6.6 – Input parameters for for the steel plates representing the Enköping culvert in Sweden

t [mm]	A [mm^2/mm]	I [mm^4/mm]	EA [kN/m]	EI [kNm^2/m]	W [kN/m/m]
3.00	3.54	1353	$7.434 * 10^5$	284.13	0.2355

In figure 6.14 results from PLAXIS of the vertical displacements of the culverts crown are compared, were results reported by Petterson. L [9] are used as a referance. It is important to highlight that the results from field presented here are not as exact as in figure 6.11A), but are only ment as a referance. All results from PLAXIS up to a backfill level of 2.25 meter were filtered as the magnitude of these is considered to be neglectible.

Three results are compared here, that is one from field, one with and one without the compaction in PLAXIS. The results with compaction shows two results pr. backfill level, that is one when the layer has been constructed and one when the compaction is finished (i.e the layer has been unloaded).

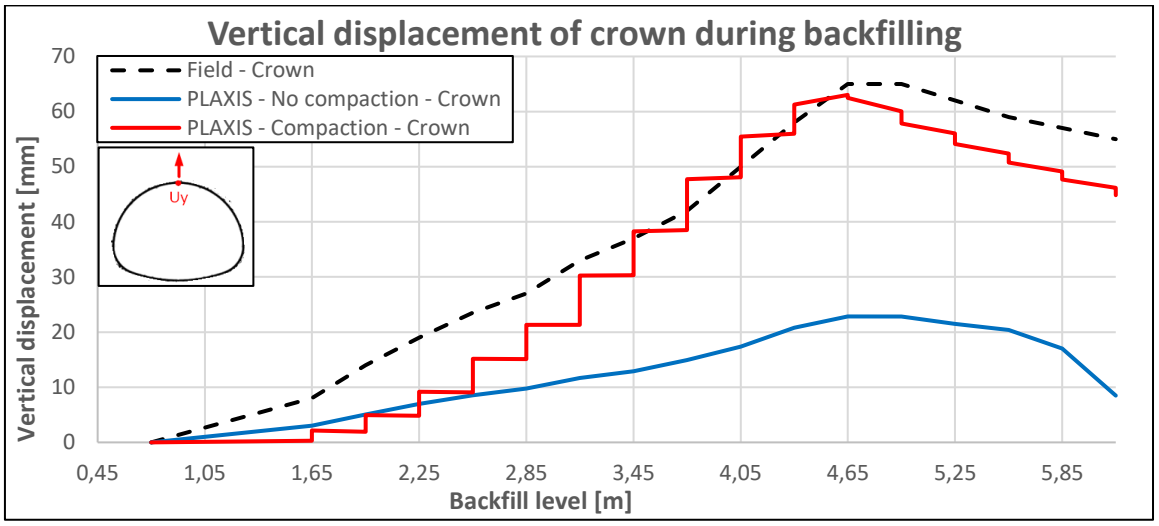

Figure 6.14 – Vertical displacements as a function of backfill level, showing results with and without compaction in PLAXIS

All three results shows a logical behaviour of the pipe. The pipe is first squeezed inwards due to the earth pressure of the backfill, which is then squeezed down again when the soil covering starts. Placing the layers alternatively with no compaction seems to highly influence the results as the maximum deflection of the crown only was in the order of 23 mm upose to 65 mm in field. «Compacting» in PLAXIS with a Hardening Soil model and using a static line load demonstrates its great ability to remember previous loading, causing an increase in displacements of 275%.

The effect of compaction in field was taken away from figure 6.14 as it was only ment as a reference, but can from figure 6.11A) also be seen to affect the results. Indeed, this effect seems more significant in PLAXIS than they were in field, but having in mind that it is a static load that plastifices these layers compared to a centrifugal force in field, some deviation must be expected.

In figure 6.15, moment distributions during backfilling is presented showing the same cases as previous. Results from two nodes are presented here, one at the crown and one at the quarter point of the culvert (ca. 45° from the center axis). Similar to the results for deflection, the effect of compaction is included.

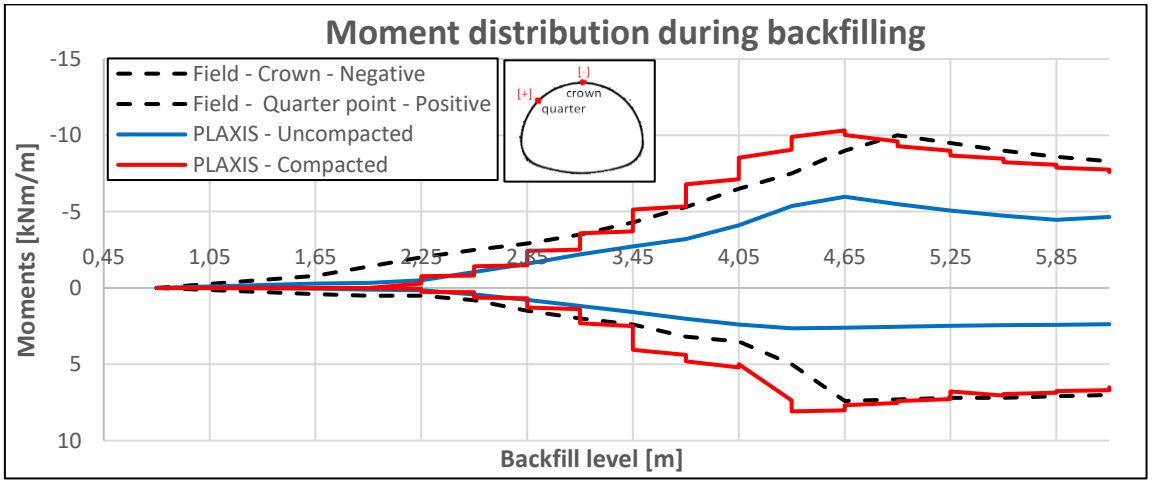

Figure 6.15 – Moment distributions at crown level and quarter point during backfilling with and without compaction in PLAXIS, compared to field measurement.

As the results shows, the moments starts to built up gradually as the backfill proceeds, where the biggest bending moments can be seen just as the backfill reaches the crown level for then to be reduced as the height of cover increases. As with the deflections, the effect of compaction can also be seen here but less significant. This has good agreement to what the field measurements demonstrated in figure 6.11.

In figure 6.16 internal thrust are presented when the backfill has reached A) crown level (0 meter height of cover), B) 0.75 meter height of cover and C) and 1.5 meter height of cover.

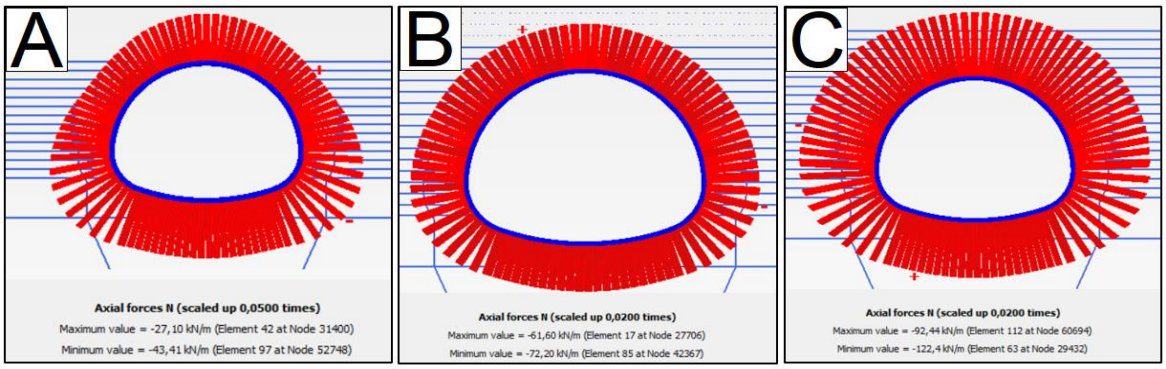

Figure 6.16 - Axial forces when the backfill has reached A) crown level, B) 0.75 meter soil cover and C) 1.5 meter soil cover

The internal thrust forces does not show as good correlation as the soil-structure interaction did. Field measurements reported an axial thrust of -120 kN/m at crown level, -128 kN/m at 0.75 meter cover and -173 kN/m at construction finish upose to -43.4 kN/m, -72.2 kN/m and -122.4 kN/m in PLAXIS. This might be related to the fact that PLAXIS is not able to catch the structural interaction between the bolted connection of each corrugated plate element.

In terms of investigating the soil-culvert interactions of this structure, this example has shown that PLAXIS is well suited for modelling this interaction. The hardening soil models ability to remember previous loads enables the user to model each step similar to procedures in field. If the materials used and the compaction equipment in field are known, then this procedure has shown to return a representative behaviour.

If it is the structural reponse of the pipe that is of interest however, one should consider to use other softwares than PLAXIS 2D. In Amer Wadi's most recent doctor thesis regarding SSCB, Abaqus was proven to be well suited for such purpose [28].

6.3.2 The Horisontal ellipse at Queens university, a test culvert from Canada 2017

This section compares the same procedure for backfilling as in section 6.2.1, to yet a full-scale test performed on a horisontal ellipse in Canada. The purpose of the full-scale test was to get a better understanding of how horizontal ellipses would behave during backfilling, when applying service loads and ultimate loads. This section will only adress the findings from backfilling.

The test were performed in a prebuilt test pit at Queen's university, Canada. The facility was built under motivation of research on various types of pipes such as concrete, polythylene and corrugated metal pipes [30]. The test pit was in total 3 meters deep, 8 meters wide and 16 meters long with a retaining wall built in the middle to divide the facility into two half. A bedding being about 0.6 meter thick was laid out and compacted to 95% SP before the test started, see figure 6.17A) and 6.17B).

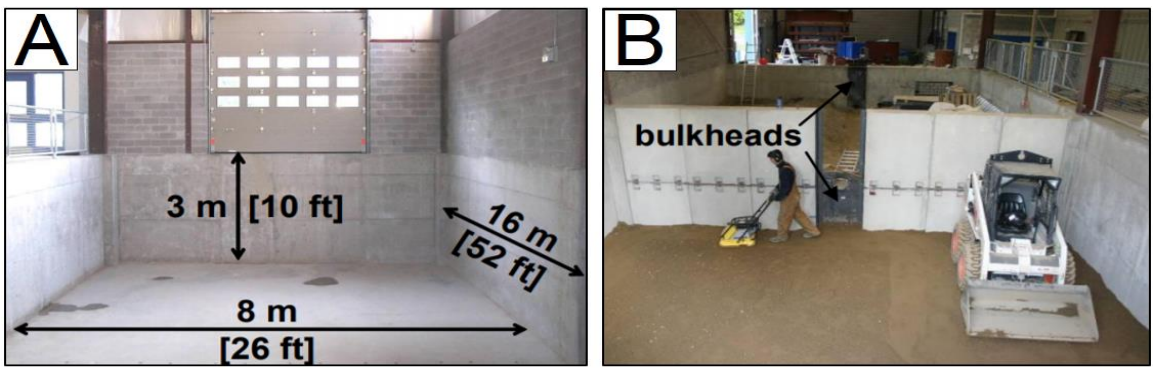

Figure 6.17 – The test pit at Queens university, showing A) Geometric properties of the pit and B) construction of the fundation

In order to build a trench for the ellipse, precast concrete blocks was placed on the sides of the pit approximately 2.1 meter away from the walls of the pit, leaving 3.8 meter of space for the pipe. A soil cover of 0.9 meter was used, and the ellipse had a height of 1.35 meter and span 1.6 meter, leaving 1.1 meters of space to backfill on each side, see figure 6.18.

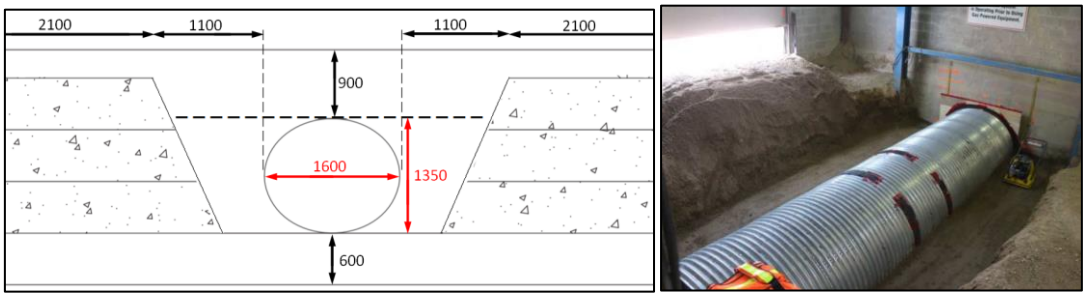

Figure 6.18 – Geometrical properties of the trench and picture from the test site (From Moore. I. D, 2017)

The sand which was used in the backfill was classified as a poorly graded sandy gravel (GP-SP) according to the Unified Soil Classification System and was used as bedding, backfill and soil cover. A bedding being 75 mm thick was premade for the ellipse and each layer in the backfill and soil cover was 300 mm thick, and was compacted with a vibrating plate tamper (Wacker wp1550AW) [30]. Summary of the soil samples collected at each backfill section are shown in table 6.7.

Table 6.7 – Summary of the backfill properties at all sections of the construction (From Moore. I. D, 2017)

	Dry density [g/cm^3]	**Water content [%]**	**Standard proctor (SP) [%]**
Bedding	2.2	3.6	96.4
Backfill to crown	2.1	4.0	92.6
Crown to top of 0.45 m cover	2.2	4.7	96.3

The displacements were measured with a DIC device (Digital Image Correlation) and strains by fiber optic sensors [30], placing them as shown in figure 6.19.

The culvert was a horisontal ellipse with a span of 1.6 meter, height 1.35 meter and lenght 6.5 meters. The steel plates of the culvert had an corrugation of 76.2 x 25.4 mm, and the steel plates was 1.82 mm thick. The culvert had a an cross-sectional area (A) of 2.26 mm^2/mm, second moment of inertia (I) of 170.4 mm^4/mm and a reported youngs modulus of 200 GPa [30].

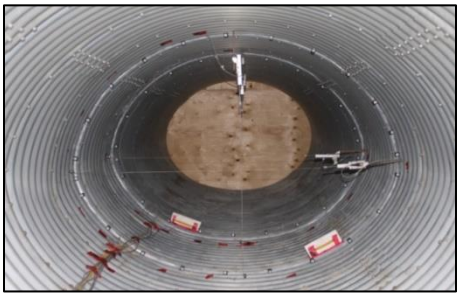

Figure 6.19 – Placing of fiber optic sensors cables and DIC targets (From Moore. I. D, 2017)

During backfilling it was reported that the culvert had a vertical diameter change of 0.9 mm, and about 1.1 mm horisontal change when the backfill had reached crown level. The culvert to then contract to -2.1 mm vertically and expanded -0.8 mm horisontally when 0.9 meter of soil cover was placed on top of it. At 0.9 meter of soil cover, the sensors at the culvert registered an internal thrust of about 30 kN/m at the horisontal axis and about 20 kN/m at the vertical axis.

The PLAXIS model was created based of the geometric properties of the test pit where it in total was 8 meters long and 2.85 meters high. The foundation was prepared in a similar manner as shown in section 6.2.1, being 0.6 meter thick and with double the unloading stiffness under the culvert compared to the free backfill ($6xE_{50}^{ref}$). The culvert was built on an 75 mm uncompacted bedding, following by backfill in layers built alternatively 300 mm thick. The inner and outer zone were not distinguished for this case.

The compaction force was set to 25 kN/m similar to the case of Enköping. In order to catch the trenchs potential effect on the horisontal support during compaction, the compaction load was extended to the end boundaries, see figure 6.20.

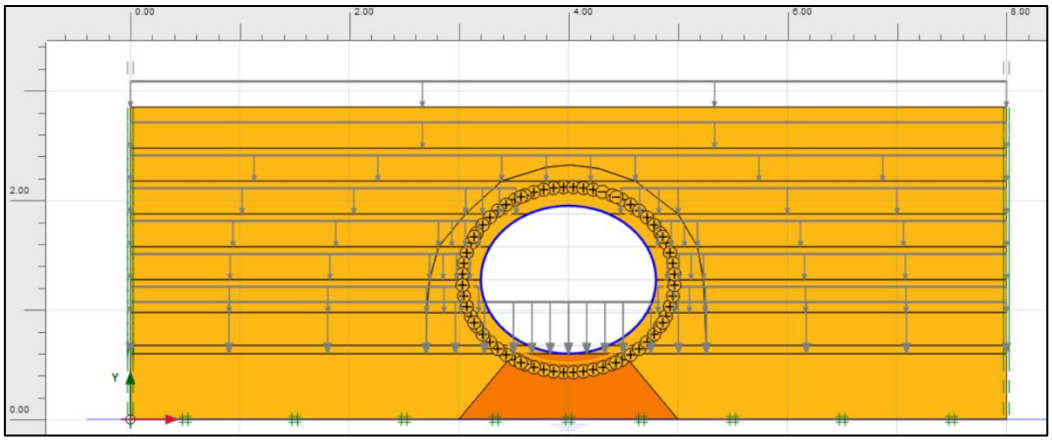

Figure 6.20 – Geometric properties of the PLAXIS model used for simulating the backfill during construction of the horisontal ellipse, Canada

With the limited information available on the backfill material, estimating stiffness parameters according to SDM (Duncan's SCI-method) were avoided as it purposes an unrealistically low secant stiffness (< 10 MPa). By knowing that the sand used for backfill in this case was classified as «GP-SP», which is the same classification as the sand at Enköping (according to the Unified Soil Classification System), it is reasonable to assume that the stiffness of this sand should not deviate that much from the sand used in Sweden.

By calculating the average degree of compaction (SP) and average dry density from the backfill and soil cover, the formula from SDM can be used for estimating the average density of the material. From table 25, an average value of 94.45% SP and 2.15 g/cm^3 for dry density is selected. Using the formulation from SDM we obtain

- $\rho = (\frac{RP}{100\%})* \rho_{s,max} = (\frac{94.45\%}{100\%})* 2.15 = 2.03$ g/cm3 $\Leftrightarrow \gamma = 19.92$ kN/m^3

Assuming that the mateiral is similar to the Enköping sand, the following parameters are estimated for the backfill and presented in table 6.8.

Table 6.8 - Input parameters for PLAXIS, showing stiffness, density, friction- and dilatancy angle

E_{50}^{ref} [MPa]	E_{oed}^{ref} [MPa]	E_{ur}^{ref} [MPa]	γ [kN/m^3]	φ [°]	ψ [°]	c [KPa]
30	30	90	19.9	36	5	1

From using a youngs modulus of 200 Gpa, the input parameters of the ellipse were obtained, see table 6.9. The weight of the steel is calculated based of a unit weight of 78.5 kN/m^3, see chapter 5.2.1.

Table 6.9 - Input parameters for for the steel plates representing the horisontal ellipse in Canada

t [mm]	A [mm^2/mm]	I [mm^4/mm]	EA [kN/m]	EI [kNm^2/m]	W [kN/m/m]
1.82	2.26	170.4	$4.518 * 10^5$	34.88	0.1429

In figure 6.21, results from A) the vertical and B) horisontal displacements of the culvert from PLAXIS during backfilling are presented, while including the reported deformation patterns measured in field as a referance [30].

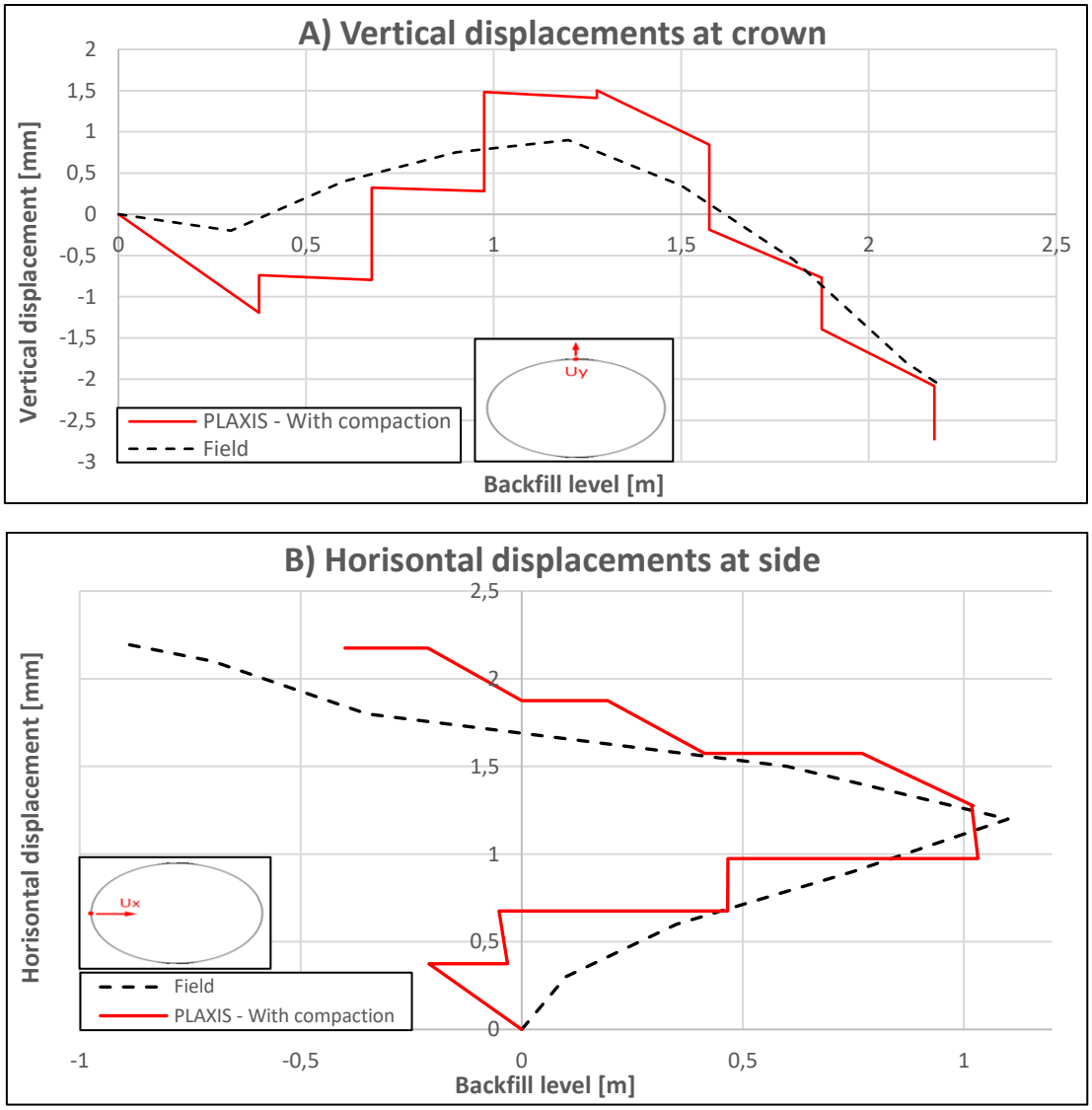

Figure 6.21 - Vertical displacements as a function of backfill level, comparing results from PLAXIS with field

As both comparisons shows, there is good agreement between the field measurements and the PLAXIS simulation. When the pipe is laid at its bedding, its own weight forces the crown displace downwards by deforming. The crown is them pushed upward again as the backfilling starts, for then to be pushed down again when the cover is laid on top. At the horisontal displacements a similar tendency can be seen, but it seems like the pipes expansion horisontally when laid at its bedding is taken away from the field results. It is concluded that the overall trend in general shows good agreement to the measurements from field.

Comparing the axial thrust to what was registered in field, similar to the Enöping case PLAXIS undershoots the thrust, see table 6.10. It is worth to mention however that the PLAXIS results shows that the thrust is higher horisontally than vertically, something which agrees with the classic formulation of ring compression theory considering smaller radius of this section, see Chapter 4.2.1.

Table 6.10 – Axial thrust at a cover height of 0.9 m, showing results at all four nodes of the culvert

		Node A	Node B	Node C	Node D
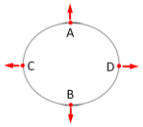	**Field**	18 kN/m	21 kN/m	30 kN/m	27 kN/m
	PLAXIS	12.12 kN/m	14.8 kN/m	17.14 kN/m	17.14 kN/m

In figure 6.22 a comparison between the bending moments measured in field are compared to PLAXIS when the backfill has reached crown level, where figure 6.22A) presents the measured bending moments from field and figure 6.22B) the bending moments from PLAXIS. One should be aware of that results from field are presented in a polar plot (i.e the quarter points are not in the position they would've been for a circular pipe) [30].

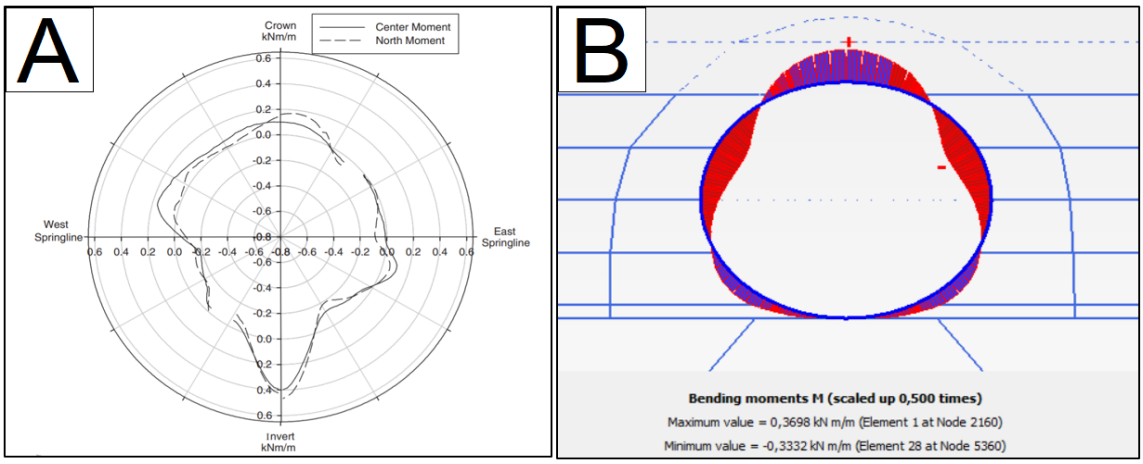

Figure 6.22 – Bending moments when the backfill has reached crown level showing results from A) field and B) PLAXIS

The results presented here are only presented as a comparison between the magnitudes from field and PLAXIS, where good agreement is found. The bending moments from field varies around -0.2 to 0.4 kN/m in field, and about -0.33 to 0.37 kN/m in PLAXIS.

6.3.3 Comments and discussion

The general conclusion from the backfill comparisons here is that there is a certain amount of information required beforehand if running a backfill similation and expecting sufficient accuracy. The aim of this chapter was to compare the generalized procedure from chapter 6.2 to these two field measurements, where it in general shows good agreement as long as certain field conditions are known.

For both these examples the same procedure was followed in PLAXIS with almost a identical backfill material as the «GP-SP sand» were used for both these cases. As was demonstrated with the Enköping case, the effect of compaction has a major influence on the end results for these structures as the deflections was increased with 275% only from introducing compaction into the simulation. From this it can be stated that using the effect of compaction when modelling is a necessity in order to catch a representative soil-structure behaviour for this kind of culvert.

According to the supplier *onesourcerental*, a vibrating plate tamper of the type WP1550AW corresponds to a centrifugal force of 15 kN/m, while a 300-500 kg vibroplate according to *dynapac*, corresponds to about 49 kN/m of sentrifugal force. Even if such details were not considered in these simulations one should be aware of them when using static line loads as compaction in PLAXIS. The compaction force might for example been overshooted in the ellipse case but the purpose of this comparison was rather more like a validation test. In the next chapters the effect of using different compaction forces are studied further, and it will show that the magnitude of the compaction loads makes a significant difference for these structures end result.

When comparing moment distributions PLAXIS showed good agreement to both cases. An intersting observation here was that when comparing the results from the horisontal ellipse to the case of Enköping, the internal bending moments on the ellipse was extremely low compared to the bending moments for Enköping. This is related to the slenderness of the ellipse compared to Enköping which leads to a lower flexibility number and, according to several authors, an overall more flexible interaction which decreases the internal bending moments developed in these structures [17-19].

The aspect that didn't correlate as good was the structural response of the pipe (i.e axial forces). The PLAXIS simulations deviated from what was measured in field, which are thought to be related to aspects such as the bolted connections and potential 3D effects between these steel plates. According to Wadi, software such as Abaqus has proven to be more suited for such analyses than PLAXIS 2D [18].

6.4 Defining stiffness parameters for 20/120 mm crushed rock and investigating the long term behaviour of flexible steel pipes in PLAXIS

This section purposes stiffness parameters for a gravel and 20/120 mm crushed rock material. The following section also provides examples on how variables such as combining different backfill materials, compaction loads and changing stiffness parameters affects the long-term capacity of a flexible culverts (i.e when the model behaves elastic), with using the Enköping culvert from Sweden as a referance.

In the case of a rigid concrete culvert the predefined gravel are to be used as the corrective layer under the transition slab while in the case of a flexible culverts, it is used for its bedding and inner zone. Based of Nordals purposed stiffness ranges for sands (15-50 MPa) [13] and the findings of section 6.3, a similar gravel is defined here but only increasing the unit weight to 20 kN/m^3.

The purpose of the analysis shown here is to investigate how changing variables affects the flexible structure after the soil model hardens (i.e the model becomes elastic). When this stage is reached, the beahaviour of the model represents something similar to a «long-term behaviour» (i.e elastic behaviour), and this behaviour is then compared to long-term field measurements for evaluation.

6.4.1 Defining stiffness parameters

A challenge with defining stiffness parameters for a 20/120 mm crushed rock material is that little to no accurate research exist on the subject. The large stone size involved in the material makes it very difficult to test in a convential triaxial- or oedometer apparatus. It is also challenging to test it isolated with convential plate loading tests as the diameter of these test apparatus is rarely larger than 300 mm, leading to high risks of larger stones influencing the results. Due to these limitations defining the stiffness of this material will be more based of others experiences, available data and common sense.

In Nålsunds doctoral thesis from 2014 [31], the stiffness of railway ballast was one of the main topics and based of plate loading tests performed at the norwegian highway between Trondheim and Stjørdal, it was purposed that the stiffness ranges of crushed rock was between 180-260 MPa. These tests were carried out on a layered pavement structure, see figure 6.23.

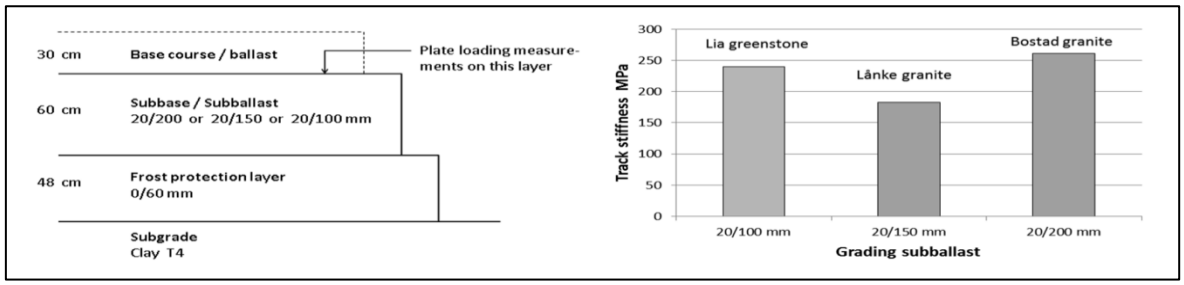

Figure 6.23 – Purposed stiffness ranges from plate loading tests at highway E6, Trondheim-Stjørdal (From Nålsund. R, 2014)

When refering to the values in figure 6.23, it should be kept in mind that when plate loading tests is performed on layered structures the underlaying materials may actually affect the results with an influence zone up to several meters. It is therefore thought that the ranges purposed by Nålsund is rough, but gives an idea of how stiff this material may become after it has been compacted.

In an interaction with a relative small culvert and taking into consideration compaction of each layer, a 20/120 mm crushed rock material can be expected to behave stiff and rigid in such interactions. One should for example not expect much flow of the material, which can be presummed from the illustrations shown in figure 6.24, where the backfill of two recent concrete culverts in Norway are presented.

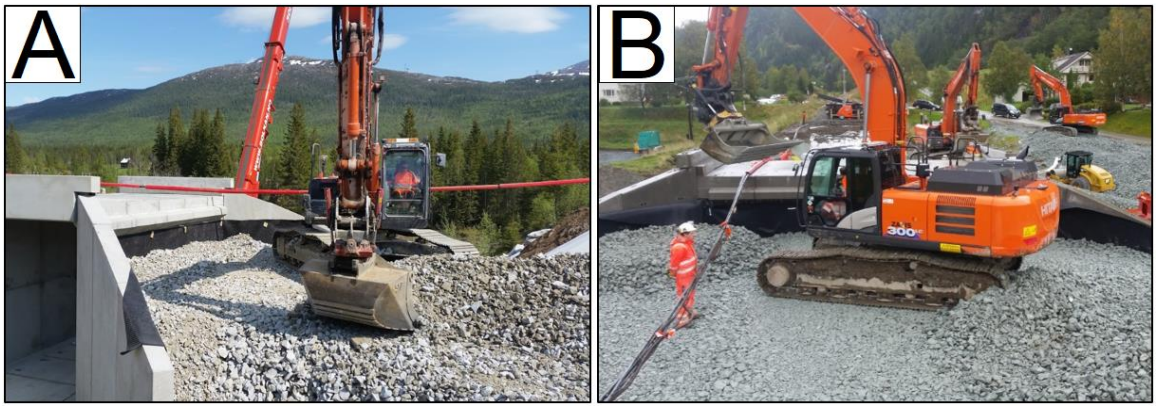

Figure 6.24 – Backfilling with 20/120 crushed rock at two culverts in Norway, showing A) Svenningdal culvert built in 2016 and B) Kilnes culvert built in 2018 (FOTO: Farbu & Gausen AS)

Visually speaking, the crushed rock is thought to behave very rigid in relation to these culverts. One way of catching this behaviour in PLAXIS is to increase the dilatancy angle, this will make it harder for the material to displace when it is being loaded from the surface which relates to the stiffness of it. A dilatancy angle of 15° is selected for the crushed rock.

The reference stiffness of this material is also expected to be higher than a sand, and a referance stiffness of 45 MPa is selected. The angle of friction is increased to 40°, and the unit weight is set to 20 kN/m^3 together with 0.1 kPa in cohesion. From this we obtain

Table 6.11 – The standardized norwegian backfill materials showing the properties of a sandy gravel and 20/120 crushed rock

	E_{50}^{ref} [MPa]	E_{oed}^{ref} [MPa]	γ [kN/m^3]	φ [°]	ψ [°]	c [KPa]
Sandy gravel	30	30	20	36	5	1
20/120 crushed rock	45	45	20	40	15	0.1

Before predefining the unloading stiffness of these materials it is very important to have in mind that it is the unloading stiffness that governs the displacements seen at the railway track during «a train passage». Shared experiences from Bane NOR has suggested that the deflections on a «moderate track» should not be larger than an order of 2.0-2.5 mm under 22.5 tonn referance axle.

Calibrating the unloading stiffness for this crushed rock were done with a simple model built from layers of Hardening soil. The material in the backfill was damped with 100% in the frequency ranges 5-50 Hz, see chapter 3.6. The railway track defined in chapter 2.3.1 was then built on top of this backfill and the «freight train» from chapter 3.2.2 was used for the simulations, see figure 6.25.

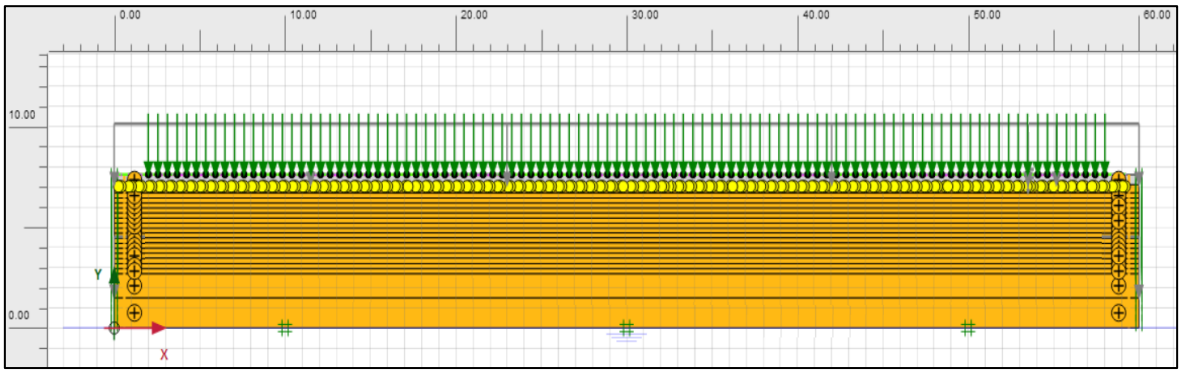

Figure 6.25 – Model conditions for calibration of the unloading stiffness for the 20/120 mm crushed rock

From running some simulations it has been found that if the unloading stiffness of the crushed rock is set to eight times the referance stiffness, the track will deflect about 1.75 mm under the bogie of two

22.5 tonn axles and about 1.5 mm under a single static axle (84.9 kN/m in plane-strain). This is also under the condition that several «train passages» has runned over the model and all plastifications are finished (i.e the model behaves completely elastic).

Decreasing the unloading stiffness to five times the referance stiffness causes the track to deflection about 2.4 mm under the bogie and 1.5 mm under a single static axle of 22.5 tonn. This is also under the prerequisite that the model has plastified and behaves completely elastic, see figure 6.26 and 6.27.

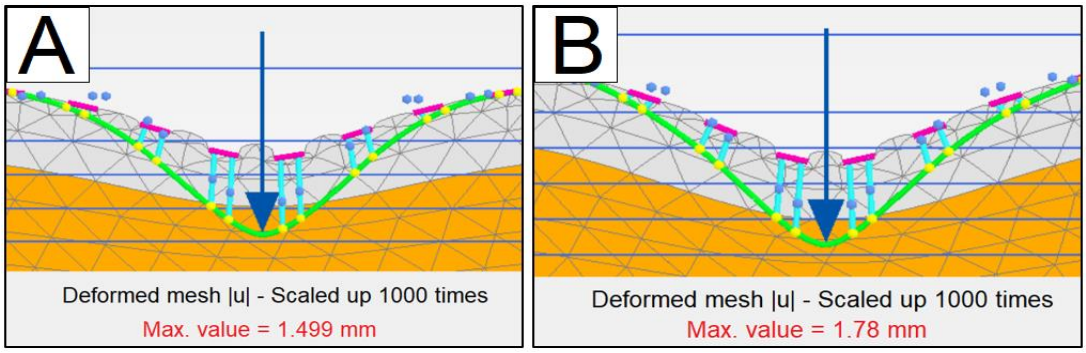

Figure 6.26 – Rail displacements under a static point load of 84.9 kN/m when A) using 360 MPa as the unloading stiffness and B) using 225 MPa as the unloading stiffness of the crushed rock

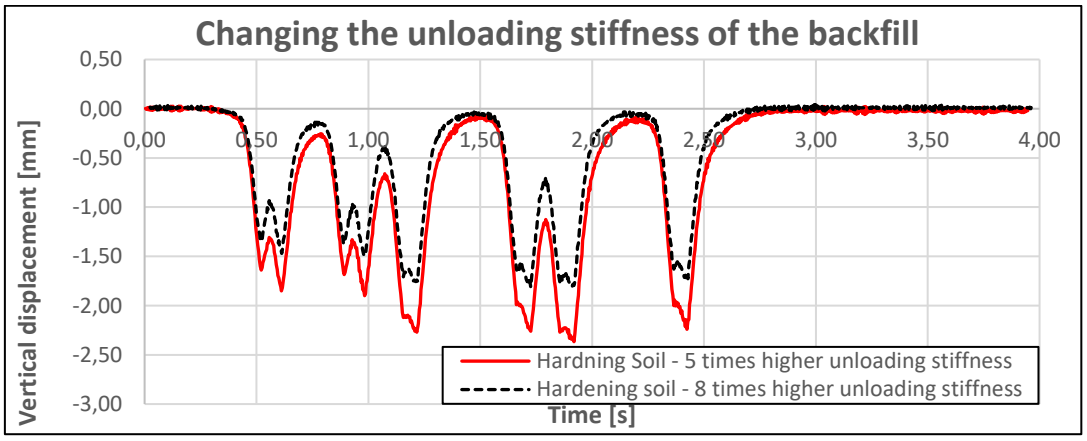

Figure 6.27 – Vertical displacement of the rail from only changing the unloading stiffness

What these results shows is that the rail displaces about 0.3 mm more in the static example when decreasing the unloading stiffness, but 0.5 mm under a bogie. From this calibration it is thought that the deflections returned from using five times the referance stiffness as unloading stiffness is more representative for a «moderate track» compared to using the higher one.

For the sand materials however, it was found in the latest stages of this project that predefining its unloading stiffness without accounting for where it is being used (i.e either around the flexible culvert or under the transition slab) was not favourable due to problems discovered with the inbuilt formulation of stress dependent stiffness in Hardening Soil, see chapter 6.1.2. It was decided as a result to not predefine the stiffness of the sand material in this report.

6.4.2 Investigating the effect of compaction, soil properties and unloading stiffness

Basing the culvert used in this simulation of the Enköping test culvert from Sweden, the effect of changing compaction loads, soil properties and increasing the unloading stiffness are investigated further. The aim of this section is to get a better understanding of how the «long-term» soil-culvert interaction (i.e when a train is passing) is affected by changing these variables in PLAXIS.

The model created for these simulations shown in figure 6.28, and shows that geometrically speaking, it is identical to the model used in chapter 6.3.1. In this model however, the compaction loads are divided

into two zones, one close to the culvert and one further out (denoted as configuration I and II). Configuration I is predefined with 25 kN/m of force in all these simulations as this has been defined as equivalent to a vibroplate in this project.

Three soil materials are used in these simulations, one at the regular backfill, on at the inner zone of the culvert, and one at the fundation. The only difference between the fundation and regular backfill is that the unloading stiffness is doubled in the fundation compared to the regular backfill.

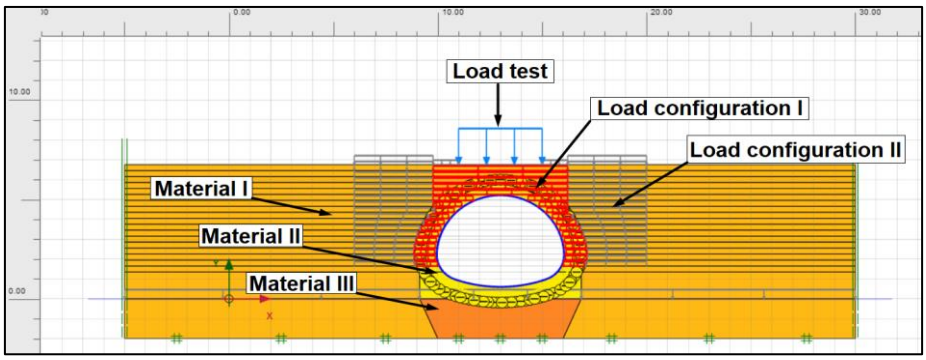

Figure 6.28 - Geometric properties of the PLAXIS model used for this simulation

Lastly, a 4.0 meter wide line load is placed on top of the culverts center axis with 200 kN/m of force, denoted as «load test» in figure 6.25. The load test is carried out to investigate how the culvert behaves when it is being subjected to surface loads as the variables of the backfill are changed.

Mainly two materials are used, that is the predefined sand and 20/120mm crushed rock material which was shown in table 6.11. In total five combinations are studied, summarized in table 6.12.

Table 6.12 – Seleceted combination of backfilling variables

Case	Description
A	**Gravel exclusively used for all three soil bodies and** • The unloading stiffness in regular backfill is 3 times the referance stiffness • The unloading stiffness in the fundation is 6 times the referance stiffness • The compaction load is set to 25 kN/m for both load configurations
B	**Gravel exclusively used for all three soil bodies,** • The unloading stiffness in regular backfill is 3 times the referance stiffness • The unloading stiffness in the fundation is 6 times the referance stiffness • The compaction load is set to 25 kN/m for config. I and 50 kN/m for config. II
C	**Gravel is used at the innerzone, 20/120 mm crushed rock in the outer zones** • The unloading stiffness in regular backfill is 3 times the referance stiffness • The unloading stiffness in the fundation is 6 times the referance stiffness • The compaction load is set to 25 kN/m for both load configurations
D	**Gravel is used at the innerzone, 20/120 mm crushed rock in the outer zones** • The unloading stiffness in regular backfill is 3 times the referance stiffness • The unloading stiffness in the fundation is 6 times the referance stiffness • The compaction load is set to 25 kN/m for config. I and 50 kN/m for config. II
E	**Gravel is used at the innerzone, 20/120 mm crushed rock in the outer zones** • The unloading stiffness in regular backfill is 8 times the referance stiffness • The unloading stiffness in the fundation is 16 times the referance stiffness • The compaction load is set to 25 kN/m for config. I and 50 kN/m for config. II

In figure 6.29 and 6.30 two plots is presented, vertical displacements of the crown and horisontal dis-placements at the culverts center axis during all backfilling stages. Each plot also presents results from the load test where two load tests are performed for each case.

The load test shows the maximum displacement of loading followed by the change in displacements when unloading. In order to investigate the effect of hardening (i.e the unloading stiffness), two load tests was performed to ensure that the culvert behaves completely elastic, see table 6.12. It should be mentioned beforehand that the results from the load test in these plots in reality were performed at the same backfill level and was only placed differently for demonstration purposes.

From figure 6.29 it can be seen that the vertical displacement of the crown is little influenced by changing the properties of the soil material in the outer zone. This can also be seen from comparing case A and B to case C and D where the displacements for case A is almost identical to case C and the displacements of case B similar to case D.

The variable which seems to contribute the most to this difference is increasing the compaction force. This can be seen for case B, D and E as increasing the compaction load to 50 kN/m at configuration II causes the crown to displace much more than using only 25 kN/m. It is also seen for case B where sand was used exclusively that the displacement of the crown is slightly higher than for case D and E.

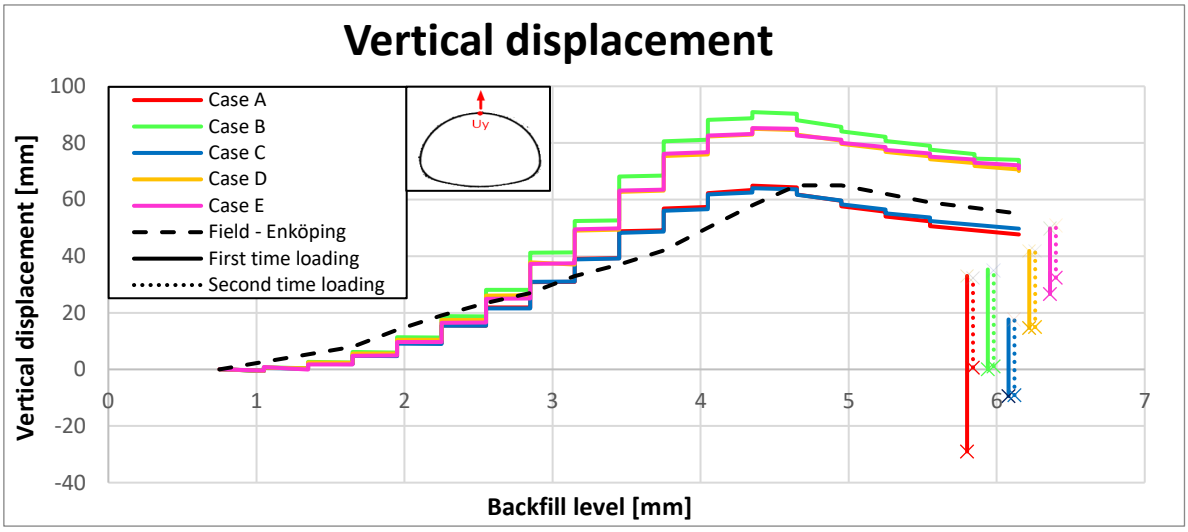

Figure 6.29 – Displacement results for all five cases including the «load test», showing vertical displacements of the crown

The load test seen in figure 6.28 shows that for Case A were it was only used sand, behaves softer than all other four cases at first time loading. Comparing case A to case B where the same material has been used, shows that despite the displacement being larger for case A compared to B, the elastic range tends to match each other after the material hardens and becomes elastic.

This cannot be seen until the second load test is performed for case A however, which suggests that the sand in combination with light compaction plastifies the backfill less than for example case C where the crushed rock was compacted with the same force, or case B were the same material was used but compacted with a larger force.

In figure 6.28 similar tendencies can be seen for case E where increasing the compaction force increased the dis-placements of the pipe, unaffectedly of the increased unloading stiffness. The elastic range however, has decreased from increasing the unloading stiffness.

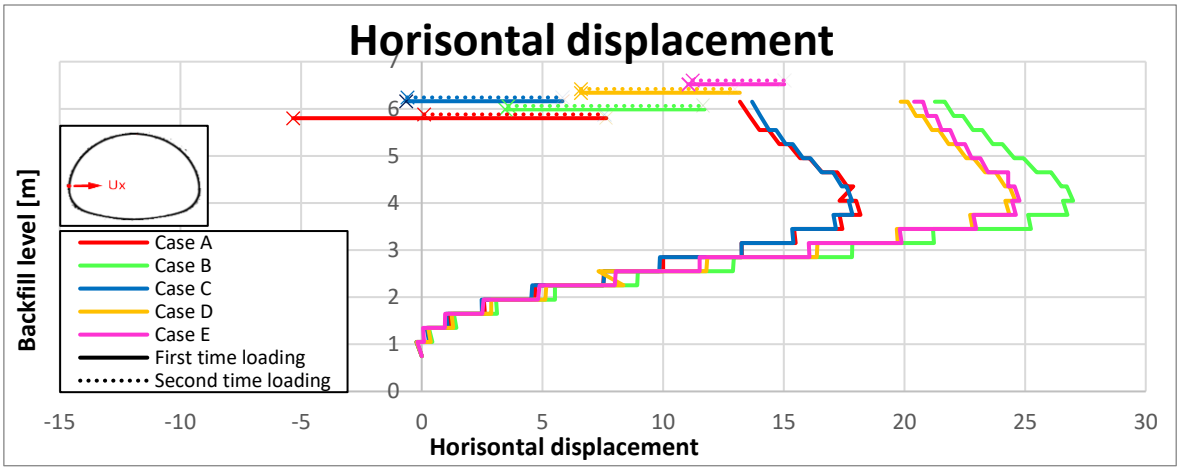

Figure 6.30 – Displacement results for all five cases including the «load test», showing horisontal displacements of the crown

The horisontal displacements in figure 6.29 shows that during backfilling, similar tendencies as for the vertical displacements occours. The low compaction force used for case A and C causes least displacements, followed by an significant increase for case D and E, and an even larger increase for case B. This tendency is better understood from investigating the internal bending moments that develops after backfill finish, see table 6.13.

Tabell 6.13 – Moment distribution after backfilling finish for all three cases (From PLAXIS)

Moments [kNm/m]	Case A	Case B	Case C	Case D	Case E
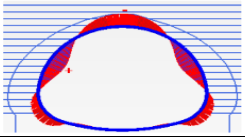	+ 8.878 - 8.219	+ 12.32 - 11.22	+ 8.708 - 8.501	+ 11.58 - 11.03	+ 11.71 - 11.23

When only using 25 kN/m as compaction force the bending moments remains similar to what was measured at Enköping [9] for both cases. Increasing the compaction force however, also causes an increase in bending moments. These results shows that the bending moments that develops during backfilling is proptional to the deformations, which also agrees with field behaviour [9,17,19]

In figure 6.31, bending moments and axial forces for case C when performing the load test is presented. The results demonstrates that exepct for some changes in sign, the magnitudes of the bending moment is nearly unaffected while the axial forces (internal thrust), increases with over 400% during the load test demonstrating that most of the loads from the surface is taken in ring compression rather than bending. This behaviour agrees good with both theory and field behaviour [9,17,18,19].

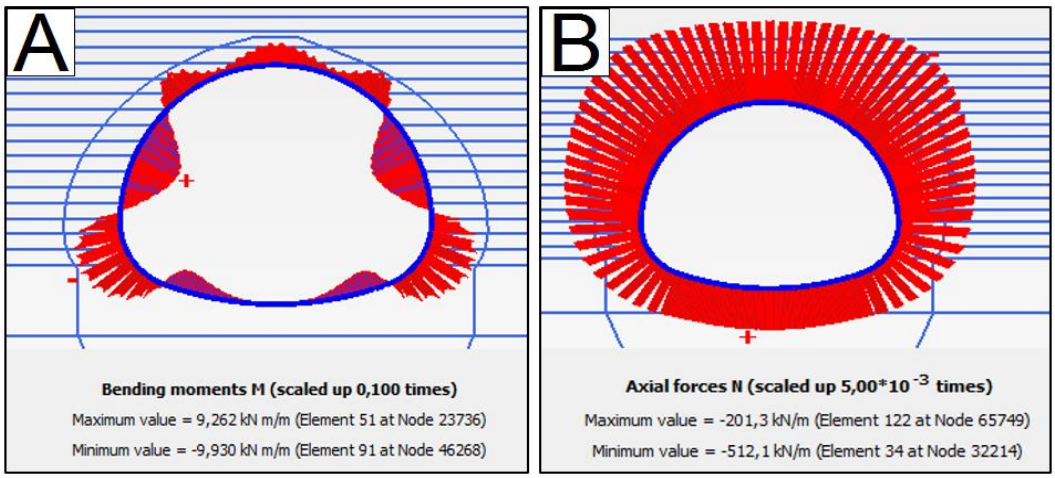

Figure 6.31 – Results from case C under the load test, showing A) bending moments and B) Axial forces (thrust)

With this it can be concluded that the deformations during backfilling in these simulations shows good agreement to behaviour in field. Most of the internal bending moments in the structure develops during backfilling which is well known to be the most critical phase in field. The deformations of the pipe is are more influenced by the compaction forces rather than the materials.

Recapping the load test from figure 6.29, it suggests that increasing the compaction force influenced the cases with crushed rock (case C, D and E) more than for the cases with only sand (Case A and B). The maximum displacement seen in the elastic range for case A were slightly reduced when increasing the compaction force for case B. When increasing the line loads in the cases with crushed rock however, the maximum displacement undergoes a tremendous reduction when comparing case C to case D.

This behaviour suggests that when a combination of sand and crushed rock is used instead of a sand explicitly combined with the use of heavier compaction equipment, creates a more rigid like resistance for the pipe, causing the pipe to better resist vertical loads which may be associated with higher vertical stiffness over the culvert seen at the surface.

This tendency is even more evident for case E with the higher unloading stiffness as both the elastic range and maximum horisontal displacement has decreased considerably. This behaviour agrees with the fact that it is the unloading stiffness that governs the elastic range in Hardening Soil models.

For all cases, it was also found that the axial forces (internal thrust) increases as the soil plastifies with time, see table 6.14. When unloading the load test, the internal thrust compared to before increases as the material hardens. Only case E deviates slightly from the other cases where the higher unloading stiffness was used.

Tabell 6.14 – Axial forces after A) backfilling and B) after load test

Thrust force [kN/m]	Case A	Case B	Case C	Case D	Case E
A) After backfilling	- 126.8	- 130.5	- 123.9	- 127.3	- 137.2
B) After load test	- 169.8	- 167.9	- 161.7	- 169.3	- 156.3
Increase	25.3 %	22.3 %	23.4 %	24.8 %	12.2 %

6.4.3 21 years of field monitoring – Two case studies from Norway

In the years of 1982-1988, two full scale field tests were carried out as a part of Vaslestads doctor thesis from 1990 [17], namely the large span culverts Dovre and Tolpinrud.

Both these structures are located in the southern part of Norway, Dovre about 350 km north, and Tolpinrud about 60 km north-west of Oslo, see figure 6.32. Information on backfilling and construction of these culverts are not the main forcuse of this section, and only brief information is given here. More information and construction and back-filling are given in [17, 26].

The Glötzl cells installed on these culverts has continously been measure-ing earth pressures for 21 years [26]. This section highlights these results as a comparison to the findings of the previous section.

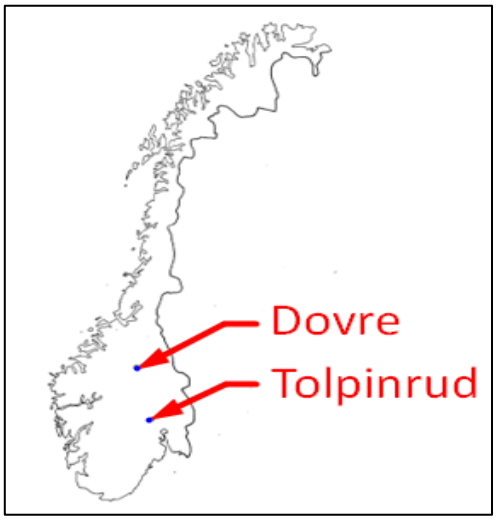

Figure 6.32 - Location of Dovre and Tolpinrud culvert

Dovre structure was a horisontal ellipse built in 1985 for animal crossings over a norwegian highway, see figure 6.33. It was built with a corrugation type MP 200x55 and had a steel thick-ness of 7 mm. The culvert had a horisontal span of 10.78 meter, was 7.13 meter high and built with 4.2 meter height of cover.

The backfill at Dovre consisted of well-graded gravel and was compacted to 97% Standard proctor in 0.3 meter thick layers.

Dovre was also installed with thrust beams on the quarter points of the structure. Results regarding these thrust beams are not adressed further in this section as thrust beams are not used any longer in modern design [19].

Regarding the field measurements, eight Glötzl cells was installed on the structure for measuring earth pressures where five of them was bolted directly to the steel and two placed above the crown to measure long term arching behaviour, see figure 6.33. Strain gauges was also installed on the structure for measuring thrust forces in the steel (not shown) for a periode of three years, reported in Vaslestad [17].

From the three years of field measurements at Dovre [17], it was found that the change in internal bending moments was insignificant in the observed periode compared to the maximum bending moment that occoured during backfilling, see figure 6.34A). The axial forces in 1985 was measured to be 489 kN/m at the crown, which gradually increased with time. In 1987 the axial forces at crown level had increased to 860 kN/m to then stabilize, see figure 6.34B).

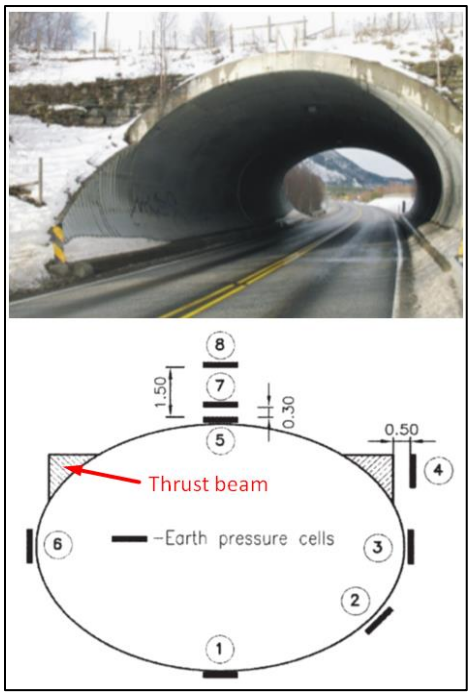

Figure 6.33 – Dovre structure showing the high-way and placing of the eight Glötzl cells

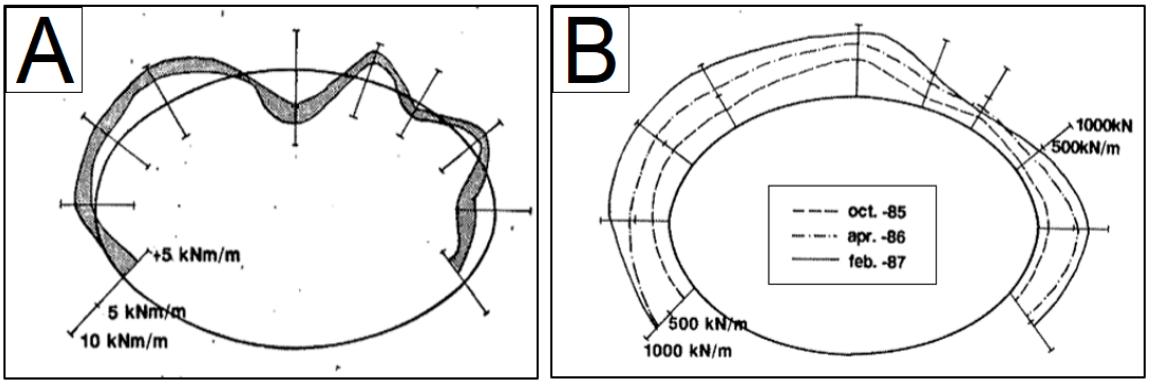

Figure 6.34 – Measurements on Dovre structure in the periode 1985-1987, showing A) change in bending moments and B) change in internal thrust forces in a periode over three years (Modified after Vaslestad. J, 1990)

The Glötlz cells that was mounted on the culvert continously measured earth pressures at the locations shown in figure 6.30 for more than 21 years. These long-term earth pressures revealed that the positive arching-effect over the culvert had remained stable for over 21 years, and the earth pressures had the tendency to first increase, for then to be decreased [19, 26]. A comparison of the initial earth pressures and the long-term earth pressures after 21 years are shown in figure 6.35.

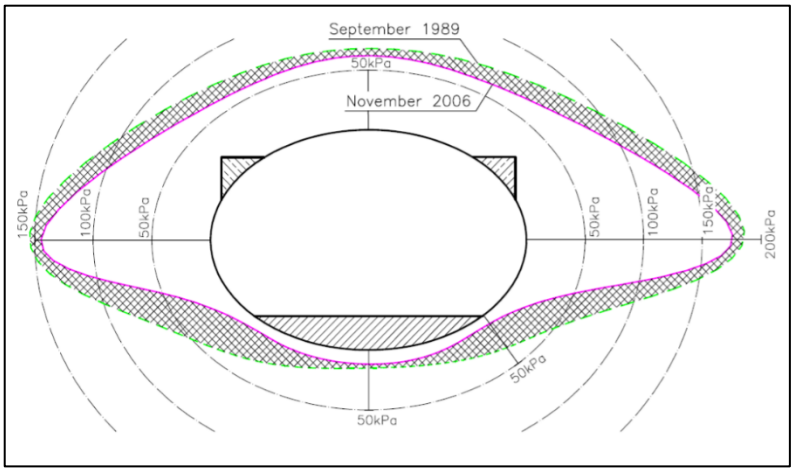

Figur 6.35 - Long-term eart pressures at Dovre structure, showing circumferential earthpressures from 1989 and 2006

Yearly results from Dovre at cell no. 3 and 6 is presented in figure 6.36 which shows that even if the earth pressures measured in 1989 were higher than in 2006, the overall tendency is that the earth pressure increases from the initial earthpressures at backfill finish. This behaviour suggests that the horisontal earth pressure tend to move towards passive state with time this despite this culvert not being subjected to any traffic loads.

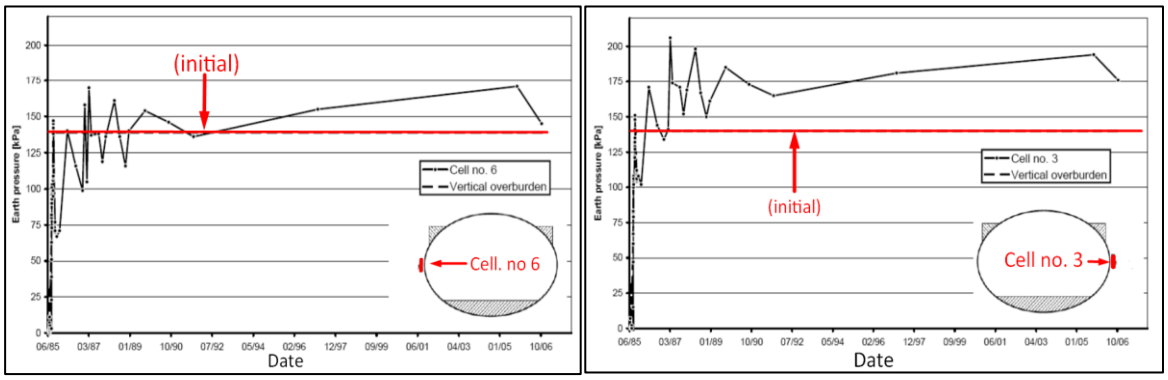

Figure 6.36 – Yearly earthpressures from 1985 to 2006, showing that the earth pressures tends to increase with time

The second case, Tolpinrud bridge was the first flexible super-span structure in Norway, and was built in 1982. The culvert was built both as railway tunnel and a bridge for road traffic, and was instrumented with a corrugation of MP 200x55 and a steel thickness of 6.8 mm. The cross-section of Tolpinrud was a pipe arch, having a span of 7.81 meter and was 6.92 meter high.

The backfill consisted of gravel and sand, and was compacted in 20 centimeter thick layers to about 97% standard proctor. The soil cover for this structure varied from 1.1 to 1.6 meters, see figure 6.37.

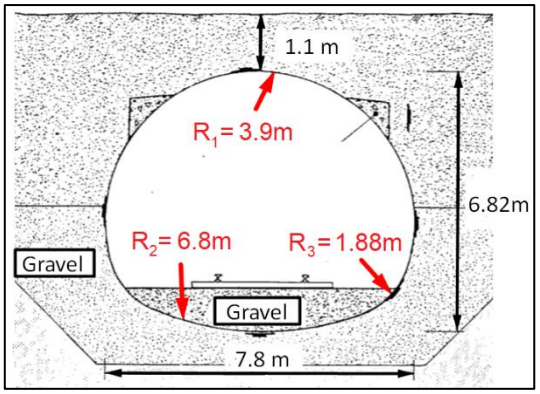

Figure 6.37 – Geometric properties of Tolpinrud structure built in 1982 (Modified after Vaslestad. J, 1990)

As with the Dovre structure, the Tolpinrud structure was also instrumented with thrust beams. Results regarding thrust beams are not discussed.

Glötzl cells was mounted at two longitudinal locations on this structure, one set of Glötzl cells at profile 25 and one set 50 meter seen from the northern end of the structure, see figure 6.38.

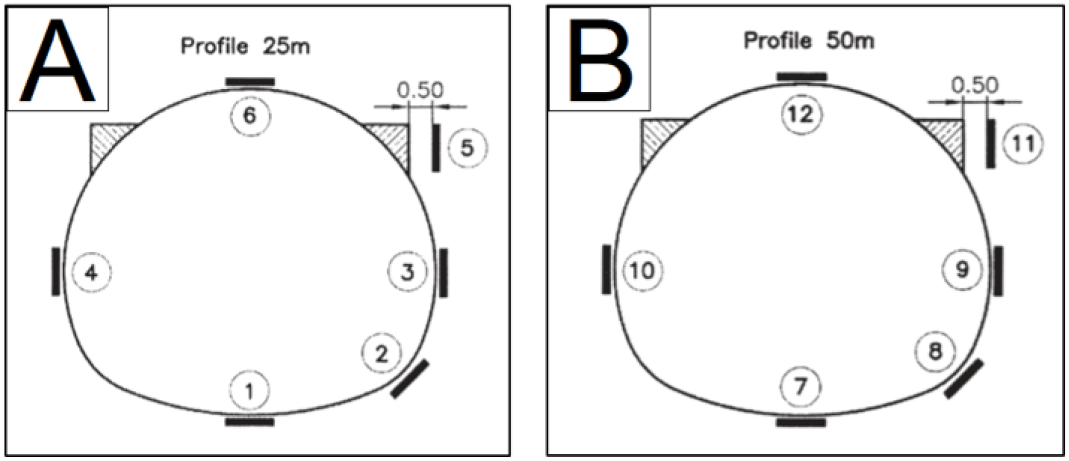

Figur 6.38 – Placing of Glötzl cells at Tolpinrud structure, showing locations at A) 25 meter and B) 50 meter seen from the northern side of the structure (Modified after Vaslestad. J, 1990)

At these locations, the Glötzl cells was measuring earth pressures for more than 21 years with the placing as shown in figure 6.358 respectively. In figure 6.39 results from earth pressure measurements at construction finished compared to 21 years are presented.

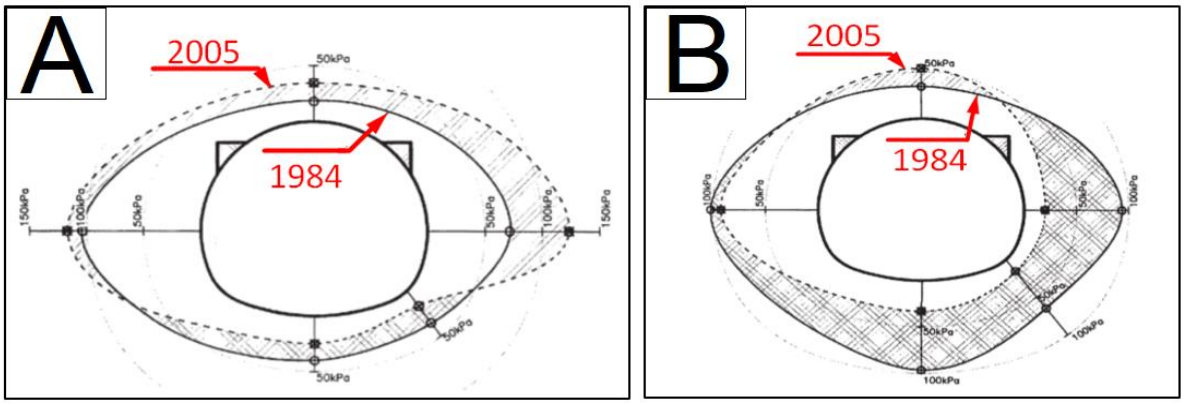

Figur 6.39 – Comparison of 21 years of earthpressure change at location A) profile 25 meter and B) profile 50 meter seen from the northern side of the structure (Modified after Vaslestad et. al, 2006)

In figure 6.40, yearly earthpressure is presented for Glötzl cell no. 3 and 4 from profile 25. The results at these locations shows that the horisontal earth pressures similar to Dovre, tends to increase with time. This suggests that the horisontal earth pressures surrounding flexible pipes tends to gradually move towards a passive state with time.

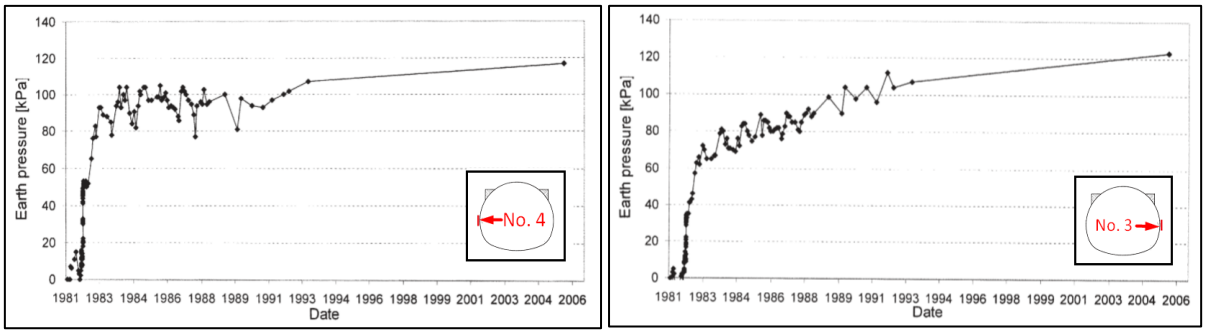

Figur 6.40 – Yearly earthpressure monitoring at cell no. 3 and 4, at profile 25 (25 meter into the tunnel, seen from north) (Modified after Vaslestad et. al, 2006)

The tendencies shown at Dovre and Tolpinrud suggests that independent of the surface conditions over these structures, flexible pipes undergoes a change in horisontal earth pressure with time which tends to increase. The three year of measurements at Dovre also showss that these structures also takes more of the overburden loads in ring compression as time passes by. This, together with the increased horisontal earth pressures suggests that the interaction flexible pipes has with its surrounding soil tends to become more and more rigid with time.

6.4.4 Dicussion

In the previous two sections, a comparison between several PLAXIS simulations and field measurements was carried out in order to investigate the effect changing materials, compaction loads or the unloading stiffness has on the surrounding forces of a burried pipe.

From PLAXIS it is found that the compaction loads used under the backfilling stages highly influences the structures overall long-term capacity. After construction finish little to no changes occours in internal bending moments compared to the change in axial forces (internal thrust). From the load test it was in general found that the internal thrust of the structure always increases as hardening of the backfill occours. This behaviour agrees god with what was measured at Dovre, see chapter 6.4.2.

The change in internal bending moments is insignificant to the change in bending moments during backfilling, while the axial forces increases tremendously when the structure is being loaded, demonstrating that the structures in the model in fact takes most of the load in ring compression. Hardening of the material in general causes the axial forces to increase, which also agrees with field behaviour.

When considering earth pressures there might be expected some uncertainty tied to the Glötzl cells. These measurements are still valuable in terms of discovering any general trends, and both results from Dovre and Tolpinrud suggested that the horisontal long-term earth pressures compared to at installation, tends to increase with time.

When increasing the unloading stiffness in PLAXIS it is seen from the load test at the horisontal displacement (fig. 6.40) that they decrease. The culvert becomes more rigid in its interaction with the surrounding soil when increasing the unloading stiffness.

From that it is the unloading stiffness that governs a soil materials long-term stiffness in a Hardening Soil model the load test revealed that this parameter also controls the rigidity of the soil-culvert interaction when the material hardens. As the earth pressures at Dovre and Tolpinrud has shown, it may be expected that this «rigidity» (i.e horisontal support) enhances with time.

When investigating earth pressures in PLAXIS no clear trend was been found from unloading-reloading the surface over the structure. A problem with investigating earth pressures around a nonuniform circular objects in PLAXIS, is that because the plate elements are modelled as small elements connected together by fixed points, there is a tendency of occouring small spikes at the interfaces which deviates the results, see figure 6.41.

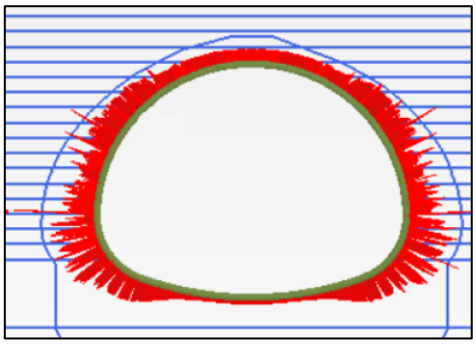

Figure 6.41 – Example of earth pressures around a circular pipe arch. Spikes deviating the results can clearly be seen at random sections of the structure

7 Final remarks, recommendations and discussions

During this project it has been performed alot of PLAXIS simulations and in this period of time, some experiences with the software has accumulated which are shared in this chapter.

7.1 General recommendations

The first point to adress is that when running dynamic analyses with moving train loads, using the track system presented in chapter 2 in combination with a Hardening Soil backfill, it requires alot of computer power. It was not able to create any of these models on the commercial computers available at the university of NTNU, and special workstations had to be used.

One should also be aware of the amount of disk space required to run these simulations. A typical sequence of simulations using a Hardening Soil model, medium mesh and running 3-5 train passages requires about 60-100 GB of disk space. Increasing the number of saved steps will increase the size of these files considerably.

7.1.1 Divergence problems and model collapse

One should be aware of some problems experienced when changing and editing existing models. In some cases after creating stages and running simulations in a given model, if that model is saved and later changed (i.e structures, adding lines or changing boundary conditions), it has been experienced that PLAXIS remembers the previous model conditions even if each phase is deleted/changed according to the new model condition and severe convergence errors might occour.

In order to avoid this problem it is in general recommended to save a template before adding any phases or saving a simulation for then to change the model conditions later. When this problem occoured in this project, it was found that the only solution at the time was to model everything from scratch again.

Another problem associated with divergence is tied to the «free-field» option (see chapter 3.3). It was found that if the model plastifies to much during a dynamic analysis then the end boundaries at the x-axis might collapse, see figure 7.1.

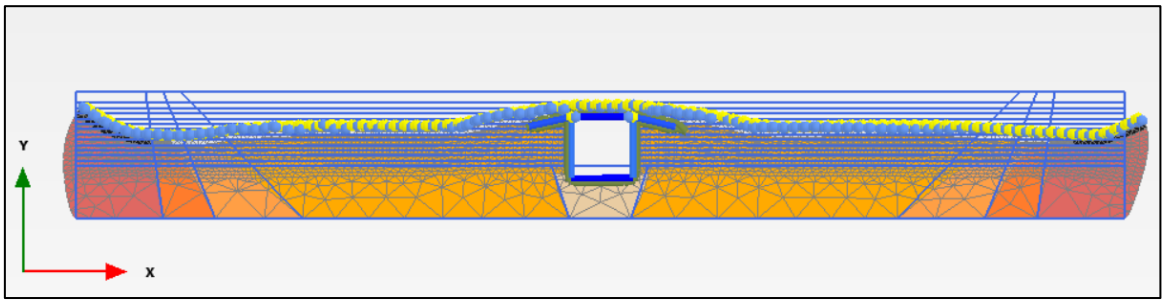

Figure 7.1 – An example of the «flow tendency» at the end boundaries of the model when using the «free-field» option

Some purposals has been made that this relates to the large plastifications of the soil at the end boundaries. A quick fix could be as simple as compacting the surface with a line load extending over the entire model. Another way of fixing this is to change the number of «max steps» in the pase explorer, but this solution is not consistent.

7.2 Soil models

When selecting soil models there are certain things one should bear in mind. It was decided in this project to stick with the Hardening Soil model for the backfill since it was the best fit for catching both the short-term (i.e construction and backfilling) and long-term behaviour of the transition zones (when the elastic state has been reached). The reason for this being the case is that simpler models such as Mohr Columb or Linear-Elastic models uses the same loading stiffness as unloading stiffness.

During this project it was found that it is possible to catch similar behaviours of flexible steel pipes during backfilling with Mohr Coloumb compared to a Hardening Soil model. This is only achievable in Mohr coloumb when keeping the line loads (compaction) activated when adding a layer on top however. When this load is unactivated again, it forces the underlying layer to remember the compaction effect for that layer when it is unactivated. This approach was used by Wadi [27,28].

For a long-term condition however, when moving train loads has passed over a culvert surrounded by a backfill modelled with Mohr Coloumb, the soil model doesn't plastify as it does in Hardening Soil which affects the final interaction forces surrounding the culvert when the model has plastified.

As has been discussed in chapter 6.3 and 6.4, a soil models ability to «trap» and remember stresses is crucial in order to catch a realistic long-term behaviour of flexible steel pipes. When these train loads has passed a flexible culvert, it is seen that the internal bending moments of the structure remains almost completely unchanged while the axial forces increases. As was shown in chapter 6.4, this behaviour agrees well to field.

At the last stages of this project however, it was found that Hardening soils inbuilt formulation of stress dependent stiffness (not covered in this report) causes the stiffness at the surface to be low, untill the surface is loaded. In the regular embankment this does not make that big of a difference but at the culvert however, both above and bellow the effective stresses are nearly zero, and only after the soil starts to displace from the train loads does the stiffness come into play.

Ways to improve this problem can either be to increase the unloading stiffness or decrease the power modulus number (m). See the inbuilt formulation of stiffness in chapter 6.1.2.

7.3 Dynamics and damping

As was discussed in chapter 3, the way these moving point loads are modelled causes severe vibrations at the entry and exit of the model. This led to a solution of damping the end boundaries of the model was used, while remaining the section at the transition zones undamped (see chapter 3.4.2). It was first aimed for keeping the transition zones completely undamped even though it has been the quasi-static aspect of the problem that has been of interest in this project.

It was found that this was only achievable with a Linear-Elastic soil model as Hardening Soil creates a «stair» at the deflections when running train simulations. The displacements seemed to increase after each point load (i.e «axle») had passed any node of the model (see chapter 3.6). This problem can either be solved from using damping or unhooking the «tension cut-of» option. One should be aware of that unhooking the tension cut-of option does not work until about 3-5 simulations has been performed.

If the dynamic aspect of this track system are to be considered, one should also be aware of some of the frequency domains that has been observed at the track. It was for example detected an unrealistic frequency domain, more specific the pad to pad passing frequency at each individual sleeper, see chapter 3.5.1. In a dynamic analysis this frequency domain should be accounted for.

To validate the dynamic aspect of the entire track system of this model one could try to compare the frequencies seen at the track in this model to a «receptance test», where the frequency domains of a real track are compared.

Bibliography

[1] Bane NOR (2017). *InterCity-prosjektet, Teknisk Designbasis for InterCity-strekningene*. Rev. 04A 13.12.2017.
Available at https://www.banenor.no/Prosjekter/prosjekter/intercity/dokumenter/

[2] Bane Nor (2019). *Teknisk regelverk*, norwegian railway normal.
Available at https://trv.jbv.no/wiki/Overbygning/Prosjektering/Sporkonstruksjoner

[3] PLAXIS (2019). PLAXIS 2D Reference Manual 2019.
Available at: https://www.plaxis.com/support/manuals/plaxis-2d-manuals/

[4] Jernbanekompetanse (2019). *Track components, rail fastening systems*. Norwegian database for textbooks on railway infrastructure.
Available at: https://www.jernbanekompetanse.no/wiki/Sporets_komponenter/Befestigelse

[5] Esveld. C (2016). *Modern Railway Track*, Digital Edition 2016, version 3.8, MRT-Productions. Revisions available at: http://www.esveld.com/

[6] Iwnicki. S (2006). *Handbook of Railway Vehicle Dynamics*, Taylor & Francis Group LCC. Digital edition, chapter 6. Track issues by Tore Dahlberg. Available at NTNU library

[7] NSB, Norsk jernbaneskole (1999). Elektrisk trekkraftmateriall.
Available at http://www.bibsys.no/

[8] Statens Vegvesen (1983). Bruprosjektering 12, Kulverter og rør. Normal, håndbok-100.
Available at https://brage.bibsys.no/

[9] Petterson. L, (2007). *Full Scale Tests and Structurual Evaluation of Soil Steel Flexible Culverts with low Height of Cover*. Report. Civil and Architechtural Engineering. Kungliga Tekniske Högskolan (KTH). Available at: http://kth.diva-portal.org/

[10] PLAXIS 2D (2015). *Ground response analysis in PLAXIS 2D*. Report. Delft University of Technology & PLAXIS. Available at www.plaxis.com

[11] Kramer. S (1996). *Geotechnical Earthquake Engineering*. Prentice-Hall International series in civil engineering and Engineering mechanics

[12] Nordal. S (2017). *Geodynamics*, Compendium. Phd Course, Lecture notes. Norwegian University of Science and Technology, Geotechnical Group.

[13] Nordal. S (2018). *Geotechnical Engineering Advanced course, lecture notes and background material*, Compendium. Norwegian University of Science and Technology, Geotechnical Group.

[14] Statens Vegvesen, Vegdirektoratet (2015). *Handbook R761, Guideline. Processcode 2 – Standard description for bridges and piers.* Available at www.vegvesen.no

[15] Statens Vegvesen, Vegdirektoratet (2014). Normal, Håndbok N400: *Bruprosjektering, prosjektering av bruer ferjekaier og andre bærende konstruksjoner*. Available at https://www.vegvesen.no/fag/publikasjoner/handboker

[16] Statens Vegvesen, Vegdirektoratet (2018). Veileder, Håndbok V220: *Geoteknikk i vegbygging*. Available at https://www.vegvesen.no/fag/publikasjoner/handboker

[17] Vaslestad. J (1990). Soil Structure interaction of buried culverts. Doctoral thesis, Norges tekniske høgskole (NTH), Geotechnical division.

[18] Duncan. M. J (1979). *Behaviour and Design of Long-Span Metal Culverts*. Vol. 105 No. GT3. Journal of Geotechnical Engineering Division

[19] Petterson. L and Sundquist. H (2014). *Design of soil-steel composite bridges*. Report 112, 5th Edition. Dept. Architectural and Civil Engineering, Royal Institute of Technology, KTH, Stockholm, Sweden. Available at http://www.diva-portal.org/

[20] Andersson. A, Karoumi. R, Sundquist. H (2012). Full scale tests and structural evaluation of soil-steel flexible culverts for high-speed railways, II European Conference. Available at http://kth.diva-portal.org/

[21] Williams. K, Mackinnon. S and Newhook. J (2012). *New and innovative developments for design and installation of deep corrugated burried flexible steel structures*. Research paper, archives of insitute of civil engineering

[22] Viacon (2015). *MultiPlate MP200, Fleksible flerplaterør i stål*. Product catalogue. Available at www.Viacon.no

[23] Machelski. C (2015). *Stiffness of railway soil-steel structure.* Article. Bridge Division, Civil Engineering Institute, Wroclaw University of Technology.

[24] Machelski. C (2014). *DEPENDENCE OF DEFORMATION OF SOIL-SHELL STRUCTURE ON THE DIRECTION OF LOAD PASSAGE.* Article. Bridge Division, Civil Engineering Institute, Wroclaw University of Technology. Available at http://www.rabdim.pl

[25] Machelski. C, Antoniszyn. G & Michalski. B (2006). *LIVE LOAD EFFECTS ON A SOIL-STEEL BRIDGE FOUNDED ON ELASTIC SUPPORTS.* Article. Bridge Division, Civil Engineering Institute, Wroclaw University of Technology. Available at http://www.rabdim.pl

[26] Vaslestad. J, Emdal. A, Kunecki. B (2007). Long-term earth pressure measurements of two large-span flexible culverts in Norway.

[27] Wadi. A (2012). *Soil Steel Composite Bridges, A comparison between the Pettersson-Sundquist design method and the Klöppel & Glock design method including finite element modelling.* Master thesis, KTH, Stockholm. Available at http://kth.diva-portal.org/

[28] Wadi. A (2019). *Soil Steel Composite Bridges, Research advamces and application.* Doctral thesis in structural engineering and bridges, KTH, Stockholm. Available at http://kth.diva-portal.org/

[29] Moore. I. D (2017). *Large-Scale Laboratory Experiments to Advance the Design and Performance of Buried Pipe Infrastructure*. Queen's University, Ellis Hall, Kingston Available at https://ascelibrary.org/

[30] Regier. C, Hoult. A. N, Moore. I. D (2017). *Laboratory Study on the Behavior of a Horizontal-Ellipse Culvert during Service and Ultimate Load Testing*. Canada. Bridge eng. Journal. Available at https://ascelibrary.org/

[31] Nålsund. R (2014). *Railway Ballast Characteristics and Performance*. Doctoral thesis. Norwegian University of Science and Technology (NTNU). Available at https://brage.bibsys.no

[32] Lysmer. J, Richart. F.E (1966). Dynamic response to footing to vertical loading. Journal of the soil mechanics and Foundations Division, ASCE, Vol. 92, No. SM1, pp. 65-91.

[33] Janbu. N (1963). *Soil Compressibility as Determined by Oedometer and Triaxial Tests*. European Conference on Soil Mechanics and Foundation Engineering, Wissbaden.

NORWEGIAN UNIVERSITY OF SCIENCE AND TECHNOLOGY
DEPARTMENT OF CIVIL AND ENVIRONMENTAL ENGINEERING

Appendix B – REPORT II

ROGER 1000 measurements for locating vertical track deviations at culvert underpassings

- ***A comparison between ROGER 1000 measurements at flexible steel-soil composite bridges and rigid concrete bearing culverts in Norway***

By Dan Sergei Sukuvara

Acknowledgement

Associated with this report, I want thank Trine-Lise Lorentsen and Terje-Vasset from Bane NOR, Peder Hembre from ViaCon and Albert Lau from NTNU.

A special thanks goes to Trine-Lise for spending time on extracting and sorting data from BaneData for me. This report would've not been feasible without her help.

For assessing the stiffness over flexible steel-soil composite bridges I was very dependent on design drawings for evaluating the transition zones. I want to thank Peder for providing me with necressary design drawings and background information for the three chosen steel culverts in this report.

I also want to thank Albert Lau and Terje for providing me with additional background information and helping with intreprent the data.

Abstract

ROGER 1000 is a measuring veichle that checks the entire railway network in Norway twice a year. A typical norwegian maintenance cycle goes as following, track deviations is first measured by ROGER 1000, these deviations is then registered as work orders with a certain priority which is then corrected by the means of maintenance.

In this report the vertical track data measured by ROGER 1000 was studied for six norwegian culvert cases, three being built of flexible steel and three being built of rigid concrete. The aim of this study was to investigate if there could be detected any correlation between the available ROGER 1000 data, stiffness variations and potential differential settlements at the transition zones of these culverts.

The general conclusion is that there has not been found any trend in track deviation for these six culverts that stands out from a normal track. Only one culvert case of flexible steel and one of rigid concrete showed some deviation at the location of the culvert, namely Holme and Jarenhaugen culvert while the rest of these cases showed nothing. It should be considered that the overall track quality at some of these locations were quite bad which might have contributed to some of the deviations seen above these culverts.

The final conclusion of this report is that there is no direct correlation seen between the deviations registered by ROGER 1000 and stiffness variations purposedly caused by these culverts.

.

Table of contents

1 Introduction

The purpose of this report is to provide practical insight of the deterioration rate of real railway transition zones in Norway. The methods used in this report is primarily interpretation of data from the measureing train «ROGER 1000», where geometric track data from the yearly inspections are studied. In addition to detecting track deviations, these ROGER 1000 measurements are also considered valuable in terms of understanding the magnitudes these track deviations at the transition zones is registered in.

The report is written in total 4 chapters. The first chapter describing prerequisites for the chosen culverts in this study, followed by background information on ROGER 1000. In total six culverts were chosen, three being made of flexible steel and three being made of rigid concrete, presented in chapter 2 and 3 respectively. The report is summarized with a discussion in the last chapter.

1.1 Methods

Due to time constraint of this project, it was only possible to investigate available data that had been registered previously. It was first decided that the best way of evaluating existing transition zones was by comparing vertical track deviations registered by ROGER 1000 with tamping frequencies. If there was any correlation between ROGER 1000 and the tamping frequency, one could make some sort of thought and conclusion on the deterioration rate of these transition zones.

After investigating and analyzing tamping data, it was found that correlating tamping frequencies to ROGER 1000 measurements involved alot of uncertainty. Tamping is often divided into several categories where the most relevant for transition zones would be «point tamping». It was concluded that even this category contained uncertainty since tamping never occours in track section less than 50 meters due to the lenght of the tamping train. Another uncertainty tied to tamping is that these workourders are based of ROGER 1000 measurements, which according to Bane NOR, may also deviate. This makes it difficult to tie the track deviations registered ny ROGER 1000 to tamping data with high certainty. An example showing tamping frequencies are shown for Holme culvert in chapter 2.2.

It was decided that the most outcome when considering the time constrain of this project would come from investigating several ROGER 1000 measurements instead of comparing them to tamping frequencies. This approach makes it possible to catch any trend in the registered deviations by ROGER 1000, which regardless of the tamping frequencies provides better understanding of the maintenance demand at these culverts.

1.1.1 Prerequisites

A prerequisite when selecting cases for comparison that the track conditions of each case, should be as similar as possible. From consulting with several people in Bane NOR, it has been suggested that the transition slab for concrete culverts was introduced somewhere around year 1990-2000. It was also found that stored ROGER 1000 measurements before year 2000 doesn't exist in Bane NORs database, Banedata. The prerequisites for these six culverts was therefore as following

- The culverts cannot have been built before year 2000
- Cases where the track is alligned completely straight over the bridge is prefered
- Only cases were the track is founded on ballast (over the bridges) is applicable
- Cases where auxiliary rails- or any other component affecting the track stiffness is avoided

1.1.2 Limitations

Some of the selected culverts have very limited information on them. For example, of all the selected concrete culverts, factors such as height of cover or cross-sectional data were not available. These variables however, makes a bigger difference for flexible culvert cases than rigid oes. As a result, only flexible culvert cases with sufficient cross-sectional data available, were chosen.

The concrete culverts were selected based of from ROGER 1000 photos tak every 0.5 meter at the track. Other than this visual check, no other technical consideration was made when chosing these culverts.

1.2 ROGER 1000 measurements for railway transition zones

Each year the entire norwegian railway network is controlled by a measuring coach named ROGER 1000. The measuring car does various checks for deviations on the track and pantograph, which is performed twice a year on the entire railway network in Norway, see figure 1.1.

Figure 1.1 - The measuring car ROGER 1000 for controlling the entire railway network in Norway (Source www.BaneNOR.no)

Any deviations registered by ROGER 1000 outside the allowable limit for that track component will be postnoted into BaneData (the norwegian railway database) as a workorder. These workorders are registered with different levels of importance, were a critical workorder for example, means that the demand for maintenance at its post is acute.

Speaking in terms of vertical track deviations which was the most relevant post for transition zones in this project, when the rail deviates up to a certain limit, that deviation will be registered as a workorder based of the limits set to the location of that railway line. In the case of a transition zone, such deviations is often tied to differential settlements which often requires tamping (maintenance) to correct. This means, if severe irregularities is registered by ROGER 1000 it is reasonable to assume that some of these deviations might be related to difference in track stiffness and differential settlements.

1.2.1 Measureing vertical track deviation with ROGER 1000

ROGER 1000 is instrumented with accelerometers and rail measurement sensor heads, a system consisting of lasers and cameras at the front of the car for scanning rail profiles. According to Esveld. C, this system is used by most modern measuring veichles for normal train speeds between 80-160 km/h [1].

The general ORIAN Rail Measurement system is reportedly made up of lasers and cameras at the front of the veichle which scans the rail at regular intervalls of 25 cm [1], see figure 1.2.

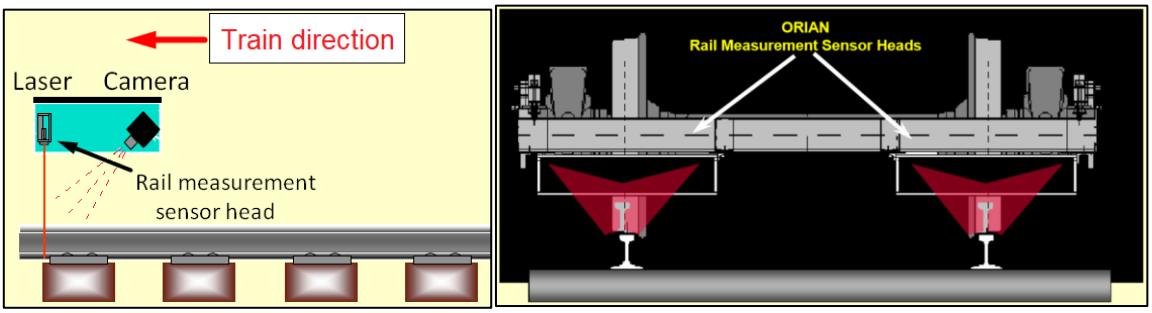

Figure 1.2 – Rail measurement system used for most measuring trains, a system built up of lasers and cameras which registers cross-sectional track data at regular intervalls (Modified after Esveld. C, 2016)

When the measuring car registers data at any given section, the rail is hit by a light from these lasers which then are recorded and analyzed by the camera system. The intrepretation from the cameras are then sent to the computers in the veichle, which then links them to kilometer data (i.e location). This scan however, is for investigating track quality, horisontal deviations, gauge distances but not the tracks vertical deviation which is deriven from the accelerometers.

According to Esveld. C [1], the vertical deviations measured by ROGER 1000 are taken from relative displacements tranducers which measures the veichle body acceleration at regular intervals. This acceleration is then double integrated with respect to time which returns the absolute spatial car body displacement. This spatial car body displacement are then compared to a teoretical profile and hence, the vertical deviation of that track section is returned.

The results for vertical track deviation are typically presented at the longitudinal axis (i.e the x-axis) presenting kilometer (location), and an y-axis presenting vertical deviation from the target profile. The results are shown in such a way that any deviation from the target profile is presented, see figure 1.3.

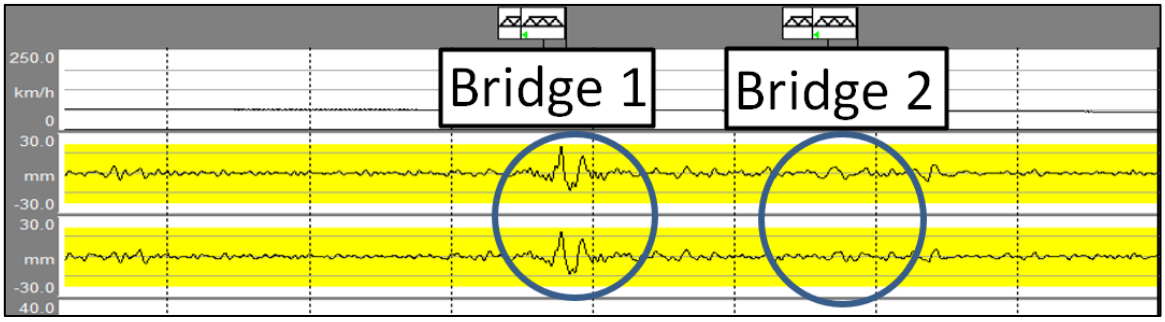

Figure 1.3 – Example: Vertical track deviations measured with ROGER 1000 at two bridges (Via Terje Vasset, Bane NOR)

The figure shows how measurements looks like directly from ROGER 1000, and shows a section across two bridges (denoted as «bridge 1» and «bridge 2»). For bridge 1 these results shows that there occours some kind of «dip» before and after passing this bridge. At bridge 2, these deviations cannot be seen however, suggesting that the track over that bridge holds the same quality as the rest of the normal track of the entire section presented in the figure.

The marked area in yellow shows the tolerated limit for vertical track deviation at that particular line, where it can be seen that bridge 1 is just bellow the acceptable limit before a work order will be registered. The magnitude of this area (i.e allowable vertical deviation of the track) is governed by the requirements set for that line, where higher speed for example leads to less of a tolerated deviation.

It should be highlighted that these measurements does not reflect track stiffness but more the track quality at the particular time ROGER 1000 passes that section. This means, in a case were the track is fixed to a stiff bridge while being founded on ballast over an embankment and no transition slabs has been used (the «worst case scenario»), such cases may also show zero deviation if the ROGER 1000 measurement are performed shortly after a maintenance cycle. These measurements must therefore be viewed more as a check rather than a quantity for evaluating track stiffness. It should also be mentioned that the measurements provided by ROGER 1000 is rough, and may show deviations themselves.

2 ROGER 1000 measurements for three cases of flexible steel-soil composite bridges

The stiffness of railway tracks over flexible steel-soil composite bridges are highly influenced by factors such as soil cover, span lenght, backfill execution and the geometry of the culvert. It was therefore considered a necessity to only use cases were design drawings were available.

Three flexible steel culverts were chosen, Sjånes culvert (built 2016), Holme culvert (built 2012) and Viker culvert (built 2012). All these cases had the cross-sections of the type «pipe arch» according to the Swedish Design Method (SDM) [3], a geometry which is the more softer types of flexible culverts compared to other profile types when thinking in terms of verticale track stiffness.

These culverts were chosen mostly based of the available design drawings and ROGER 1000 photos, but also because they had a relative large span lenght compared to their soil cover, a factor which is crucial when assessing the stiffness transition problem for a railway track.

The three culverts are located in the middle and southern part of the country, as shown in figure 2.1. Exact coordinates for each culvert are also given in table 2.1.

Figure 2.1 – Location of Sjånes, Holme and Viker culvert in Norway (From Bing maps)

Table 2.1 – Location coordinates for all three culverts

	Latitude [°N]	Longitude [°E]
Sjånes culvert	66.27127342° N	13.98277598° E
Holme culvert	63.80950167° N	11.45683034° E
Viker culvert	61.33532932° N	10.27328908° E

From the available ROGER 1000 data, a interwall 500 meter before and after each culvert was specified for each case. This was specified for all the chosen culvert cases in this report in order to be able to distinguish the deviations at the culverts from the deviations at the free track to exclude, and get a overview on the local conditions, which is very important when trying to locate the source of these deviations.

As the ROGER 1000 data will show, the vertical deviations for each case (in general) varies quite alot. This can be tied to the difference in allowable deviation for each of these locations, but also other variables such as local backfill or soil conditions. For comparison reasons, a maximum and minimum vertical deviation in the plots (the y-axis) is set to $\pm$ 40 mm for all cases.

According to the measuring department from Bane NOR, it is also reasonable to expect some deviation from the results in respect the kilometer data. Under circumstances such as wet weather conditions, creep and slip forces at the contact patch between wheel and rail can according to Bane NOR, cause up to 20-30 meter deviation in the kilometer data. An interwall of 25 meter before and after each culvert was therefore specified as «transition zone», a section where deviations are considered to possibly be related to the culverts.

2.1 Sjånes steel-soil composite culvert

Sjånes is a flexible Steel-Soil Composite Bridge (SSCB) built at the railway line «Nordlandsbanen» in year 2016. The culvert is located at kilometer 489 according to the referance system for Nordlandsbanen, a few kilometers south from the city Mo i Rana, see figure 2.2.

Figure 2.2 – Location of Sjånes culvert at «Nordlandsbanen» in mid Norway (After Bing maps)

The culvert was built with a steel corrugation of the type, MP 200x55 with 6 mm thick steel plates. The cross-section is of the type «pipe arch», i.e it consist of three radiis. The profile of this culvert is of the more wider types of pipe arch, labeled as «VM-profile» according to ViaCons profile classification system [4]. These profile types keeps the necessary foundation level to a minimum with the cost of being softer in terms of surface loads. More on profile types can be found in the SDM-manual [3] or ViaCon product catalogue.

According to the design drawings, this culvert spans about 4 meter, is about 3.1 meters high and 18 meters long.

The design drawings also specifiy that the backfill at this case consist of a sandy gravel with a maximum fraction of 32 mm, corresponding to a «base course material» in the SDM-manual [3]. The height of cover seen from the bottom of a sleeper to the crown of the culvert, varies between 0.93 to 1.3 meter, see figure 2.3.

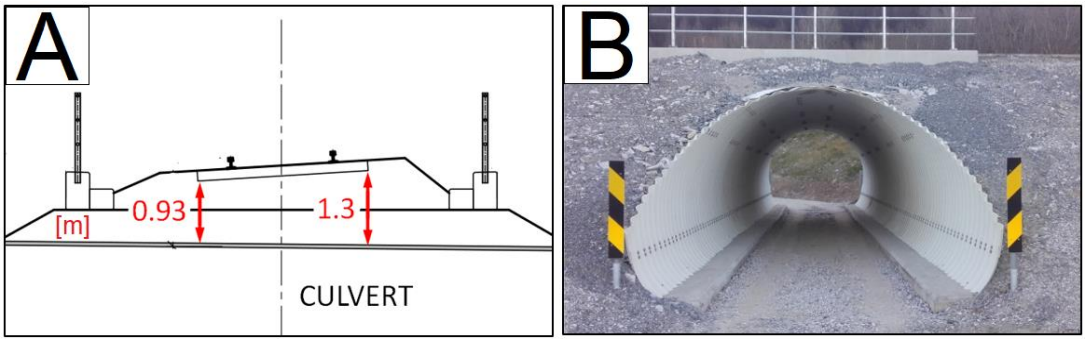

Figure 2.3 – Illustration of A) Soil cover conditions and B) photo from the site at Sjånes (Source: ViaCon Norway)

It is important to be aware of that this culvert is built in a slack curve with a radius ranging between 1200 to 3000 meter, which is the reason for the height of cover varying along the sleeper in figure 2.3. Photos from the site and a ROGER 1000 photo shown in figure 2.4 .

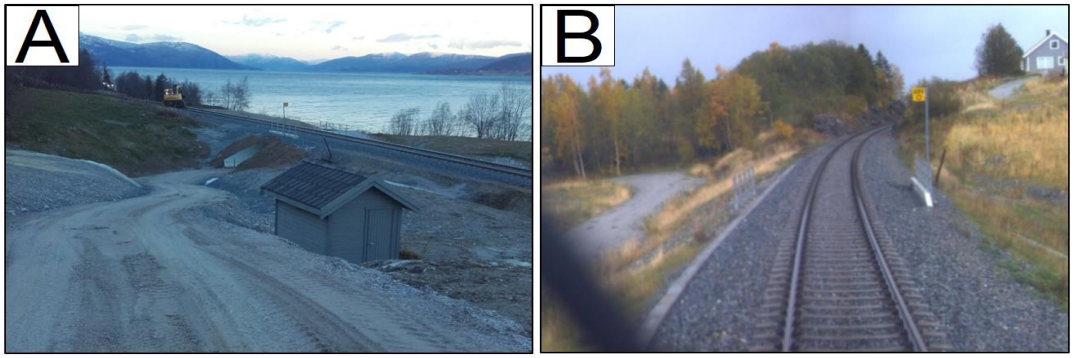

Figure 2.4 – Site conditions showing A) placing of the culvert in relation to the track and B) ROGER 1000 photo taken a few meters before passing the culvert (Source: ViaCon Norway and Bane NOR)

2.1.1 ROGER 1000 results

This section discusses the ROGER 1000 results presented on page 7–9. Since this culvert is relatively new, only measurements from 2017 and 2018 were available.

What these plots show is a 1000 meter section of ROGER 1000 measurements with the culvert placed in the middle of the plot. The results in these plots shows the vertical deviation with respect to the target profile, which is defined as zero along the y-axis.

The general trend from these results is that it is hard to make any conclusion of these results in respect to the culvert. In alot of these measurements, it can be seen that the noise (i.e vertical deviation) is consistent over the entire 1000 meter section. In general, the quality of this track is bad which can be seen at the measurements from 10.03.17, evidently worsening after three months (15.06.17).

When ROGER 1000 is traveling in the uposite direction of the 15.06.17 measurements, the new measurements from 17.06.17 shows similar deviations along the track which validates the previous tendencies. Some peaks can now be seen at the culverts location from the measurements of 15.06.17 and 17.06.17, but still gives no ground to state that these deviations has anything to do with the stiffness of the track above the culvert, as similar peaks can be found at kilometer 488.8-488.9 (100-200 meter before the culvert).

From the measurement peformed 01.06.18 and 03.06.18 it can be seen that the noise has been significantly reduced, suggesting that maintenance of the track has been performed. The overall conclusion of this particular case is that there is no ground to claim that the transition zone of this culvert contribute to any additional maintenance.

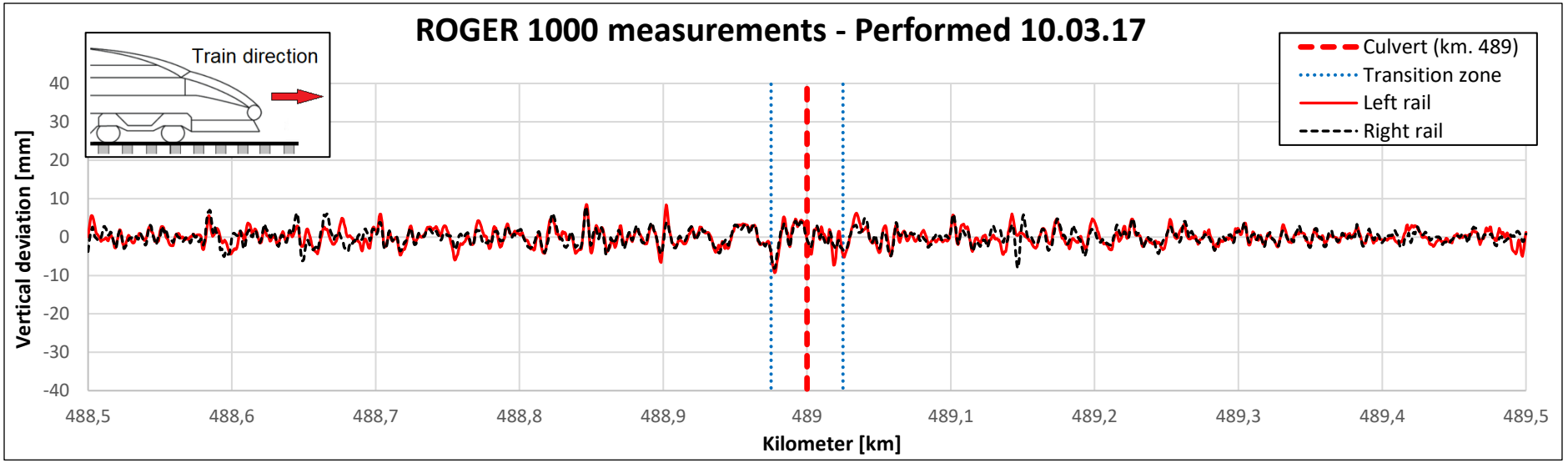
ROGER 1000 measurements - Performed 10.03.17
Train direction
Culvert (km. 489)
Transition zone
Left rail
Right rail
Vertical deviation [mm]
40
30
20
10
0
-10
-20
-30
-40
488,5
488,6
488,7
488,8
488,9
489
489,1
489,2
489,3
489,4
489,5
Kilometer [km]

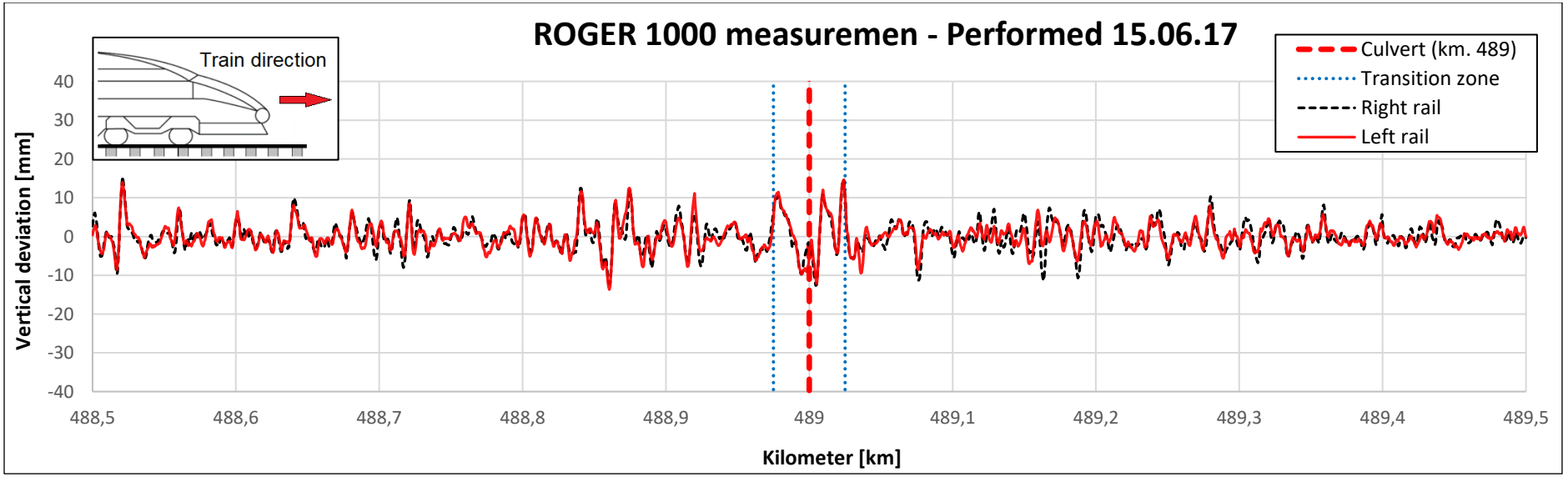
ROGER 1000 measuremen - Performed 15.06.17
Train direction
Culvert (km. 489)
Transition zone
Right rail
Left rail
Vertical deviation [mm]
40
30
20
10
0
-10
-20
-30
-40
488,5
488,6
488,7
488,8
488,9
489
489,1
489,2
489,3
489,4
489,5
Kilometer [km]

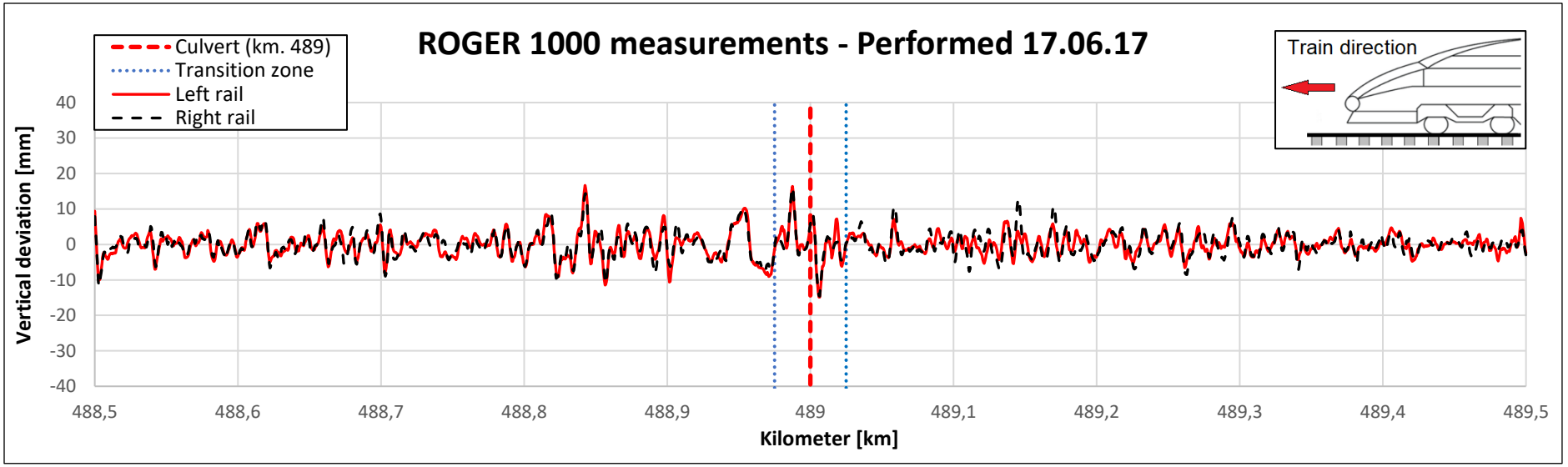
ROGER 1000 measurements - Performed 17.06.17
Culvert (km. 489)
Transition zone
Left rail
Right rail
Train direction
Vertical deviation [mm]
40
30
20
10
0
-10
-20
-30
-40
488,5
488,6
488,7
488,8
488,9
489
489,1
489,2
489,3
489,4
489,5
Kilometer [km]

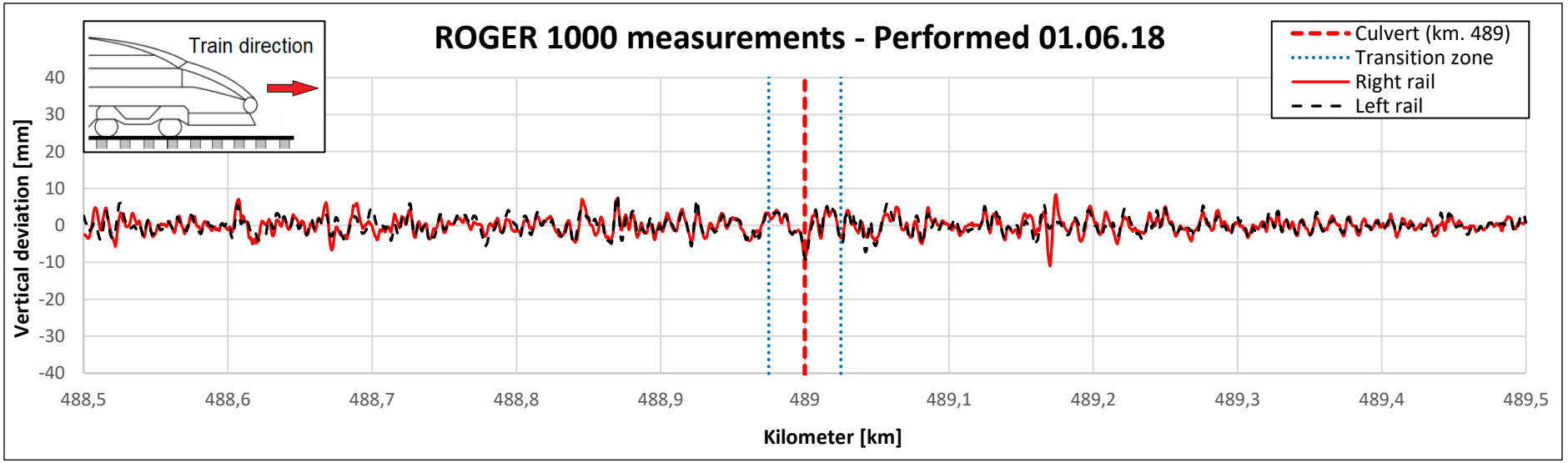
ROGER 1000 measurements - Performed 01.06.18
Train direction
Culvert (km. 489)
Transition zone
Right rail
Left rail
Vertical deviation [mm]
40
30
20
10
0
-10
-20
-30
-40
488,5
488,6
488,7
488,8
488,9
489
489,1
489,2
489,3
489,4
489,5
Kilometer [km]

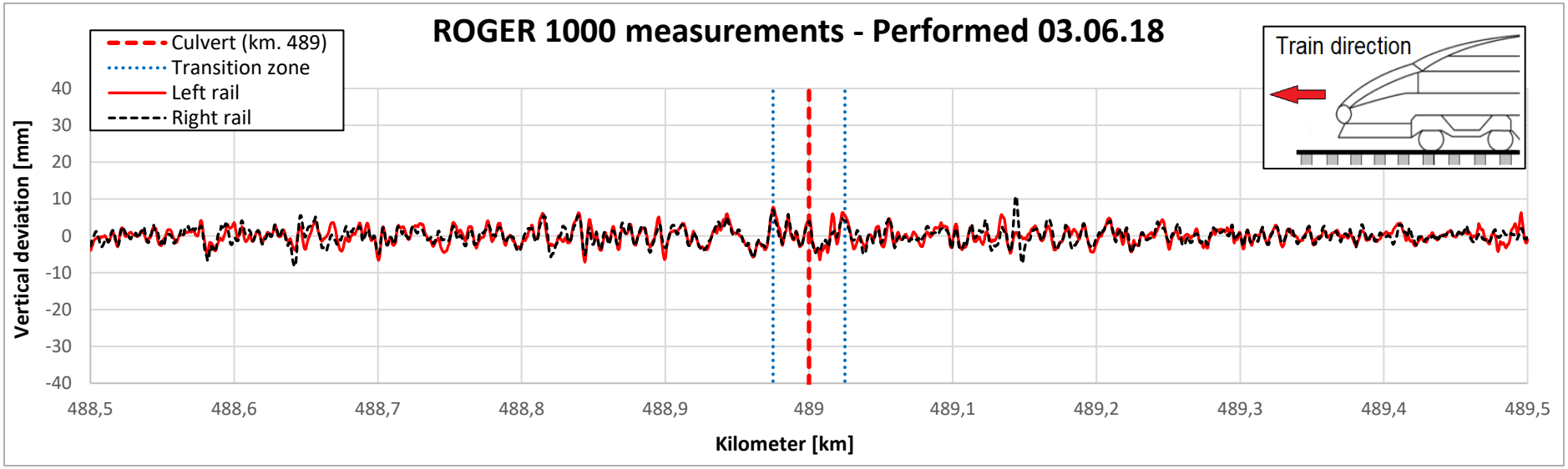
ROGER 1000 measurements - Performed 03.06.18
Culvert (km. 489)
Transition zone
Left rail
Right rail
Train direction
Vertical deviation [mm]
40
30
20
10
0
-10
-20
-30
-40
488,5
488,6
488,7
488,8
488,9
489
489,1
489,2
489,3
489,4
489,5
Kilometer [km]

2.2 Holme steel-soil composite culvert

Holme culvert was built in year 2012 at the railway line «Nordlandsbanen». The culvert is located at kilometer 98.882, a few kilometers north from the city Verdalen, see figure 2.5.

Figur 2.5 – Loaction of Holme culvert at Nordlandsbanen

Holme culvert is similarly to Sjånes, built with a steel corrugation MP 200x55 and 6 mm thick steel plates. The cross-section of this culvert is also of the type pipe arch. Similar to the geometry of Sjånes, it is of the wider types of pipe arch labeled as «VM-profile» in ViaCons classification system [4].

Holme spans about 5.8 meter, is 22.8 meter long and has a lowest height of cover at about 1.1 meter seen from the bottom of the sleepers, see figure 2.6A).

Similar to Sjånes, Holme was also built in a slack curve with a radius ranging in between 1200 to 3000 meter, see figure 2.6B). This results in the height of cover also be differentiating, where the lowest being about 1.1 meter.

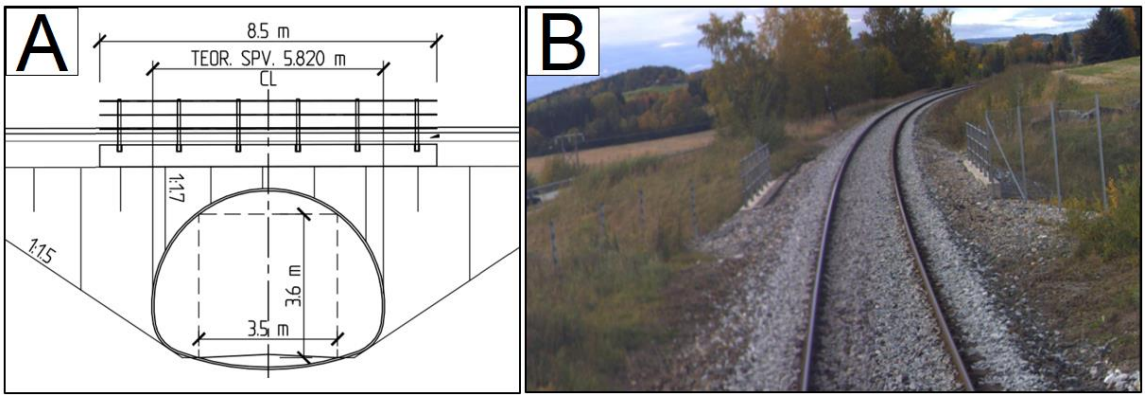

Figure 2.6 – Illustration of A) geometric conditions for the bridge in relation to the track and B) ROGER 1000 photo from the site a couple of meters before passing the culvert (Source: ViaCon Norway and Bane NOR)

2.2.1 ROGER 1000 results

This section discusses the ROGER 1000 measurements presented from page 12-14 with tamping data presented on page 11. Upose to Sjånes, some peaks in this case was located at the location of the culvert.

From the oldest measurements available (31.05.11), the noise is can be seen to be consistent over the entire 1000 meter section of the plot. About two years later (16.09.13) some peaks deviating from the rest of the noise is located above the culvert. This deviation is in the order of 10 mm, and are likely related to Holme culvert. But the root cause however, remains unknown as this peak is only seen at the right rail (compared to the left rail).

About a year later (19.09.14), this peak at the culvert is removed, which suggests that some maintenance has occoured between these measurements. In the same plot however, a new peak is located about 30-40 meters away from the culvert, but this peak is outside the dashed lines «transition zone» and involves to much uncertainty for it to be assumed to be related to the culvert.

Two years later (27.09.16), another peak is found at the culvert but the largest peak from this measurement, is found ca. 100 meter in front of the culvert. These measurements reveals that it is not only the culvert which causes deviations but also random sections of the free track. These findings gives an idea of how much the culvert in fact are affecting the track quality.

One year later (18.06.19) a significant peak is seen at the the culvert, deviating within a order of 10 mm. From the measurements performed this time, significant deviations of the track is only seen above the culvert, suggesting that the culvert contributes to some irregularities.

In figure 2.7 available tamping data is presented, and shows various maintenance operations that has occoured over the years. It can be seen that four tamping cycles of the kind «point tamping» has occoured at the location of the culvert, over a lenght of about 100 meter.

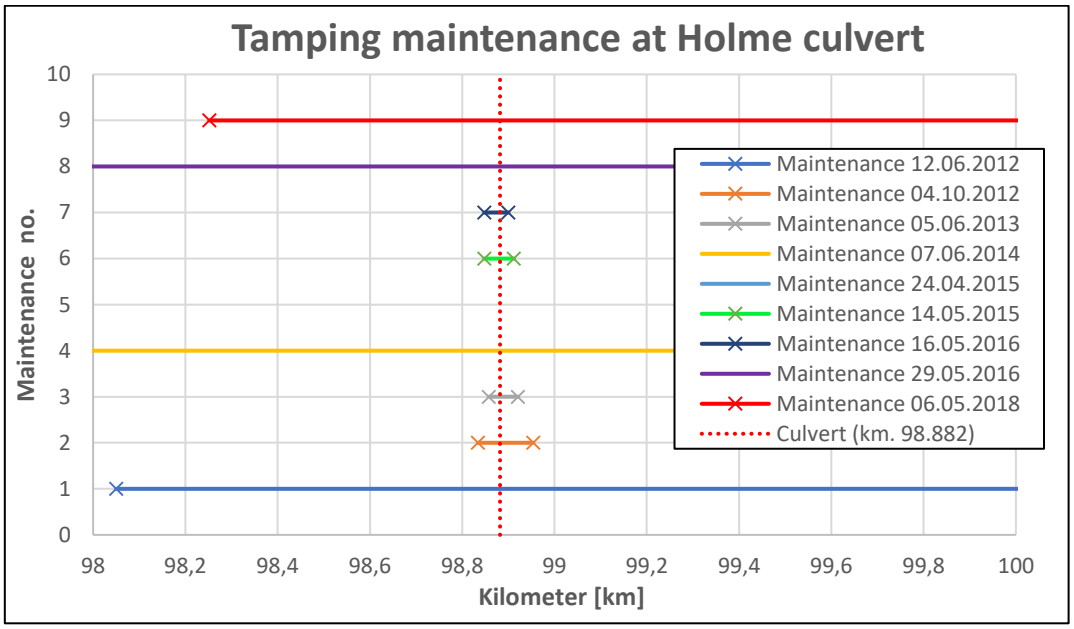

Figure 2.7 – Sorted tamping data for Holme culvert (Available via Bane NOR)

Whats important to highlight about tamping data is that the «point tamping» (i.e the concentrated tamping at the culvert) is based of ROGER 1000 results. According to the measurement division from Bane NOR, when a peak from ROGER 1000 deviates 20-40 meter from a bridge, it is often automatically assumed that this peak is related to the bridge and point tamping is requested as a result.

By comparing the point tamping from 05.06.2013 to the ROGER 1000 measurements performed 16.09.13, it is seen that the results are either inconsistent or the effect of tamping noneffective as the significant peak at the culvert occours only 3 months after this tamping scheme.

The third point tamping (14.05.15) are probably related to the ROGER 1000 measurements performed 19.09.14. As seen from these measurements, the peak is located about 30-40 meters away from the culvert. But this doesn't necessary mean that they're related to the bridge.

The last peak located at the bridge from ROGER 1000 (18.06.17), is seen about one year after a contious tamping cycle has been performed (29.05.16). This peak is probably related to the culvert as it is located inside the dashed line defined as «transition zone».

The results from this culvert shows that ROGER 1000 is able to catch deviations, likely caused by the culvert. The results from this case shows that some deviations in track geometry are probably related to the culvert, but doesn't say anything about the source of the problem. Comparing to the tamping datas the results are not always consistent. From the available data it is seen that tamping doesn't always get rid of the problem either.

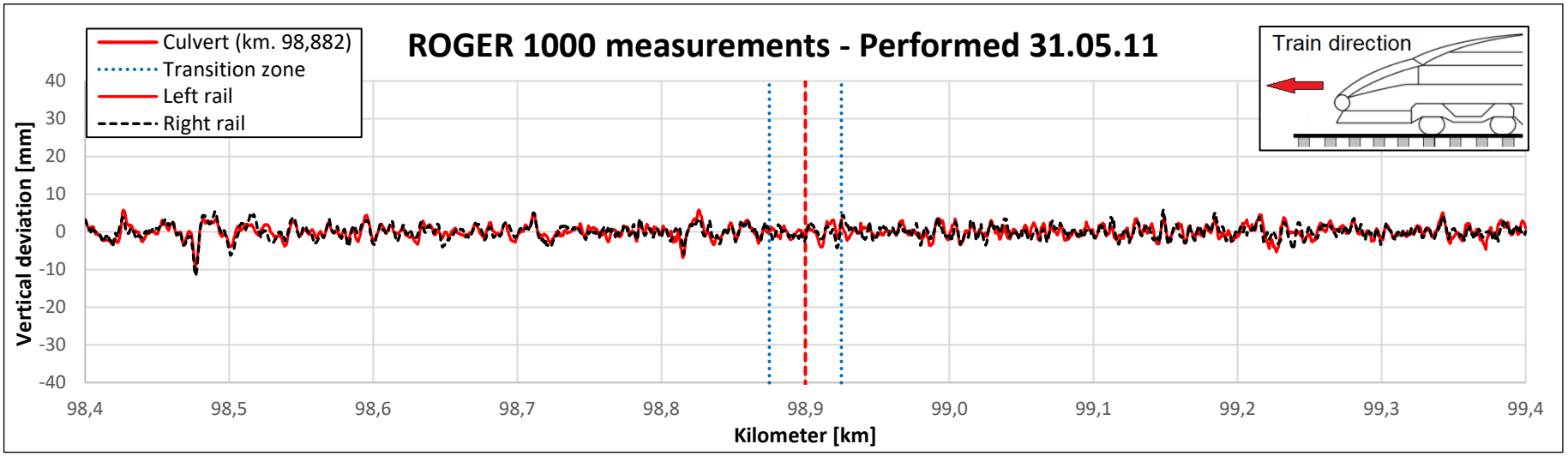
ROGER 1000 measurements - Performed 31.05.11
Culvert (km. 98,882)
Transition zone
Left rail
Right rail
Train direction
Vertical deviation [mm]
40
30
20
10
0
-10
-20
-30
-40
98,4
98,5
98,6
98,7
98,8
98,9
99,0
99,1
99,2
99,3
99,4
Kilometer [km]

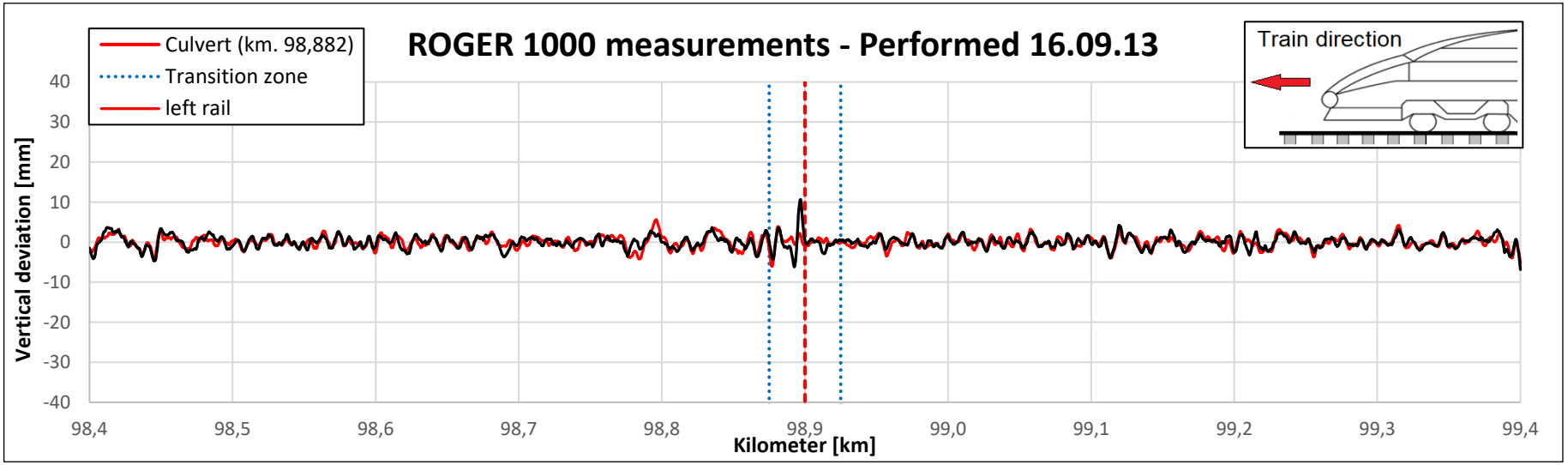
ROGER 1000 measurements - Performed 16.09.13
Culvert (km. 98,882)
Transition zone
left rail
Train direction
Vertical deviation [mm]
40
30
20
10
0
-10
-20
-30
-40
98,4
98,5
98,6
98,7
98,8
98,9
99,0
99,1
99,2
99,3
99,4
Kilometer [km]

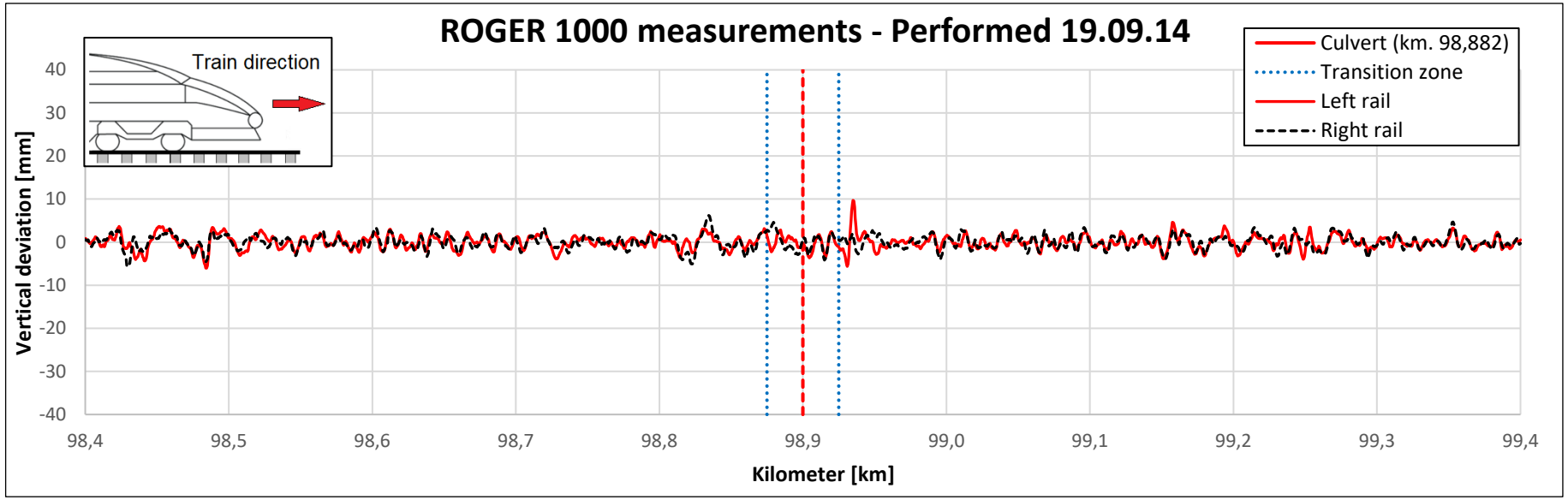
ROGER 1000 measurements - Performed 19.09.14
Train direction
Culvert (km. 98,882)
Transition zone
Left rail
Right rail
Vertical deviation [mm]
40
30
20
10
0
-10
-20
-30
-40
98,4
98,5
98,6
98,7
98,8
98,9
99,0
99,1
99,2
99,3
99,4
Kilometer [km]

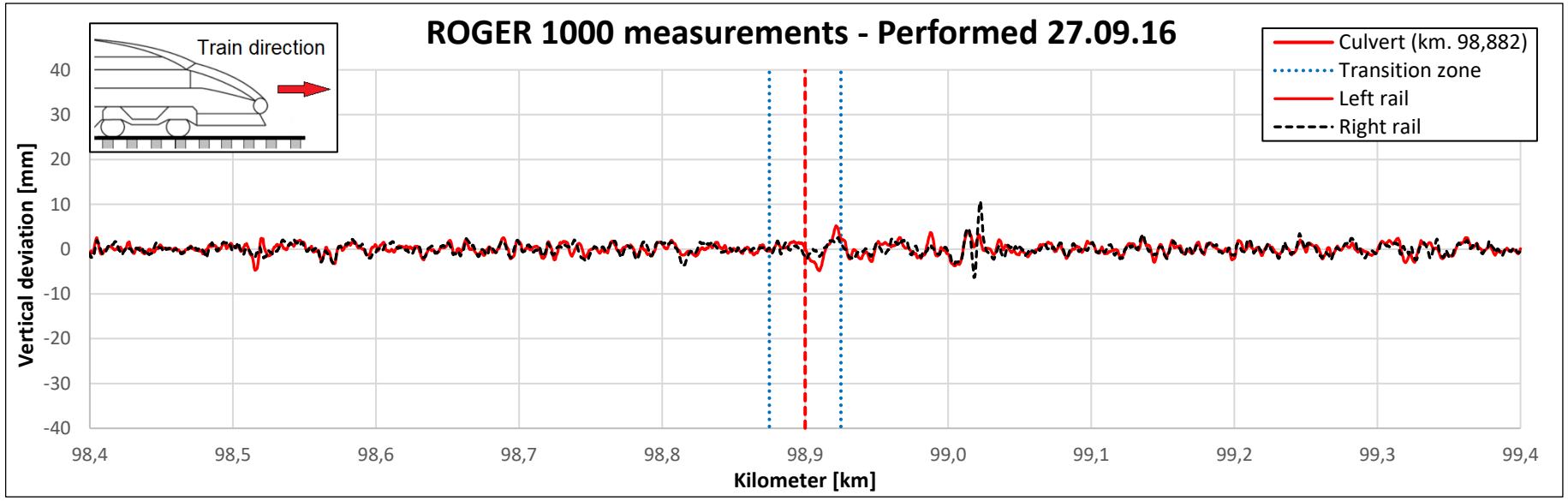
ROGER 1000 measurements - Performed 27.09.16
Train direction
Culvert (km. 98,882)
Transition zone
Left rail
Right rail
Vertical deviation [mm]
40
30
20
10
0
-10
-20
-30
-40
98,4
98,5
98,6
98,7
98,8
98,9
99,0
99,1
99,2
99,3
99,4
Kilometer [km]

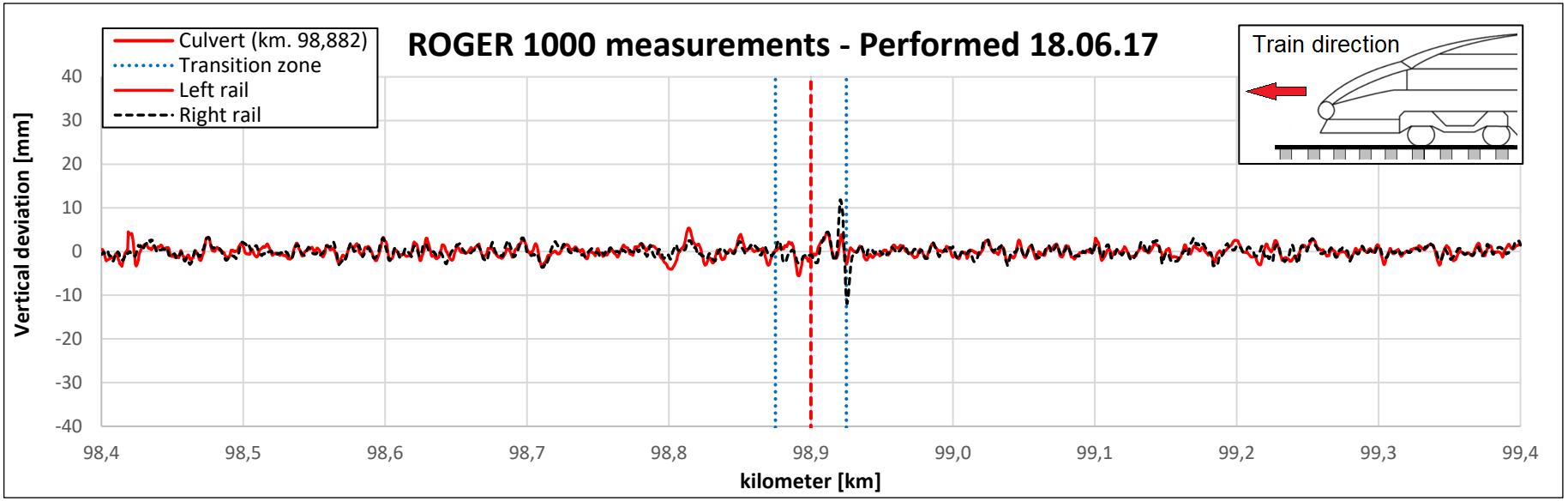
ROGER 1000 measurements - Performed 18.06.17
Culvert (km. 98,882)
Transition zone
Left rail
Right rail
Train direction
Vertical deviation [mm]
40
30
20
10
0
-10
-20
-30
-40
98,4
98,5
98,6
98,7
98,8
98,9
99,0
99,1
99,2
99,3
99,4
kilometer [km]

2.3 Viker steel-soil composite culvert

Viker culvert was built in year 2012 at the railway line «Dovrebanen», and is located at kilometer 217.357, a few kilometers away from the small village Tretten, see figure 2.8.

The culvert is built with a cross-secion of the type pipe arch, and is made of the more shallower types compared to the VM-profile used at Holme and Sjånes, denoted as «VT-profile» in ViaCons classification system [4].

According to design drawins, this culvert spans about 5 meter horisontally and is approximately 5 meters high. Judging from the design drawings, the soil cover seem to be about 1.4-1.6 meters, see figure 2.9A).

Viker culvert was built at a straight track section as shown from the ROGER 1000 photo in figure 2.9B).

Figure 2.8 – Location of Viker culvert at Dovrebanen

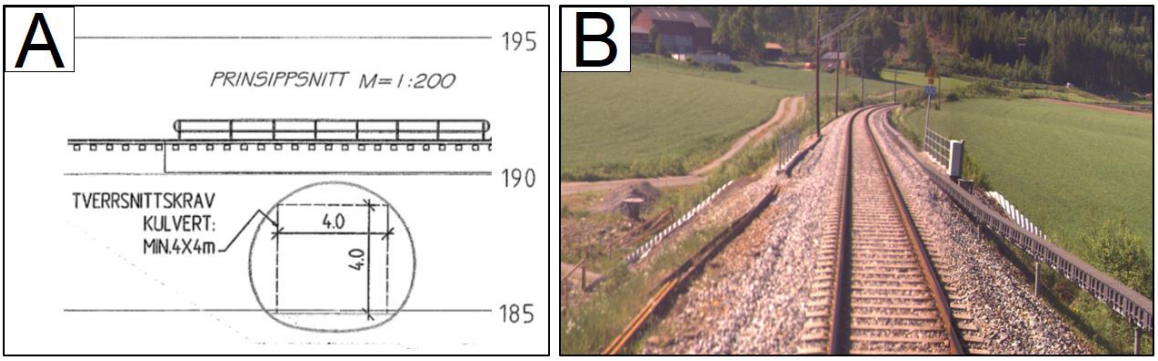

Figure 2.9 - Illustration of A) geometric conditions for the bridge in relation to the track and B) ROGER 1000 photos before passing the culvert (Source: ViaCon Norway and Bane NOR)

2.3.1 ROGER 1000 results

The results shown on page 16-18 are discussed in this section. Similar to Sjånes, no peaks cause by the culvert that certainly deviates from the rest of the 1000 meter intervall can be seen in this case.

From the intervall kilometer 217.15 – 217.35, there is some peaks that can be seen from several measurements regularly, but not above the culvert. These measurements are the ones from (22.05.14), (19.09.15) and (01.10.16) while little to no noise is seen at the culvert. At kilometer 217.55 and 217.7 some spikes also seem to occour frequently for these measurements.

The data from this case suggests that Viker culvert does not cause any additional deviation in track geometry compared to the free track.

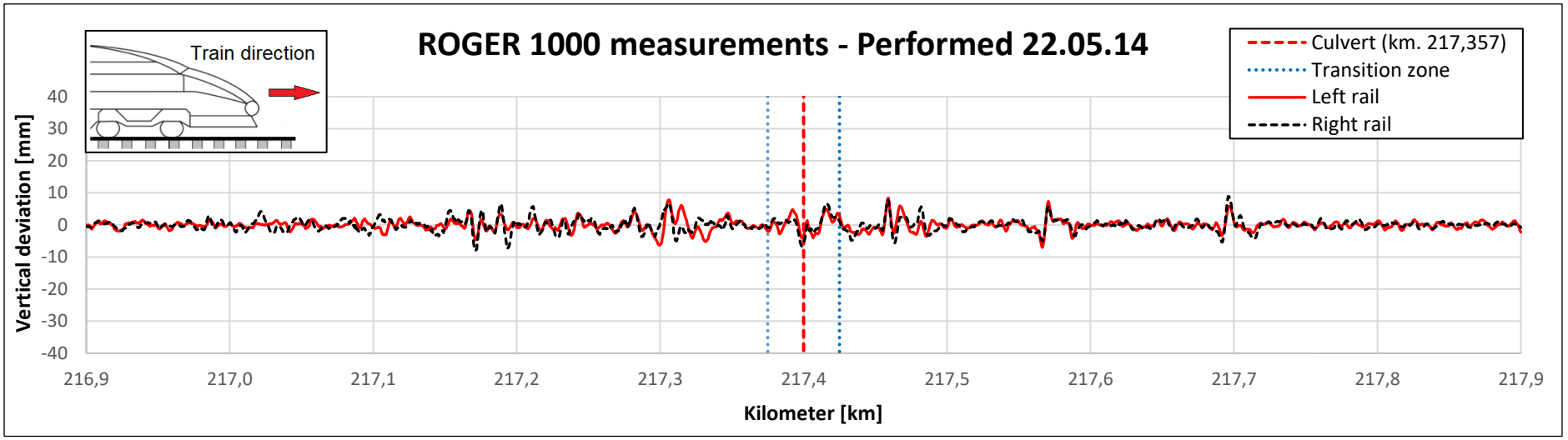
ROGER 1000 measurements - Performed 22.05.14
Train direction
Culvert (km. 217,357)
Transition zone
Left rail
Right rail
Vertical deviation [mm]
40
30
20
10
0
-10
-20
-30
-40
216,9
217,0
217,1
217,2
217,3
217,4
217,5
217,6
217,7
217,8
217,9
Kilometer [km]

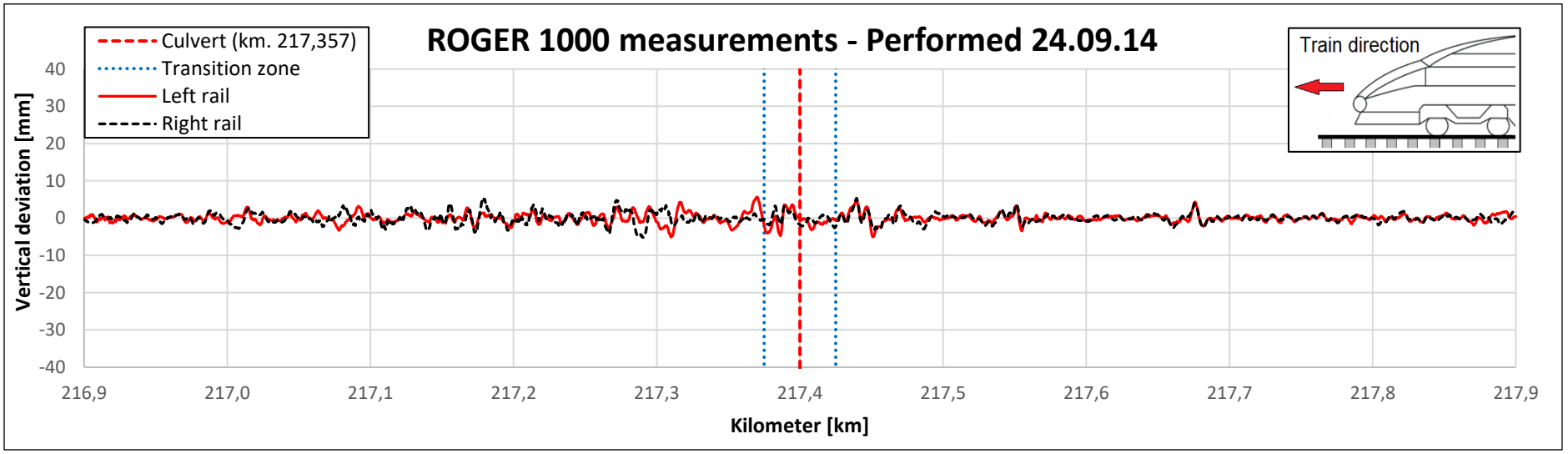
ROGER 1000 measurements - Performed 24.09.14
Culvert (km. 217,357)
Transition zone
Left rail
Right rail
Train direction
Vertical deviation [mm]
40
30
20
10
0
-10
-20
-30
-40
216,9
217,0
217,1
217,2
217,3
217,4
217,5
217,6
217,7
217,8
217,9
Kilometer [km]

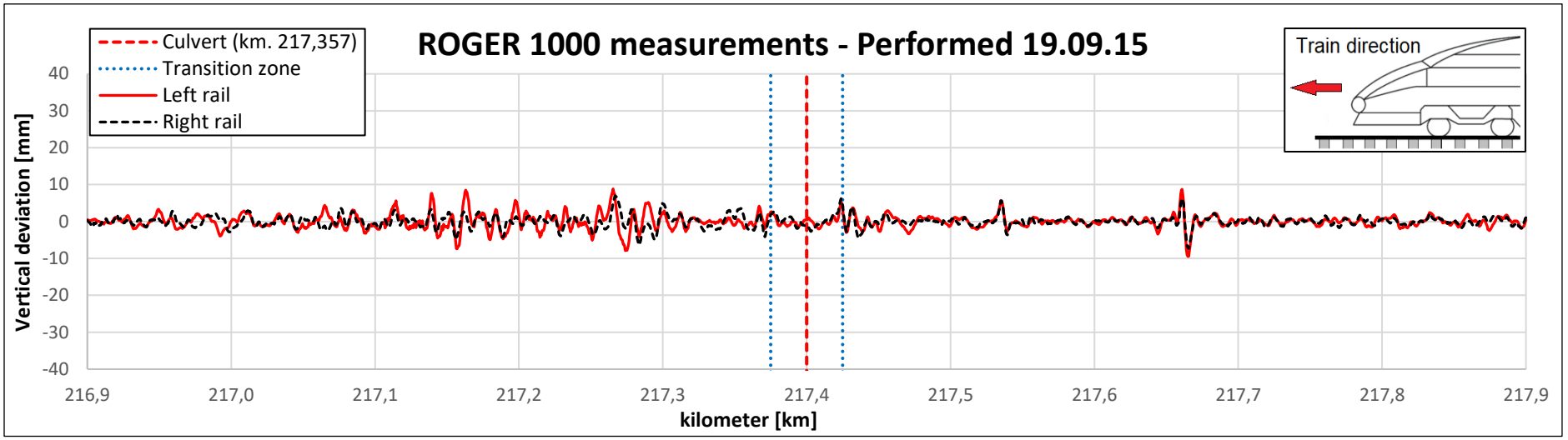
ROGER 1000 measurements - Performed 19.09.15
Culvert (km. 217,357)
Transition zone
Left rail
Right rail
Train direction
Vertical deviation [mm]
40
30
20
10
0
-10
-20
-30
-40
216,9
217,0
217,1
217,2
217,3
217,4
217,5
217,6
217,7
217,8
217,9
kilometer [km]

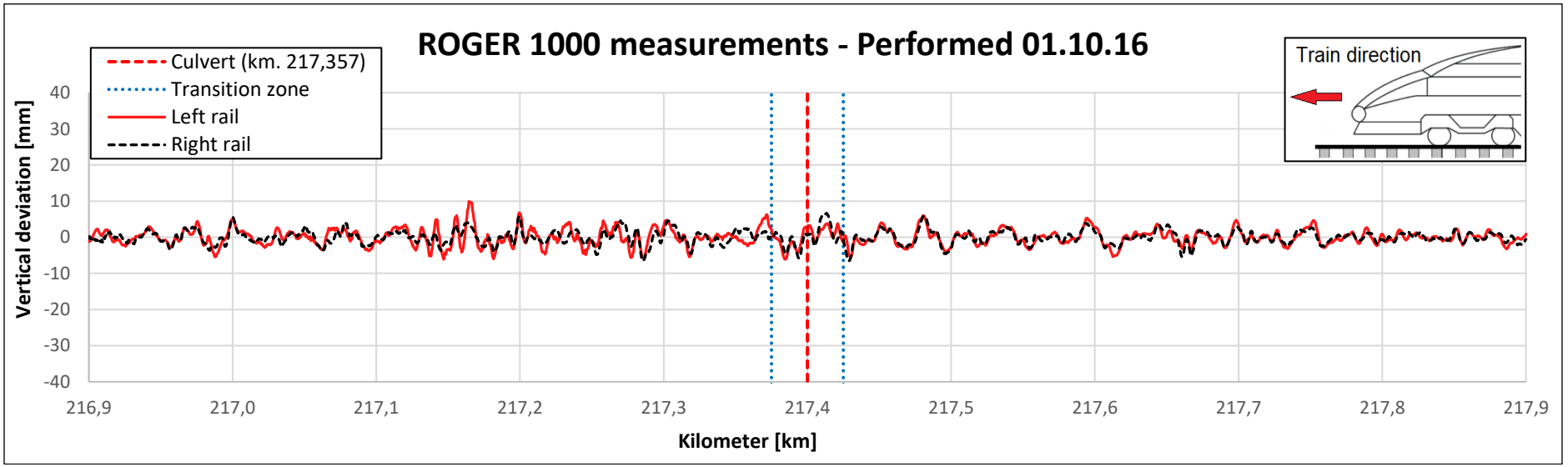
ROGER 1000 measurements - Performed 01.10.16
Culvert (km. 217,357)
Transition zone
Left rail
Right rail
Train direction
Vertical deviation [mm]
40
30
20
10
0
-10
-20
-30
-40
216,9
217,0
217,1
217,2
217,3
217,4
217,5
217,6
217,7
217,8
217,9
Kilometer [km]

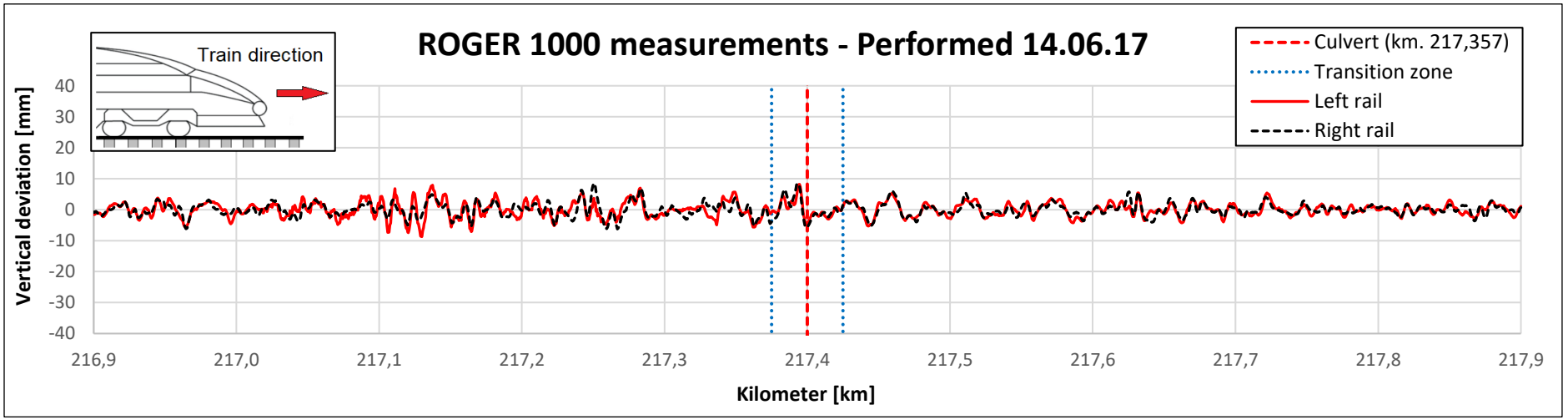
ROGER 1000 measurements - Performed 14.06.17
Train direction
Culvert (km. 217,357)
Transition zone
Left rail
Right rail
Vertical deviation [mm]
40
30
20
10
0
-10
-20
-30
-40
216,9
217,0
217,1
217,2
217,3
217,4
217,5
217,6
217,7
217,8
217,9
Kilometer [km]

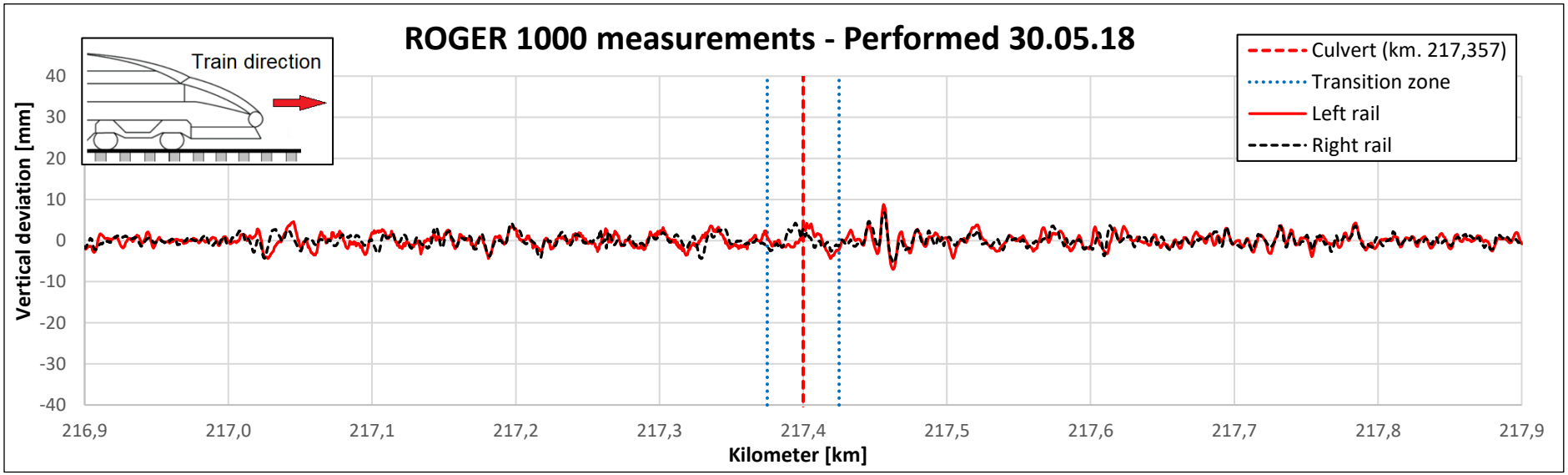
ROGER 1000 measurements - Performed 30.05.18
Train direction
Culvert (km. 217,357)
Transition zone
Left rail
Right rail
Vertical deviation [mm]
40
30
20
10
0
-10
-20
-30
-40
216,9
217,0
217,1
217,2
217,3
217,4
217,5
217,6
217,7
217,8
217,9
Kilometer [km]

3 ROGER 1000 measurements for three cases of rigid concrete culverts with transition slabs

When chosing cases for rigid concrete culverts it has been a challenge to find cases where design drawings were available and the criterias set for the local conditions were met. The three cases presented in this chapter was therefore mostly defined on the basis of ROGER 1000 photos, where it was ensured that curves were avoided and the height of cover was as low as possible. This decision was based of the presumption that the geometry of rigid concrete culverts does not cause that big of a difference compared to cases of flexible steel culverts.

Three rigid concrete culverts were chosen, Svenningdal culvert (built 2016), Vinstradalsveien culvert (built 2000) and Jarenhaugen culvert (built 2011). These culverts are located in the middel and southern part of the country, see figure 3.1. Exact coordinates for each culverts is also shown in table 3.1.

Figure 3.1 – Location at Svenningdal, Vinstradalsveien and Jarenhaugen concrete culvert in Norway (Source: Bing maps)

Tabell 3.1 – Location coordinates for all three culverts

	Latitude [°]	Longitude [°]
Svenningdal culvert	65.44200662° N	13.39377466° E
Vinstraveien culvert	62.51435352° N	9.60784839° E
Jarenhaugen culvert	60.00650904° N	10.02493990° E

Similar to the cases with flexible steel, a intervall 500 meter before and after each culvert is specified (along the x-axis of the plots). These culvert is located at their exact location by kilometer data, with an interval of ± 25 meter before and after the culvert (labeled as «transition zone»). A limit of ± 40 mm in vertical deviation (the y-axis) is also specified for all three cases.

3.1 Svenningdal concrete culvert

Svenningdal culvert was built in year 2016 and is located at kilometer 355.665 at the railway line «Nordlandsbanen», a few miles south from the city Mosjøen, see figure 3.2.

Even though no design drawings were available for this culvert, pictures from installation and backfilling was, see figure 3.3. These illustrations shows A) backfilling and compaction, B) when the backfill has reached the level of the transition slab and C) overfilling.

What valuable with these pictures is that they provide some information on the materials involved in the backfill aswell as how the installation has been carried out. It can be seen that 20/120 mm norwegian crushed rock has been used exclusively for the entire backfill and a light vibroplate has been used to compact the material bellow the transition slab, a procedure which is common according to the current norwegian regulations.

Figure 3.2 – Location of Svenningdal concrete culvert at «Nordlandsbanen» (Source: Bing maps)

Figure 3.3 – Installation and backfilling of Svenningdal culvert in 2016, showing A) compaction work, B) when the backfill has reached the slab level and C) Overfilling (Source: Farbu & Gausen AS)

In figure 3.4 ROGER 1000 photos is shown for demonstration of the site conditions at the track, showing that the track in this case is alligned completely straight over the culvert.

Figure 3.4 – ROGER 1000 photo before the measuring veichle is passing Svennindal culvert (Source: Bane NOR)

3.1.1 ROGER 1000 reuslts

This section discusses the ROGER 1000 data presented on page 21-22. In general, these results shows that the track quality at this location compared to other cases is good. For the first two measurements (performed 15.06.17 and 05.10.17), it can be seen that the deviations is relatively small and consistent over the entire 1000 meter section of the plot and there is no indication of the culvert causing any additional deviation.

One year later, the ROGER 1000 measurements shows that the track quality has worsen. But this only applies at sections outside the location of the culvert, for example at kilometer 355.2 to 355.3, kilometer 355.45 to 355.5 and kilometer 355.75-355.8.

The two years of ROGER 1000 measurements for this particular case shows that there is no indication of this culvert causing any additional track deterioration.

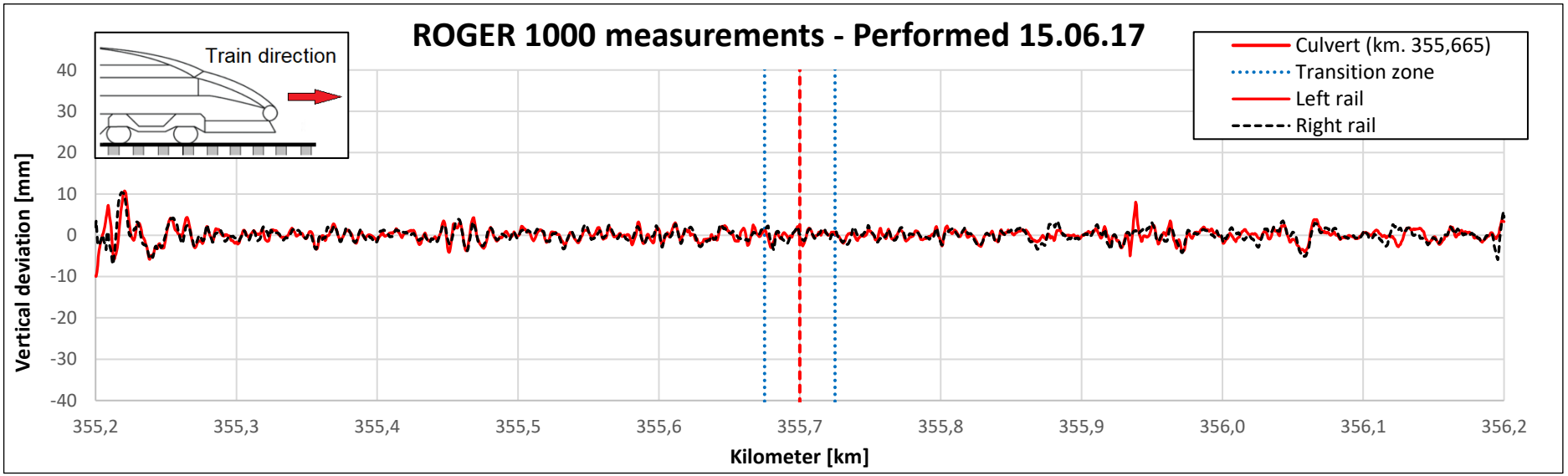
ROGER 1000 measurements - Performed 15.06.17
Train direction
Culvert (km. 355,665)
Transition zone
Left rail
Right rail
Vertical deviation [mm]
40
30
20
10
0
-10
-20
-30
-40
355,2
355,3
355,4
355,5
355,6
355,7
355,8
355,9
356,0
356,1
356,2
Kilometer [km]

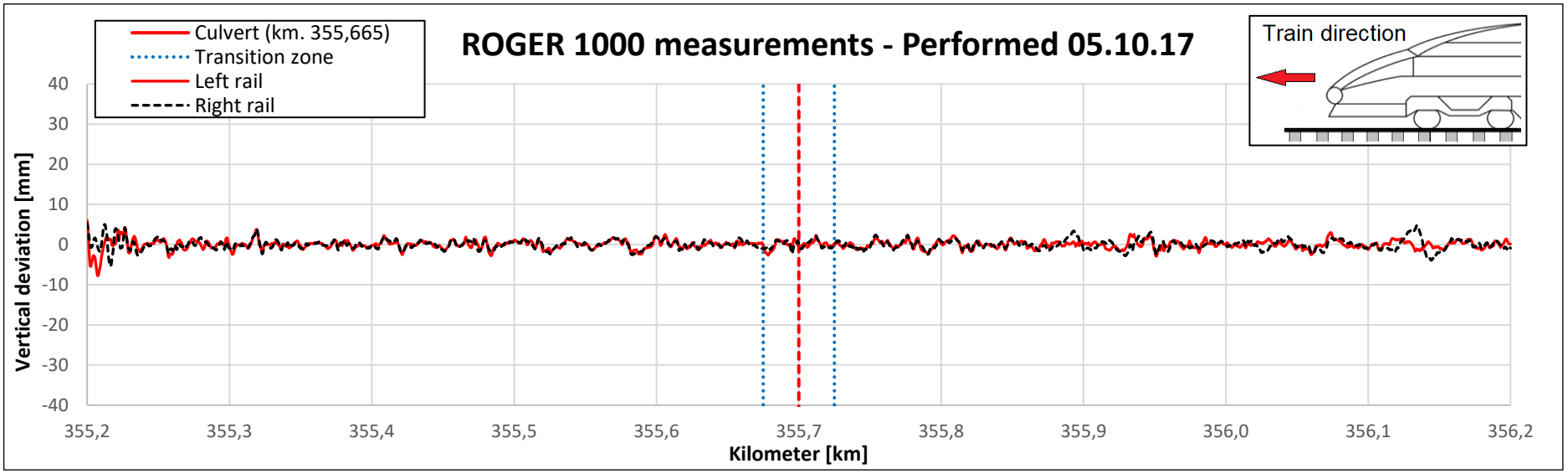
ROGER 1000 measurements - Performed 05.10.17
Culvert (km. 355,665)
Transition zone
Left rail
Right rail
Train direction
Vertical deviation [mm]
40
30
20
10
0
-10
-20
-30
-40
355,2
355,3
355,4
355,5
355,6
355,7
355,8
355,9
356,0
356,1
356,2
Kilometer [km]

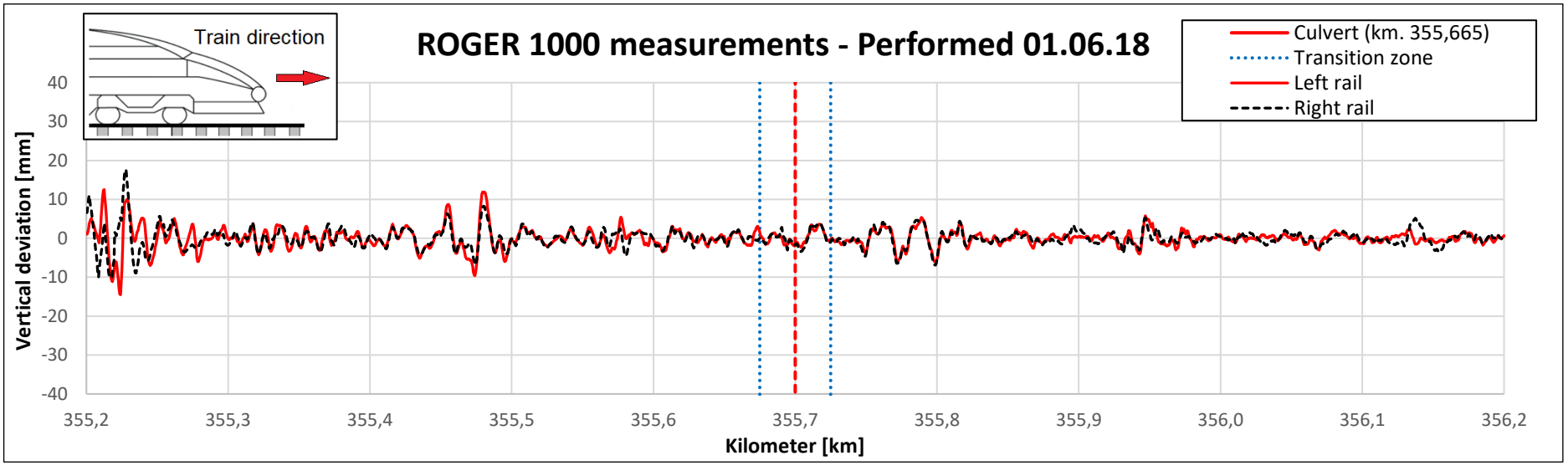
ROGER 1000 measurements - Performed 01.06.18
Train direction
Culvert (km. 355,665)
Transition zone
Left rail
Right rail
Vertical deviation [mm]
40
30
20
10
0
-10
-20
-30
-40
355,2
355,3
355,4
355,5
355,6
355,7
355,8
355,9
356,0
356,1
356,2
Kilometer [km]

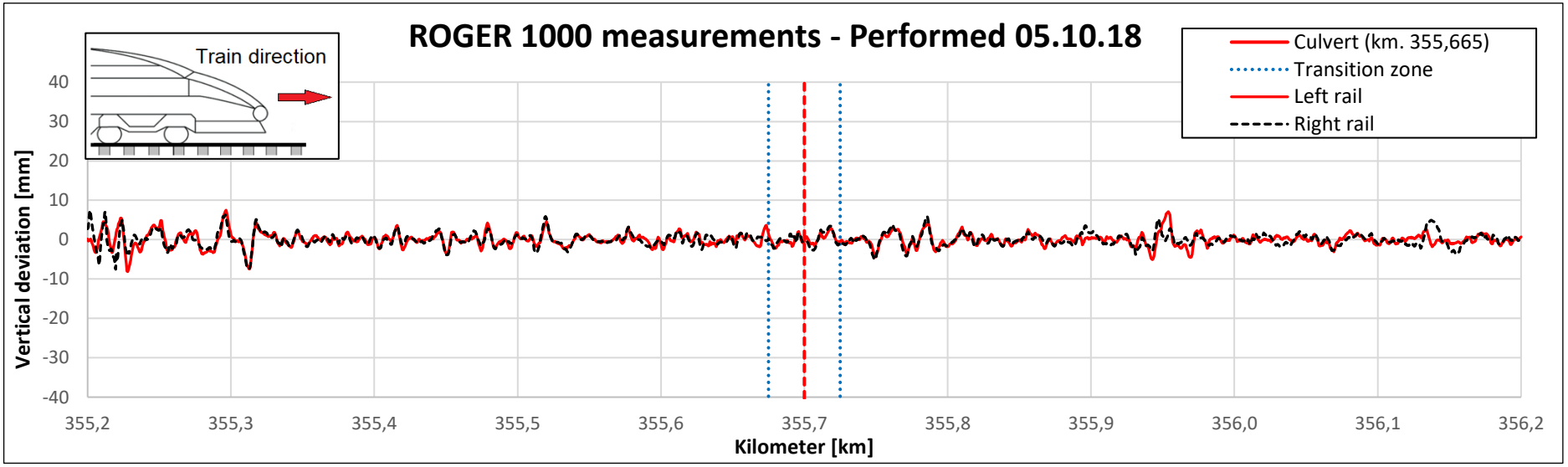
ROGER 1000 measurements - Performed 05.10.18
Train direction
Culvert (km. 355,665)
Transition zone
Left rail
Right rail
Vertical deviation [mm]
40
30
20
10
0
-10
-20
-30
-40
355,2
355,3
355,4
355,5
355,6
355,7
355,8
355,9
356,0
356,1
356,2
Kilometer [km]

3.2 Vinstradalsveien concrete culvert

Vinstradalsveien culvert was built in year 2000, and is located at kilometer 418.82 at the railway line «Dovrebanen», a few miles south from the city of Oppdal, see figure 3.5.

The available data for this culvert was very limited, and only ROGER 1000 photos were used when evaluating the local conditions surrounding this culvert.

In figure 3.6 a ROGER 1000 photo is shown, where it can be seen that the culvert is built in a very slack curve. The culvert has a relative shallow height of cover which makes this case representative for the stiffness transition problem. It can also be seen that the culvert is used as a road crossing, suggesting that its cross-section is also suffiently large.

From the fact that this culvert was built in year 2000, it can also be assumed that it has been instrumented with a transition slab.

Figure 3.5 – Location Vinstradalsveien concrete culvert at «Dovrebanen» (Source: Bing maps)

Figure 3.6 – ROGER 1000 photo taken coach a couple of meters before passing the culver (Source: Bane NOR)

3.2.1 ROGER 1000 results

This section discusses the ROGER 1000 data presented on page 25-27. For this culvert, only data from 2010-2018 were available. The track quality of the 1000 meter intervall taken at the location of this culvert generally seems to be bad.

From the measurements performed 28.04.10, deviations up to 18 mm in the free track is seen. These deviations however is almost neglectible at the location of the culvert compared to their magnitude at the free track, for example at kilometer 418.3-418.75 and kilometer 419-419.3.

Similar is seen two years later (23.05.12), where a lot of deviations is seen at most sections of the free track expect at the location of the culvert. This trend continous for the measurements performed in the later years such as 18.09.15, 19.05.16, 30.09.16 and 24.05.18.

These measurements suggests quite the uposite of whats commonly been described in the litterature [5], that stiffness variations causes increased track forces and hence, increasing the maintenance frequency. For this particular case, the track quality at the culvert always seemed to be better compared to the quality at the free track, suggesting that the deterioration rate above the culvert in fact was slower. This might be related to the backfill being made of higher quality material compared to the free embankment.

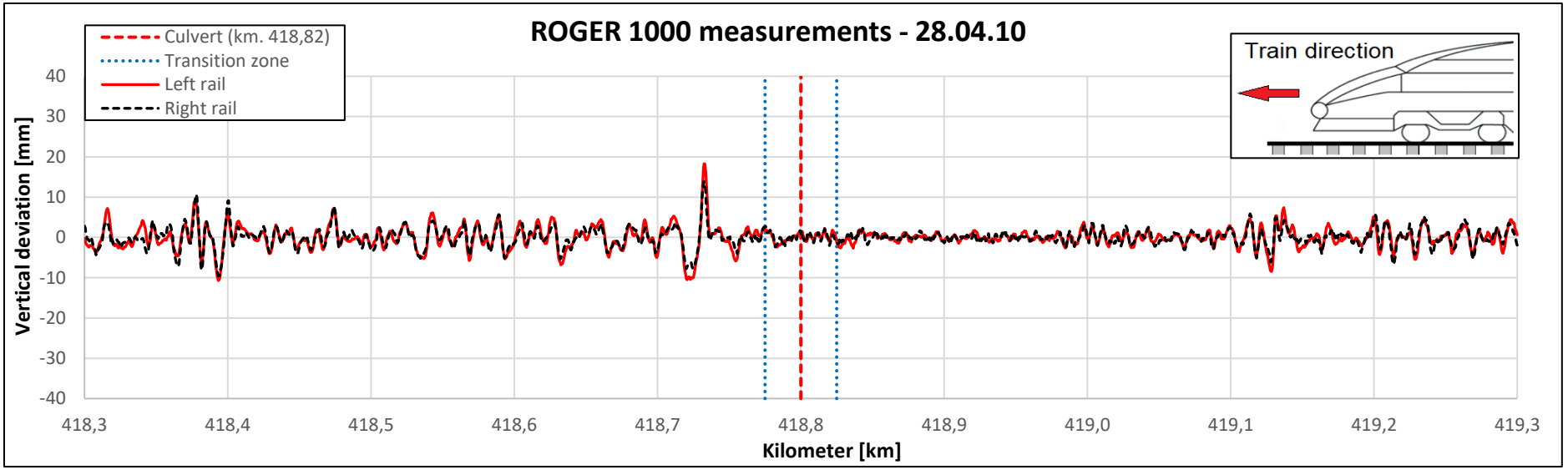
ROGER 1000 measurements - 28.04.10
Culvert (km. 418,82)
Transition zone
Left rail
Right rail
Train direction
Vertical deviation [mm]
40
30
20
10
0
-10
-20
-30
-40
418,3
418,4
418,5
418,6
418,7
418,8
418,9
419,0
419,1
419,2
419,3
Kilometer [km]

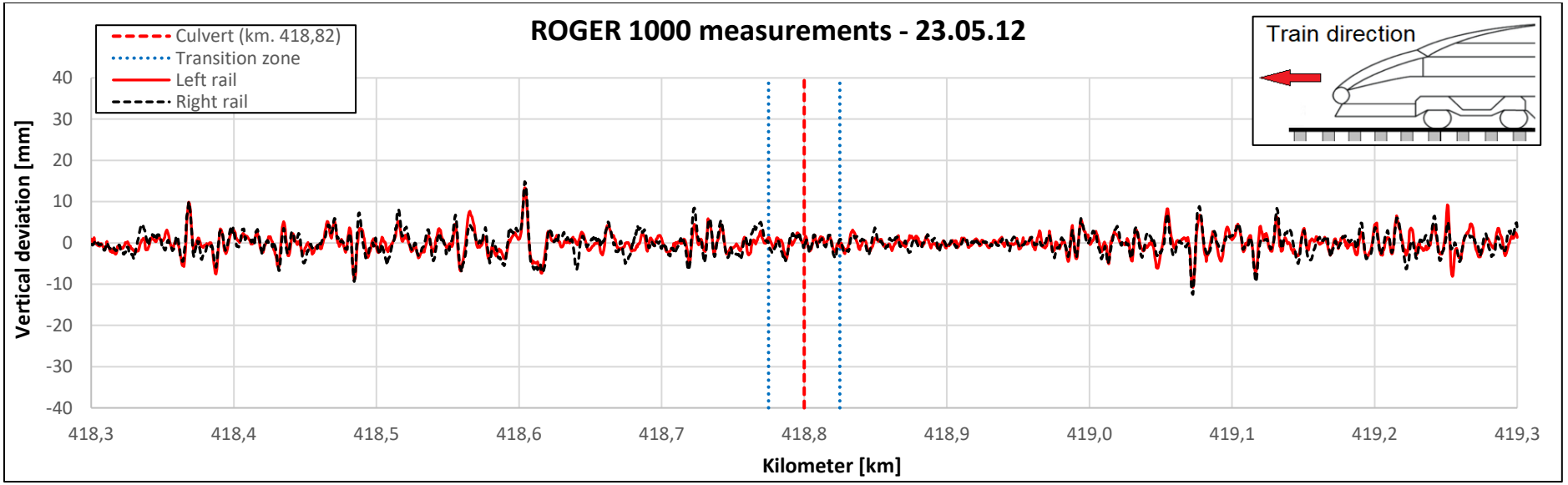
ROGER 1000 measurements - 23.05.12
Culvert (km. 418,82)
Transition zone
Left rail
Right rail
Train direction
Vertical deviation [mm]
40
30
20
10
0
-10
-20
-30
-40
418,3
418,4
418,5
418,6
418,7
418,8
418,9
419,0
419,1
419,2
419,3
Kilometer [km]

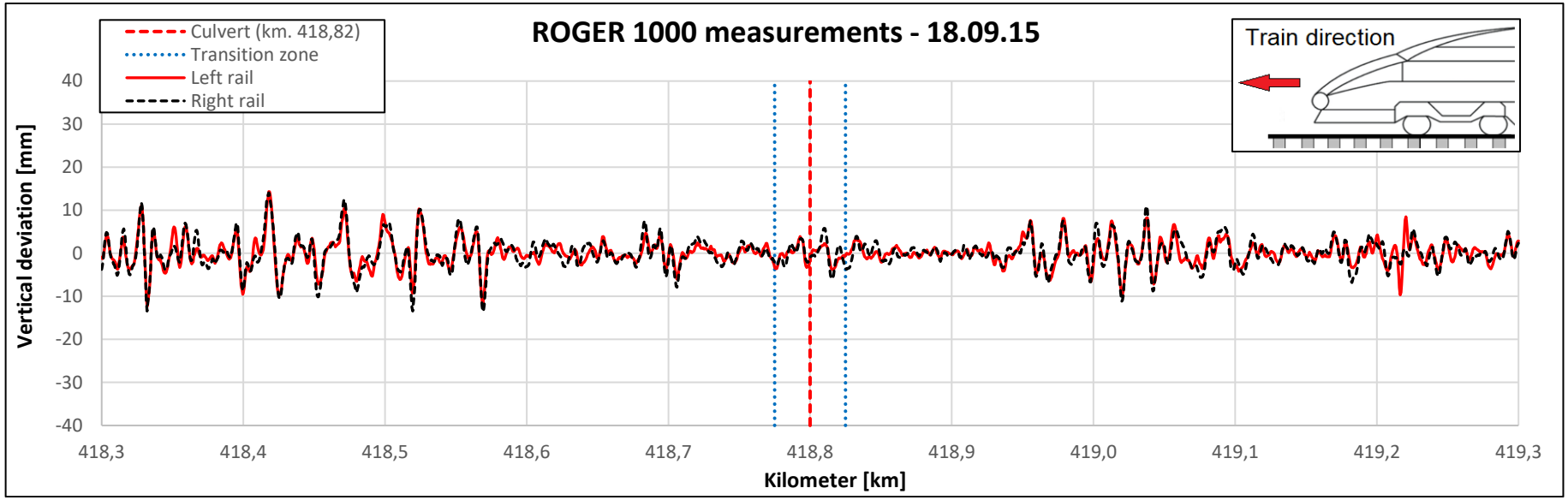
ROGER 1000 measurements - 18.09.15
Culvert (km. 418,82)
Transition zone
Left rail
Right rail
Train direction
Vertical deviation [mm]
40
30
20
10
0
-10
-20
-30
-40
418,3
418,4
418,5
418,6
418,7
418,8
418,9
419,0
419,1
419,2
419,3
Kilometer [km]

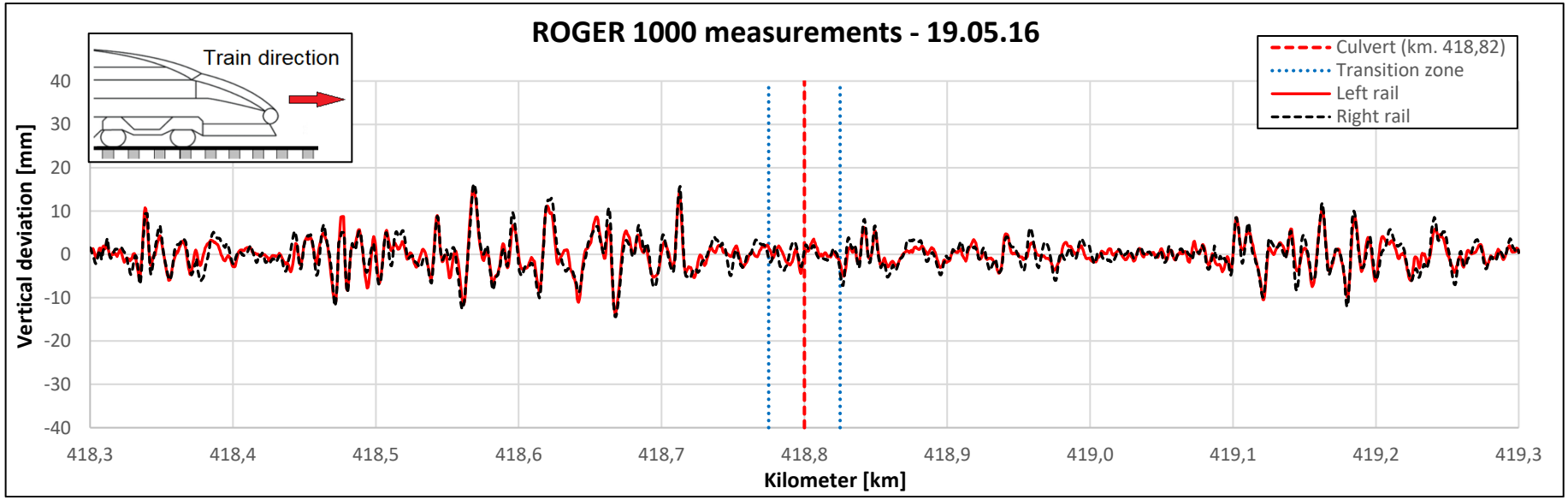
ROGER 1000 measurements - 19.05.16
Train direction
Culvert (km. 418,82)
Transition zone
Left rail
Right rail
Vertical deviation [mm]
40
30
20
10
0
-10
-20
-30
-40
418,3
418,4
418,5
418,6
418,7
418,8
418,9
419,0
419,1
419,2
419,3
Kilometer [km]

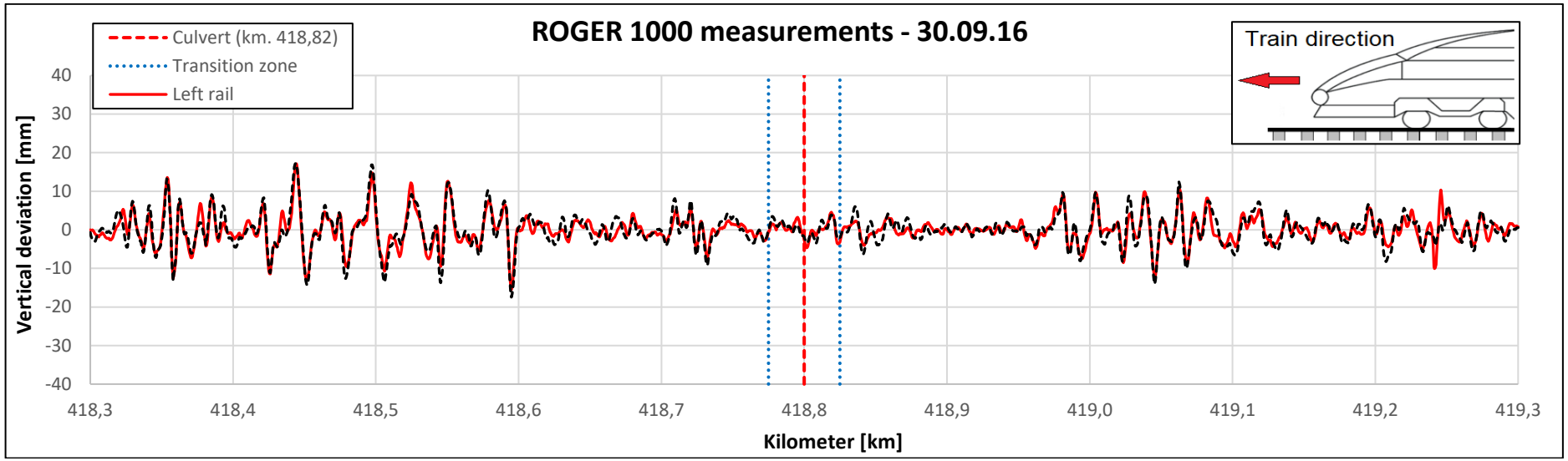
ROGER 1000 measurements - 30.09.16
Culvert (km. 418,82)
Transition zone
Left rail
Train direction
Vertical deviation [mm]
40
30
20
10
0
-10
-20
-30
-40
418,3
418,4
418,5
418,6
418,7
418,8
418,9
419,0
419,1
419,2
419,3
Kilometer [km]

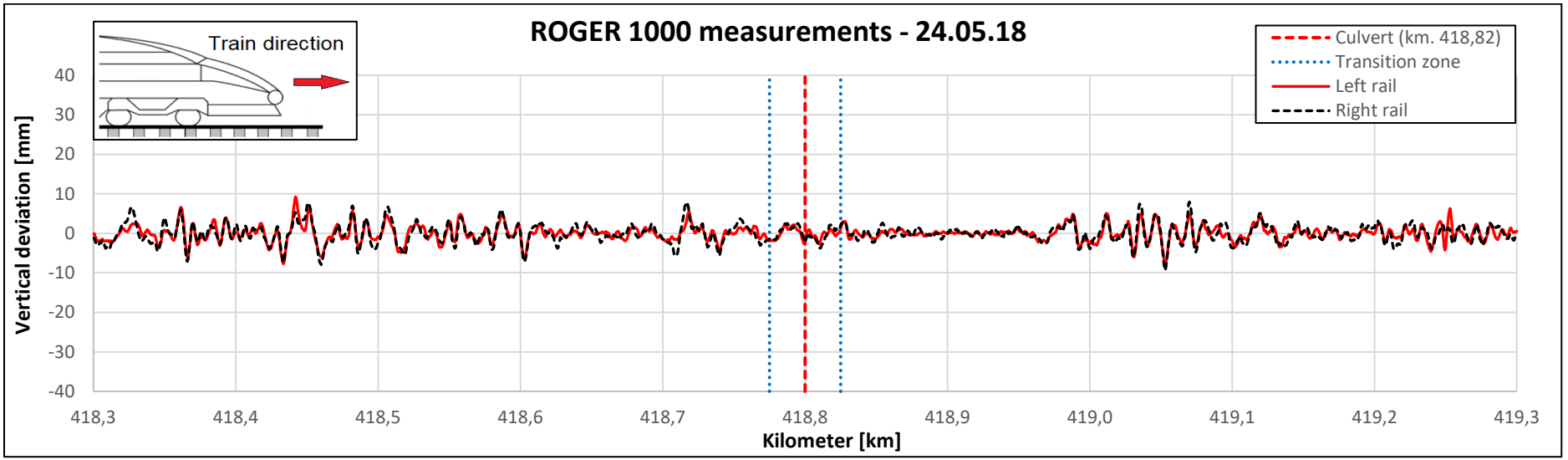
ROGER 1000 measurements - 24.05.18
Train direction
Culvert (km. 418,82)
Transition zone
Left rail
Right rail
Vertical deviation [mm]
40
30
20
10
0
-10
-20
-30
-40
418,3
418,4
418,5
418,6
418,7
418,8
418,9
419,0
419,1
419,2
419,3
Kilometer [km]

3.3 Jarenhaugen concrete culvert

Jarenhaugen culvert was built in year 2011, and is located at kilometer 100.448 at the railway line «Randsfjordbanen» between the cities of Hokksund and Hønefoss, see figure 2.16.

Similar to Vinstradalsveien culvert, the data available for this culvert was very limited and only ROGER 1000 photos were used when evaluating the local conditions surrounding the culvert.

A ROGER 1000 photo is shown in figure 3.8, where it can be seen that the culvert is built in a straight track section. It can also be seen that the height of cover is relative shallow, which makes this culvert a good case for this study.

Since this culvert was built long after year 2000, it can be thrusted that it has been instrumented with a transition slab.

Figure 3.7 – Location of Jarenhaugen culvert at «Randsfjordbanen» (Source: Bing maps)

Figure 3.8 - ROGER 1000 photo showing the transition zone a few meters before the culvert (Source: Bane NOR)

3.3.1 ROGER 1000 results

This section discusses the ROGER 1000 data presented on page 33-35. In uposition to the other cases, some deviations for this case was found at the culvert. These deviations however, are not as consistent as the deviations seen at the free track and no direct conclusion regarding the source of them could be made.

From the measurements in 2011 (26.05 and 01.09), the overall noise is consistent over the section of 1000 meter except for three locations, at kilometer 99.95, 100.52 and 100.73.

One year later (18.04.12) these spikes is still visible, but now some deviation at the culvert and kilometer 100.28 can also be seen. The amplitude of the deviation seen at the culvert is quite big, but not as big as the one seen at kilometer 100.52.

One year after this measurement (23.04.14), all the mentioned deviations has increased. Whats interesting here is that now both the entry and exit of the culverts transition zone can be seen. These deviations however, is not the most critical (i.e largest) deviation of this measurement.

Moving to the last available ROGER 1000 measurement from 12.09.14, the spikes has been significantly reduced, removing the spikes completely previously seen at the culvert, suggesting that some tamping has occoured. Even from this measurement the deviations previously seen at kilometer 99.95 and 100.52 is still visible.

The results from this case shows that deviations over rigid culvert underpassings can also be captured by ROGER 1000 if their large enough. These deviations similar to Holme steel-soil composite culvert (chapter 2.2), are not consistent and no conclusion regarding the stiffness variation the follows this culvert can be made.

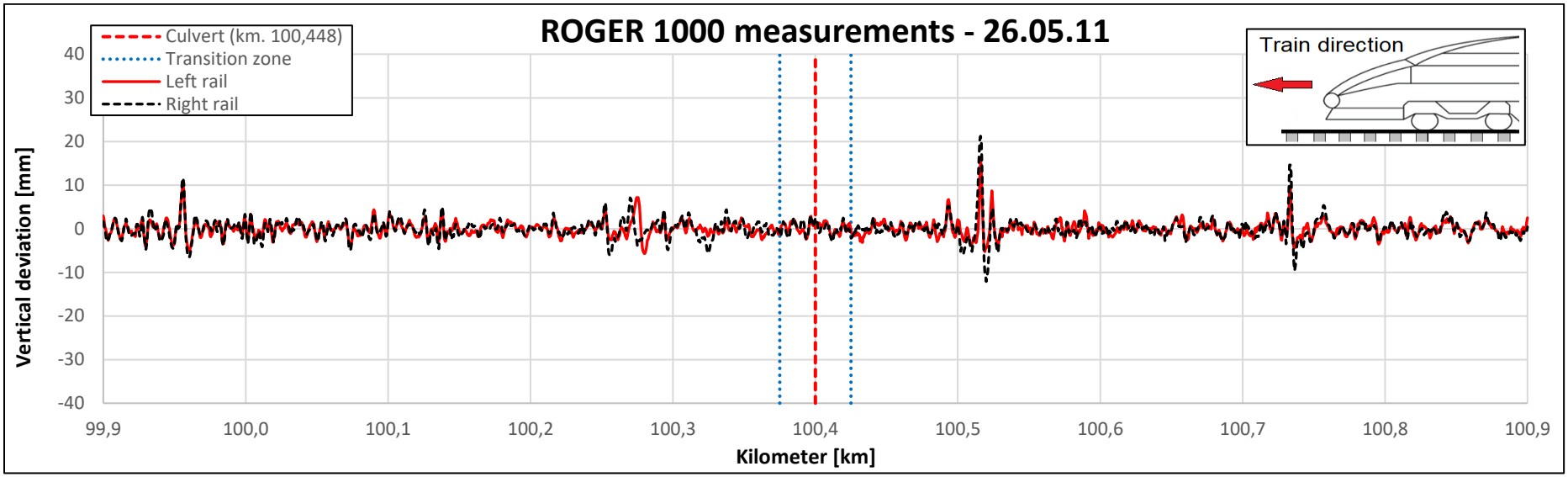
ROGER 1000 measurements - 26.05.11
Culvert (km. 100,448)
Transition zone
Left rail
Right rail
Train direction
Vertical deviation [mm]
40
30
20
10
0
-10
-20
-30
-40
99,9
100,0
100,1
100,2
100,3
100,4
100,5
100,6
100,7
100,8
100,9
Kilometer [km]

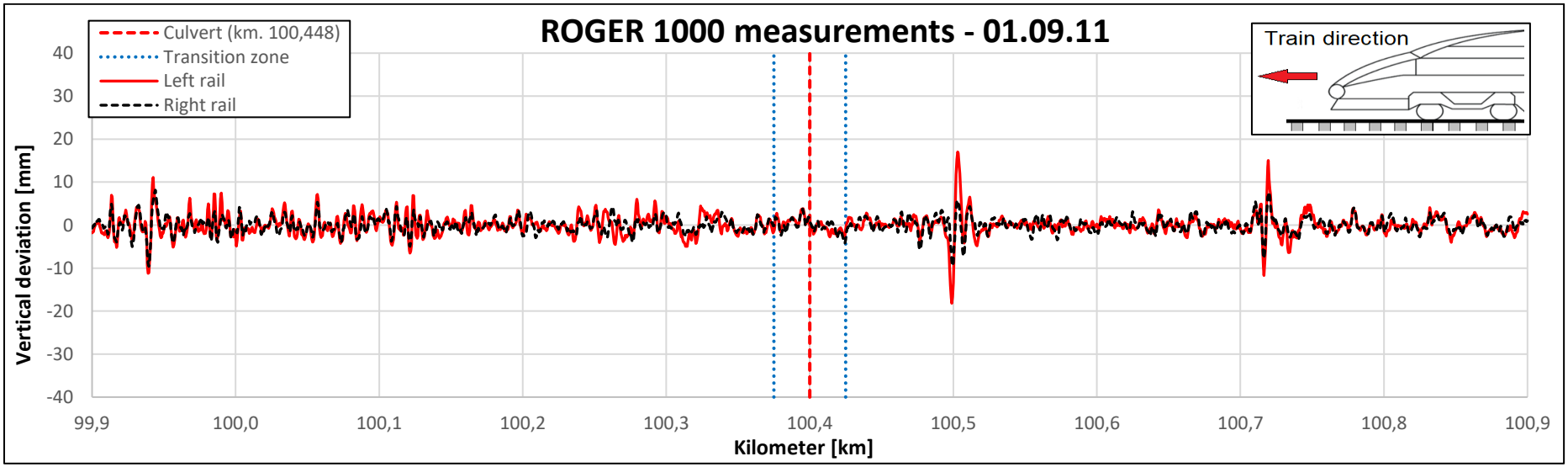
ROGER 1000 measurements - 01.09.11
Culvert (km. 100,448)
Transition zone
Left rail
Right rail
Train direction
Vertical deviation [mm]
40
30
20
10
0
-10
-20
-30
-40
99,9
100,0
100,1
100,2
100,3
100,4
100,5
100,6
100,7
100,8
100,9
Kilometer [km]

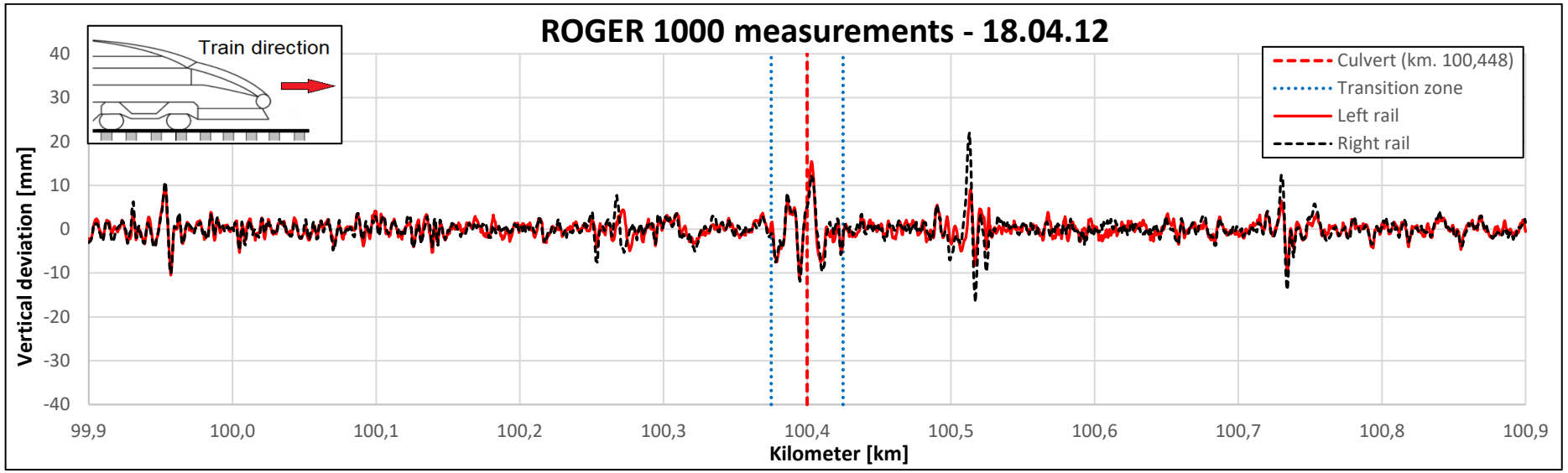
ROGER 1000 measurements - 18.04.12
Train direction
Culvert (km. 100,448)
Transition zone
Left rail
Right rail
Vertical deviation [mm]
40
30
20
10
0
-10
-20
-30
-40
99,9
100,0
100,1
100,2
100,3
100,4
100,5
100,6
100,7
100,8
100,9
Kilometer [km]

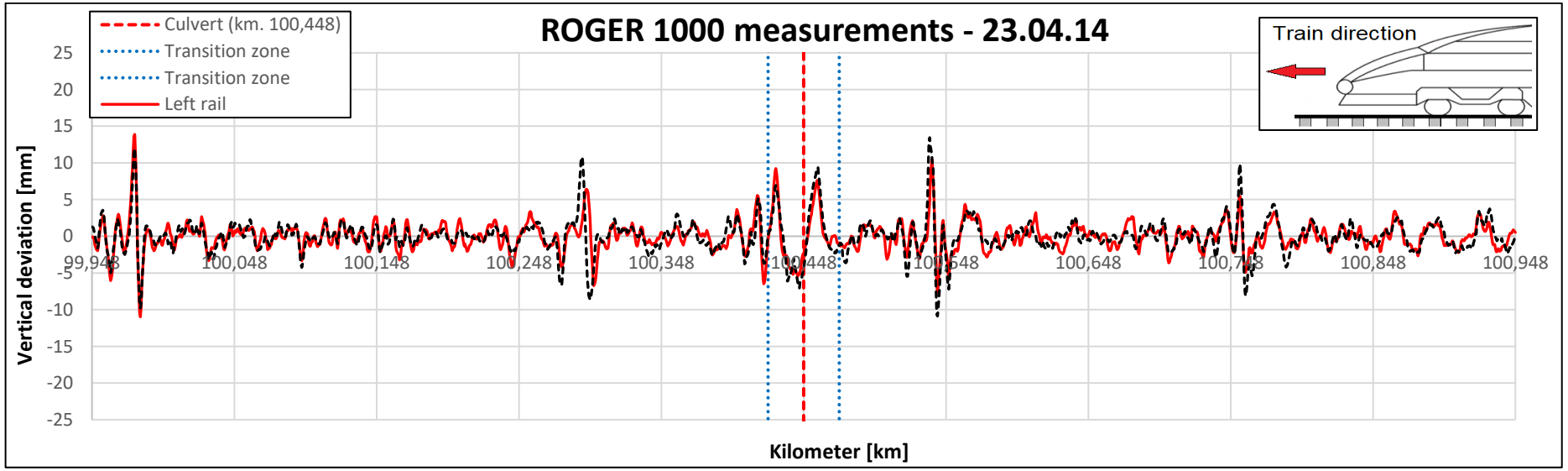
ROGER 1000 measurements - 23.04.14
Culvert (km. 100,448)
Transition zone
Transition zone
Left rail
Train direction
Vertical deviation [mm]
25
20
15
10
5
0
-5
-10
-15
-20
-25
99,948
100,048
100,148
100,248
100,348
100,448
100,548
100,648
100,748
100,848
100,948
Kilometer [km]

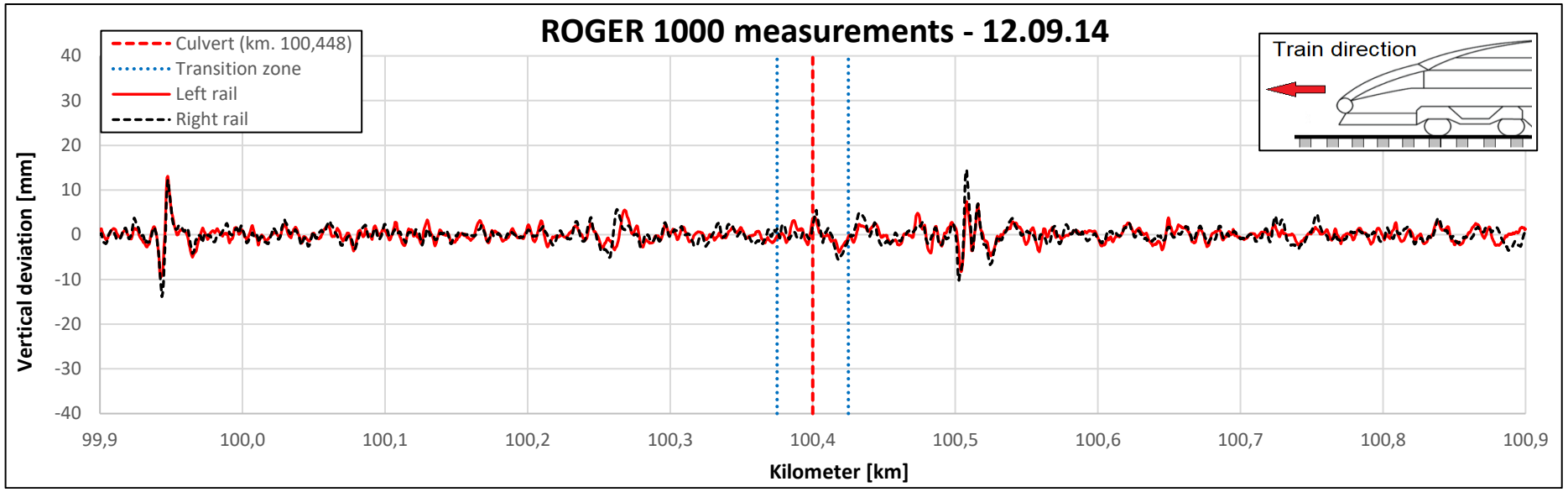
ROGER 1000 measurements - 12.09.14
Culvert (km. 100,448)
Transition zone
Left rail
Right rail
Train direction
Vertical deviation [mm]
40
30
20
10
0
-10
-20
-30
-40
99,9
100,0
100,1
100,2
100,3
100,4
100,5
100,6
100,7
100,8
100,9
Kilometer [km]

4 Discussion and conclusion

In this report six cases of culvert underpassings bellow railway tracks was investigated with ROGER 1000 data. The purpose of this study was to investigate if vertical track deviations captured by ROGER 1000 could be used to investigate any irregularities and tie them to stiffness variations purposedly caused by these culverts.

The general conclusion is that the deviations captured by ROGER 1000 is very dependent on local conditions and not as much affected by these culverts as one might think. For example, at the site of Svenningdal culvert the typical deviations of the track ranged between $\pm$ 5 mm. Compared to the vertical track deviations seen at Jarenhaugen culvert, the deviations could reach up to 20 mm. Such variations for example, suggests that the overall track quality at Svenningdal was better than at Jarenhaugen.

Another aspect which should be thought of is the allightment of the track. In curves for example, the aspect of horisontal track forces may also influence the behaviour over these culverts as was seen from the 16.09.13 measurement at Holme culvert, where only the right rail deviated from the target profile.

Yet a variable which should be mentioned, is track conditions. At the location of Sjånes and Holme for example, available data from Bane NOR shows that 49E1 rails were used at the location of Sjånes, while 54E3 rails at Holme which is about 12% stiffer in bending [6]. Such local conditions definitely makes an impact to the overall track stiffness. An interesting observation here was that despite this being the case, it was Holme culvert that showed most track deviations and not Sjånes.

From the results of the three steel soil composite bridges the overall noise compared to the target profile seemed to be consistent at Sjånes culvert. In this case the height of cover was as shallow as 0.93 meter, suggesting that the change in track stiffness caused by the culvert is not a significant problem.

Some deviations in track profile related to steel culverts could only be seen for the Holme case, where several measurements revealed spikes at the culvert location which clearly stood out compared to the spikes at the free track. Comparing this again to the Viker culvert which had about the same span lenght, no significant deviation in vertical track allignment was found for the last case. These findings suggests that the deviations seen from ROGER 1000 are not consistent in cases of flexible steel culverts.

Similar to the cases with flexible steel, the deviations found for the selected concrete culverts are not consistent either. In the first two cases, Svenningdal and Vinstradalsveien, little to no deviation that deviated from the general noise at that site was seen. At the Vinstradalsveien case, quite the uposite of the expected behaviour was revealed. The section over the culvert (about 100 meter before and after) was the only section were the deviations were small compared to the rest of the free track. These results are in uposition to the classic statement that stiffness variations at railways tracks always increases the deterioration rate and need for maintenance.

Only at the last concrete case (Jarenhaugen), could some irregularities be tied to the culvert. Again, these amplitudes compared to the amplitudes seen at the free track did not stand especially out. They could aswell be related to the local conditions instead of the culvert.

From these six cases the overall conclusion is that there is no direct correlation seen between stiffness variations at culvert underpassings and ROGER 1000 data, both in the case of rigid concrete and flexible steel cases. Since the ROGER 1000 data is the basis behind most of the maintenance that is carried out on the railway network, it can from this be stated that there is no direct correlation between increased corrective maintenance frequency and stiffness variations either.

Whats important to be aware of when evaluating transition zones is local conditions, and especially track conditions over the bridge. When bad solutions such as fixing the track to the bridge is avoided (which was the case for all these culverts) the deterioration purposely caused by these culverts is not any more significant compared to the regular deterioration rate at the free track.

Bibliography

[1] Esveld. C (2016). *Modern Railway Track*, Digital Edition 2016, version 3.8, MRT-Productions. Revisions available at: http://www.esveld.com/

[2] Vasset. T (w/o year). *ROGER 1000 MÅLEVOGN*, infrastrukturdivisjonen – vedlikeholdsstab, Norsk jernbaneskole. Available at: www.jernbaneskolen.no

[3] Petterson. L and Sundquist. H (2014). *Design of soil-steel composite bridges*. Report 112, 5th Edition. Dept. Architectural and Civil Engineering, Royal Institute of Technology, KTH, Stockholm, Sweden. Available at http://www.diva-portal.org/

[4] Viacon (2015). MultiPlate MP200, Fleksible flerplaterør i stål. Product catalogue. Available at www.ViaCon.no

[5] European Rail Research Institute (ERRI), Specialists Committee (1999). *ERRI D 230.1/RP 3: Bridge ends, embankment structure transition*, State of the art report.

[6] Bane Nor (2019). Teknisk regelverk, norwegian railway normal. Available at https://trv.jbv.no/wiki/Overbygning/Prosjektering/Sporkonstruksjoner

NORWEGIAN UNIVERSITY OF SCIENCE AND TECHNOLOGY
DEPARTMENT OF CIVIL AND ENVIRONMENTAL ENGINEERING

Appendix C – REPORT III

The transition zone of Gouda railway culvert

- ***Results and discussions of a case study performed on a rigid concrete bearing culvert on piles from Netherland***

By Dan Sergei Sukuvara

Abstract

This report discusses and highlights the results from the comprehensive monitor programme that was carried out on a railway culvert near Gouda Goverwelle, Netherland. The culvert was a 2x2 square concrete culvert instrumented with transition slabs, and the circumstances surrounding this culvert was very special, it was founded on rigid piles while the free track was built on top of a sand fill directly on top of a soft clay, which settled for about 1.0 mm pr. month.

Whats valuable about this case is the extent the field measurements were carried out to, providing unique insight in potential fall pits and soil behaviour under the transition slab. Alot of the results related to the differential settlements of the clay has been filtered away, and the focuse of this report has primarily been on the results which are considered more applicable for most types of concrete culverts instrumented with transition slabs.

The results for this case shows that if the volume of the materials bellow a transition slab has the ability to change with time, adding ballast and tamping only provides a quick fix. These measurements also suggests that the end of the transition slab which extends into the backfill, more or less always becomes the weakest section of the transition zone where the stiffness will be lowest, and where a softer backfill material will only will contribute to the problem.

Table of contents

1 Introduction

This report highlights and discusses the findings from a culvert located at Gouda Goverwelle in Netherland, were a comprehensive field survey was performed at the site in the periode of 2008-2009 under motivation from Delft Cluster, Pro Rail and Deltares [1]. The results from the field investigations was later used as a basis for two doctoral theses from 2011 and 2013 [5,6], and has according to authors involved in the project later led to changes in Pro Rails regulation of the transition slab.

The culvert was a small 2x2 meter square concrete culvert founded on piles in soft clay, and had over several years caused high maintenance problems. One of the main factors leading up to the study on this culvert was the unusual high tamping frequency in the transition zones [2].

1.1 History and description of the culvert

The field testing on the culvert was carried out at the railway link Utrencht-Gouda, east of the Gouda Goverwelle station. The original railway link was built in 1855 on a typical Dutch soft soil with two tracks. The line was later widened in 1995 to a four line track by adding two more tracks at the nortern side of the existing line.

Associated with the widening of the line, the original culvert was also rebuilt and prolonged. The culvert is located approximately 500 meters east from Gouda Goverwelle station, as shown in figure 1.1.

Figure 1.1 – The Utrencht-Gouda railway line and location of the stiff square concrete culvert (Source: Google maps)

The culvert was a small squared, box culvert with a 2x2 meter cross section which origi-nally was built in 1852 out of masonry. Parts of old embankment that was rebuilt is still made of the old masonry that was initially used for the culvert.

Associated with the extension of the track in 1995, the new section of the culvert was built with prefabricated concrete elements [1].

The main purpose of the culvert was to allow for water to flow between the northern and southern side of the embankment, see figure 1.2.

Figure 1.2 – Southern side of the box culvert during a train passage. The water table can be seen at surface level (From Hölscher. P and Meijers. P 2009)

The track section which was involved in the monitor programme was the most recent, northern-most track (track no. 1) as illustrated in figure 1.3.

The train traffic at this track consists mostly of various types of passenger trains, but some freight train passages were also measured during the testing [4]. The train traffic at this track travels foremost in one direction, from east to west and the maximum allowable speed at the railway line was 140 km/t [1,5].

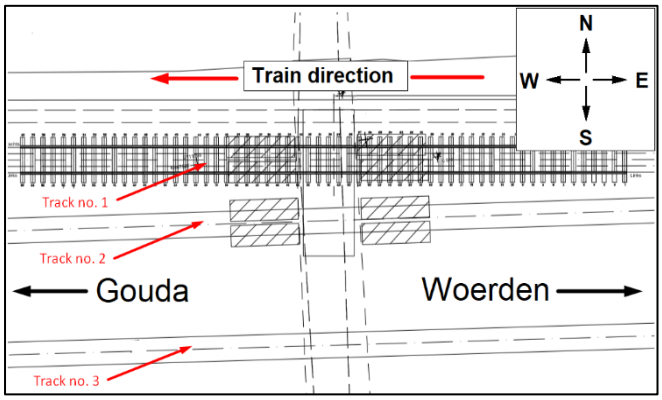

Figure 1.3 – Location of the track (no. 1) with train direction foremost going towards Gouda station (Modified after design drawings from Hartman A.D, 2008)

Tied to the extension of the line in 1995, the whole foundation of the extended part at the culvert was also rebuilt, replacing the old shallow piles with a combination of steel tube and square concrete piles [3]. These piles penetrates the soft clay down to a stiffer sand layer, about 11 meters bellow the top of the embankment. This provided a rigid fundation for the culvert in respect to the embankment which was founded directly on the soft clay.

The new part of the culvert was designed with an integrated corbell to connect the transition slab and the bridge. According to the design drawings, the slab was placed directly upon the corbell with no reinforced connection allowing for the slab to rotate freely [1,3], see figure 1.4.

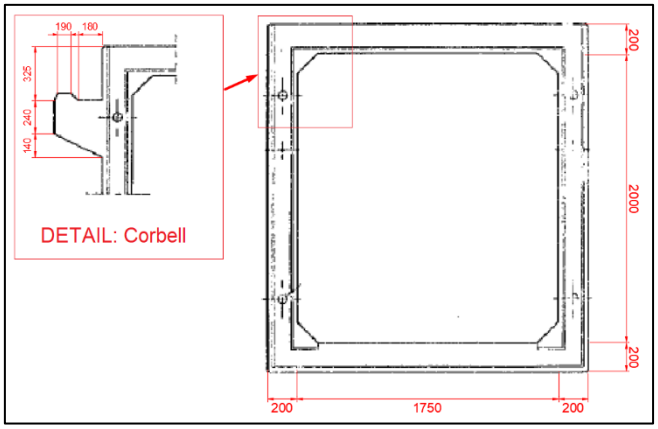

Figure 1.4 – Dimensions of culvert according to design drawings (Modified after design drawings from Hartman A.D, 2008)

The approach slab was initially built with a lenght of 4.0 meters, thickness 0.3 meter and slope 1:40 [2]. At construction finish, the culvert had a total length of 51,25 meter perpendicular to the embankment, crossing all four railway tracks [1].

2 Mapping of the ground conditions

Before the static and dynamic field measurements were carried out, an comprehensive field survey was performed at the site beforehand to map the current ground conditions. The field survey compromized in total 7 Cone Penetration Tests (CPT), one Vertical Seismic Profile Test (VSPT) and several Ground Penetration Radar tests (GPR) at the locations shown in figure 2.1.

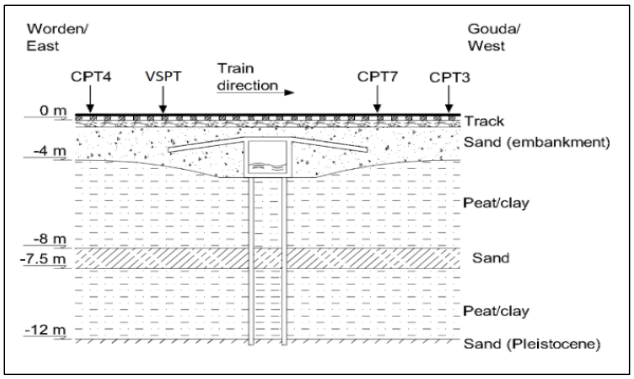

Figure 2.1 – Cross section of the culvert northernmost side, showing the positioning of the measurements including the interpertated soil profile (Modified after Coelho. B, 2011)

Cone penetration test no. 4 (CPT4) and the vertical seismic profiling (VSPT) was performed on the left/east side of the culvert, while CPT7 and CPT3 was performed at the culverts right west side as shown in figure 2.1.

The interpretations of the CPT tests suggested that the embankment was rather heterogeneous being about 4 meter thick, followed by a very low cone resistance with an increase in porepressure for about 7 meters, suggesting a soft clay layer. Along this clay layer, a sandlayer was also present with a varying thickness being about 8 meters deep.

At approximately 12 meters depth, there was located a stiff Pleistocene sand layer which the piles under the culvert was founded on. The CPT results used for interpertating the soil profiles are presented in figure 2.2, showing the tip resistance at the three locations (CPT3, CPT4 and CPT7 from figure 2.1).

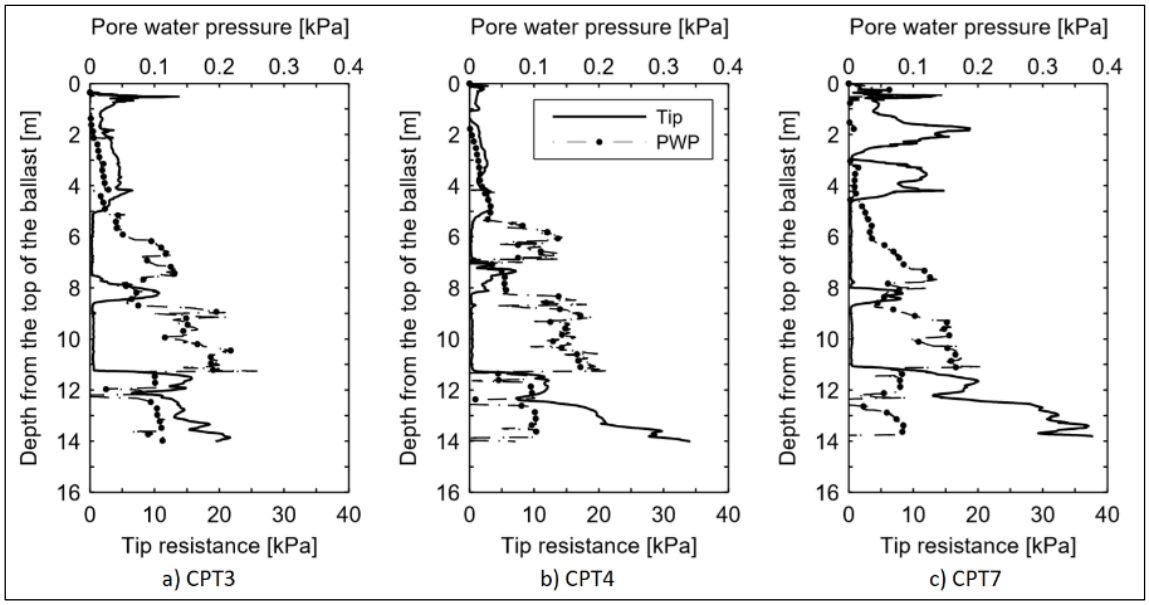

Figure 2.2 – CPT results: Showing tip resistance and porewater pressure (PWP) for the three cone penetration locations, where a) shows CPT3, b) CPT4 and c) CPT7 (Modified after Coelho. B, 2011)

The measured vertical seismic profile are presented in figure 2.3, where figure a) shows tip resistance of the test, b) the friction ratio and c) the interpreted shear wave velocity profile. It should be noted that the shear wave velocity profile shown in figure 5c) are intreprentation of the original results by Coelho. B [5] whereas the raw data were reported by Hartman. D [1].

Figure 2.3c) shows that the shear wave velocities were about 60 to 80 m/s in the soft clay layer, and about 140 m/s for the sand and embankment layers. This suggests that the stiffness of the Pleistocene layer were in the same range as the stiffness of the embankment.

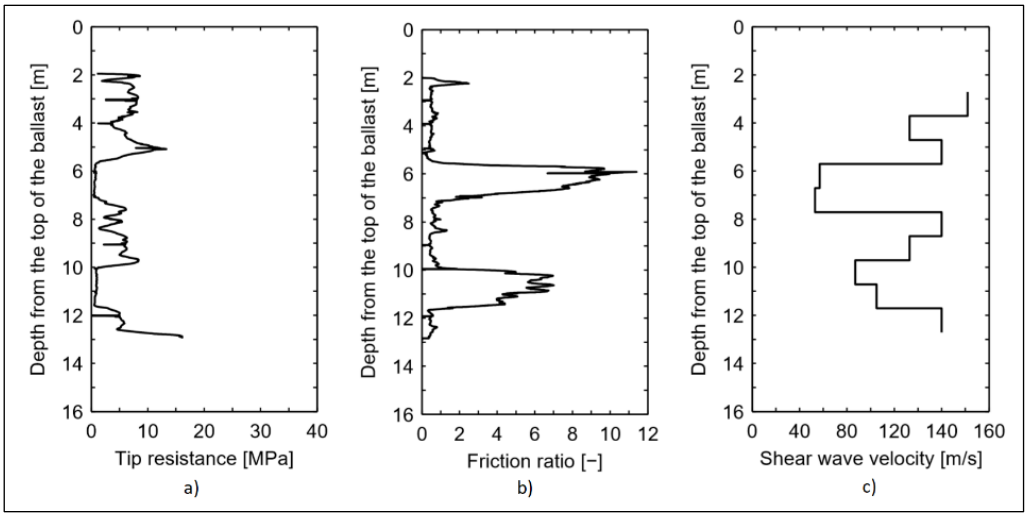

Figure 2.3 - VSPT results: Showing a) tip resistance, b) friction ratio and c) the interpreted shear wave velocity profile from the Vertical Seismic Profile Test performed at the culverts east side (After Coelho. B, 2011)

For mapping of the current position of the transition slab and ballast thickness, Ground Penetration Radar tests (GPR) was used together with hand dug trial pits for validation. There was reported some deviation between the GPR results and hand dug trial pits due to the ballast being mixed into the embankment material over the years. This mixing was not studied in detail, but field observations at the site suggested that the mixed zone was about 20 centimer thick [2].

Figur 2.4 shows that the ballast thickness over the slab in 2008 could reach up to 0.8 - 1.2 meter, while the ballast thickness on top of the culvert remained at about 0.5 meter. From the measurement results, it is evident that the ballast thickness both above the slab and culvert has increased tremendously over the years as it only was 0.3 meter at construction finish. At the end of both transition slabs, it seems like there is a tendency of accumulating an even larger ballast thickness than everywhere else, suggesting that the toe of the slab has requried more ballast supplementation and tamping compared to the rest of the track at this location.

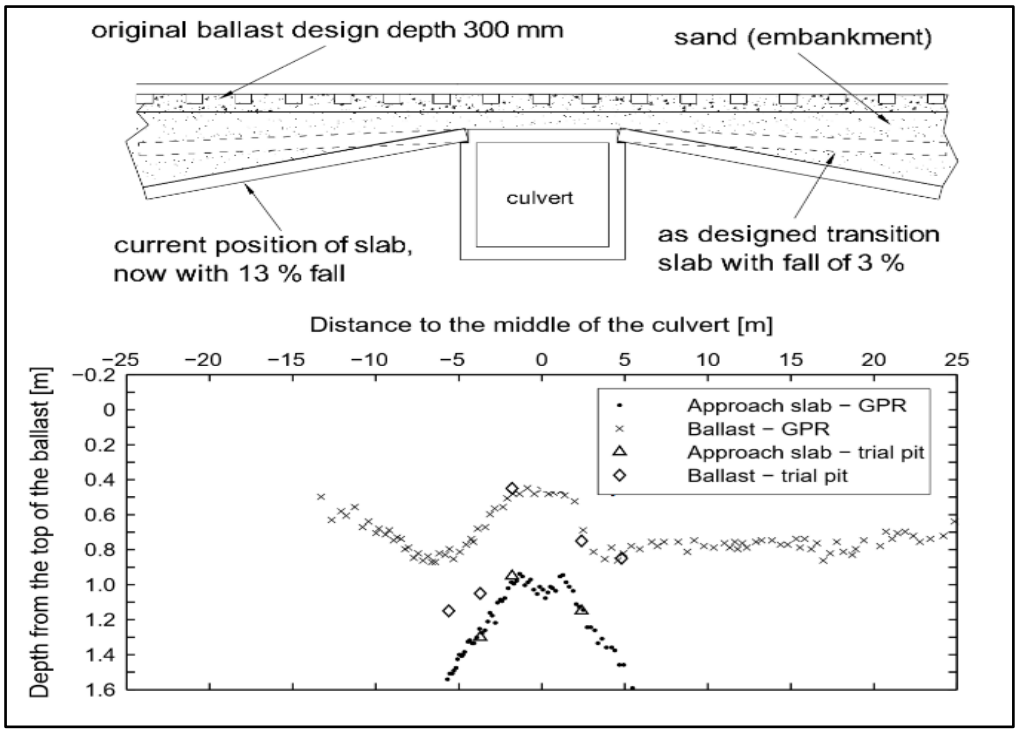

Figure 2.4 - Illustration and GPR results: The ballast thickness over the slab and positioning in 2008, suggest that the plate has rotated tremendously over the years (Modified after Coelho. B, 2011)

From the figure it can be seen that the originally designed slope of the transition slab was about 3%, and has over a periode of 13 years has it increased its elevation to about 13%. Such large rotation corresponds to a vertical displacement of 0.64 meter at the slabs toe (i.e end point) [2], and explains the especially thick ballast at this section compared to everywhere else.

2.1 Estimating the elastic modulus of the backfill

According to Nordal, a good way of estimating the small strain stiffness of soils is from interpreting shear wave velocity measurements [12,13]. In order to compare the case of Gouda Goverwelle to other cases, the shear wave velocities measured by the Vertical Seismic Profile Tests (VSPT) are therefore used in order to back calculated and estimate the elastic modulus of this embankment. This would make the measurements more comparable to other cases.

According to Nordal and Kramer [11,12,13], the shear wave velocity of any soil medium can be expressed through the shear modulus and specific density as

$$V_s = \sqrt{\frac{G}{\rho}} \qquad \text{(Eq. 2.1)}$$

and

$$G = \frac{E}{2(1+\nu)} \qquad \text{(Eq. 2.2)}$$

where

G being the shear modulus
ρ being the specific soil density
v being the possions ratio of the soil
E being the elastic modulus

Inserting (Eq. 2.2) into (Eq. 2.1) and isolating the elastic modulus, gives

$$E = 2(1+v)*\rho*v_s^2 \qquad \text{(Eq. 2.3)}$$

Since no information was given on the sand material used in the backfill, the specific density must be assumed. For doing so, one should bear in mind that this embankment was built in year 1995, which means it has settled for quite a while.

As later demonstrated in section 4.1.1 and 4.1.2 however, the soft clay beneath the embankment also settled autonomously for about 1.0 mm each month, which might have affected the compaction of this sand over the years. It is therefore difficult to know exactly how well this sand has been compacted.

Based of the experiences made from two full scale fieldmeasurements involving backfilling with a poorly sandy gravel (after the Unified Soil Classification System), the specific density of those sands after being compacted was ranging in between 1920 – 2030 kg/m^3 [14,15]. Based of these numbers, a specific density of 1900 kg/m^3 is specified for this embankment.

According to Nordal, the possions ratio for most sands in an odeometer apparatus normally ranges between 0.3-0.4 [13]. According to the norwegian public road administration (Statens Vegvesen), it is a normal practice to assume a higher possions ratio, up to 0.5 when estemating the stiffness of a layered pavement superstructure [16]. The way of thinking here is that compacted materials has a better ability to distribute vertical loads than loose ones, i.e the possions ratio can be expected to be higher than 0.3 in this case.

Two calculations are performed with the expression in Eq. 2.3, that is using a possions ratio of 0.3 and 0.5, leading up to the following parameters

- $v_s \approx 140$ m/s
- $\rho \approx 1900$ kg/m^3
- $v \approx 0.3\text{-}0.5$

Inserted into equation 2.3, we obtain

- $E_{(v=0.3)} = \frac{2(1+0.3)*1900*140^2}{10^6} = 96.82$ MPa
- $E_{(v=0.5)} = \frac{2(1+0.5)*1900*140^2}{10^6} = 111.72$ MPa

From this rough estimation based of the VSPT-results, the elastic modulus of the sand in the backfill is thought as to be in the range of 95-115 MPa.

3 The monitoring programme (2008-2009)

To better understand the mechanisms of the transition zone at Gouda Goverwelle, a monitoring program was performed in the period of May 2008 to June 2009. The goal of the programme was to investigate and understand both the long term quasi-static behaviour of the track and transition slab, but also the dynamic behaviour of train-track interactions of the transition zone during train passages.

Since the embankment was founded directly on soft clay while the culvert on piles, a regular differential settle-ment rate between the embankment and culvert was expected. This evidently caused a regular maintance of the transition zone which for the most parts involved tamping and adding ballast for levelling and aligning the track. The monitor program was consequently carried out to get a better understanding of the correlation between the tamping frequency and the deterioration of the track.

The static testing was performed in a period of total 10 months between september 2008 – june 2009, enclosing a full maintance cycle. The dynamic tests were performed at two different days, the first one being approximately 2 months after the previous maintenance cycle, and the second test about 7 months after. Table 3.1 gives a complete overview of the monitoring programme.

Table 3.1 – Complete overview of the monitor programme performed between 2008-2009 (Modified after Coelho. B, 2011)

Period	Maintenance	Static measurements	Dynamic measurements
March 2008	Performed between 06.03.08 and 03.05.08 (details missing)		
April 2008			
May 2008			First test performed 04.05.08
June 2008			
July 2008	Performed 08.06.08		
August 2008			
September 2008		Inclinometer measurements starts 08.09.19	
October 2008	Performed 07.10.08	Levelling starts 07.10.08	
November 2008		Pore water pressure (PWP) starts 24.11.08	
December 2008			
January 2009		Levelling starts 24.01.09	
February 2009			
March 2009			
April 2009		Hanging sleepers starts 21.04.09	
May 2009		Hanging sleepers stops 05.09.09	Second test performed 05.05.09
June 2009	Performed 30.06.09	PWP stops 08.06.09 Levelling stops 12.06.19	

3.1.1 Test setup for the static long-term measurements

The static long-term field measurements included monitoring of the horisontal and vertical movement of the embankment and railway track, porewater pressure measurements on both sides of the culvert, and the development of hanging sleepers over time after a maintenance cycle.

The levelling was carried out by the use of a electronic theodolite once a month which leveled the position of the rail in respect to the lines pylons [2,5]. The groundwater table was measured by the means of piezometers, while horisontal movement of embankement with inclometers. The hanging distance, (i.e gap between sleeper and ballast) was measured with a void indicator device.

3.1.2 Test setup for the dynamic short term measurement (May 2008)

The first dynamic test was performed in may 2008, approximately two months after the last tamping cycle. According to Coelho. B [5], the setup for this measurement involved eleven geophones (denoted as G), three triaxial and six uniaxial accelerometers (denoted T and A), and one high speed video camera.

Most of the geophones were placed directly on top of the wooden sleepers (G1-G7), while geophone G8 and G9 was placed directly on top of the approach slab. The triaxial accelerometers was placed in the soil at 1.0 meter (T1) and at 3.0 meters depth (T2-T3). Only two uniaxial accelerometer was used during this test, where accelerometer (A16) was placed at the same location as geophone (G9) in the soil above the approach slab for validating the results. Uniaxial accelerometer (A12) was placed in the soil at the end of the second approach slab (i.e exit of the approach slab) as shown in figure 3.1.

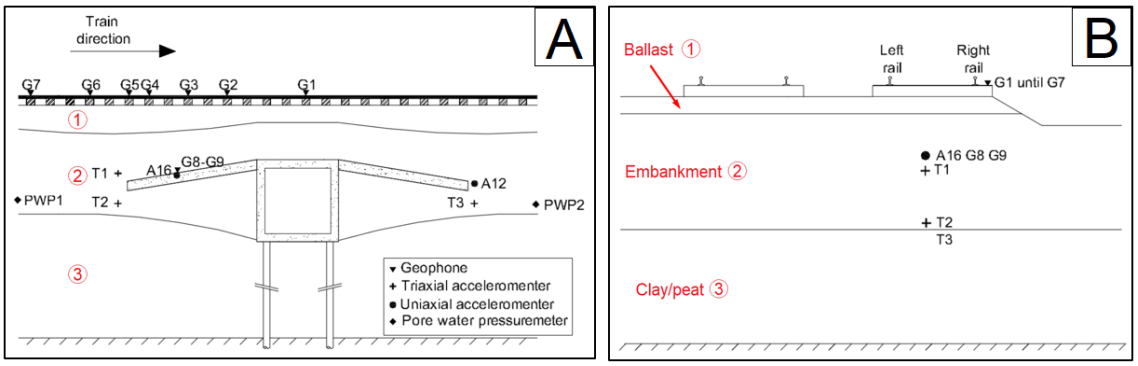

Figure 3.1 - Placing of the measuring equipment for the first dynamic test in 2008, showing each of their location in respect to the culvert and track (Modified after Coelho. B, 2011)

All geophones were adjusted to only measure vertical motions expect for geophone G8, which only measured the horisontal movement for that location. Geophone G9 was placed at the same location as accelerometer A16 to validate the results. The high speed camera were also used for validating the results of the geophones mounted on top of the wooden sleepers (G1-G7).

In total 14 train passages was monitored during the first dynamic test, with the properties as presented in table 3.2.

Of the measured train passages, there was in total

- 3 train passages of the type IDD
- 4 train passages of the type ICM
- 2 train passages of the type ILC
- 5 train passages of the type Mat V

More information about the trains are provided in [4,5].

Table 3.2 – Properties of the trains passing the culvert during the first dynamic test in May 2008 (From Coelho. B, 2011)

Train type	Velcity range [km/h]	Static axle load [kN]
Intercity double deck train set (IDD)	114-130	126-192
Intercity single deck train set (ICM)	98-129	97-143
Locomotive with carriages (ILC)	126-130	160-215
Local train (Mat V)	89-114	95-136

3.1.3 Test setup for the dynamic short term measurements (May 2009)

The second test was performed 7 months after the last tamping cycle (07.10.08), and provided the new information from the previous dynamic test (04.05.08) the devices was now placed in new positions. In this test, 9 geophones (denoted $\bar{G}$) was used, 12 uniaxial accelerometers (denoted $\bar{A}$), four triaxial accelerometers (denoted $\bar{T}$) and two strain gauges (denoted $\bar{S}$). The strain gauges was used to measure the dynamic axle loads, positioned as shown in figure 3.2.

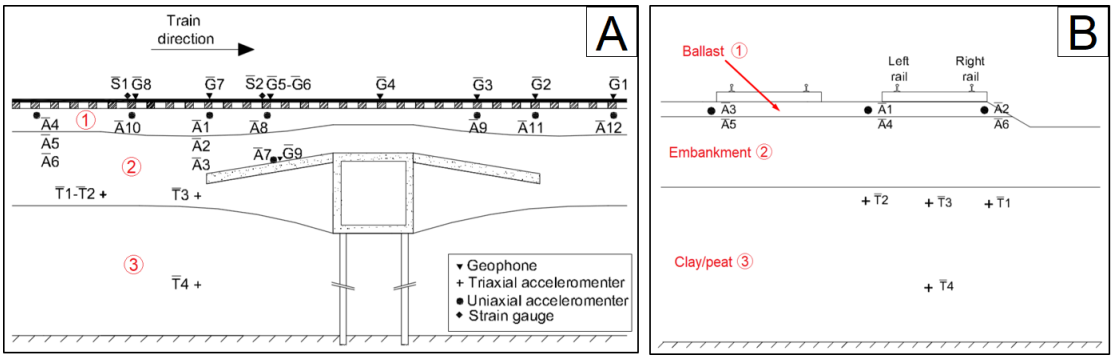

Figure 3.2 - Placing of the measuring equipment for the second dynamic test in 2009, showing each of their location in respect to the culvert and track (Modified after Coelho. B, 2011)

Eight of the geophones was placed directly on top of the sleepers ($\bar{G}1$-$\bar{G}8$) while one geophone ($\bar{G}9$), was placed directly on the middle of the slab at accelerometer ($\bar{A}7$) for validation, see figure 3.2.

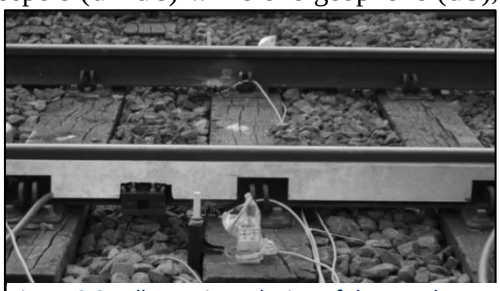

Figure 3.3 – Illustration: Placing of the geophones on top of the sleepers (From Coelho. B, 2011)

Exepct for accelerometer ($\bar{A}7$), all uniaxial accelerometers was placed in the ballast as shown in the figure 3.2 ($\bar{A}1$-$\bar{A}6$, $\bar{A}8$-$\bar{A}12$). All triaxial accelerometers was placed in the soil ($\bar{T}1$-$\bar{T}4$) and the strain gauges placed on the rail, see figure 3.2 and 3.3.

For validating the results from the geophones and accelero-meters, the high speed camera was also used here as a validation check for this test.

Table 3.3 - Properties of the trains passing the culvert during the second dynamic test in May 2008 (From Coelho. B, 2011)

Train type	Velcity range [km/h]	Static axle load [kN]
Passenger train (Sprinter T1)	65-105	76-124
Passenger train (Sprinter T2)	67-110	76-124
Local train (Mat V)	86-106	95-136

A total of 13 train passages occoured during the second dynamic test, see table 3.3.

Of the measured train passages, there was in total

- 7 trains of the type Sprinter T1
- 4 trains of the type Sprinter T2
- 3 trains of the type Mat V

More information about the trains are provided in [4, 5].

4 Analysis of the static long-term behaviour of the transition zone

In the following section, results of the monitoring programme presented in Hölscher. P and Meijers. P final report [2] are discussed. The intent of this section is to provide a better basis for under-standing the correlation between tamping, settlement rate, development of hanging sleepers and slab behaviour with respect to time.

4.1.1 Tamping, settlement rates and hanging sleepers

After the last tamping cycle of October 2008, the settlement rate of the track was monitored by leveling a section of the track that covered the transition zone and culvert. The results from the monthly levelling are presented in figure 4.1.

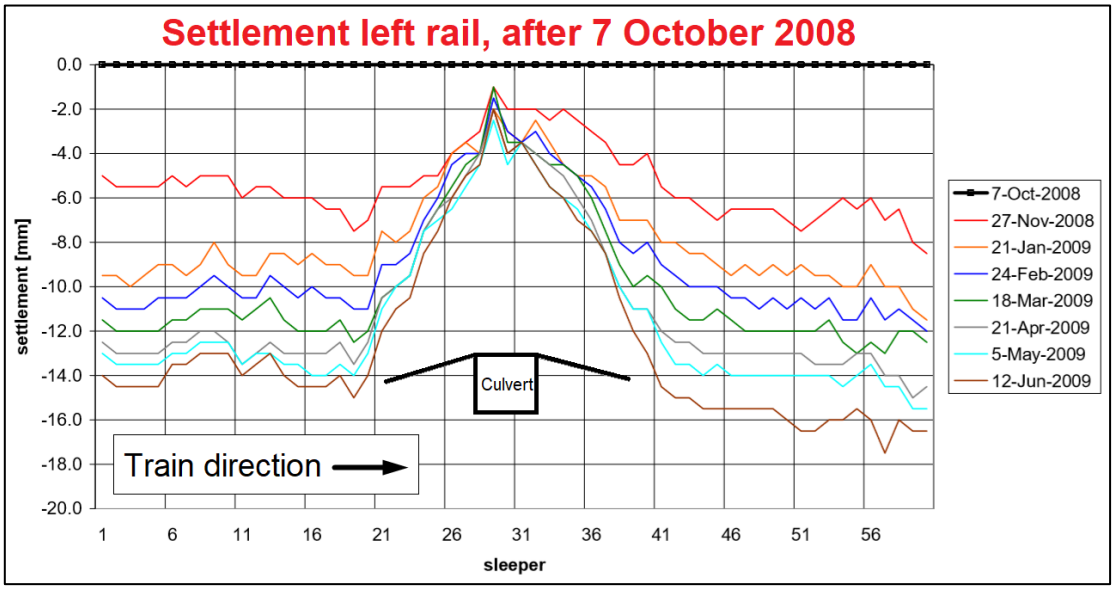

Figure 4.1 –The settlement of the left rail after a tamping cycle in October 2008, showing monthly results of track settlements clearly giving indications of the culverts placing (Modified after Hölscher. P, Meijers. P, 2009)

On top of the culvert, figure 4.1 shows that the settlement is limited to about 2-4 mm, while the settlements are continously increasing towards the embankment. The results seen at the end of the transition slabs also suggests that the track at the exit of the culvert settles slightly more than track at the entry. This shows that train direction does matter it terms of deterioration of a transition zone.

Considering the soft clay in the subsoil, some autonomous settlements could be expected beforehand due to consolidation of the clay. Using the pylons and track as reference points, the autonomous settlement in the free track were measured to be in the order of 1 mm/month [2]. These results shows good correlation with the monthly levelling as time passed by and the autonmous settlements started to dominate the settlement behaviour.

From inspecting the settlement rate at each individual sleeper, the rate varied in between 3-4 mm for the first month, then decreases towards the autonomous settlement rate of 1.0 mm pr. month. The reason for this happening after tamping, was thought to be because the vibrations involved in the tamping procedure caused the structure of the ballast developed from compaction of normal train traffic to be changed, destroying the actual stable configuration of the ballast and restarting the intial densification stages over again [5].

Over time, the measurements showed that the autonomous settlements would govern the total settlement rate when the ballast had reached its stable configuration again. From comparing the measured settlement rates at different sleepers to classic time dependent functions for the densification of ballast, the average settlement rate shows a reasonable fit when the initial stages had surpassed, suggesting that some rearrangment has taken place, see figure 4.2.

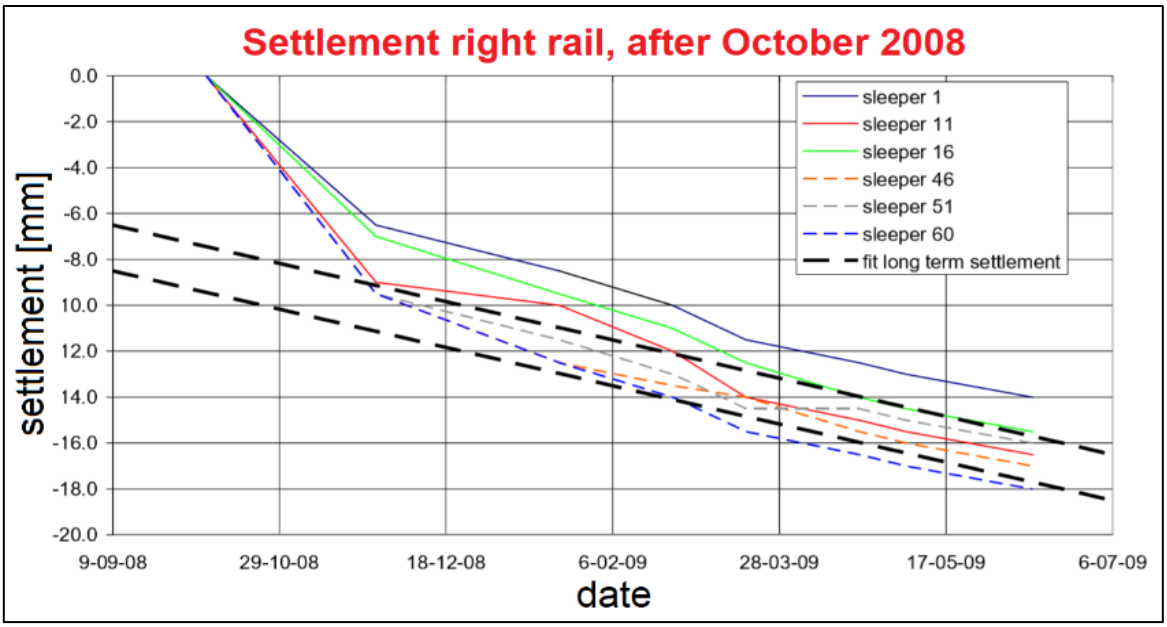

Figure 4.2 - The settlement rate of individual sleepers, showing that the rate decreases with time (After Hölscher. P, 2009)

It was also found that the densification rate of the ballast in the free embankment compared to the densification rate at the culvert and slab was lower (i.e the initial settlements surpassed faster at the culvert compared to at the free track) [2,5,6].

The reason for this is thought to be tied to these locations differences in soundboard properties bellow the ballast, where the concrete under the ballast would provide a much better soundboard than the embankment, strongly influencing the quality of the compaction achived by tamping [2].

The differential settlement was also correlated to check the potential for hanging sleepers, where Vortok de-vices were used to measured hang-ing distance of the sleepers about 7 weeks after the previous tamping cycle, see figure 4.3.

These results showed that the track shortly after a maintenance cycle had the tendency of hanging above the slab which gradually decreased towards the free embankment. This is tied to the local conditions where the culvert was founded on piles while the embankment settled autonomously about 1 mm pr. month, inveditably causing the sleepers to hang over time.

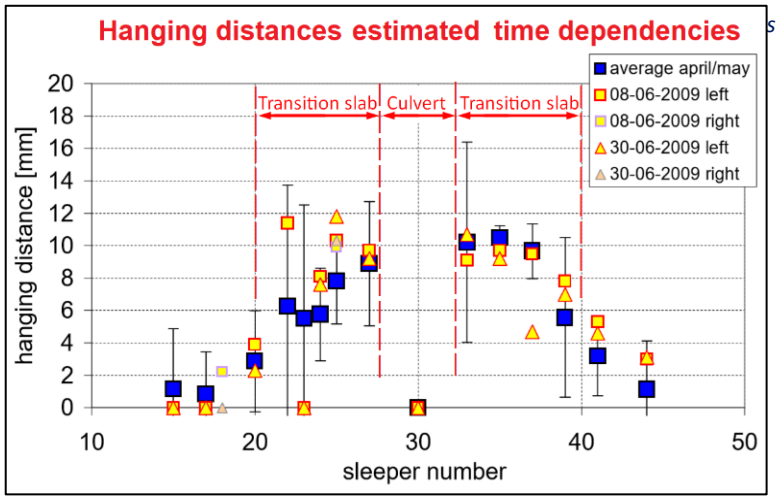

Figure 4.3 – Measured time dependent hanging distances with the Vortoc device (After Hölscher. P, Meijers. P, 2009)

As figure 4.3 shows, in the middle of the culvert (sleeper no. 30) no hanging distance can be observed. Above both approach slabs closest to the culvert, a maximum hanging distance of 10 mm i seen, gradually decreasing as the distance from the culvert increases. At about 7-8 meters from the culvert (about 15 sleepers), the hanging distance decreases to almost zero again.

To better understand the hanging phenomena, a analytical model was developed by Hölscher. P [2]with the intent to better understanding the influence settlement had on the development of hanging sleepers.

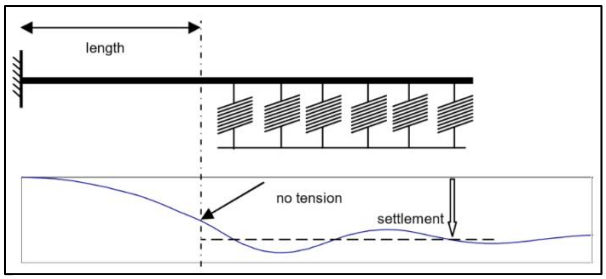

Figure 4.4 – Analytical model for development of hanging sleepers (After Hölscher. P, Meijers. P, 2009)

Indeed, the autonomous settlements from consolidation would inevitably lead to hanging sleepers, but this model provides a better basis for assessing the correlation between tamping, settlements and this development with respect to time.

In this theoretical model the track above the culvert was assumed to be completely fixed while in the free embankment, assumed to be founded on elastic springs, see figure 4.4.

By knowing that the rails at the Utrench line were of the type 54E1 and having alot of field data available, the track properties and spring stiffness could be estimated and the model used to calculate the correlation between differential settlements and development of the free hanging lenght of the track [2], see figure 4.5.

The figure shows that a differential settlement of 2.5 mm results in a free hanging distance of about 4 meter, and even the slightest settlement would to a degree lead to hanging sleepers.

After 50 days from the last tamping cycle, levelling data from figure 4.1 showed that the track settled approximately 3 mm above the culvert and 10 mm at the end of the approach slab.

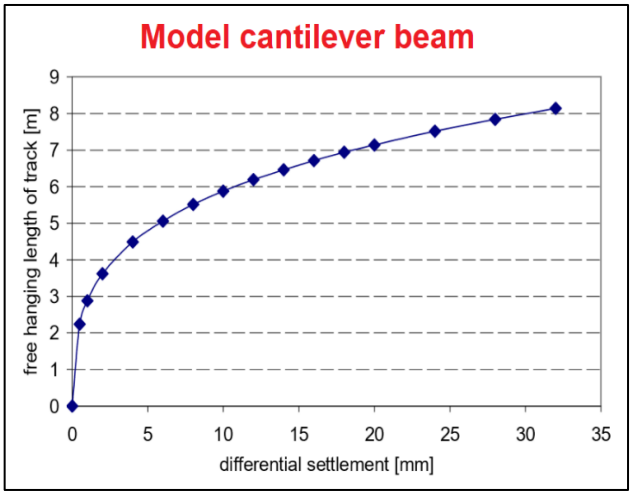

Figure 4.5 – Free hanging distance of the track as a function of track settlement (After Hölscher. P, Meijers. P, 2009)

Having the autonomous settlement rate of 1 mm/month in mind, this phenomenom was thought to be more related to the tamping than the consolidation [2,6]. The embankment provided a poor soundboard under the ballast compared to the concrete of the culvert, leading to a poorer degree of compaction after tamping which increased the potential for differential settlements between these two sections [2].

4.1.2 Slab behaviour

Based of the levelling results from October 2008 to June 2009, figure 4.6 shows the average settlement development over time above the transition slab [2].

From the 9 months of levelling data, it can clearly be seen that the ballast settles more at the end of the slab compared to the free embank-ment or everywhere else. Recapping the results from the field survey in chapter 2, it was evident from a combi-nation of hand dug holes and GPR mea-surements that the slab had rotated from its original slope of 3 % to 13 % after 13 years, which explains this occourance.

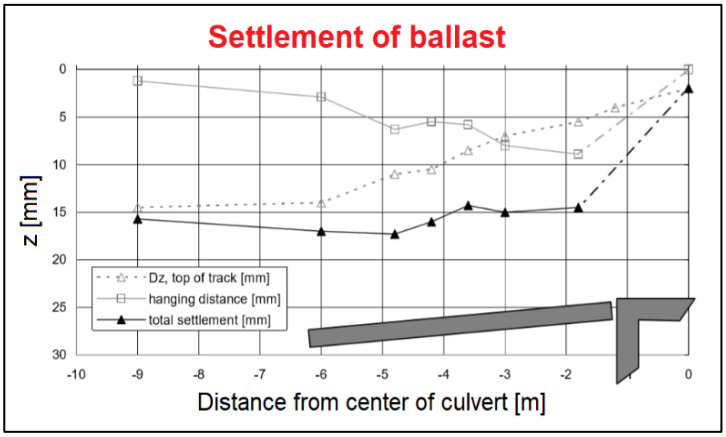

Figure 4.6 – The development of ballast settlement measured at the top of the ballast above the transition slab, suggesting that the slab has especially becomed a weak point (After Hölscher. P, Meijers. P, 2009)

This corresponded to a total vertical settlement at the end of the slab of about 0.64 meter, which explains the reason for the increased ballast thickness at the end of the slab and the larger potential for differential settlements which often occoured after each tamping cycle.

To even better understand the settlement behaviour at the approach slab, two settlement points was installed at each side of the culverts slab, see figure 4.7.

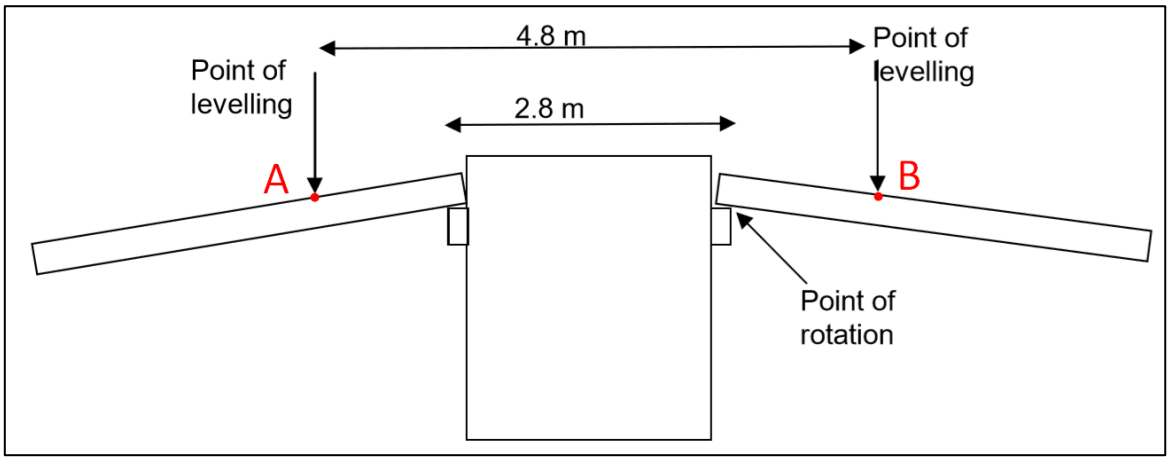

Figure 4.7 –Instrumentation of measuring points for assessing the rotation of the slab (After Hölscher. P, Meijers. P, 2009)

Extrapolations of the results at these points showed that the settlement rate of the slabs toe was about 2.5 times higher than the autonomous settlement rate of the clay (1.0 mm/month) [2]. Recapping the results from figure 2.4 that showed that the ballast thickness above the slab was about 10-20 cm thicker than it was at the adjecent embankment, backs up the hypothesis that the high settlement rate at the approach slabs originated more from the mechanisms bellow the slab rather than above.

The increased ballast thickness at the end of both slabs suggested some kind of downward flow of the material under the slab, and two checks were made in order to investegations them. First a check for flow (volume-change) was made, then compared to a predictive modell for the settlement rates. The evaluation of volume change was assumed to be sufficient for explaining the 2.5 times higher settlement rate at the slab compared to the autonomous settlement of the free embankment [2].

When inspecting the potential for flow of the backfill material, it was appropriate to assume that the sand under the slab could not densify any more, which makes its volume constant. As shown in figure 4.8, three sources of change in volume were considered for this culvert:

- Settlement of the peat clay layer resulting in a loss ($\Delta V_{subsoil}$) of the sand in the backfill
- Settlement of the approach slabs toe (ΔV_{top}) due to difference between autonomous settlement and slab settlement which were 2.5 times higher
- Potential of flow under the culvert ($\Delta V_{culvert}$)

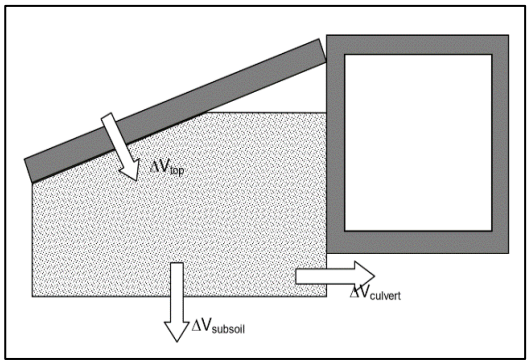

Figure 4.8 – Principal sketch: Potential for flow of sand backfill material (From Hölscher. P, Meijers. P, 2009)

For transforming the axle loads from the trains to the slab, a certain contact lenght under the slab is required. In order for the principles of this model to be realistic, it was assumed that from all the train passages over the years, the slab must have settled sufficient and the minimum contact lenght must have been present as shown in figure 4.9A).

Another presumption was that the additional settlements must have had their origin from the sand being able to move away from the slab in the terms of flow, as purposed in figure 4.9B). More assumption for this model are provided in [2].

Comparing the two cases of this model, it was possible to reason for the increased settlement rate tendency beneath the slab compared to the autonomous settlement rate in the subsoil.

Assumptions made for both cases was that for a minimal case, a contact lenght ($L_{contact}$) of 1.0 meter with an effectiv width (B_{eff}) of 1.0 meter for sand to flow beneath the culvert was assumed. For a maximal case, a contact lenght of 3.0 meter with an effective width (B_{eff}) of 2.0 meter for the sand to flow beneath the culvert is assumed.

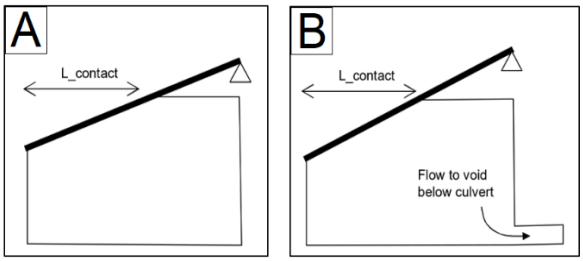

Figure 4.9 – Illustration: Simple beam founded on one freely rotating support and in the free embankment where A) shows before increase in settlements, and B) shows after increase in settlements (From Hölscher. P, Meijers. P, 2009)

By comparing the flow rate (i.e settlement causing the change in fill height at the point of rotation) as a function of the autonomous settlement rate of subsoil, to the settlement rate of the tip of the slab for these two cases, it is shown that the settlement rate of the slab always ends up at 1.5-2.5 times higher than the settlement of the subsoil [2], see figure 3.10.

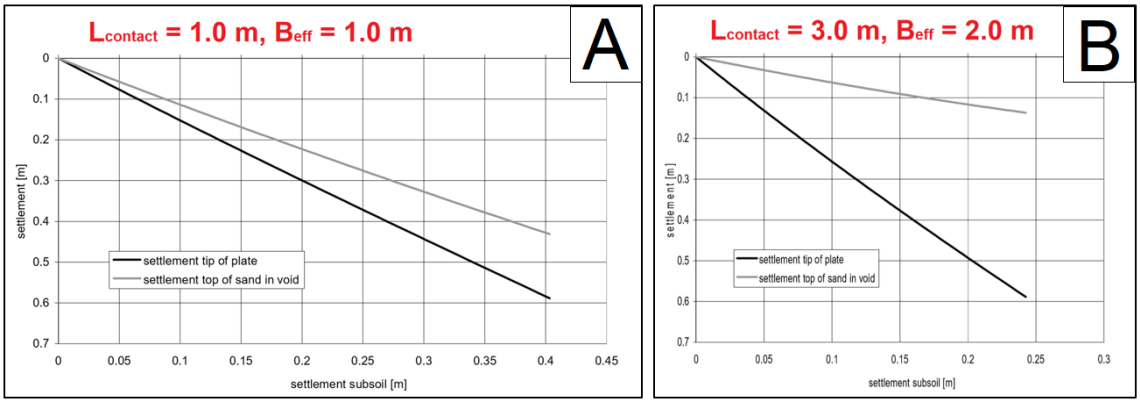

Figure 4.10 – Settlement ratio between the tip of the plate and top of sand in the void in the case of A) a contact lenght of 1.0 meter and effective width 1.0 meter, and B) a contact lenght of 3.0 meter and effective width 2.0 meter (Modified after Hölscher. P, Meijers. P, 2011)

These findings provides a good explaination for why the end of the slab always seemed to settle more and become the weakest point at the Gouda Gouverwelle culvert.

As a comparison, a static solution based on Brinch-Hansen theory for bearing capacity showed that a contact lenght of about 1-2 meter for a slab was required to carry the load of passing trains. This quantity is however rough, since the cyclic and dynamic loads from a train passage may increase the required contact lenght. From the fact that the soil volume beneath the slab also changed with time, it was still assumed that this prediction model gave a reasonable explaination for the increased settlement rate at the endpoint of the slab [2].

5 Analysis of the tracks dynamic behaviour

Results from the dynamic measurements performed at Gouda Govervelle are presented in this section. Alot of focuse from the authors involved in these field measurements has been assessing the hanging sleepers at the transition zone [2,5,6], but are less prioritized in this report as the main intent is to study the general aspect of the dynamic behaviour which should be applicable for other culvert cases. Most of the dynamic results presented in this chapter was processed by Bruno Coelho in 2011 [5].

5.1.1 First dynamic test (May 2008)

This test was performed to both check the reliability of the different measuring devices but also to provide a better basis for placing the devices in the second dynamic test.

To check the reliability of these measurements, geophone G5 which was placed directly on top of a sleeper above the slab was compared to the displacement measured by the high speed camera. A comparison between these devices were made during a ILC train passage at 130 km/h, see figure 5.1.

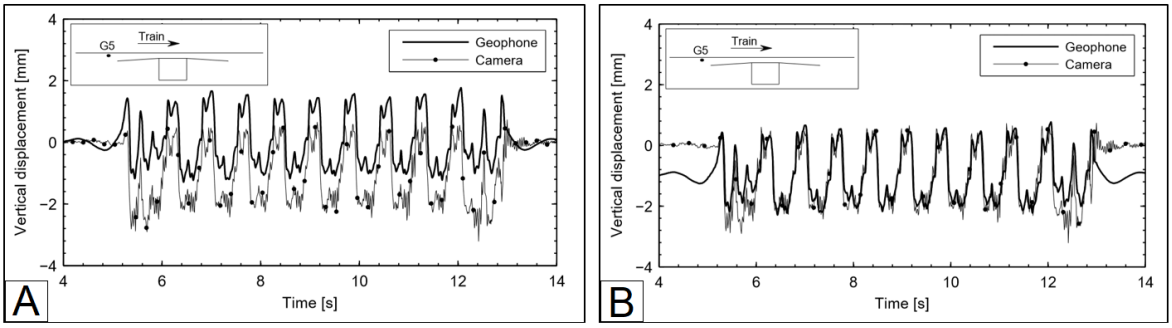

Figure 5.1 –Comparison between the vertical displacement measured by geophone (G5) and high speed camera, where A) shows before filtering and B) after filtering the results (Modified after Coelho. B, 2011)

As the initial results from figure 3A) shows, there is good agreement in the peak to peak response but poor correlation between the vertical displacements. By removing the DC component of the frequency domain, the data was then shifted downwards as shown in figure 3B) were a better correlation was found.

From the same train passage, it was also found good agreement between the vertical displacement measured by accelerometer A16 and the displace-ments measured by geophone G9 above the approach slab, see figure 5.2.

As the results from the figure shows, both in magnitude of the displace-ments and the peak to peak value does the comparison correlate well.

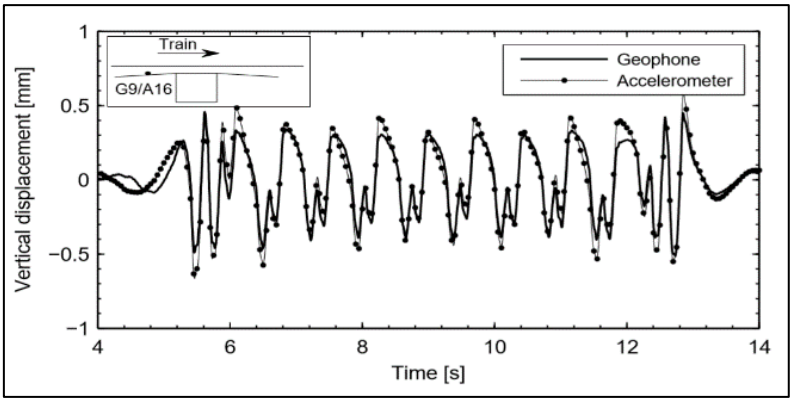

Figure 5.2 – A comparison between the vertical displacement measured by geophone G9 and accelerometer A16 (From Coelho. B, 2011)

For assessing the general behaviour of this transition zone three geophone measurements are presented in figure 5.3, showing the vertical displacement versus time at the free track (G7), above the approach slab (G3) and above the culvert (G1). These measurements were performed about 2 months after the previous tamping cycle.

The figure shows that the maximum peak displacement was approximately 1.5 mm in the free track (G7, fig. 5.3A), 6 mm above the approach slab (G3, fig. 5.3B) and 0.7 mm above the culvert (G1, fig. 5.3C).

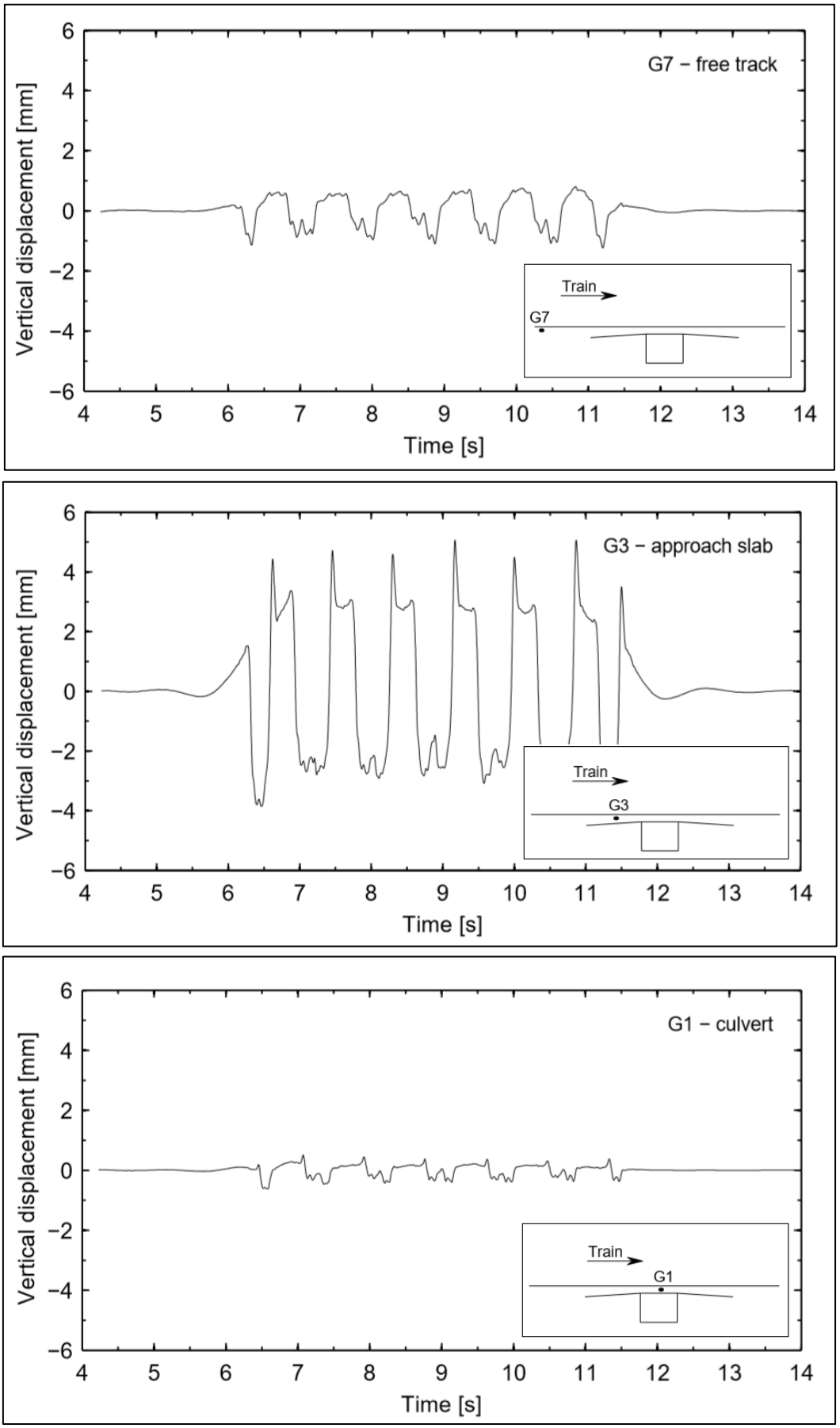

Figure 5.3 - Vertical displacement of ballast measured by geophone G7, G3 and G1 (Modified after Coelho. B, 2011)

As the results from figure 5.3 shows, the displacements are tremendously increased above the approach slab, showing that it is the weakest point with the lowest stiffness in the transition zone. For all geophone measurements at the sleepers, the vertical displacement seemed to move upwards simultaneously when each axle was passing the geophones, but can best be seen above the approach slab (G3) where there are spikes clearly moving upwards. This were thought to be associated with the sleepers hanging at this measuring point [5], which was confirmed from the static measurements, see chapter 4.1.1.

The average maximum displacements for all train passages over the the geophones are presented in figure 5.4, which shows that the track at the end point of the slab («toe») clearly deviates from both the free embankment and culvert.

As the train is moving into the slab, the displacement measurements of the sleepers shows that it occours some kind of «dip» in the beginning of the slab (G7-G4) and (G4-G1), see figure 5.4.

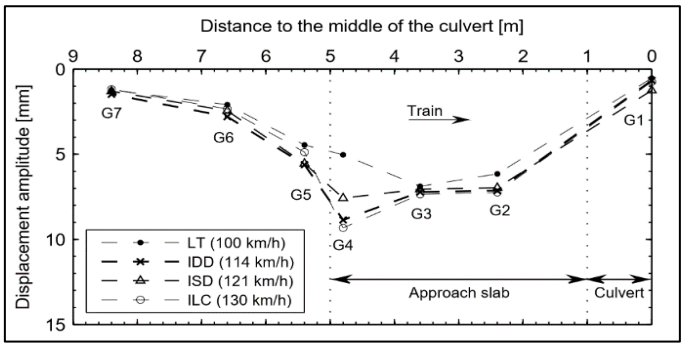

Figure 5.4 –The average displacement amplitude for all train passages clearly that the slab causes a dip in the transition from embankment to slab (From Coelho. B, 2011)

The dynamic results from the track showed good compliance with the static monitoring programme in section 2.1, which also showed that the settlement rate was up to 2.5 times higher at the slabs end section compared to the autonomous settlement rate at the free track (i.e in the clay).

5.1.2 Second dynamic test (May 2009)

As with the first dynamic test, the first task during this test was to validate the results by comparing the geophone and accelerometer measurements with the high speed camera. A good correlation between geophone ($\bar{G}7$) and the camera measurement was found, see figure 5.5A). For further comparison, accelerometer ($\bar{A}7$) was compared to geophone ($\bar{G}9$), which also showed good correlation, see figure 5.5B).

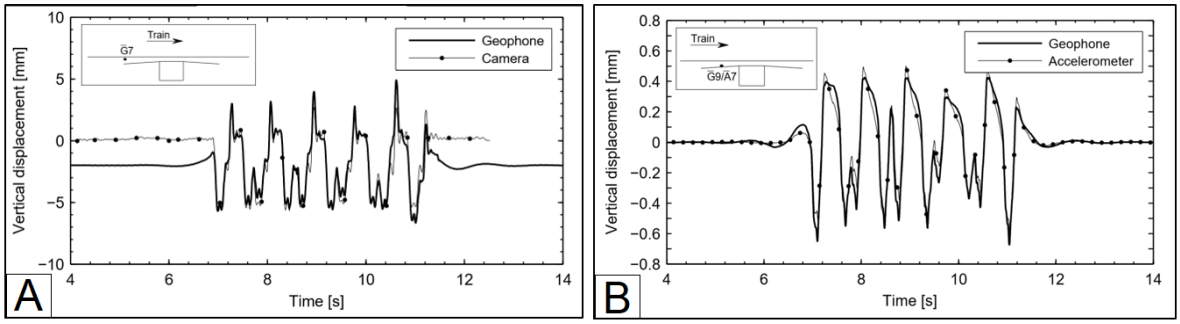

Figur 5.5 - Comparison between A) the vertical displacement measured by geophone ($\bar{G}7$) and high speed camera, and B) the vertical displacement measured by geophone ($\bar{G}9$) and accelerometer ($\bar{A}7$) (Modified after Coelho. B, 2011)

The tendency of hanging sleepers at the first dynamic test in 2008 was also studied further in this test by placing two pairs of accelerometers and geophones at the entry and exit of the transition zones at each side of the culvert. The geophones was placed directly on top of the sleepers while the accelerometers in the ballast.

By comparing the vertical displacements of sleeper and ballast, the severity of hanging sleepers could be assessed. As figure 5.6 shows, before the approach slab the difference between sleeper displacement ($\bar{G}8$) and ballast displacement ($\bar{A}10$) is very small. On top of the approach slab the difference in sleeper displacement ($\bar{G}7$) and ballast displacement ($\bar{A}2$) is about 9 times higher, clearly demonstrating that the sleepers in fact are hanging above the slab, see figure 5.6A) and 5.6B).

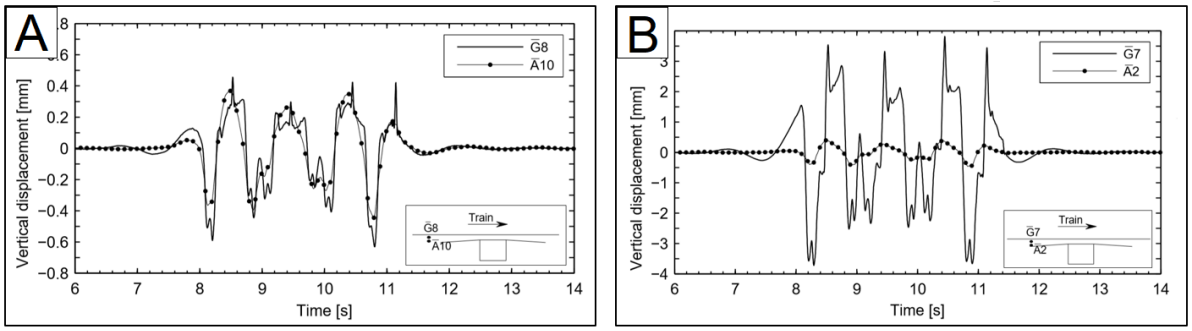

Figure 5.6 –Comparison between the vertical displacement of sleeper and ballast in A) before the approach slab and B) above the approach slab (Modified after Coelho. B, 2011)

By comparing the average peak to peak displacements along the track, it was found that the same displacement pattern occoured as previous seen in the dynamic test from 2008, see figure 5.6. In this test however, the displacement of the transition slab both at the entry and exit of the culvert were measured, and it was found that the slab on both sides displaced more than the culvert and free embankment.

The results showed that at the entry of the culvert, the maximum downward displacements of the sleepers occoured at the middle of the slab, while at the exit of the culvert the displacements on the end of the slab with a slightly larger magnitude. This suggests that a stiff to soft transition leads to larger sleeper displacements than a soft to stiff transition, see figure 5.7A).

By inspecting the ballast displacements further, it can be seen that the displacements of the track is larger on the left side compared to the right, suggesting that the dynamics and deterioration rate is more severe when the train is moving from a soft to stiff condition compared to the latter case, see figure 5.7B).

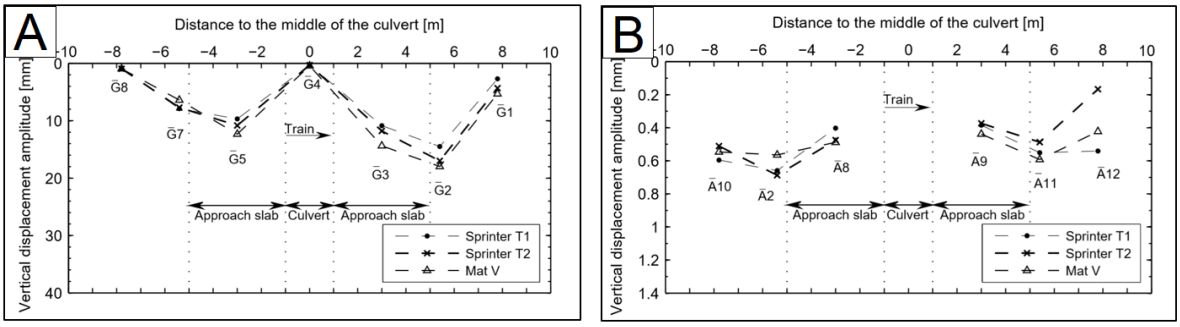

Figure 5.7 – Illustration: Average peak to peak displacement for devices located A) along the track on top of the sleepers, and B) along the track kon top of the ballast (Modified after Coelho. B, 2011)

By comparing the displacments from the first test to the second test, it was possible to evaluate the development of settlement with time at the different locations for infication of the long term behaviour of the transition zone, see table 5.1.

Table 5.1 – Average peak to peak displacement during the first and second dynamic test exposing the developing displacement pattern with time (From Coelho. B, 2011)

Year	G7 and $\bar{G}8$ [mm]	G3 and $\bar{G}5$ [mm]	G1 and $\bar{G}4$ [mm]
2008	1.24	6.83	0.76
2009	0.8	11.23	0.31
Ratio 09/08	0.64	1.65	0.4

It was found that in the free track (G7 and G$\bar{8}$) and on top of the culvert (G1 and (G$\bar{4}$), the displacementrate decreases over time. On the approach slab however (G3 and (G$\bar{5}$), a clear increase is seen which suggests that the deterioration rate above the slab accelerates.

Lastly, the dynamic train loads were also measured by the means of strain gauges, which according to Coelho. B measures within 5% accuracy [5].

One strain gauge were placed on the rail at the free embankment and one at the rail above the slab. The strain gauges were mounted on the rail web along its neutral axis to prevent the bending of the rails to influence the results, see figure 5.8.

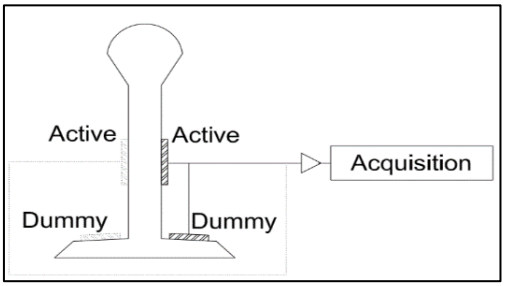

Figure 5.8 –Principles for placing the strain gauges on the rail along the neutral axis (From Coelho. B, 2011)

In figure 5.9, the strain gauge results ($\bar{S}1$ and $\bar{S}2$) during a Sprinter T1 passage are presented, showing that the axle loads increases from a maximum peak at about 180 kN at the free embankment (figure 5.9A), to a maximum peak at about 240 kN above the slab (figure 5.9B), proving that an dynamic amplification has taken place with about 25% increase.

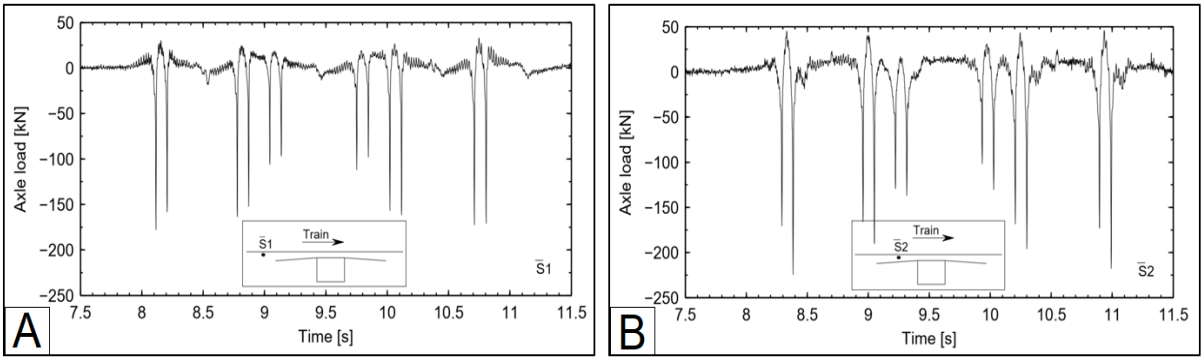

Figur 5.9 – Illustration: Dynamic axle loads during a Sprinter T1 train passage at 96 km/h, showing A) results from the free track and B) results above the approach slab (Modified after Coelho. B, 2011)

The measurements from the strain gauges were also used for defining dynamic amplification factors by calculating the ratio between dynamic and static axleload [5] after the following expression

$$\text{Dynamic amplification} = \frac{Load^{dynamic}avarge}{Load^{static}average} \quad \text{(Eq. 5.1)}$$

where

$$\text{Load}_{\text{average}} = \frac{\Sigma\, Maximum\ wheel\ load}{Number\ of\ wheels} \quad \text{(Eq. 5.2)}$$

Figure 5.10 presents the dynamic amplification factors for all trains at the measuringpoints in the free embankment ($\bar{S}1$) and the approach slab ($\bar{S}2$). These results shows that the amplification on average, is higher above the slab than in the free embankment, but that the amplification factors in the free embankment is more variable than above the slab, see figure 20A) and 20B).

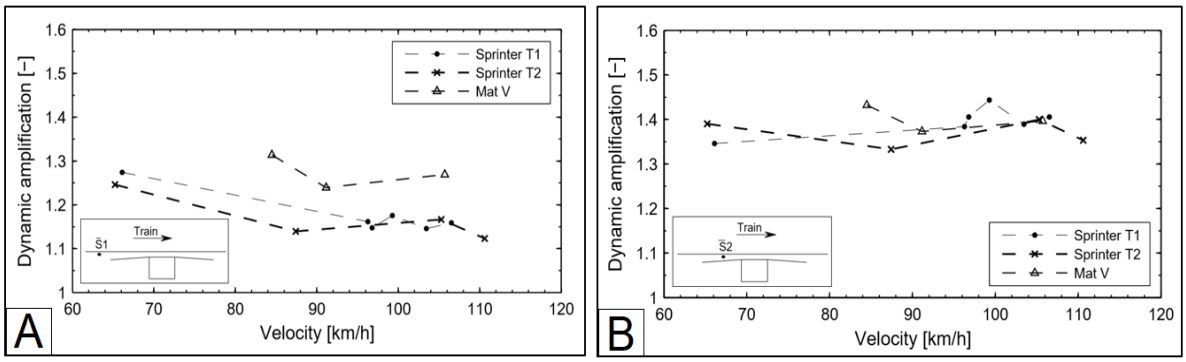

Figure 5.10 - Dynamic amplification factors in A) the free embankment and B) above the approach slab during several train passages derived from equation 1 and 2 (Modified after Coelho. B, 2011)

The reason for this variety is tied to the fact that the amplification above the slab is governed by the hanging sleepers and rail curvature which dominates the load behaviour while at the free embank-ment the support is better and the dynamic amplification will be smaller and more dependent on train speed, train types and axle loads [5].

From the average dynamic axle loads (Eq. 5.1) and the average peak to peak displacements during a train passage, an average dynamic stiffness could also be estimated. For comparison, the average dynamic stiffness at the middle of the approach slab was about 9 times smaller than in the free track, see figure 7A) and 7B).

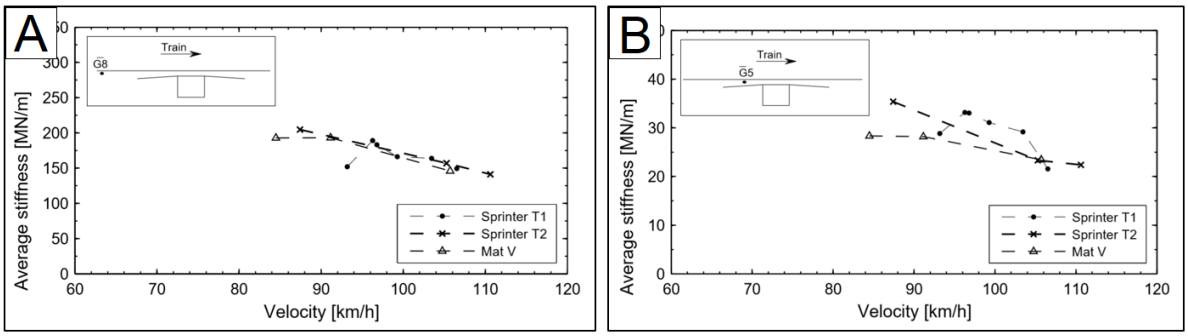

Figure 5.11 –The average dynamic stiffness on A) the free track and B) in the middle of the transition slab (Modified after Coelho. B, 2011)

Following the same principles for calculating the average stiffness by using the displacements of the ballast instead of the sleepers, it is found that the «apparent stiffness» over the culvert is about 1.5 times higher that of the free track [5].

It is important to highlight that this is called apparent stiffness because the value is more like a ratio than a stiffness as the results from the loads were not measured at the same position as the displacement-.

6 Discussion and summay

This report was written to highlight and discuss some of the findings from the comprehensive field monitor programme that was carried out at the railway culvert of Gouda Goverwelle. Despite this culvert being a very special case, some of the tendencies and magnitudes revealed from the field measurements are still thought of as being relevant for most types of concrete culverts instrumented with transition slabs.

An interesting observation here was that the toe area of the slab always seemed to be the weakest point in this transition zone compared to the rest of the track, even shortly after a maintenance cycle. Indeed, the autonomous settlements at the site would eventually cause this behaviour to worsen with time and eventually cause this section to become the weakest point. But this tendency was already seen at the first dynamic measurement which according to Coelho. B, was performed at a time when no observations of the sleepers hanging was made for that measuring point.

When comparing the displacements from the dynamic test of 2008 to 2009, it was found that the displacement ratio (i.e increase with time) above the culvert and in the free track was slowing down (i.e the ratio was less than 1.0). But on the slab however, it seemed to be accelerating (i.e a ratio higher than 1.0). According to the study performed by Hölscher and Meijers, this was related to the sand in the backfill being able to flow bellow the slab, causing the volume beneath the slab to change over time, the contact lenght of the slab to decrease, evidently causing it to rotate. This explains the especial increased ballast thickness above the slab compared to the other sections of the track.

Another interesting finding was that the ballast seemed to densify faster above the culvert compared to the free track, which suggests that ballast supplementing and regular tamping at this site was not that effective. This phenomena is also purposedly related to the stiffness of the subsoil where it in this case was particulary soft. Its worth mentioning that the tamping trains for this particular case were not specified, and more modern trains such as Stopfexpress 09-4X (used at «Gardemoenbanen», a railway line in Norway) has the ability to tamp (elevate the track) and compress (compact) the ballast in one single operation, decreasing the initial densification of the ballast after tamping.

It was also found from these measurement that the trains moving direction had a direct influence on the tracks response. When the train was moving from the embankment (soft medium) to the culvert (stiff medium), the dynamic responses was more severe compared to a transition between culvert and embankment as the ballast would settle more. When the train was moving from the culvert (stiff medium) to the embankment (soft medium), the track displacement during any train passage was larger compared to at the entry. This indicates that a stiff to soft transition causes larger track displacements than the latter case, but a soft to stiff transition causes more severe dynamics.

What these findings demonstrates is the importance of controlling the backfill material bellow the transition slab, and that corrective maintenance such as ballast supplementation and tamping in general only provides a temporarly fix. The suggestion from this study is that the softer the backfill material under the slab is, the more potential is there for that section of the track to «dip» when the trains are passing over from the free track over to the transition slab.

If its ensured that the material bellow the slab is well compacted and cannot flow over time there is no proof of that the stiffness reduction at the slabs end point is enough to increase the deterioration rate of the transition zone with time for a general case. If the material by any chance has the ability to flow however, the end result might be as demonstrated with Gouda Goverwelle, where the slabs intent of providing a graduall stiffness transition for the track had completely failed, and only moved the problem to the end of the transition slab.

Bibliography

[1] Hartman A.D (2009). Railway transition zones and switches. Factual report fieldtest monitoring, Deltares. Available at https://repository.tudelft.nl/

[2] Hölscher. P, Meijers. P (2009). Analysis of track and soil behaviour at transition zones – Case study near Gouda Goverwelle, Deltares. Available at https://repository.tudelft.nl/

[3] Hartman. A.D (2008). Delft Cluster Railway transition zones & switches. Factual report short-term measurement 2008. Available at https://repository.tudelft.nl/

[4] Hölscher. P, Hartman. A.D (2009). Delft Cluster Railway transition zones & switches. Factual report short-term measurement 2009. Available at https://repository.tudelft.nl/

[5] Coelho. B (2011). Dynamics of railway transition zones in soft soils. Doctoral thesis, TU Delft. Available at https://repository.tudelft.nl/

[6] Ferreira Silva. J (2013). *Long-term behaviour of railway transitions under dynamic load, application to soft soil sites*. Doctoral thesis, University Nova De Lisboa. Available at https://repository.tudelft.nl/

[11] Kramer. S (1996). *Geotechnical Earthquake Engineering*. Prentice-Hall International series in civil engineering and Engineering mechanics

[12] Nordal. S (2017). *Geodynamics*, Compendium. Phd Course, Lecture notes. Norwegian University of Science and Technology, Geotechnical Group.

[13] Nordal. S (2018). *Geotechnical Engineering Advanced course, lecture notes and background material*, Compendium. Norwegian University of Science and Technology, Geotechnical Group.

[14] Moore. I. D (2017). *Large-Scale Laboratory Experiments to Advance the Design and Performance of Buried Pipe Infrastructure*. Queen's University, Ellis Hall, Kingston Available at https://ascelibrary.org/

[15] Petterson. L, (2007). *Full Scale Tests and Structurual Evaluation of Soil Steel Flexible Culverts with low Height of Cover*. Report. Civil and Architechtural Engineering. Kungliga Tekniske Högskolan (KTH). Available at: http://kth.diva-portal.org/

[16] Statens Vegvesen, Vegdirektoratet (2018). *Retningslinjer, Håndbok R211: Feltundersøkelser*. Available at https://www.vegvesen.no/fag/publikasjoner/handboker